Oxidative Medicine and Cellular Longevity

Antioxidants and Free Radicals in the Phototoxicity of Drugs and Nanomaterials

Lead Guest Editor: Daoud Ali
Guest Editors: Hui-Min D. Wang and Madhukar Saxena

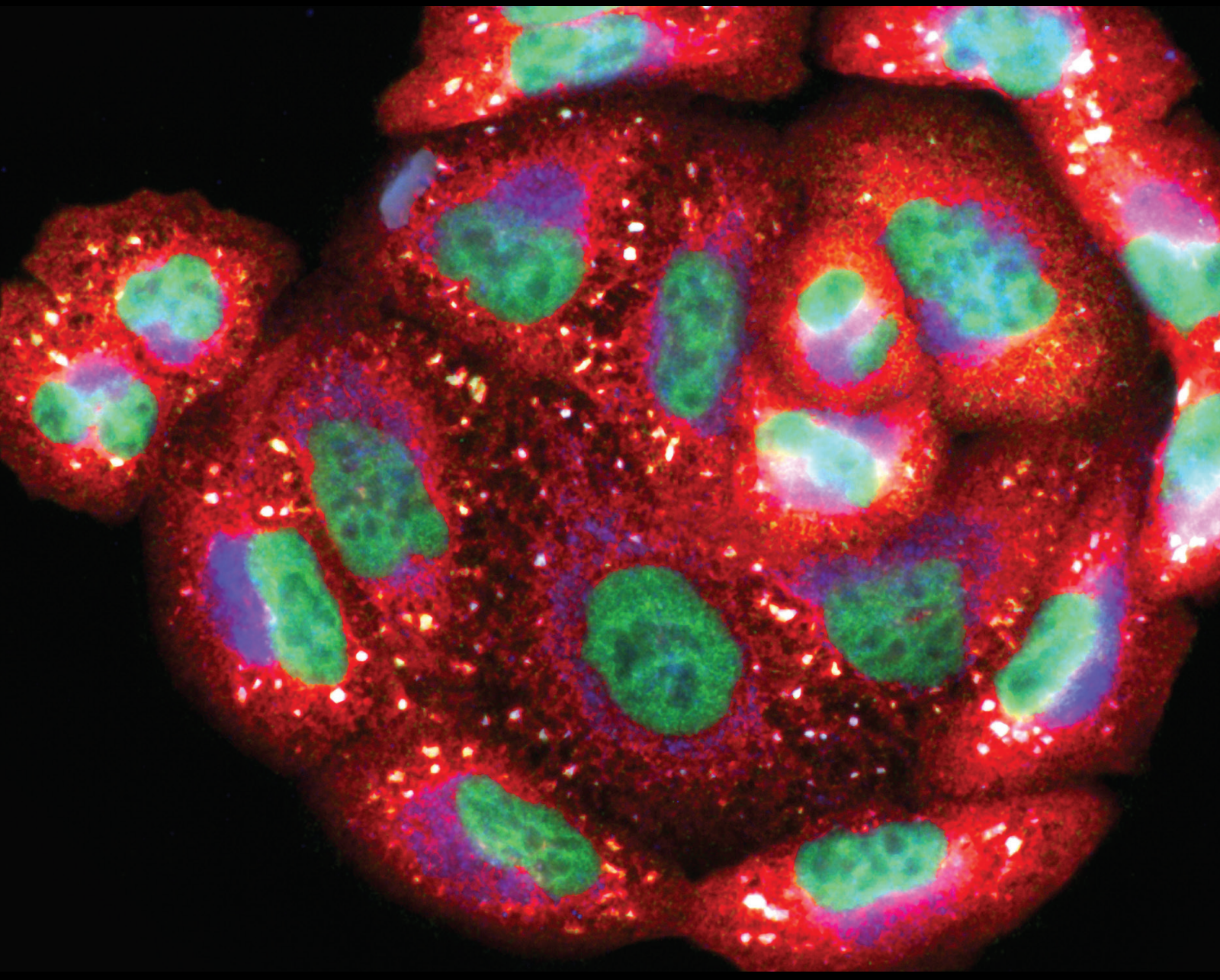

Antioxidants and Free Radicals in the Phototoxicity of Drugs and Nanomaterials

Oxidative Medicine and Cellular Longevity

Antioxidants and Free Radicals in the Phototoxicity of Drugs and Nanomaterials

Lead Guest Editor: Daoud Ali
Guest Editors: Hui-Min D. Wang and Madhukar Saxena

Contents

Different Doses of β-Cryptoxanthin May Secure the Retina from Photooxidative Injury Resulted from Common LED Sources
Cemal Orhan, Mehmet Tuzcu, Hasan Gencoglu, Emre Sahin, Nurhan Sahin, Ibrahim Hanifi Ozercan, Tejas Namjoshi, Vandita Srivastava, Abhijeet Morde, Deshanie Rai, Muralidhara Padigaru, and Kazim Sahin
Research Article (15 pages), Article ID 6672525, Volume 2021 (2021)

Mechanism of Intestinal Flora and Proteomics on Regulating Immune Function of *Durio zibethinus* Rind Polysaccharide
Huimin Jiang, Jinmei Wang, Qiongxin Liang, Shengjun Jiang, Changyang Ma, Yan Zhang, and Wenyi Kang
Research Article (20 pages), Article ID 6614028, Volume 2021 (2021)

Oxidative Stress Mediated Cytotoxicity, Cell Cycle Arrest, and Apoptosis Induced by *Rosa damascena* in Human Cervical Cancer HeLa Cells
Mai M. Al-Oqail, Nida N. Farshori, Ebtesam S. Al-Sheddi, Shaza M. Al-Massarani, Quaiser Saquib, Maqsood A. Siddiqui, and Abdulaziz A. Al-Khedhairy
Research Article (11 pages), Article ID 6695634, Volume 2021 (2021)

Hindawi
Oxidative Medicine and Cellular Longevity
Volume 2022, Article ID 9355692, 17 pages
https://doi.org/10.1155/2022/9355692

Research Article

Adipose-Derived Stem Cell-Incubated HA-Rich Sponge Matrix Implant Modulates Oxidative Stress to Enhance VEGF and TGF-β Secretions for Extracellular Matrix Reconstruction *In Vivo*

Yu-Shen Cheng,[1] Hung-Hsun Yen,[2] Chung-Yen Chang,[1] Wei-Chih Lien,[3,4] Shu-Hung Huang,[5,6] Su-Shin Lee,[5,6] Lin Wang,[7] and Hui-Min David Wang[4,6,8,9]

[1]*Department of Chemical and Materials Engineering, National Yunlin University of Science and Technology, Douliou, Yunlin 64002, Taiwan*
[2]*Department of Fragrance and Cosmetic Science, Kaohsiung Medical University, Kaohsiung 807, Taiwan*
[3]*Department of Physical Medicine and Rehabilitation, National Cheng Kung University Hospital, College of Medicine, National Cheng Kung University, Tainan 701, Taiwan*
[4]*Ph.D. Program in Tissue Engineering and Regenerative Medicine, National Chung Hsing University, Taichung 402, Taiwan*
[5]*Division of Plastic Surgery, Department of Surgery, Kaohsiung Medical University Hospital, Kaohsiung 807, Taiwan*
[6]*Collage of Medicine, Kaohsiung Medical University, Kaohsiung 807, Taiwan*
[7]*College of Chemistry & Pharmacy, Northwest A&F University, Yangling, Shaanxi 712100, China*
[8]*Graduate Institute of Biomedical Engineering, National Chung Hsing University, Taichung 402, Taiwan*
[9]*Department of Medical Laboratory Science and Biotechnology, China Medical University, Taichung 404, Taiwan*

Correspondence should be addressed to Lin Wang; wanglin0317@nwsuaf.edu.cn
and Hui-Min David Wang; davidw@dragon.nchu.edu.tw

Received 13 May 2021; Accepted 20 November 2021; Published 17 January 2022

Academic Editor: Alin Ciobica

This study demonstrated both adipose-derived stem cells (ASCs) *in vitro* and *in vivo* combined with three-dimensional (3D) porous sponge matrices on implant wound healing. Sponge matrices were created from hyaluronic acid (HA), collagen (Col), and gelatin (Gel), constructing two types: HA-L (low content) and HA-H (high content), to be cross-linked with 1-ethyl-3-(3-dimethylaminopropyl) carbodiimide (EDC). Fourier transform infrared spectroscopy method verified carboxyl groups of HA and amino groups of Col and Gel reacting between the raw materials and scaffolds to identify the successive cross-linking. The swelling ratios of two types of sponge matrices were analyzed by water absorption capabilities, and the results displayed both over 30-fold dry scaffold weight enhancements. In biodegradation tests, matrices were hydrolyzed over time by three cutaneous enzymes, hyaluronidase, lysozyme, and collagenase I. ASCs from rats were cultured within the HA-H scaffold, demonstrating higher antioxidative abilities and secretions on related genes and proteins compared to the other two groups. The ASC HA-H matrix promoted cell proliferation to stimulate capillary angiogenesis inducer secretions, including vascular endothelial growth factor (VEGF) and transforming growth factor-β (TGF-β). *In vivo* histological examinations showed ASCs from implanted HA-H implant transported into the subcutis, and rat skin cells also infiltrated into the original matrix zone to increase the extracellular matrix (ECM) reconstructions. Our experimental data revealed that the ASC HA-H sponge implant was effective in improving wound repair.

1. Introduction

The human skin covers the entire body, has an average surface area of nearly 1.6 m^2 in a human adult, and acts as the first line of defense against external factors. The skin comprises three layers: epidermis, dermis, and subcutis [1]. During cell differentiation, the epidermis divides into the stratum corneum, granulosum, and spinosum and basal layer [2]. The basal layer consists of basal cells, which act as daughter cells, continuously dividing and moving toward the outer layer of the skin. The dermis area is the supportive connective tissue between the epidermis and the underlying hypodermis and includes two layers: the dermis papillary and reticular layers. The human dermis contains sweat glands, hair roots, nervous cells, fibers, and blood capillaries and lymph vessels. The subcutis, also called the hypodermis, lies below the dermis and is used for fat storage. It contains loose connective tissues and fat lobules and has larger blood vessels and nerves than the dermis [2].

Stem cells are biological undifferentiated cells which differentiate to specialized ones and divide into producing more stem cells and are found within multiple organism tissues [2, 3]. In mammal organisms, stem cells comprise two broad kinds: embryonic and adult stem cells, whereby the former are found in blastocyst inner cell mass and the latter are purified from various tissues [4]. In adult creatures, progenitor and stem cells work as the healing medical staffs to the body, supporting matured organs. There are three identified available resources of autologous adult stem cells: (1) adipose tissue (lipid cell), which is required for extraction by liposuction; (2) bone marrow, which is needed for extraction by harvest, that is, drilling into bone (typically the femur or iliac crest); and (3) blood, which is necessitated for extraction through apheresis, wherein blood is drawn from the donor (similar to a blood donation) and passes through a machine that extracts the stem cells and returns other portions of the blood to the donor [5]. Adipose-derived stem cells (ASCs) ideally possess other unique properties, including abundant proliferation, minimally invasive procedures for collections, and easy adaptation when transplanted into a host [6, 7]. ASCs can be isolated from a plentiful source of adipose tissues recovered through lipoaspirations, which have become a routine plastic procedure with the increasing prevalence of obesity and the extra lipid accumulation [7]. These subcutaneous adipose tissues greatly contribute to research and other medical applications. ASCs have presented to own the DNA regenerative defective ability, having crucial positive impacts on extensively damaged oxidative stress cells or tissues [8]. It was identified that reactive oxygen species (ROS) improved stem cell differentiations and assisted reprogramming them into induced pluripotent stem cells (iPSCs), and on the other hand, ROS were related to the premature aging and malignant cell transformation. High oxidative stress hinders wound repair and slows the healing process. Since ASCs were discovered, several summary points have been revealed on their differentiations and wound-healings and tissue-engineering capacities [7–10]. We also have published several papers to demonstrate this finding [3, 11–14].

Designing specific therapeutic properties can help to decrease the morbidity and mortality from full-thickness skin wounds by using skin substitutes [15]. Nowadays, tissue engineering approaches apply three-dimensional (3D) skin substitutes including tissue cells, scaffold matrices, and surrounding signals, to accomplish this goal. In the past few decades, various potential scaffold matrices were developed from synthetic and natural polymers for tissue repairs and regenerations, according to the principles of tissue engineering [16, 17]. 3D porous matrices serve as temporary templates to guide new tissue reproduction and provide sufficient porosity for body fluids to transport nutrients and oxygen [18]. Biomaterials, including hyaluronic acid (HA), collagen (Col), and gelatin (Gel), which are the major components of human connective tissues, soft tissues, and the skin, ideally serve as physical support edifices of the extracellular matrix (ECM) [19, 20]. The present study hypothesized that HA, Col, and Gel could be cross-linked together into a 3D porous matrix and used as a cultured construction for ASC proliferations. This ASC matrix implant was assessed for biocompatibilities and characteristics *in vitro*, ex vivo, and *in vivo* for skin wound repair. We found out this implant was positively and potentially applied in wound healing.

2. Materials and Methods

2.1. Preparation of Porous Matrices. HA (molecular weight: 2–2.1 million daltons; Kibun Food Chemicals Co., Japan), Col (molecular weight: 64,000 daltons; Sigma-Aldrich Co., St. Louis, MO, USA), and Gel (molecular weight: 5,000 daltons; Sigma-Aldrich Co.) were initially dissolved into 100.0 mL deionized water. The raw material ratio for HA-L (low HA content) was HA : Col : Gel = 2.43 : 36.58 : 60.99 (g/g, %), and another for HA-H (high HA content) was 38.46 : 23.08 : 38.46 (g/g, %). Both homogeneously mixed solutions were dispensed at −80°C into a specific dish, which had the same curvature as contact lenses. The frozen mixtures were lyophilized in a freeze dryer (FDU-1200, Eyela Co., Japan). 1-Ethyl-3-(3-dimethylaminopropyl) carbodiimide (EDC, Sigma-Aldrich Co.) was then added to the mixture and thoroughly mixed at 4°C to form a solution with a mass ratio of EDC : mixture of 1 : 12, and the cross-linking reaction solution was stirred for 24 h. After the cross-linking was completed, the films were rinsed thrice with deionized water and lyophilized again. The freeze dryer was under harsh conditions for sterilization and HA-L dry weight of 5.22 ± 0.01 g and HA-H dry weight of 5.30 ± 0.01 g.

2.2. In Vitro Matrix Characterization: Fourier-Transform Infrared Spectroscopy (FTIR) Scanning. FTIR is a type of light signal applied to acquire the infrared spectrum of absorption or emission of gas, liquid, or solid materials. FTIR spectrometer 2000 system (PerkinElmer, OH, USA) was used for the simultaneous collections of high-spectral-resolution data over wide spectral ranges. A matrix sample was made into a slight powder, mixed with KBr powder (1 : 8), dried in a 70°C oven for 24 h, and compressed into pellets for FTIR examination over a wavenumber range

between 400 and 4,000 cm^{-1} with a scanning speed of 2.5 cm/s and a resolution of 2 cm^{-1}.

2.3. In Vitro Matrix Characterization: Swelling Ratio. The swelling ratios of matrices were determined by a conventional gravimetric procedure [21] and were performed on samples immersed in phosphate-buffered saline (PBS) at pH 7.4 using a thermostatic water bath at 25°C. Samples were made of similar sizes for the examinations (approximately 10.0 mm in diameter in circle shape and 2.0–3.0 mm in thickness). The weights of the swollen matrix samples (W_0) were determined immediately after removing excess water with tissue paper. The equilibrium weight of the swollen gel samples (W_1) was obtained until no measurable weight increase was observed. The swelling ratio was calculated as follows:

$$\text{Swelling ratio} = \frac{W_1 - W_0}{W_0}\ (\text{fold}). \quad (1)$$

2.4. In Vitro Matrix Characterization: Enzymatic Degradations. Three enzymes, hyaluronidase, lysozyme, and collagenase I (Sigma-Aldrich Co.), were used for the degradation of two types of matrices. Hyaluronidase and lysozyme are important enzymatic proteins of the ECM metabolism which catalyzes the degradation of the dermal ECM surrounding glycosaminoglycans [22]. They hydrolyze glycol bonds of HA 1,4-β-linkages between *N*-acetyl-*D*-glucosamine residues and *N*-acetylmuramic acid. Collagenase I specifically targets the relatively loose region (Gly775-Leu/Ile776) of the Col triple helix domain. Waterless matrices (30.0 ± 0.03 mg) were absorbed in 1 mL PBS buffer (pH 7.4) with hyaluronidase (30 and 50 U/mL) for 4-, 8-, and 12-day incubations, to examine two matrix degradation rates. A similar protocol was used for lysozyme (10,000 and 30,000 U/mL) degradations for 2, 4, and 6 days. In collagenase I biodegradation tests, 10.0 and 20.0 U/mL collagenase I were suspended in 1.0 mL 0.1 M Tris–HCl with 0.05 M $CaCl_2$ (pH 7.4), and matrices were immersed for 4, 8, and 12 h. All reactions were incubated at 37°C, and 0.2 mL of 0.25 M ethylenediaminetetraacetic acid (EDTA, Sigma-Aldrich Co.) was added to terminate the reactions at the specified time points. At the end of the evaluation periods, the remaining matrices were washed three times in distilled water and finally lyophilized for the final weight amounts. The degradation ratio was calculated as the percentage via dividing the difference between the residual weight (W_n) and original weight (W_0) by the original weight (W_0):

$$\text{Degration ratio}(\%) = \frac{W_n - W_0}{W_0} \times 100\%. \quad (2)$$

2.5. Collections of Adipose Tissues from Sprague–Dawley (SD) Rats. Adipose tissues were harvested from six male SD rats (BioLASCO Taiwan Co., Ltd), which weighed approximately 300–400 g. The rats were first anesthetized by intraperitoneally injecting Zoletil 50. Their inguinal areas were then cut out to collect approximately 10 g of adipose tissue. The Institutional Animal Care and Use Committee at National Chung Hsing University approved the described procedures (NCHU-IACUC No. 106–123). Since the collected adipose tissues still contained erythrocytes, Dulbecco PBS (D-PBS) buffer was used to rinse the adipose tissues and remove most of the erythrocytes. The tissues were scraped into a tube, washed with D-PBS buffer, and centrifuged at 750 × g for 5 min, similar to the protocol described by Bergonzi et al. [23]. The upper layer was then transferred into a new test tube using a sterile pipette and was washed at least twice. A second centrifugation was performed (750 × g for 5 min), and the tissues were transferred into tubes containing Dulbecco's modified Eagle medium (DMEM, Thermo Fisher Scientific Co., Waltham, MA, USA) with 1 mg/mL collagenase, 0.2 mM ascorbic acid 2-phosphate, and 2 mM n-acetylcysteine (NAC). The tubes were submerged for 3 h at 37°C and centrifuged at 750 × g for 5 min to separate the collagenase solution. The precipitate was washed following the centrifugation and cultured for 24 h into DMEM with 10% fetal bovine serum (FBS), 2.0 mM NAC, and 0.2 mM ascorbic acid 2-phosphate in a 5% CO_2 incubator. Any unattached cells were removed using PBS. 25 cm^2 flasks were prepared, each containing 5.0 mL keratinocyte serum-free medium (SFM) with 10% FBS, 100 U/mL penicillin, and 100.0 mg/mL streptomycin. The medium was replaced every other day. Cells were prepared for subculture, and any excess was stored in a liquid nitrogen tank.

2.6. Fluorescence Microscopy Image of Ex Vivo ASC Matrix. After a centrifugation, cell pellets (2×10^5 cells/mL) were mixed with 5 mL PKH26 (Sigma-Aldrich Co.), a red fluorescent dye that was stained for cell membrane labeling. The mixtures were then sunk for 5 min at 25°C according to the experimental protocol and were vortexed for 30 sec. Excess PKH26 was washed with a complete medium. A monolayer of PKH26-labeled ASCs was reseeded into two types of matrices at a density of 1×10^5 cells/mL. PKH26-labeled cells from both matrices were harvested in a Cell Proliferation Kit II [2,3-bis(2-methoxy-4-nitro-5-sulfophenyl)-2H-tetrazolium-5-carboxanilide, XTT; Life Technologies, CA, USA] assay for the cell proliferation measurement and viewed using a fluorescence microscopy (Eclipse Ti-U; Nikon, Japan) for the cell morphology [3].

2.7. Measurement of Intracellular ROS Level in ADSC. ROS-sensitive fluorescent dye, 2′,7′-dichlorofluorescin diacetate (DCFDA) was applied to determine if the HA-rich sponge matrix downregulated the intracellular oxidative stress level in cells [24, 25]. In order to observe the sample antioxidative properties, cells were precultured within two types of biomaterials for 24 hrs. Afterward, it was rinsed with warm PBS solution and incubated within 20 μM DCFDA-contained PBS at 37°C and 5% CO_2 for 30 min, to replace a fresh cell medium and to wash cells at least 3 times with PBS. Using trypsin/EDTA, we cut away the focal adhesion cell anchored to the culture dish. The cellular fluorescent intensity was analyzed with Guava® easyCyte Flow Cytometers (Merck KGaA, Darmstadt, Germany) at 485 nm excitation and 530 nm emission for 2,7-dichlorofluorescein (DCF) detection.

2.8. Scanning Electron Microscopy (SEM) Image of Ex Vivo ASC Matrix. SEM is a technique of electron microscope applied to acquire images of a sample via scanning the surface through a focused electron beam. The electrons interact within sample atoms to produce multiple signals which contain the information about the sample compositions and the surface topography. The morphological characteristics of the ASC (5×10^3 cells/mL) HA-H porous matrix implants were observed using a SEM (JSM-5300; JEOL Co., MA, USA) [3]. Cells were cultured in keratinocyte-SFM with 10% FBS, 100 U/mL penicillin, and 100 mg/mL streptomycin in a 5% CO^2 incubator. Matrices were fixed in 2.5% glutaraldehyde in 0.1 M sodium phosphate buffer (pH 7.2) overnight, postfixed in 1% osmium tetroxide for 1 h, dehydrated in ethanol, and dried at the critical point. Dried samples were coated with gold using a sputter coater (JEE-4X/5B; JEOL) at an ambient temperature. We took images with a cell-free matrix and ASC HA-H porous matrix implant cultured for 14 and 42 days in suitable view scales.

2.9. Examination of Ex Vivo Cell Proliferation Ratio. The principle of XTT is similar to MTT, and the final product of XTT is water-soluble. In our previous research [3], we found that XTT examination on the proliferation rate in the scaffold was more accurate than the MTT assay. An aliquot of the cell suspension (5×10^3 cells/mL) was injected into each matrix. Cells were cultured as in previous procedures. On days 1, 3, 5, and 7, the XTT assay was applied to detect cell proliferation. This platform detects one of the mitochondrial functions, i.e., the reduction of XTT into a formazan product. Each well received 400 μL XTT medium, and the plate was dipped for 2 h. A microplate reader (Stat Fax, Palm City, FL, USA) was applied to measure cellular XTT optical density at 450 nm. The percentage of cell proliferation was calculated by subtracting the absorbance of the blank from the total absorbance (A) on each time interval. The result was then divided by the difference between the absorbance on day 1 (A_1) and that of the blank as shown:

$$\text{Percentage of cell proliferation} = \frac{A - A_{\text{blank}}}{A_1 - A_{\text{blank}}} \times 100\%. \quad (3)$$

2.10. Implanting ASC HA-H Matrix in Animals. According to the ex vivo cell proliferation ratio protocol, 4×10^5 cells/mL were seeded in a $2 \times 3\,\text{cm}^2$ matrix. Before seeding, ASCs were stained with PKH26 for histology and immunofluorescence detection [14]. The HA-H matrix only and ASC HA-H matrix were implanted in the back of adult male SD rats weighing 320 ± 20 g. SD rats were housed in an animal facility at 22°C and a relative humidity of 55% with a 12 h light–dark cycle. Food and sterile tap water were available ad libitum. All procedures were approved by NCHU-IACUC No. 106-123. The dorsum subcutis of SD rats was implanted with two types of ASC-cultured matrices under anesthesia with 2.0%–2.5% isoflurane (Halocarbon Products Co., GA, USA) in O_2.

2.11. Histological Detection of ASC HA-H Matrix Implant by Hematoxylin and Eosin (H&E) and Immunohistochemistry Staining. 4′,6-Diamidino-2-phenylindole (DAPI, AAT Bioquest Co., CA, USA) is a fluorescent stain which binds powerfully to double-strand DNA in adenine–thymine-rich regions. DAPI is a well-known nuclear counter mark to apply in multicolor fluorescent techniques and following the protocols of Sigma-Aldrich Co. to stain skin tissue cells. ASCs were stained with PKH26 and then seeded in a matrix. SD rats were sacrificed in seven days after the implant surgery by an overdose of CO_2. The ASC implant dorsum and normal skins were separated for histological examination using H&E staining and for fluorescent observations [26]. The section used for H&E staining was formalin-fixed and embedded in paraffin; 10 μm thick sections were cut and mounted on glass slides. The sections were deparaffinized in xylene and stained with H&E. For fluorescence observations, an optimal cutting temperature compound (OCT; Finetek Co., CA, USA) was used to bind the tissue at −80°C. The frozen sections were cut into 10 μm thick slices by a Shandon cryotome (FSE, Thermo Fisher Scientific Co.), rinsed three times with PBS buffer for 5 min, and mounted with FluoroQuest™ Mounting Medium containing DAPI. The same procedures were used for microscopy, as described in the previous paragraph for fluorescence microscopy of *in vivo* tissue matrix.

2.12. Quantitative Real-Time Polymerase Chain Reaction (qRT-PCR). The qRT-PCR method is a technique used for evaluating gene expression levels by measuring the cDNA products after each cycle of PCR amplifications. For qRT-PCR, a reactive mixture containing SYBR Green Master Mix (Qiagen, Valencia, CA, USA) templates and primers was used. All qRT-PCR reactions were accomplished by a StepOnePlus™ System (Thermo Fisher Scientific Co.). The reactions were carried out according to the following program: cDNA templates were initiated at 95°C, annealed at 60°C, and elongated at 72°C, and all steps were repeated with 40 cycles of amplifications. At the end of the annealing stage of the experiments, we began to determine the fluorescence acquisition [27]. The targeted gene primers are shown in Table S1.

2.13. Western Blot Analysis. Western blot is a famous method to separate proteins and to identify them, and the sample sources are from the cell cultures or sacrificed tissues. Specific binding antibodies for corresponding proteins were fitted to analyze the performances of the proteins in our rat tissues. Western blot analysis is the primary method for transferring proteins, which is termed electroblotting. Lysates were centrifuged at $20{,}000 \times g$ for 30 min, and the protein concentrations within the supernatant solution were determined with a bicinchoninic acid (BCA) protein assay kit (Pierce Co., Rockford, IL, USA). Equal amounts of protein were separated by sodium dodecyl sulfate-polyacrylamide gel electrophoresis (SDS-PAGE) and then electrotransferred to a nitrocellulose polyvinylidene difluoride (PVDF) membrane (PALL Life Science, Ann Arbor, MI, USA) using an electrical current. Then, the membrane

was washed with 1x TBST (Tris-buffered saline, 0.1% Tween 20) to remove traces of skim milk and placed in the TBST box. The membrane was immersed with respective primary antibodies and incubated with the horseradish peroxidase-conjugated second antibodies for 1 h and then treated with enhanced chemiluminescence (ECL) detection reagents (PerkinElmer, ECL1 : ECL2 = 1 : 1, Spokane, WA, USA). The protein signals after ECL treatments were visualized by a Mini Size Chemiluminescent Imaging System from Life Sciences (Thermo Fisher Scientific Co.) and were measured to detect the bands [14].

2.14. In Vivo Secretions of Angiogenic Growth Factors by ASC HA-H Matrix Implant. Sacrificed tissues were collected to detect secretions of proangiogenic cytokines on days 1, 3, 5, and 7 [14]. According to the manufacturer's instructions, we made an enzyme-linked immunosorbent assay (ELISA) to determine the amounts of vascular endothelial growth factor (VEGF) and transforming growth factor-β (TGF-β) secreted by two ASC-implanted tissues following ELISA development kits (BlueGene Biotech Co., Shanghai, China). Briefly, 10 mg skin tissue was collected from rats, cut into pieces, and suspended in lysis buffer overnight to extract protein. 100 μL samples were added into ELISA plates which coated the VEGF and TGF-β antibody and were incubated at room temperature for 2 h. After incubation, 100 μL of Streptavidin-HRP Conjugate was added for 30 min and detection by spectrophotometer at 620 nm.

2.15. Statistical Analysis. Differences between the vehicle control group and ASC-treated matrix groups *in vitro*, ex vivo, and *in vivo* assays were analyzed by Student t-test. One-way ANOVA was applied for statistical comparisons between the vehicle control group and experimental groups. A significant difference ($*$) was defined as $p < 0.05$, and a highly significant difference ($**$) was defined as $p < 0.01$.

3. Results and Discussion

3.1. Chemical Cross-Linking Reaction for Extracellular Matrix-Like Porous Matrices. HA, an anionic and nonsulfated high molecule glycosaminoglycan, is found in connective, epithelial, and neural tissues. It is one of the key components of wound repair, significantly contributing to the stimulation of initiation, release, and regulation of angiogenic growth factors [28]. HA not only plays a diversity of roles in pathologic and physiologic issues but also is employed extensively in clinical and skin cosmetic applications as a biomedical agent and drug delivery system supplement. The main restriction of HA is because of rapid degradation, short half-life property, and its accordingly low bioavailability in vivo. In our aim to conquer the above weaknesses, HA is typically subjected to chemical modifications [29]. Col is the major component of ECM and comprises approximately 70%–80% of dry skin weight [30]. As one of the elements, Col has many advantages, including biocompatibility, low toxicity, and nonimmunogenic properties. Gel is a partial hydrolysis product of Col and can be manufactured easily in an inexpensive approach. Gel is a common supplement to support biomaterial product physical and structural stability and is usually used in the chemical, food, and pharmaceutical industries. The construction of 3D matrices via cross-linking has become one of the main strategies for creating porous matrices [31]. We expected to cross-link these three components modifying the matrix degradation rates, water absorption, and biomechanical characteristics, thus further improving their biocompatible implant applications. In this study, EDC was used as a chemical cross-linking agent, which is a zero-length cross-linking agent (i.e., the agent itself is not incorporated into the macromolecule) [32], to directly connect to two different reactive groups demonstrating the chemical scheme in Figure 1(a). The activated intermediate agent reacted with the carboxyl groups of HA and with various amine side chains of Col and Gel and linked HA to Col and Gel forming a porous matrix. Using lyophilization, we could obtain a sponge-like matrix using the above method, and the following steps tested the characteristics of the porous matrix cellular in vitro, ex vivo, and in vivo.

3.2. Porous Matrix Characterization: FTIR Scanning. FTIR spectroscopy glowed a beam light containing multiple frequencies at once and evaluated the beam absorption by the material. Next, the beam light was modified containing a different frequency combination to give a second result point. This process was repeated multiple times, and then, a computer calculated all the results and worked backward to infer the absorption of every wavelength [3]. Through our preliminary studies, we found the enhancements of HA contents in the biomaterial assisted the ASC proliferations. However, the high viscosity was a big manufacturing problem while the HA concentration was augmented in the reaction solution. We applied two HA concentrations for our further implant examinations. FTIR spectra of the matrices along with their individual polymer components are shown in Figure 1(b). In FTIR spectra of all components, peaks at 1,655 and 1,560 cm^{-1} correspond to amide I for the C=O stretching vibration and amide II for the N–H bending vibration. The peak area at 1,455 cm^{-1} corresponds to the C–N bending. In the pure HA spectrum, peak areas at 1,042 and 1,080 cm^{-1} correspond to C–O–C and C–O stretching, respectively. The absorption peaks at 1,400 cm^{-1} corresponded to the symmetrical stretching of vibration bands of the carboxyl groups. The absorption peaks of the amide group in the matrix polymers highly overlap with those newly cross-linked by the EDC amide groups in the HA-L and HA-H matrices. Therefore, no prominent new absorption peaks were observed in the HA-L and HA-H spectra.

3.3. Porous Matrix Characterization: Swelling Ratios. The swelling of polymeric 3D materials is a mechanic fluid diffusion-interrelated process to contain the liquids. The swelling ratio measurement is a low-molecular solvent content within an elastomeric matrix network and is characteristically accounted as the proportion of either the volume or the mass of the matrix in the swollen status compared to that of the dry status [3]. Three types, HA-L matrix, HA-H

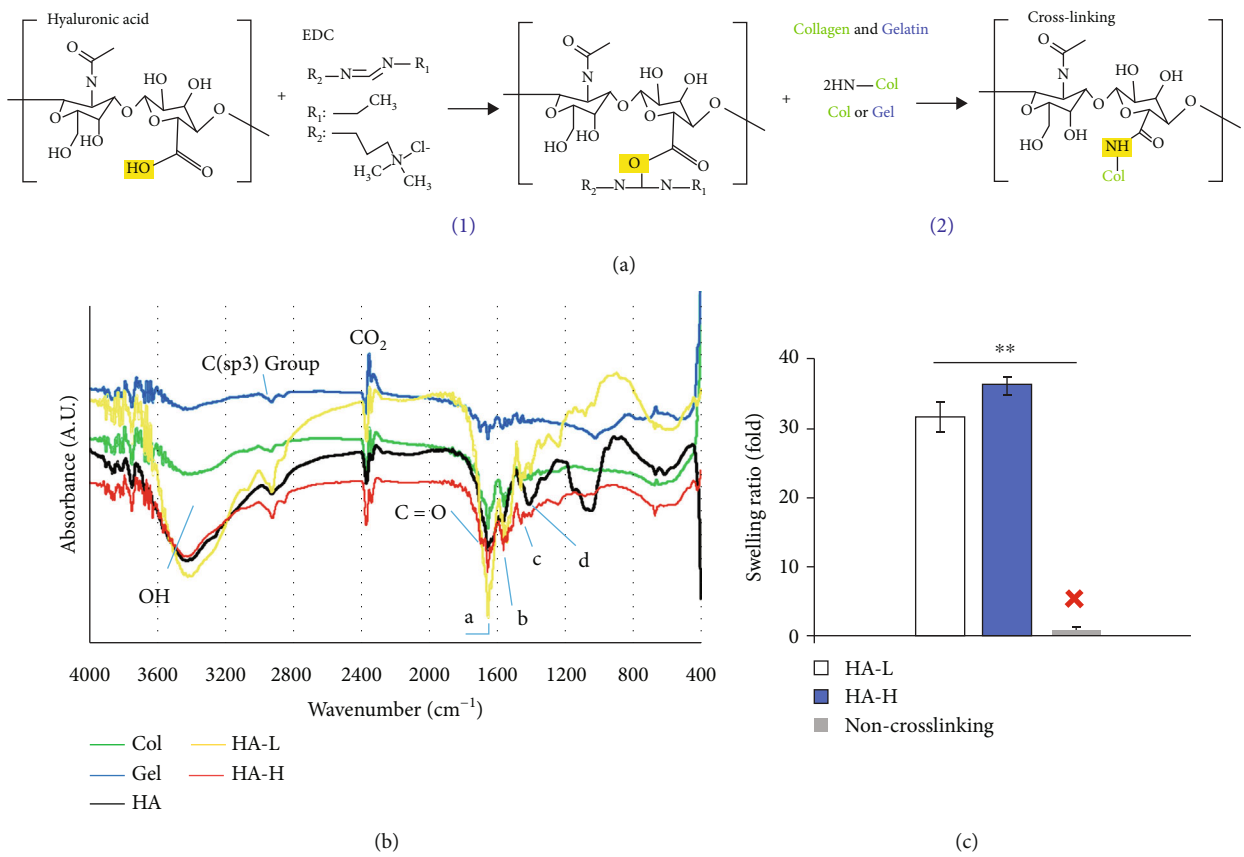

Figure 1: (a) The two-step chemical synthesis process for cross-linking matrices: (1) the cross-linking agent, EDC, linked HA with another organic molecule to form the activated intermediate acid anhydride. (2) The carboxyl groups of the activated intermediated product reacted with the amino group of Col or Gel to complete the cross-linking reaction. (b) FTIR spectra absorbance vs. wavenumber (cm^{-1}) data: HA (black), Col (green), Gel (blue), HA-L (yellow), and HA-H (red); absorbance (A.U.) and wavenumber (cm^{-1}). The molecules overlapped at ~1700 cm^{-1}, indicating an amide bond for the C=O stretching vibration. (c) The swelling ratio of testing samples: HA-L/HA-H/non-cross-linking. The white and blue bars represented HA-L and HA-H implant matrices, respectively. Without cross-linking, the scaffold was not formed in the water phase solution. Each value was represented as the mean values ± standard deviation (SD) ($n = 3$). The level of significance was designated as $^{*}p < 0.05$ and $^{**}p < 0.01$.

matrix, and non-cross-linked raw materials, were tested for their abilities to absorb water using the swelling ratio assay. A high swelling ratio indicates a scaffold can transport nutrients and oxygen into the wound body around the zone. The swelling ratios are shown in Figure 1(c). The non-cross-linked materials were dissolved in water immediately (within 2 min) and could not even maintain their hydrogel type in the PBS buffer; therefore, the swelling ratio was zero. On the other hand, the cross-linked HA-L and HA-H matrices could absorb approximately 31.2 ± 2.4- and 36.5 ± 1.8-fold PBS buffer than the dry matrix masses, respectively. According to our experience, HA has a good water absorption, and the absorption value is difficult to increase after reaching a certain maximum plateau value. Therefore, to increase the absorption ability from 31.2-folds to 36.5-folds is a significant improvement.

3.4. Porous Matrix Characterization: Enzymatic Degradations. Therapeutic wound implants are temporary healing template structure materials, and biocompatible matrices need to be degraded eventually in the body. The degradation rate of a potent matrix should not be too high to ensure the sufficient time period is available for cells to proliferate and spread around the wound area. Besides, a matrix should not be a morphologically robust solid because it is not necessary to keep it in the individual's body permanently. Biological degradations of HA-H and HA-L matrices were determined by measuring a loss in the weight following three enzymatic degradations. The rates were assayed using in vitro hyaluronidase, lysozyme, and collagenase I, and these enzymes react with certain chemical functional groups of our matrix components. Hyaluronidase and lysozyme enzymatic proteins hydrolyze the HA glycol bonds. After six days of incubation, the percentages of biodegradation of HA-H and HA-L matrices with 30 U/mL hyaluronidase were 22.1 ± 1.3% and 26.5 ± 1.0%, and the values with 50 U/mL were 26.3 ± 1.5% and 29.8 ± 2.3% for two matrices, respectively, in Figure 2(a). The percentages of biodegradations in both matrices with 10,000 U/mL lysozyme were 18.2 ± 0.3% and 35.7 ± 3.0% after 12 days of the incubation time interval, and those with 30,000 U/mL were 24.3 ± 0.7% and 40.8 ± 1.3%, respectively, in Figure 2(b). Collagenase I

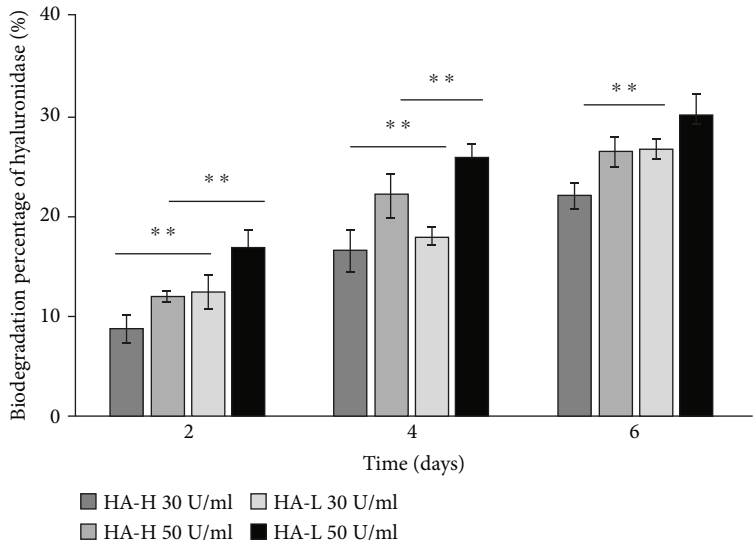

(a)

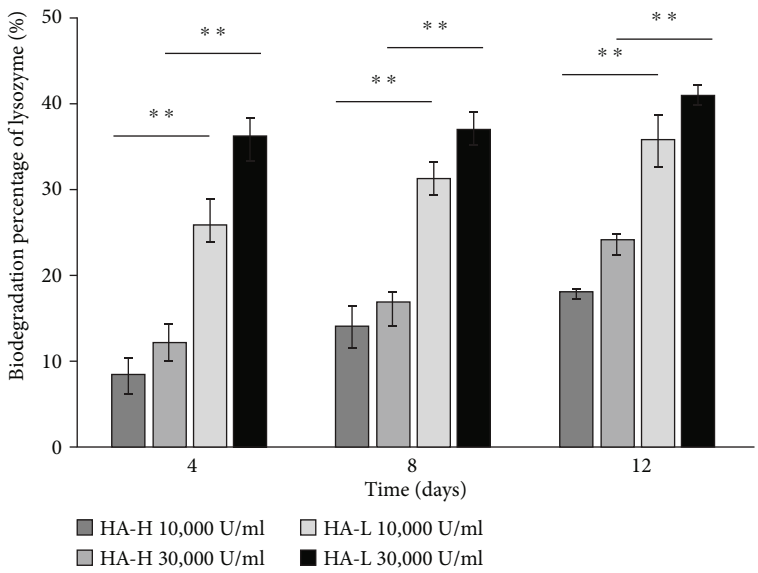

(b)

Figure 2: Continued.

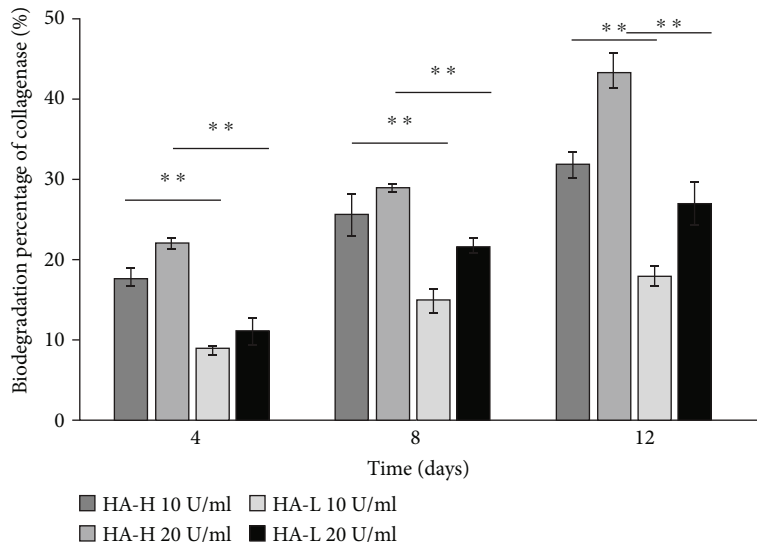

(c)

Figure 2: The matrix's HA glycoside was degraded by hyaluronidase and lysozyme, while the matrix's Col and Gel amino acid groups were degraded by collagenase. (a) Higher degradation percentages of hyaluronidase on HA-L matrix than on HA-H type. (b) Higher degradation percentages of lysozyme on HA-L matrix than on HA-H type. (c) Consistent increase of biodegradation percentages of collagenase in both type-tested matrices. Col and Gel molecular equivalent values were lower in HA-H matrix to make it easier to be hydrolyzed by collagenase I. Each value was represented as the mean values ± standard deviation (SD) ($n = 3$). The level of significance was designated as $^{*}p < 0.05$ and $^{**}p < 0.01$.

cleaves the n-[3-(2-furyl)acryloyl]-L-leucyl-glycyl-L-prolyl-L-alanine (amino acid: FALGPA) groups of Col and Gel into FAL and GPA. After 12 h of reactions with 10 U/mL collagenase I, the biodegradation percentages of HA-H and HA-L matrices were 31.4 ± 1.5% and 17.4 ± 1.0%, and for two matrices with 20 U/mL for a half day, the hydrolysis ratios for two matrices were42.9 ± 2.5%and26.7 ± 2.7%, respectively, in Figure 2(c). Our data revealed two matrices were degraded in dosage- and time-dependent manners. In addition, a specific enzyme is just for the specific raw material component group, and it will be discussed in the following sections.

ECM plays an important role in supporting the base structure of new dermis and also assists fibroblasts in providing a framework of the base structure. Furthermore, ECM absorbs the growth factors and related protease of cells to help during wound repair periods [31]. HA was speculated to improve the secretion of ECM, which causes new dermis to be denser. The previous statement leads to ECM transcription, causing further regulation of differentiation into fibroblasts genes [32]. In different wound phases (inflammation, proliferation, and maturation), HA can play a role in inflammatory response moderation, reepithelialization, and scar tissue remodeling [33, 34]. HA is thought to be indispensable to decrease scars and is considered to reduce fibrosis during wound healing [35], and it is a main component in injury repair and a proangiogenic element in tissue engineering materials [36]. It reduces inflammatory reactions, oxidative stresses, and pain levels of wounds and increases vasculogenesis and angiogenesis for the regeneration [37, 38]. We take this antioxidative advantage to increase HA equivalent concentration normality within the 3D porous matrix implant improving the reduction of inflammation. Col plays a key role in each phase of the wound healing process, including proliferation, migration, and differentiation and is one of the most promising biological materials for such applications [39, 40]. In tissue engineering for wound dressing, Gel has many advantages, including being inexpensive and nonimmunogenic. Col, HA, and Gel generally possess well-controlled biodegradabilities and biocompatibilities, and to give a three-component physical matrix structure, we used EDC for the cross-link reaction to assist the hurt skin in would healing. As we know, a suitable biomaterial should contain both soft and tough properties in a suitable range to prevent it from being too stiff and damaging the tissues [40]. We found HA showed less affections on the hard mechanical and biological properties compared to the influences of Col and Gel. The excessive amounts of Col and Gel cause high rigidity of the porous matrix, and this is not good for wound repair [3]. HA ratio is an effective target raw material of ECM composition to augment pliability, and we raised the amount of HA material to slow the degradation rate in further studies. In addition, it is unsatisfying to see that the matrix degraded before the wound has not yet been repaired, due to the rapid completion of the biomaterial. HA is a degradable molecule; after the cross-link reaction with Col and Gel polymers, the sponge matrix has a long sustaining time issue. The water absorption property of HA is very well, but a limitation value exists which leads to similar water absorption amount between two materials. Despite the similar water absorption abilities of two scaffolds, HA-H showed better performance in other biochemical examinations including cell proliferations and VEGF expressions. We tried to enhance the

concentration of HA up until the viscous limitation for the manufacturing operation. Skin cells secrete protease enzymes to degrade and digest matrices to generate sufficient space for cell proliferations and movement [8], and the matrices in this study were tested for their biological degradation. Hyaluronidase and lysozyme hydrolyze HA, whereas collagenase I degraded Col and Gel. In the enzymatic degradation reactions within examination time interval, a general pattern was shown: three specific enzymes degraded the glycol chemical bonds or FALGPA amino acid groups within two types of matrices, leading to similar results. We found out HA-L matrices had higher degradation rates with hyaluronidase and lysozyme than HA-H matrices because of the high HA contents with weak resistance to both enzymes [41]. Interestingly, collagenase I at high dosage showed the maximum matrix degradation percentage in the HA-H type, whereas collagenase I at slight concentrations presented the lowest value in the HA-L matrix. The HA-H matrix had a higher molecular equivalent in HA which is opposite to Col and Gel and with a lower resistance to collagenase I to digest Col and Gel. Hence, Col and Gel molecular equivalent values were lower in the HA-H matrix to make it easier be hydrolyzed by collagenase I. It was the reason why HA-L matrices were with lower biodegradations. Moreover, ECM contained certain cell growth factors to be as a regional warehouse; our HA-L matrix allowed the regional and speedy cellular growth factor-mediated active functions without resyntheses.

3.5. Ex Vivo ASCs Cultured in Matrices Evaluated by the Fluorescent Microscopy and Cell Proliferations. The cluster of differentiation (CD) marker is the biochemical description applied to the recognitions and research on the cellular surface supporting target biomolecules for the immunophenotyping [3]. In 2007, Schäffler and Büchler showed CD markers, differentiation capacities into various cell types, and clinical applications of ASCs [8]. In light of biochemistry and physiology, CD markers can work in many ways, frequently acting as peptide ligands or receptors essential to the physiological signals and functions. Currently, there are over 300 verified types of CD markers. Originally, CD90 was revealed as a thymocyte antigen of about 30 kDa with heavy N-glycosylated glycophosphatidylinositol conserved located on the cellular surface peptide, combining a single V-like immunoglobulin domain protein [42]. CD90 is utilized as one of the more popular indicators in a range of pluripotency stem cells, including ASCs. CD105 is a fragment of the TGF-β receptor complex, belonging to the cell surface type I membrane glycoprotein [43]. It is involved in angiogenesis and, consequently, is vital in stem cell proliferation and tumor metastasis in humans. CD146 is expressed in fetal and adult organ stem cells and is also recognized as the melanoma cell adhesion molecule anchored on the cellular surface in the body [44]. We identified the CD markers to verify where our rat ASCs belong, presented in the supplementary data in FigureS1.

In biochemical definitions, autologous stem cells are acquired from the human body, as someone may bank his or her own cells for medical elective therapies in the future, and among all category stem cell types, the autologous harvestry is in the lowest risky protocol for immune concerns [5]. Adult stem cells are often employed in surgical operations, such as in dermal repair and bone marrow transplantation. Scientists can manually grow, differentiate, and transform stem cells into particular cell types with hallmarks consistent with diverse tissues and organs, such as human skin and bones [45]. Embryonic stem cells and autologous cell lines obtained via somatic cell have also been proposed for positive therapies as future candidates [4]. An obvious interplay exists between the donor age and cell passage issues, which must be considered in developing cell-based therapies for future clinical applications. The data from diabetic rat wound healing research indicated stem cell injections, including bone marrow-derived mesenchymal stem cells (MSCs) and ASCs, resulting in faster wound repair [35]. ASCs prove an alternative origin of versatility stem cells to be differentiated into various tissue cells. ASCs have some advantages over other versatility stem cells, as seen in the following examples: adipose tissue is easy to be obtained, there is no immunological rejection of autologous transplanted cells, and it can be applied to a wide range of body tissues. A study on chronic diabetic foot ulcers included a 29-day treatment with an autologous graft comprising autologous skin fibroblasts combined with autologous stem cells on biodegradable Col membranes. The graft was directly applied to the wound and injected into the edges of the wound on days 1, 7, and 14. As a result, the injury size was decreased, and the vascularity of the dermis and dermal thickness of the wound were increased [46]. ASCs were chosen to be cocultured with our matrices because of their ability to regenerate and develop into specialized cells.

People frequently experience skin trauma suffering; thus, skin wound repair is highly significant in therapy medicine. To construct a tissue engineering healing unit which aids injuries is one of the approaches to help remedial processes, and matrices should be first tested for biocompatibility; i.e., they should not be harmful to normal cells and the body; otherwise, the patient's condition will be worsened. When a matrix is biocompatible, cells grow easily and fast, and the whole healing process is accelerated to recover. To observe the morphology of ASCs proliferating within the matrices, the cells were cultured in vitro in Petri dishes for 14 days. ASCs were stained with PKH26 and observed using a fluorescent microscope. The two rows, Figure 3(a), (A–C) and (D–F), show ASCs in HA-L and HA-H matrices photographed under white light and red fluorescence as well as the merged views (bar = 100 μm). The matrices provided a 3D porous structure in which the porosity width was around 100–200 μm for ASC migrations, and the microscope could only focus on one layer to observe ASCs in the matrices. All images showed ASCs with oval-shape morphologies. ASCs were seeded into two types of matrices, and the cell proliferation rates were examined using XTT assay on days 1, 3, 5, and 7, and the medium was changed every other day (Figure 3(b)). To compare with the experimental group on day 1, the cell viability showed enhancements between the control (onefold) and day 7 ASCs (>threefolds). Both types of matrix cell viabilities presented similar results in

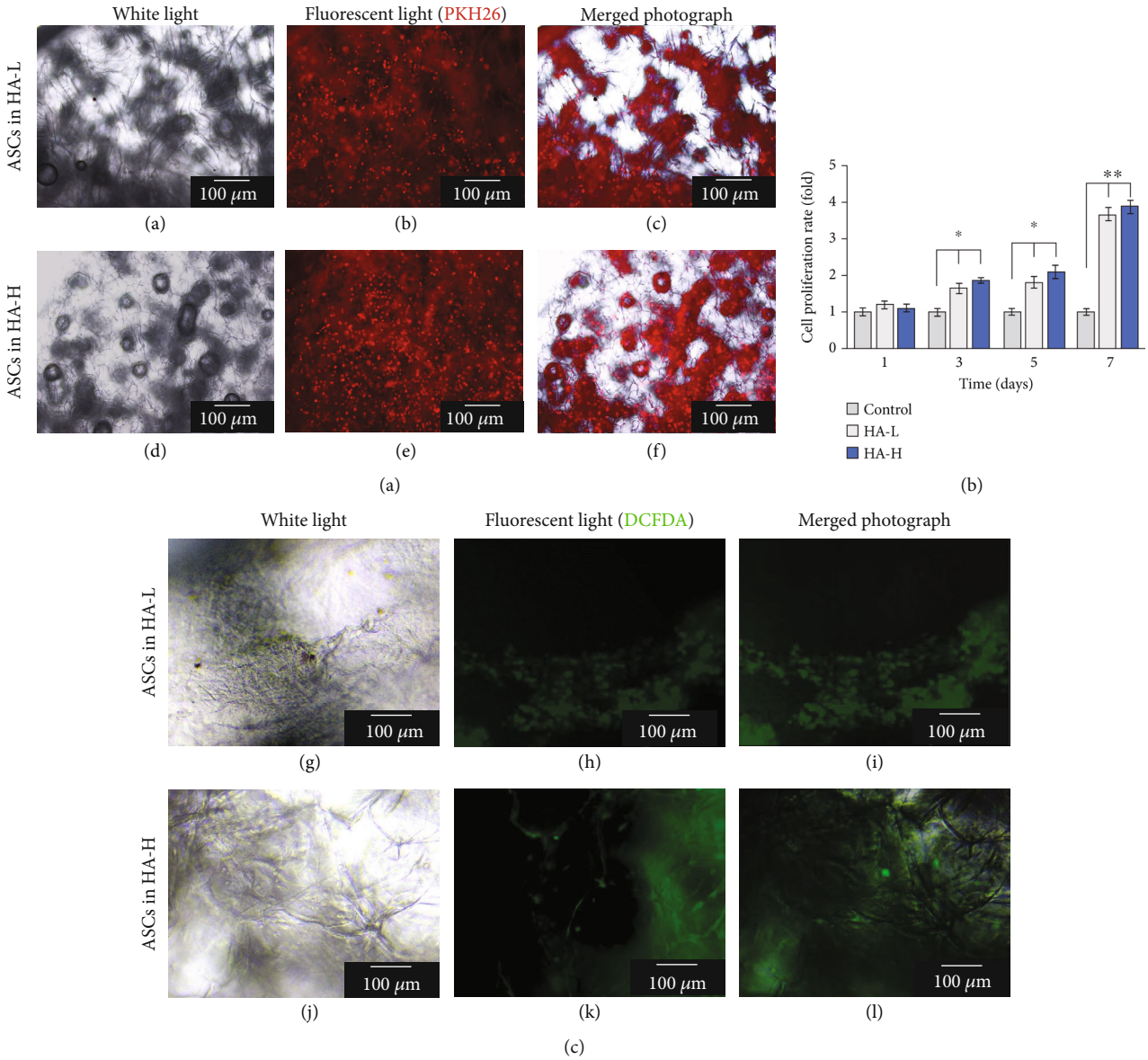

Figure 3: (a) View of cultured ASCs within two types of matrices under a fluorescence microscope. (A) and (D): The left column images were viewed under the white light. (B) and (E): The middle column images were viewed under the red fluorescence microscope. (C) and (F): The right column images were merged photographs of the first and second column ones (bar = 100 μm). (b) Steady enhancements of the cell proliferation rates for the vehicle control and HA-L and HA-H matrices. ASCs showed higher values cultured in HA-H matrix than in the HA-L one within a 7-day period culture. (c) The DCFDA assay results presented that HA-H matrix decreased ROS production in oxidative stress property assay. The photo representing order sequence (G)–(L) was similar as part demonstration (A)–(F). Each value was represented as the mean values ± SD ($n = 3$). The level of significance is designated as $^{*}p < 0.05$ and $^{**}p < 0.01$.

time-dependent manners, and HA-H groups showed slight augmentations compared to HA-L groups during the experimental periods. Antioxidative capacity is an important issue for wound healing because of the core function on reducing the radical-induced degradation and scavenging free radicals of repair cells and tissues. We already published several papers to demonstrate that oxidative lessening is beneficial to human health, especially in rejuvenation applications [47–49]. For measuring the antioxidative properties on the testing samples of interest, the cellular experimental platform was carried out in practice. DCFDA staining is a typical quantitative method for the intracellular H_2O_2 amounts to survey redundancy oxidation stresses. The damaged wound is a trigger for endogenous superoxide production and inflammatory activated cells formed ROS which release the fluorescent wavelength intensity to be identified [50–52]. To determine whether the HA-H matrix suppresses oxidative reactions, we investigate ROS generations in a cell-based measurement. The injured wound is an inducer for endogenous superoxide secretions, and inflammation-activated cells produced ROS which emitted the fluorescent intensity to be detected. In Figure 3(c), it was demonstrated

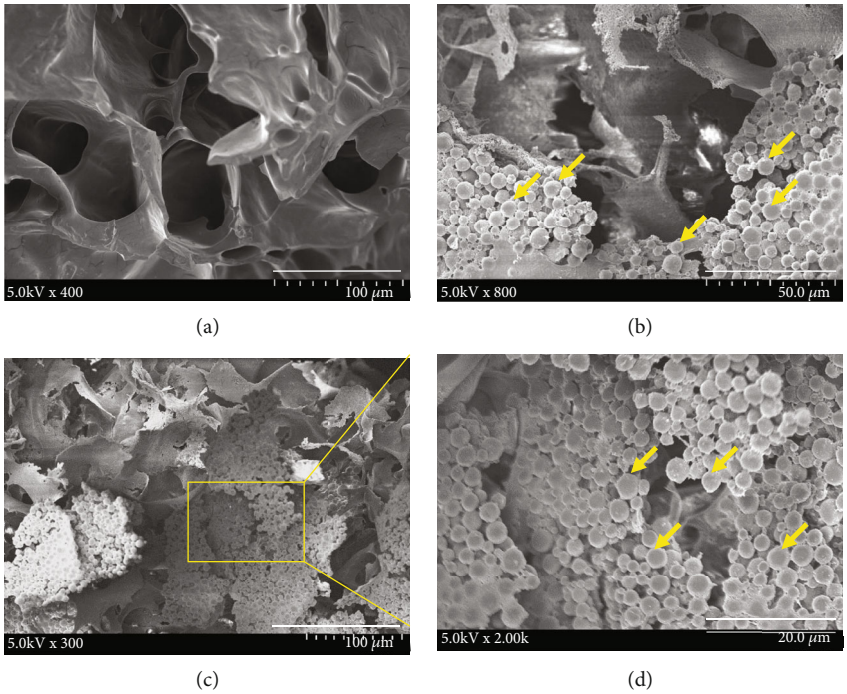

Figure 4: (a) SEM surface view of HA-H matrix only (without ASC culture) (bar = 100 μm). (b) SEM surface view of HA-H matrix with ASC culture for 14 days (bar = 50 μm). (c) SEM analysis of a 42-day ASC distribution on HA-H matrix (bar = 100 μm) and (d) an enlarged lateral view (bar = 20 μm).

that the HA-H matrix gradually reduced oxidative stresses, and we discovered that this biomaterial inhibited the production of cellular ROS successfully.

3.6. Ex Vivo ASCs Cultured in Matrices Evaluated by SEM. For SEM measurements, a specimen is usually necessary to be entirely dry, since the specimen chamber is at a high vacuum condition, and the living cells, tissues, and organisms are required chemical fixations to stabilize and preserve the physiological structures. We aimed to construct a biocompatible matrix with a porous feature to help with nutrient and oxygen transportation from the entire body to the damaged area. ASC morphologies within HA-H matrix samples were also estimated using SEM. In Figure 4(a), a lateral view of HA-H matrix without ASC cultivation was shown, exhibiting interconnected open-pore morphology (bar = 100 μm). We continually illustrated a lateral view of ASCs cultured in the HA-H matrix which is a longer period. In Figure 4(b), the matrix which was split after ASC fostering for 14 days was presented, demonstrating a good proliferative consequence (bar = 50 μm). ASCs were widely dispersed in the HA-H matrix after 42 days of culture (Figures 4(c) and 4(d)). An enlarged view of the yellow-framed area was illustrated (bar = 20 μm), and ASCs completely invaded the HA-H matrix.

During a 7-day period, cell proliferation rates in HA-L and HA-H matrices increased 3.5- and 4.2-folds compared with the original cell growths on day 1. The fluorescent examination images of the 14-day phenomena could identify ASC migrations and proliferations into two types of matrices. Next, ASCs proliferated for a longer time interval of 42 days to cover the surface of the HA-H matrix, and we discovered that ASCs migrated completely to the superficial around the matrix in the SEM images. Many types of cells bind to ECM components via focal adhesions connecting with actin filaments of the cell and via hemidesmosomes connecting with intermediate keratin filaments. Cellular adhesion is a mechanism for cell to attach and to interact with nearby cells by cell-adhesion molecules on the surface and cellular transmembrane proteins. In SEM, the fixed ASC tissue matrix was dehydrated to be detected. The air-drying protocol made our sample shrink and collapse, and we replaced the aqueous medium within the cells by the organic solvent of acetone achieving the real physiological structure discoveries.

3.7. In Vivo Histological Examination of Implanted ASC HA-H Matrix. The histological study of a tissue specimen is sectioned, stained, and examined by a light microscopy to observe the formations, structures, and functions. Our histological examinations of the rat skin and ASC matrix implant were performed by tissue sections. The goal was to evaluate skin histology with the implant of ASC HA-H matrix biocompatibilities and repair consequences. In Figures 5(a) and 5(b), both demonstrated the normal skin structure and a tissue section with the matrix implant only, respectively, and H&E staining revealed the matrix's and skin's histological characteristics (bar = 100 μm). In Figures 5(c)–5(e), ASCs were stained with PKH26, and ASC HA-H matrices were sewn within the rat skin dermis for 7 days. It was shown that the skin accepted the ASC HA-H implant, and ASCs not only existed within the implant matrix but also

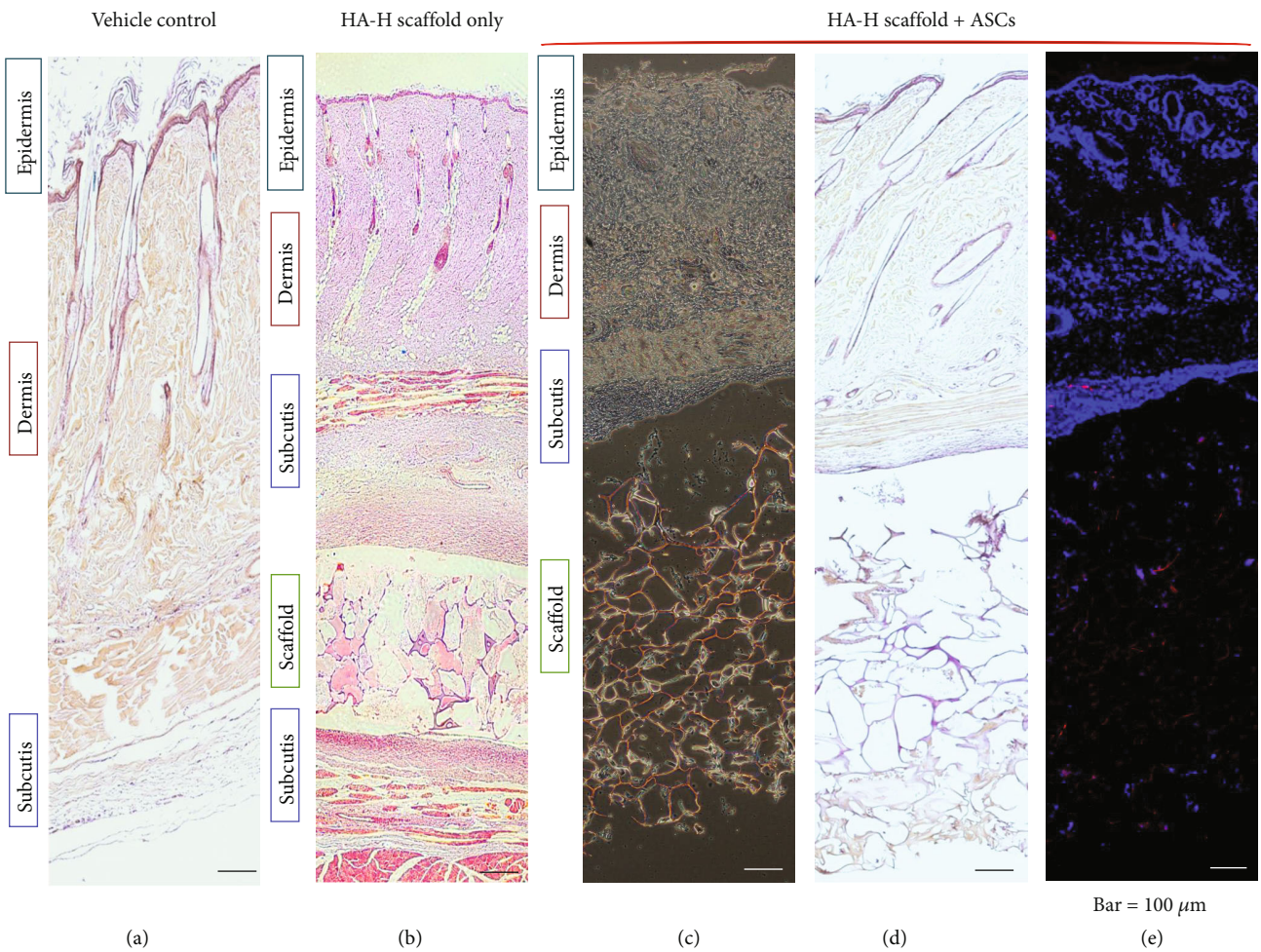

Figure 5: Histology images of wound beds. (a) Normal rat skin with paraffin section; (b) HA-H matrix was implanted into the rat skin. (c–e) ASC HA-H porous matrix was implanted within the rat skin. (c) Viewed with white light, (d) histochemical staining with the paraffin section, and (e) histochemical staining with the frozen section in fluorescent light. ASCs were dyed in PKH26 with a red color, and the blue color was a matrix surrounding tissue cells with DAPI staining.

migrated from the matrix into the subcutis-emitted red fluorescent light in Figure 5(e). Our ASC HA-H matrix implant provided ECM dynamic behaviors to regulate the cell functions, including segregating tissues from one another, supporting cells, and regulating intercellular communications. To compare the normal skin biopsy with the implanted skin, there is no significant or obvious dissimilarity between these histological sections. This suggested that the ASC matrix implant did not induce skin immune responses in vivo. We found that the matrix could be integrated with dermal multiple layers, and ASCs infiltrated into surrounding tissues. There was no significant difference between the normal skin and the ASC HA-H implant on histological examinations.

3.8. The Gene and Protein Expression Levels of Both ASC Biomaterial Implants. mRNA expression levels of two rat skin-implanted ASC matrices and the vehicle control via qRT-PCR are shown in Figure 6(a). There are three popular downstream wound healing network signals of mitogen-activated protein kinases (MAPKs): p38 mitogen-activated protein kinase (p38), mitogen-activated protein kinase kinase (MEK), and extracellular signal-regulated kinase (ERK). p38, MEK-1/2, ERK-1/2, and NF-κB were at higher expression intensities of ASC implant tissues in the HA-H type than in the vehicle control group and HA-L one. These genes were positively related to wound repair, and MEK-1/2 and NF-κB presented strong dramatic increase values more than five-folds [53]. In Figure 6(b), we illustrated protein expression amounts of the rat skin-implanted ASC matrix and the vehicle control one in western blot. It was shown that p38, MEK-1/2, and NF-κB were at higher expression quantities in the HA-H group compared with the vehicle control and HA-L groups (Figure S2). We presented a consilience result in both mRNA and protein expressions on our ASC HA-H matrix implant in vivo.

ECM-related genes and proteins are generally applied in cellular culture systems to preserve precursor and stem cells in an undifferentiated status in vitro during the induction of differentiated smooth muscle, endothelial, epithelial, and other cell types [38]. In molecular biology, p38 is responsive and activates via stress factors including

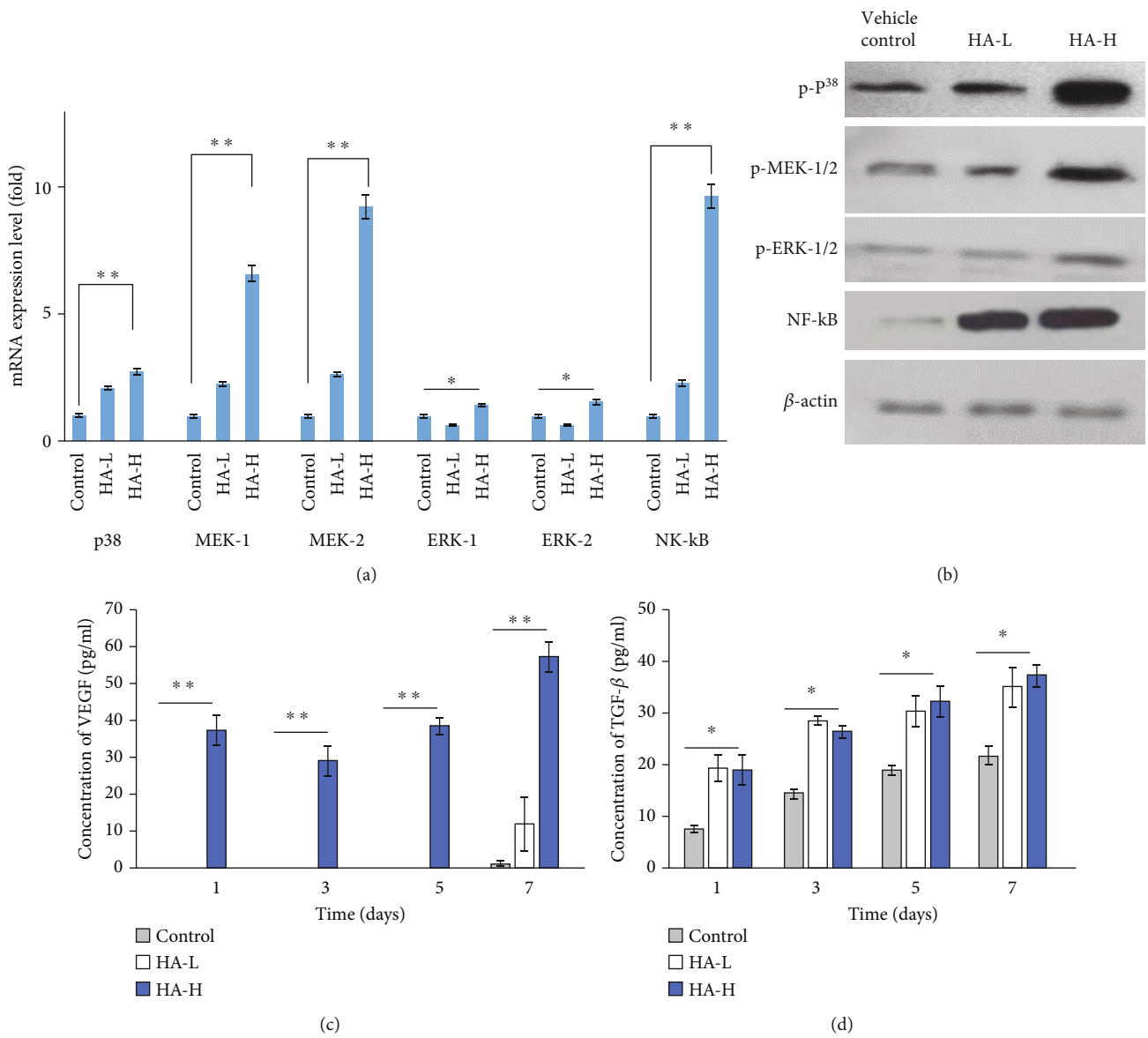

Figure 6: (a) The wound repair gene expression levels of ASCs from the vehicle control and both matrix implants in vivo. (b) The related protein expression amounts in the dish (vehicle control) and two types of implants. (c) VEGF-secreted concentrations (pg/mL) and (d) TGF-β secretions (pg/mL) of the vehicle control and two implants tested over a 7-day period. Each value was represented as the mean values ± SD ($n = 3$). The level of significance was designated as $^{*}p < 0.05$ and $^{**}p < 0.01$.

ultraviolet irradiation, osmotic pressure, heat shock, and inflammatory cytokines, which are related to cellular growth, proliferation, angiogenesis, autophagy, and apoptosis. MEK is one of the MAPK signaling proteins and is also activated in melanoma [54]. If MEK is suppressed, the cellular differentiation is blocked, and the cell programmed death is induced. ERKs are broadly expressed protein kinase and intracellular signaling biomolecules related to cell activities, such as the regulation of mitosis and meiosis functions in differentiated cells. There are two similar protein kinases called ERK-1 and ERK-2, and the phosphorylation of ERKs leads to the activation of the kinase activities. The protein product of the protooncogene enhances p38 activity and therefore causes markedly high activity of the transcription factor NF-κB [46]. NF-κB is usually adjusted from intracellular pathways which integrate signals from the immune system and the neighboring tissues. Tyrosine receptor-linked kinases, p38, MEK, ERK, Ras, and Raf were involved in a pathway network connecting an extracellular signal to MAPK activation. ECM-involved proteins can be applied to sustain the 3D cell culture for dermal modeling developments in vitro. p38 MAP kinase was discovered to trigger mitosis mechanism in adult mammalian system, and our present work has been conducted to support the positive potential in human skin implant regenerations.

3.9. Secretions of Wound Healing Growth Factors on VEGF and TGF-β. For wound repair, the injury tissue requires

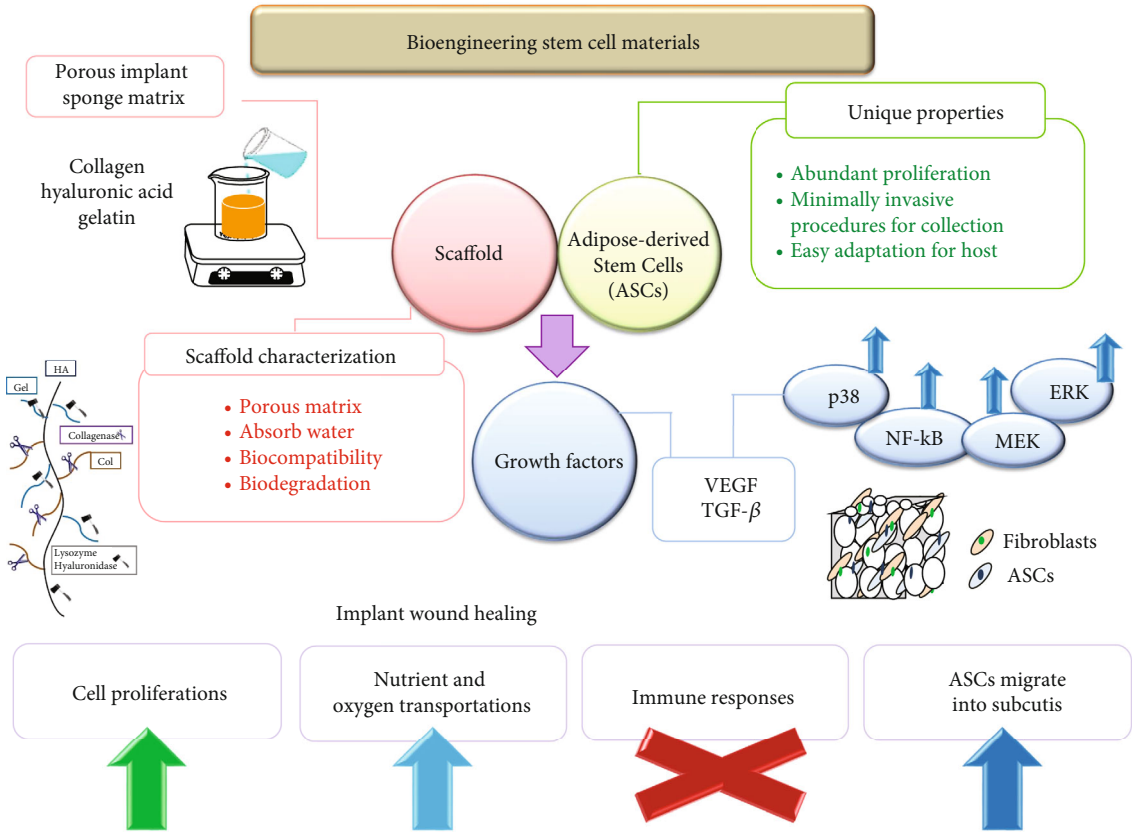

Figure 7: ASC HA-H porous biocompatible matrix cartoon chart for the wound repair.

many growth factors to stimulate hurt cell regeneration. VEGF and TGF-β are growth factors secreted by several cells, including platelets, macrophages, keratinocytes, fibroblasts, and ASCs [49]. Moreover, neutrophils, endothelial cells, and smooth muscle cells secrete VEGF. In this study, we tested secreted VEGF and TGF-β from ASC implants and injured zone tissues in Figures 6(c) and 6(d). VEGF concentrations in HA-L implants were too low to measure until seven days and compared to HA-H types were 12.23 ± 7.35 and 57.19 ± 4.10 pg/mL on day 7, and TGF-β amounts in HA-L and HA-H matrices were 36.81 ± 4.31 and 39.06 ± 2.03 pg/mL, respectively. A low ROS level helps cell proliferation as cell-cycle progression is activated and driven by growth factors. A review article by Gimble and Nuttall highlighted three categories of ASC secretions, including adipokines, cytokines, and secreted proteins [10]. Studies have pointed out that regulating HA affects the angiogenesis-related growth factors (e.g., VEGFA, VEGFB, hepatocyte growth factor (HGF), platelet-derived growth factor A (PDGFA), and PDGFC), causing enhanced tissue proliferation [49, 55]. VEGF is worth mentioning as a growth factor in dermal wound healing because it assists cell proliferation, migration, and angiogenesis. It is a major moderator in endothelial cell growth, proliferation, permeability, and migration of physiological and pathological angiogenesis. VEGF synergistically collaborates with other cytokines to enhance dermal damage tissue healing and to accelerate wound repair processes. ECM reconstructions are essential and secreted, synthesized, organized, and deposited via facilitations of VEGF around the wound surroundings. We discovered that VEGF secretion of cytokine response mediators in ASCs was greater in that HA-H matrix. We found that VEGF and TGF-β were upregulated in response to the ASC HA-H implant stimulus, and ECM was induced as well, possibly contributing to the upregulation the nutrient transcripts and above-mentioned protein interactions. Our implant generated an integrated response to ECM stiffness and TGF-β, a potent agonist of skin differentiation. The combination of ECM stiffness and exogenous TGF-β induced stem cell gene expressions more strongly than either worked via a p38 MAPK-dependent mechanism alone. This investigation has shown that autocrine VEGF and TGF-β pathway mechanisms were compensatory elements of ECM reconstructions in wound repair and were contingent upon the signaling in a feedback positive loop with p38, ERK, and NF-κB.

Angiogenesis is the physiological process through which new blood vessels from preexisting vessels are formed in the earlier stage of vasculogenesis. Angiogenesis continues the growth of the vasculature by processes of sprouting and splitting. VEGF and TGF-β are presented to be major contributors for the angiogenesis to increase the number of capillaries in a given network. The capillary endothelial cells proliferate to show signs of tube structures upon stimulations by VEGF, TGF-β, and FGF-β. VEGF upregulation is a main factor of the physiological responses to exercise, and its role in angiogenesis is suspected to be a possible treatment in vascular injuries and skin damage. VEGF is

an effective stimulator of angiogenesis, and in the presence of this growth factor, plated endothelial cells grow and migrate, eventually forming tube structures resembling capillaries. VEGF causes a massive signaling in endothelial cells and binds to VEGF receptor 2 to start a tyrosine kinase pathway which stimulates the production of factors to variously stimulate vessel permeability, proliferation/survival, migration, and finally differentiation into mature blood vessels. Mechanically, VEGF is upregulated with muscle contractions as a result of enlarged blood flow to affected areas. The amplified blood flow also causes a large increase in the mRNA productions of VEGF receptors 1 and 2.

The inflammation reaction is mainly involved in wound healing that is in early terms. If it is not properly adjusted, it will lead to abnormal wound healing. Based on our data, these HA fragments can stimulate ASCs to produce inflammation reaction cytokines, which transfer inflammatory signals to phagocytes and other dermis reaching the injury site. TGF-β is one of the most important cytokines involved in cellular growth, adhesion, migration, and ECM precipitation. TGF-β presents in the early terms of wound healing and adjusts ASC responses. A HA-rich surrounding contributed to the promotion of an inflammatory reaction during the wound healing course through activating proinflammatory phenotypes in ASCs [35]. HA modulates the proinflammatory cytokines to decrease oxidative stress and to enhance the skin wound repair [54]. The importance of inflammation mediators derived from the HA-H matrix-treated stem cells for activating the immune response was shown based on the activation of human blood leukocytes [36]. In injury repair procedures, TGF-β produced from similar cells compared to VEGF is essential in wound contraction, angiogenesis, cell penetration, connective tissue regeneration, inflammation, fibrotic scar formation, and reepithelialization [55]. TGF-β-treated ASCs induced higher expressions of type I Col along with cell cycle regulatory proteins and migration of fibroblasts. Considering the master cytokine leading to fibrosis, TGF-β supports defense of the normal tissue areas around wounded surroundings by forming granulations for the infections. It permits penetration of fibroblasts and the talk of fibroblasts to myofibroblasts, forming constrictive forces to help injury closures on ECM developments. To sum up, we prepared an ASC HA-H porous matrix for a promising implanted biomaterial in wound repair applications (Figure 7).

4. Conclusions

This study discovered that the HA-H matrix provided an optimal pore size and has a high water absorption level. The swelling ratios of both sponge matrices were analyzed by water absorption capabilities, and the results displayed that both have over 30-fold dry scaffold weight enhancements. In biodegradability experiments, two sponge implants could be degraded by three various human dermal enzymes. The ASC HA-H implant had an antioxidative ability to offer an increased cell proliferation rate and greater levels of VEGF and TGF-β amounts in related genes and proteins compared to other two groups and did not induce any immune responses *in vivo*. Overall, the study confirmed that the ASC HA-H implant can act as potent ECM for skin regeneration, and we recommend further investigations of the clinical properties be conducted on human skin wound healing.

Data Availability

The data used to support the findings of this study are available from the corresponding authors upon request.

Conflicts of Interest

The authors declare no competing financial and nonfinancial interests.

Authors' Contributions

Yu-Shen Cheng and Hung-Hsun Yen contributed equally to this work.

Acknowledgments

We thank Miss Tsz-Yee Lo (Department of Fragrance and Cosmetic Science, Kaohsiung Medical University) and Miss Marikris Racho (Department of Biology, San Diego State University) for their assistance. This work was supported by grants from the Ministry of Science and Technology (MOST 109-2221-E-005-012); we also thank the ENABLE Projects of NCHU (ENABLE:110ST001G). Wei-Chih Lien carried out his work under the auspices of the Ph.D. Program in Tissue Engineering and Regenerative Medicine, National Chung Hsing University and National Health Research Institutes.

Supplementary Materials

Table S1: wound repair-targeted sequences used in this study. Figure S1: *ex vivo* rat ASCs were cultured in HA-H matrix to evaluate by the fluorescent microscopy. The positive signals: CD90, CD105, and CD146; the negative signals: CD11b and CD31. Figure S2: western blot images. *(Supplementary Materials)*

References

[1] H.-M. Wang, Y.-T. Chou, Z.-L. Hong et al., "Bioconstituents from stems of Synsepalum dulcificum Daniell (Sapotaceae) inhibit human melanoma proliferation, reduce mushroom tyrosinase activity and have antioxidant properties," *Journal of the Taiwan Institute of Chemical Engineers*, vol. 42, no. 2, pp. 204–211, 2011.

[2] S. MacNeil, "Progress and opportunities for tissue-engineered skin," *Nature*, vol. 445, no. 7130, pp. 874–880, 2007.

[3] H. M. Wang, Y. T. Chou, Z. H. Wen, C. Z. Wang, C. H. Chen, and M. L. Ho, "Novel biodegradable porous scaffold applied to skin regeneration," *PLoS One*, vol. 8, no. 6, article e56330, 2013.

[4] K. Németh, A. Leelahavanichkul, P. S. Yuen et al., "Bone marrow stromal cells attenuate sepsis via prostaglandin E_2-dependent reprogramming of host macrophages to increase their

interleukin-10 production," *Nature Medicine*, vol. 15, no. 1, pp. 42–49, 2009.

[5] D. Siniscalco, C. Giordano, U. Galderisi et al., "Intra-brain microinjection of human mesenchymal stem cells decreases allodynia in neuropathic mice," *Cellular and Molecular Life Sciences*, vol. 67, no. 4, pp. 655–669, 2010.

[6] J. Buschmann, S. Gao, L. Härter et al., "Yield and proliferation rate of adipose-derived stromal cells as a function of age, body mass index and harvest site–increasing the yield by use of adherent and supernatant fractions?," *Cytotherapy*, vol. 15, no. 9, pp. 1098–1105, 2013.

[7] F. Uzbas, I. D. May, A. M. Parisi et al., "Molecular physiognomies and applications of adipose-derived stem cells," *Stem Cell Reviews and Reports*, vol. 11, no. 2, pp. 298–308, 2015.

[8] A. Schäffler and C. Büchler, "Concise review: adipose tissue-derived stromal cells—basic and clinical implications for novel cell-based therapies," *Stem Cells*, vol. 25, no. 4, pp. 818–827, 2007.

[9] J. M. Gimble, A. J. Katz, and B. A. Bunnell, "Adipose-derived stem cells for regenerative medicine," *Circulation Research*, vol. 100, no. 9, pp. 1249–1260, 2007.

[10] J. M. Gimble and M. E. Nuttall, "Adipose-derived stromal/stem cells (ASC) in regenerative medicine: pharmaceutical applications," *Current Pharmaceutical Design*, vol. 17, no. 4, pp. 332–339, 2011.

[11] Y. C. Wu, Y. C. Wang, W. T. Wang et al., "Fluorescent nanodiamonds enable long-term detection of human adipose-derived stem/stromal cells in an in vivo chondrogenesis model using decellularized extracellular matrices and fibrin glue polymer," *Polymers*, vol. 11, no. 9, p. 1391, 2019.

[12] C. K. Chang, H. D. Wang, and J. C. Lan, "Investigation and characterization of plasma-treated poly(3-hydroxybutyrate) and poly(3-hydroxybutyrate-co-3-hydroxyvalerate) biopolymers for an in vitro cellular study of mouse adipose-derived stem cells," *Polymers*, vol. 10, no. 4, p. 355, 2018.

[13] Y.-W. Chang, Y.-C. Wu, S.-H. Huang, H.-M. D. Wang, Y.-R. Kuo, and S.-S. Lee, "Autologous and not allogeneic adipose-derived stem cells improve acute burn wound healing," *PLoS One*, vol. 13, no. 5, article e0197744, 2018.

[14] S. H. Huang, S. H. Wu, S. S. Lee et al., "Fat grafting in burn scar alleviates neuropathic pain via anti-inflammation effect in scar and spinal cord," *PLoS One*, vol. 10, no. 9, article e0137563, 2015.

[15] Y. Kong, Z. Hou, L. Zhou et al., "Injectable self-healing hydrogels containing CuS nanoparticles with abilities of hemostasis, antibacterial activity, and promoting wound healing," *ACS Biomaterials Science & Engineering*, vol. 7, no. 1, pp. 335–349, 2021.

[16] R. Lakshmanan, U. M. Krishnan, and S. Sethuraman, "Polymeric scaffold aided stem cell therapeutics for cardiac muscle repair and regeneration," *Macromolecular Bioscience*, vol. 13, no. 9, pp. 1119–1134, 2013.

[17] J. Buschmann, L. Härter, S. Gao et al., "Tissue engineered bone grafts based on biomimetic nanocomposite PLGA/amorphous calcium phosphate scaffold and human adipose-derived stem cells," *Injury*, vol. 43, no. 10, pp. 1689–1697, 2012.

[18] E. Bellas, M. Seiberg, J. Garlick, and D. L. Kaplan, "In vitro 3D full-thickness skin-equivalent tissue model using silk and collagen biomaterials," *Macromolecular Bioscience*, vol. 12, no. 12, pp. 1627–1636, 2012.

[19] M. W. Tibbitt and K. S. Anseth, "Hydrogels as extracellular matrix mimics for 3D cell culture," *Biotechnology and Bioengineering*, vol. 103, no. 4, pp. 655–663, 2009.

[20] K. Yu, F. Lu, Q. Li et al., "In situ assembly of Ag nanoparticles (AgNPs) on porous silkworm cocoon- based wound film: enhanced antimicrobial and wound healing activity," *Scientific Reports*, vol. 7, no. 1, p. 2107, 2017.

[21] P. Valero, S. Giannakis, R. Mosteo, M. P. Ormad, and C. Pulgarin, "Comparative effect of growth media on the monitoring of E. coli inactivation and regrowth after solar and photo-Fenton treatment," *Chemical Engineering Journal*, vol. 313, pp. 109–120, 2017.

[22] Z.-C. Yao, C. Zhang, Z. Ahmad, J. Huang, J.-S. Li, and M.-W. Chang, "Designer fibers from 2D to 3D - Simultaneous and controlled engineering of morphology, shape and size," *Chemical Engineering Journal*, vol. 334, pp. 89–98, 2018.

[23] C. Bergonzi, A. Di Natale, F. Zimetti et al., "Study of 3D-printed chitosan scaffold features after different post-printing gelation processes," *Scientific Reports*, vol. 9, no. 1, p. 362, 2019.

[24] Y.-T. Chen, C.-J. Kao, H.-Y. Huang et al., "Astaxanthin reduces MMP expressions, suppresses cancer cell migrations, and triggers apoptotic caspases of in vitro and in vivo models in melanoma," *Journal of Functional Foods*, vol. 31, pp. 20–31, 2017.

[25] C. J. Kao, H. Y. Chou, Y. C. Lin, Q. Liu, and H. M. David Wang, "Functional analysis of macromolecular polysaccharides: whitening, moisturizing, anti-oxidant, and cell proliferation," *Antioxidants*, vol. 8, no. 11, p. 533, 2019.

[26] P. F. Wu, C. C. Chiu, C. Y. Chen, and H. M. D. Wang, "7-Hydroxydehydronuciferine induces human melanoma death via triggering autophagy and apoptosis," *Experimental Dermatology*, vol. 24, no. 12, pp. 930–935, 2015.

[27] P. H. Li, Y. P. Chiu, C. C. Shih et al., "Biofunctional activities of Equisetum ramosissimum extract: protective effects against oxidation, melanoma, and melanogenesis," *Oxidative Medicine and Cellular Longevity*, vol. 2016, Article ID 2853543, 9 pages, 2016.

[28] R. Stern, "Hyaluronan in cancer biology," *Seminars in Cancer Biology*, vol. 18, no. 4, p. 237, 2008.

[29] C. Saturnino, M. S. Sinicropi, O. I. Parisi et al., "Acetylated hyaluronic acid: enhanced bioavailability and biological studies," *BioMed Research International*, vol. 2014, Article ID 921549, 7 pages, 2014.

[30] L. Sun, W. Gao, X. Fu et al., "Enhanced wound healing in diabetic rats by nanofibrous scaffolds mimicking the basketweave pattern of collagen fibrils in native skin," *Biomaterials Science*, vol. 6, no. 2, pp. 340–349, 2018.

[31] C. Q. Li, B. Huang, G. Luo, C. Z. Zhang, Y. Zhuang, and Y. Zhou, "Construction of collagen II/hyaluronate/chondroitin-6-sulfate tri-copolymer scaffold for nucleus pulposus tissue engineering and preliminary analysis of its physico-chemical properties and biocompatibility," *Journal of Materials Science Materials in Medicine*, vol. 21, no. 2, pp. 741–751, 2010.

[32] R. Palao-Suay, M. R. Aguilar, F. J. Parra-Ruiz et al., "α-TOS-based RAFT block copolymers and their NPs for the treatment of cancer," *Polymer Chemistry*, vol. 7, no. 4, pp. 838–850, 2016.

[33] H. Y. Haung, Y. C. Wang, Y. C. Cheng et al., "A novel oral astaxanthin nanoemulsion from Haematococcus pluvialis induces apoptosis in lung metastatic melanoma," *Oxidative*

Medicine and Cellular Longevity, vol. 2020, Article ID 2647670, 13 pages, 2020.

[34] J. H. Yoon, K. Cho, T. J. Garrett, P. Finch, and M. Maden, "Comparative Proteomic Analysis in Scar-Free Skin Regeneration in Acomys cahirinus and Scarring Mus musculus," *Scientific Reports*, vol. 10, no. 1, p. 166, 2020.

[35] Y.-R. Kuo, C.-T. Wang, J.-T. Cheng, G.-S. Kao, Y.-C. Chiang, and C.-J. Wang, "Adipose-derived stem cells accelerate diabetic wound healing through the induction of autocrine and paracrine effects," *Cell Transplantation*, vol. 25, no. 1, pp. 71–81, 2016.

[36] E. L. Pardue, S. Ibrahim, and A. Ramamurthi, "Role of hyaluronan in angiogenesis and its utility to angiogenic tissue engineering," *Organogenesis*, vol. 4, no. 4, pp. 203–214, 2008.

[37] G. Gocmen, O. Gonul, N. S. Oktay, A. Yarat, and K. Goker, "The antioxidant and anti-inflammatory efficiency of hyaluronic acid after third molar extraction," *Journal of Cranio-Maxillo-Facial Surgery*, vol. 43, no. 7, pp. 1033–1037, 2015.

[38] L. C. Lin, C. Y. Chen, C. H. Kuo et al., "36H: a novel potent inhibitor for antimelanogenesis," *Oxidative Medicine and Cellular Longevity*, vol. 2018, Article ID 6354972, 12 pages, 2018.

[39] L. Mei, R. Fan, X. Li et al., "Nanofibers for improving the wound repair process: the combination of a grafted chitosan and an antioxidant agent," *Polymer Chemistry*, vol. 8, no. 10, pp. 1664–1671, 2017.

[40] J. Li, Y. Zhang, S. Yang et al., "The beneficial effects of edible kynurenic acid from marine horseshoe crab (Tachypleus tridentatus) on obesity, hyperlipidemia, and gut microbiota in high-fat diet-fed mice," *Oxidative Medicine and Cellular Longevity*, vol. 2021, Article ID 8874503, 13 pages, 2021.

[41] C. Mendes, D. P. dos Santos Haupenthal, R. P. Zaccaron et al., "Effects of the association between photobiomodulation and hyaluronic acid linked gold nanoparticles in wound healing," *ACS Biomaterials Science & Engineering*, vol. 6, no. 9, pp. 5132–5144, 2020.

[42] X. Cao, Y. Wang, C. Wu et al., "Cathelicidin-OA1, a novel antioxidant peptide identified from an amphibian, accelerates skin wound healing," *Scientific Reports*, vol. 8, no. 1, p. 943, 2018.

[43] Y. W. Lin, P. S. Liu, K. A. Pook, and L. N. Wei, "Glyburide and retinoic acid synergize to promote wound healing by anti-inflammation and RIP140 degradation," *Scientific Reports*, vol. 8, no. 1, p. 834, 2018.

[44] M. Zhao, G. Altankov, U. Grabiec et al., "Molecular composition of GAG-collagen I multilayers affects remodeling of terminal layers and osteogenic differentiation of adipose-derived stem cells," *Acta Biomaterialia*, vol. 41, pp. 86–99, 2016.

[45] C. Qi, L. Xu, Y. Deng, G. Wang, Z. Wang, and L. Wang, "Sericin hydrogels promote skin wound healing with effective regeneration of hair follicles and sebaceous glands after complete loss of epidermis and dermis," *Biomaterials Science*, vol. 6, no. 11, pp. 2859–2870, 2018.

[46] J. Vojtassak, L. Danisovic, M. Kubes et al., "Autologous biograft and mesenchymal stem cells in treatment of the diabetic foot," *Neuro Endocrinology Letters*, vol. 27, Suppl 2, pp. 134–137, 2006.

[47] C. Y. Chen, K. C. Cheng, A. Y. Chang, Y. T. Lin, Y. C. Hseu, and H. M. Wang, "10-Shogaol, an antioxidant from Zingiber officinale for skin cell proliferation and migration enhancer," *International Journal of Molecular Sciences*, vol. 13, no. 2, pp. 1762–1777, 2012.

[48] H. Y. Chou, C. Lee, J. L. Pan et al., "Enriched astaxanthin extract from Haematococcus pluvialis augments growth factor secretions to increase cell proliferation and induces MMP1 degradation to enhance collagen production in human dermal fibroblasts," *International Journal of Molecular Sciences*, vol. 17, no. 6, p. 955, 2016.

[49] C. Y. Chen, C. C. Chiu, C. P. Wu, Y. T. Chou, and H. M. Wang, "Enhancements of skin cell proliferations and migrations via 6-dehydrogingerdione," *Journal of Agricultural and Food Chemistry*, vol. 61, no. 6, pp. 1349–1356, 2013.

[50] H. M. Wang, L. Fu, C. C. Cheng et al., "Inhibition of LPS-induced oxidative damages and potential anti-inflammatory effects of Phyllanthus emblica extract via down-regulating NF-κB, COX-2, and iNOS in RAW 264.7 cells," *Antioxidants*, vol. 8, no. 8, p. 270, 2019.

[51] H. Y. Chou, D. L. Ma, C. H. Leung, C. C. Chiu, T. C. Hour, and H. D. Wang, "Purified astaxanthin from Haematococcus pluvialis promotes tissue regeneration by reducing oxidative stress and the secretion of collagen in vitro and in vivo," *Oxidative Medicine and Cellular Longevity*, vol. 2020, Article ID 4946902, 13 pages, 2020.

[52] H.-Y. Chou, H.-M. D. Wang, C.-H. Kuo et al., "Antioxidant graphene oxide nanoribbon as a novel whitening agent inhibits microphthalmia-associated transcription factor-related melanogenesis mechanism," *ACS Omega*, vol. 5, no. 12, pp. 6588–6597, 2020.

[53] N.-F. Chen, W.-F. Chen, C.-S. Sung et al., "Contributions of p38 and ERK to the antinociceptive effects of TGF-β1 in chronic constriction injury-induced neuropathic rats," *The Journal of Headache and Pain*, vol. 17, no. 1, pp. 1–9, 2016.

[54] K. C. Yang, C. C. Wu, W. Y. Chen, S. Sumi, and T. L. Huang, "L-Glutathione enhances antioxidant capacity of hyaluronic acid and modulates expression of pro-inflammatory cytokines in human fibroblast-like synoviocytes," *Journal of Biomedical Materials Research Part A*, vol. 104, no. 8, pp. 2071–2079, 2016.

[55] Y. Ito, "Growth factor engineering for biomaterials," *ACS Biomaterials Science & Engineering*, vol. 5, no. 11, pp. 5597–5609, 2019.

Hindawi
Oxidative Medicine and Cellular Longevity
Volume 2021, Article ID 5598291, 13 pages
https://doi.org/10.1155/2021/5598291

Research Article

A Novel Biocompatible Herbal Extract-Loaded Hydrogel for Acne Treatment and Repair

Ying-Yi Lin,[1] Shu-Hsu Lu,[2] Rong Gao,[3] Chia-Hung Kuo,[4] Wen-Hisn Chung,[5] Wei-Chih Lien,[6,7,8] Ching-Chou Wu,[9,10] Yong Diao,[11] and Hui-Min David Wang[1,8,12,13]

[1]*Graduate Institute of Biomedical Engineering, National Chung Hsing University, Taichung City 402, Taiwan*
[2]*Division of Cardiology, Department of Internal Medicine, Kaohsiung Armed Forces General Hospital, Kaohsiung City, Taiwan*
[3]*Deloitte Institute of Biology, Yangtze River Delta Research Institute, Tsinghua University, Beijing, China*
[4]*Department of Seafood Science, National Kaohsiung University of Science and Technology, Kaohsiung City, Taiwan*
[5]*Department of Plant Pathology, National Chung Hsing University, Taichung City 402, Taiwan*
[6]*Department of Physical Medicine and Rehabilitation, National Cheng Kung University Hospital, College of Medicine, National Cheng Kung University, Tainan 704, Taiwan*
[7]*Department of Physical Medicine and Rehabilitation, College of Medicine, National Cheng Kung University, Tainan 701, Taiwan*
[8]*Ph.D. Program in Tissue Engineering and Regenerative Medicine, National Chung Hsing University, Taichung City 402, Taiwan*
[9]*Department of Bio-Industrial Mechatronics Engineering, National Chung Hsing University, Taichung City 402, Taiwan*
[10]*Innovation and Development Center of Sustainable Agriculture, National Chung Hsing University, Taichung City 402, Taiwan*
[11]*School of Medicine, Huaqiao University, Quanzhou, Fujian Province 362021, China*
[12]*Graduate Institute of Medicine, College of Medicine, Kaohsiung Medical University, Kaohsiung City, Taiwan*
[13]*Department of Medical Laboratory Science and Biotechnology, China Medical University, Taichung City, Taiwan*

Correspondence should be addressed to Yong Diao; diaoyong@hqu.huaqiao.edu.cn
and Hui-Min David Wang; davidw@dragon.nchu.edu.tw

Received 19 February 2021; Revised 16 July 2021; Accepted 25 September 2021; Published 2 November 2021

Academic Editor: Amit Kumar Nayak

A novel herbal extract-loaded gel containing several biofunctional extracts, including green tea, *Zingiber officinale* Rosc, *Phyllanthus emblica*, and salicylic acid, was developed for acne vulgaris. These natural raw materials were blended with suitable dosages of gelatin and carboxymethyl cellulose (CMC) to produce a biocompatible herbal gel. The physical chemistry properties of the hydrogel were determined by Fourier transform infrared spectroscopy (FTIR), thermal gravimetric analysis (TGA), rheometry, and scanning electron microscopy (SEM), and the hydrogel showed good mechanical and morphological characteristics. The herbal extract-loaded hydrogel mimicked extracellular matrix properties and showed good antioxidant and anti-inflammatory properties and various advantages, serving as a potential wound dressing material because of its high moisture retention ability, wound exudate absorption behavior, and biocompatibility. It exhibited moderate-high antioxidative and anti-inflammatory qualities that were important for dermis wound closure. The clinical trial results showed that most patients experienced moderate to high healing rates, and four of twenty-four individuals (16.67%) had recovery area ratios greater than 80%. This herbal extract-loaded hydrogel has effective ingredients and excellent mechanical properties as a bioactive dressing agent for acne treatment.

1. Introduction

Acne vulgaris is an unpleasant facial skin problem with a prevalence of 80% and affects social interactions, especially for teenagers [1]. The presence of acne can reduce self-esteem and self-confidence; therefore, an effective treatment is beneficial to quality of life for adolescents. Four major causes of acne include (1) high sebum production from

sebaceous glands, (2) blockade of keratinization within pilosebaceous follicles, (3) rapid growth and proliferation of microorganisms such as *Propionibacterium acnes*, and (4) an immune inflammatory response and swelling fortification around pilosebaceous follicles [2].

Acne development is triggered by interactions between the sebostatic reaction associated with sebum deregulation and inflammatory reactions. Various complementary medicines, such as natural product extracts, plant oils, and antimicrobial peptides, have few side effects [2–4]. Previous studies showed that green tea polyphenols with anti-inflammatory and antibacterial characteristics heal acne infections and reduce sebum secretion in the dermis [5]. Ginger constitutes have antiseptic and anti-inflammatory properties and increase cellular migration [6–8]. *Phyllanthus emblica* fruit extract powder abated antioxidative stress injuries and suppressed inflammatory responses [9, 10]. The antimicrobial activities of *P. emblica*, green tea, and ginger have been investigated by a number of previous studies [11–13]; these active extracts showed antibacterial activity against gram-positive bacteria (*Staphylococcus aureus*) and gram-negative bacteria (*Escherichia coli* and *Pseudomonas aeruginosa*). Salicylic acid dissolved skin debris, which clogged pores and caused acne progression as a lipophilic agent, thus decreasing corneocyte cohesion and promoting desquamation, particularly of the hydrophobic upper layers in the stratum corneum [1]. Previous studies by this group showed that these bioactive components can be used to treat acne through biofunctions.

A biomedical hydrogel dressing fabricated from natural extracts was used as a scaffold to efficiently deliver active constituents for acne repair and to reconstruct skin tissue [14]. Gelatin is a denatured protein product from collagen that is present at high levels within the extracellular matrix and is usually used in the biomedical and pharmaceutical industries [15–17]. Gelatin is accessible, economical, non-poisonous, and biocompatible and has weak antigenic properties and many peptide sequences, such as arginine glycine-aspartic acid, which increases cellular adhesion [18]. Carboxymethyl cellulose (CMC) is also a harmless biocompatible material used for wound repair [19]. CMC compensates for the poor cohesion of gelatin in a wound healing gel when used as a base polymer.

Herbal extract-loaded hydrogels enhance water retention, absorb exudate around the wound site, increase pliability and biocompatibility, and resemble extracellular matrix in a wound dressing material. In our previously published paper, we showed that our hydrogel was biocompatible and nontoxic to foreskin fibroblasts and significantly improved cell viability in a cell viability assay [20]. Moreover, the hydrogel combined with the herbal extracts was applied in an extensive wound to assess the curing ability. However, investigations of the physical-mechanical properties of hydrogels are lacking. Thus, we studied the physical chemistry properties of herbal extract-loaded hydrogels by Fourier transform infrared spectroscopy (FTIR), TGA, rheometry, and scanning electron microscopy (SEM) and analyzed the healing effect on the treatment of acne vulgaris in this research.

2. Materials and Methods

2.1. Green Tea Extract. Green tea leaves were extracted using hot water at 85–95°C, and a 5.0% solid content was achieved by applying 5 liters of hot water per kg of tea leaves. The solution was filtered using a 10-micron polypropylene filter bag and concentrated to 20% (*w*/*v*) after low-temperature vacuum drying. The extract was obtained by adding maltodextrin at a weight ratio of 2 : 1. Green tea extracts were frozen at -35°C, freeze-dried for 72 hours (0–50 hours at below 0°C and 50–72 hours increasing to 45°C), and pulverized to produce a fine tea extract powder with an average grain size of 1.0–10 μm.

2.2. P. emblica Fruit Extract. P. emblica fruit extract powder was donated by Herden Technology Corporation Company (Taiwan), frozen at -35°C for 10–12 hours, and dried at 6°C for 35 hours to achieve a moisture content of less than 5.0% (*w*/*v*). The dried *P. emblica* fruit was mixed with hot water at a ratio of 1 : 5 to produce a 5.0% solid content for extraction, and then, the mixture was filtered using a 10-micron polypropylene filter bag. After concentration in a vacuum, the concentration of the extract solution was increased to 10% *w*/*v*. An additional extract of maltodextrin at a ratio of 1 : 1 (10% *P. emblica* content, 10% maltodextrin; *w*/*v*) was blended. *P. emblica* condensate was frozen at -35°C, freeze-dried for another 72 hours (0–50 hours at 0°C and 50–72 hours at 45°C), and ground to a powder for dissolution into dimethyl sulfoxide. Dulbecco's modified Eagle's medium at suitable doses (0.05, 0.1, 0.25, 0.5, and 1 mg/mL) was used to dilute the cells for the subsequent experiments.

2.3. Ginger (Z. officinale Rosc.) Extract. Ginger or ginger root is widely used as a flavor spice and folk medicine because it has been reported to have potential anti-inflammatory, antioxidative, antithrombosis, and possible antiallergic effects in previous papers [6, 8]. Experimental ginger material was purchased from Shennong Valley Farm Co. (Taiwan), washed and sterilized, and cut into thin slices. The slices were dried in a low-temperature environment until they were easily broken and then filtered through a 40-mesh screen for sterilization using ozone.

2.4. Preparation of Herbal Ingredients. The three extracts underwent extraction using water and alcohol. All natural herbal extracts in powder form (green tea, ginger, and *P. emblica* fruit) and salicylic acid were mixed in specific proportions, and water and ethanol were added. The mixtures were stirred at 95°C for 24 hours, and the extract was allowed to settle for 12 hours for further stratification. The supernatant was sterilized and filtered using 0.22 μm nylon filter membranes, irradiated with UV, and stored at room temperature.

2.5. Herbal Extract-Loaded Hydrogel Preparation. To determine the coating properties of polymer gels and adhesion at ambient temperature, a 9% (*w*/*w*) aqueous herbal extract gelatin solution and 10% (*w*/*w*) alcohol herbal extract CMC solution were prepared. A 1–10 mL aqueous sterile

water extract was added to 0.09–0.9 g gelatin and stirred to dissolve at 100°C to produce a 9% (*w*/*w*) herbal gelatin colloidal solution. The 9% (*w*/*w*) gelatin solution and the 10% (*w*/*w*) CMC solution without herbal extracts at a ratio of 10 : 1 were compared with other hydrogels. Distilled water and ethanol were used as solvents to form nonherbal hydrogels. The herbal extract-loaded hydrogels were mixed at various ratios with gelatin/CMC solution, gelatin was dissolved in aqueous herbal extract, and CMC was dissolved in alcoholic herbal extract. Herbal hydrogels with different ratios of gelatin-herbal water extract/CMC-herbal alcohol extract were named nonherbal hydrogels, hydrogels (10 : 1), hydrogels (1 : 1), and hydrogels (1 : 10). The freeze-dried hydrogel was prepared with a freeze dryer (FDU-1200, Korea) and observed using a microscope and SEM. The dried hydrogel patches were comminuted to fine powder to allow FTIR analysis and thermal gravimetric analysis (TGA).

2.6. FTIR. FTIR (PerkinElmer Spectrum 100) was applied from 4000 to 450 cm^{-1} at room temperature to obtain information about the biochemical compositions of the herbal extract-loaded hydrogels. The FTIR spectra of pure CMC, pure gelatin, nonherbal hydrogel, hydrogel (10 : 1), hydrogel (1 : 1), and hydrogel (1 : 10) were used to identify different functional groups. The interactions between CMC, gelatin, and herbal extracts were determined by the spectral signals.

2.7. TGA. TGA was performed using a PerkinElmer DMA 7e dynamic mechanical analyzer to determine the storage modulus of our biocompatible herbal extract-loaded hydrogels. Small dried powder quantities (0.5 to 5 mg) were wrapped and placed in a platinum pan. All samples were heated from 30 to 700°C at a heating rate of 10°C/min in an isolated environment that was purged of air. The TGA data were plotted as temperature versus weight (%) and heat flow (mW/mg) to verify the thermal behaviors of the hydrogels.

2.8. Rheology Properties. The mechanical properties of hydrogels with different ratios of CMC and gelatin were evaluated on a rheometer. The reaction solutions of hydrogels were mixed in a syringe and quickly placed on the plate of a Brookfield DV-III Ultra rheometer (Brookfield Asset Management Inc, Canada). The sample was placed in the cylindrical vessel and allowed to equilibrate at a specific temperature. To control the temperature, the water jacket of the stainless steel cylindrical vessel was connected to a constant temperature bath. The temperature was maintained at 25 ± 0.1°C. The viscosity reading was taken after 60 s for each sample [21–23]. Rheological measurements of the polymer-based nonherbal hydrogel and herbal hydrogel (10 : 1) were performed using a rheometer and three different methods. (1) A strain sweep test was used to obtain the critical strain; (2) a temperature sweep test was used to determine the storage modulus of the hydrogels; and (3) a shear rate sweep test was used to determine the viscosity of the herbal extract-loaded hydrogels [24]. The strain sweep test measured the storage modulus of the hydrogel samples for a strain from 0.1 to 100%. The temperature sweep test was performed at 0.5% strain, and the temperature was increased from room temperature to 50°C at 1 rad/s. A shear rate sweep test with a shear rate of 1/s from 0.1 to 100 at 25°C was used to measure the viscosity of the nonherbal hydrogel and hydrogel (10 : 1) samples.

2.9. SEM. Scanning electron microscopy was applied to determine the surface morphology. Sample preparation for SEM images was performed according to previous papers [3]. The hydrogels were allowed to reach swelling equilibrium and cut into small pieces to expose the inner surface and then pretreated with freeze-drying to completely remove the water. Freeze-dried hydrogel (10 : 1) samples were analyzed using a TOPCON scanning electron microscope (ABT-150S, Tokyo, Japan) at an acceleration voltage of 15 kV. Dried patches were sectioned using a scalpel, and cross-sections were coated with platinum and then placed on an optimally sized aluminum stub using double-sided tape. The gold coating of 300 A on the stub was deposited using gold sputtering. The structural morphology of hydrogel patches was scanned, and photomicrographs were captured.

2.10. Determination of 1,1-Diphenyl-2-picrylhydrazyl (DPPH) Scavenging Activity. The mechanism for DPPH scavenging activity involved the DPPH reagent accepting an electron or hydrogen radical to become a stable molecule to detect oxidative activity. Hydrogen was produced when DPPH reacted with antioxidant agents. The amount of DPPH and its absorbance decreased, and the absorbance was measured spectrophotometrically at 517 nm [10]. Vitamin C (100 μM) was used as a positive control due to its superior antioxidant properties. One microliter of different concentrations of herbal polymer-based hydrogel was added to 99 μL DPPH solution (0.1 mg/mL). Various sample amounts were dissolved in methanol for each well to yield a final working volume of 100 μL. Distilled water was used as the control. Absorbance was measured using a spectrophotometer, and the DPPH value was plotted for comparison with the initial concentration of DPPH to determine the reduction by the antioxidant. The scavenging capacity (%) was calculated as

$$\text{Scavenging ability (\%)} = \left[1\text{-}\left(\frac{A_{\text{Sample}}}{A_{\text{Blank}}}\right)\right] \times 100\%. \quad (1)$$

2.11. Metal Chelating Ability. The chelation of ferrous ions in hydrogel samples was measured using a procedure developed in previous studies [25]. A 10 μL aliquot of 2 mM $FeCl_2{\cdot}4H_2O$ solution was mixed with 1 μL of different concentrations (0.5–50 mg/mL) of samples. When the sample solution was added to 20 μL of 5 mM ferrozine, the complexes of ferrous ions and ferrozine changed color. A lower absorbance signified better metal chelating activity. The absorbance was measured spectrophotometrically at 562 nm. Distilled water was used as the control. A 100 μM EDTA solution was used as a positive control. The chelating ability was calculated using a formula similar to Equation (1).

Figure 1: (a) The FTIR data and (b) the characteristic peaks for pure CMC, gelatin, and herbal extract-loaded hydrogels at various mixing ratios with or without herbal extract. The different hydrogel samples included nonherbal hydrogels, hydrogels (1 : 1), hydrogels (1 : 10), and hydrogels (10 : 1).

2.12. Case Report. For the clinical trials, twenty-four clinical subjects were treated with the herbal polymer-based hydrogel for a period of two weeks by a dermatologist. The Institutional Review Board proof is shown in Figure S1 (M2019011). All individuals who participated in this study provided written informed consent to publish these details (Table S1). All skin conditions were recorded before and after the treatments, and the recovery area for inflamed acne wounds was quantified using ImageJ software (National Institutes of Health, Bethesda, USA). The results

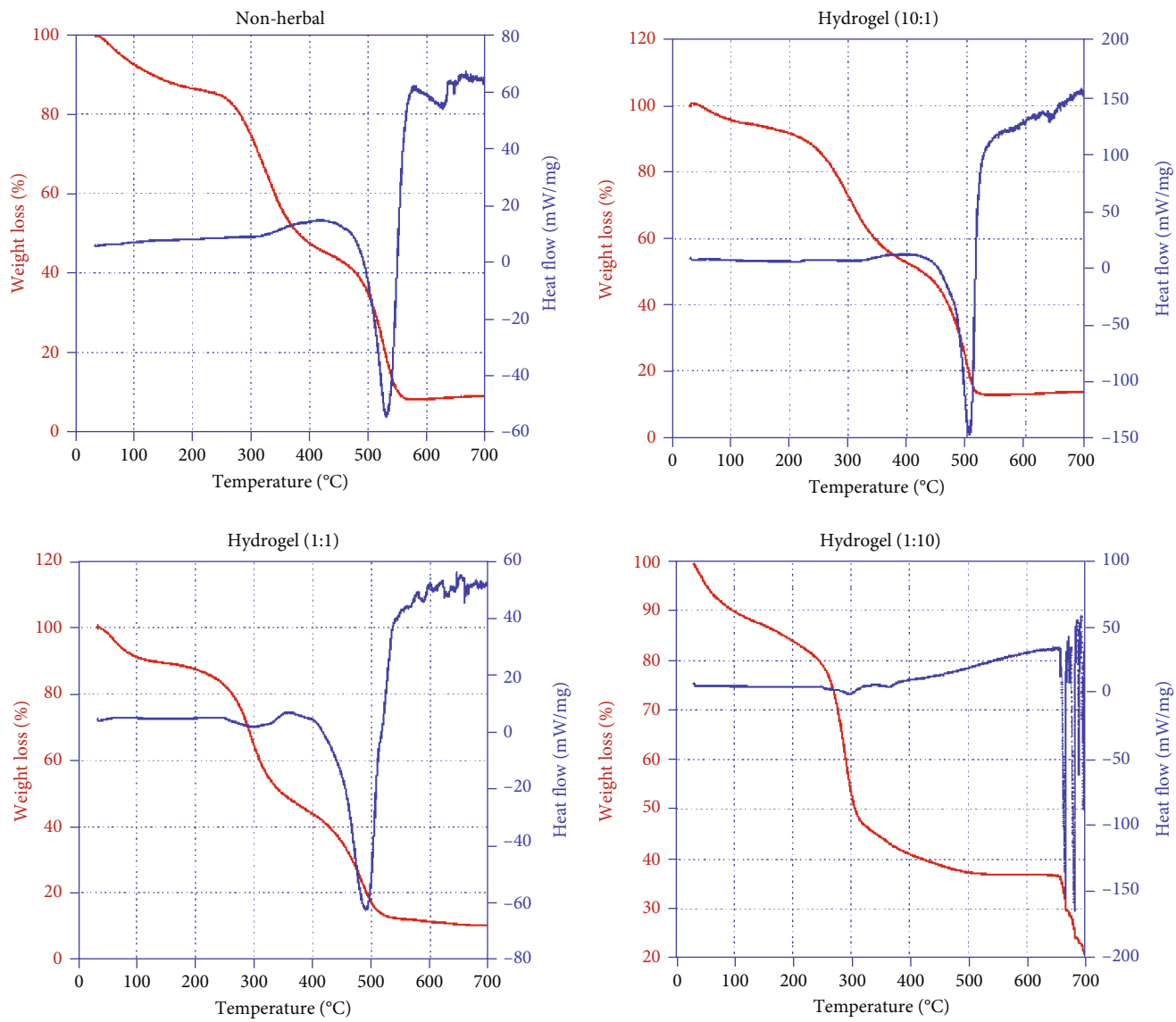

Figure 2: TGA results for the nonherbal hydrogel, hydrogel (1 : 1), hydrogel (1 : 10), and hydrogel (10 : 1) samples. The thermal properties of the samples were determined using a thermal analyzer to determine weight loss and heat flow.

are shown in Table S1. The wound healing rate (%) was calculated using

$$\text{Wound healing rate (\%)} = \frac{W_b - W_a}{W_b} \times 100\%, \qquad (2)$$

where W_b is the wound area before treatment and W_a is the wound area after treatment.

2.13. Statistical Analysis. Differences between the *in vivo* experiments for the vehicle control group and the herbal polymer-based gel group were analyzed using Student's t -test. One-way ANOVA was used for statistical comparisons between the vehicle control group and experimental groups. A significant difference (∗) was defined as $p < 0.05$.

3. Results

3.1. Hydrogel Composition. To determine the optimal blending ratio for CMC solution with alcohol herbal extract and gelatin solution with aqueous herbal extract, the configurations of hydrogels with various mixing ratios of two types of solutions were measured. We named the nonherbal hydrogel (gelatin/CMC only) and the hydrogels with gelatin/CMC: herbal extract ratios of 10 : 1, 1 : 1, and 1 : 10 nonherbal hydrogel, hydrogel (10 : 1), hydrogel (1 : 1), and hydrogel (1 : 10), respectively. The solution formed an herbal extract-loaded hydrogel, and the solvent in the nonherbal hydrogel was substituted with dilute water and 95% ethanol. Figure S2(A-D) presents the results for the alcohol herbal extract CMC solution, the aqueous herbal extract gelatin solution, and the final hydrogel. During the gelatin process, the hydrogel became stratified, and the precipitate was

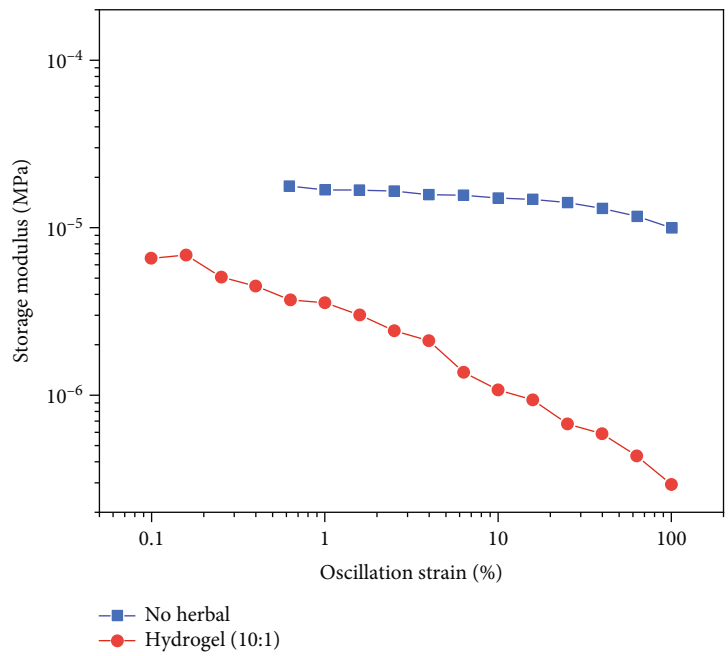

(a)

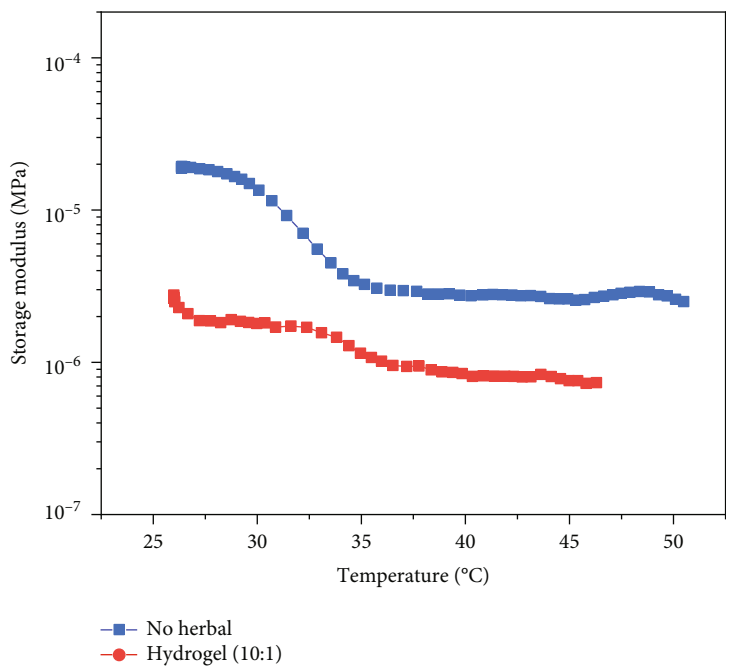

(b)

Figure 3: Continued.

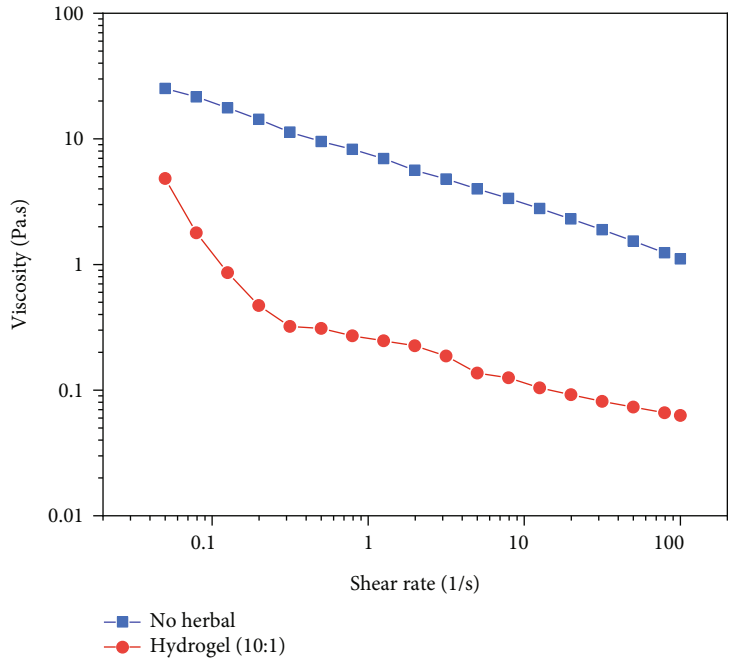

(c)

Figure 3: (a) The rheological properties of the storage modulus for a strain sweep ranging from 0.1 to 100% for the nonherbal hydrogel and hydrogel (10 : 1). (b) The relationship between temperature and the storage modulus for the nonherbal hydrogel and hydrogel (10 : 1) at 25°C. (c) The viscosity of the nonherbal hydrogel and hydrogel (10 : 1). The shear-thinning behavior of herbal extract-loaded hydrogels was characterized by an increasing shear rate from 0.1 to 100 (1/s).

deposited in the bottle of the tube as the volume of the gelatin solution increased. Figure S2(D) shows that the herbal hydrogel with a blend ratio of 1 : 10 was separated into two layers, and the precipitate was insoluble. Incomplete formation of hydrogel (1 : 10) was noted. Figure S2(E) shows freeze-dried samples with various blend ratios.

3.2. Hydrogel Evaluation by Structural, Thermal, and Morphological Analyses

3.2.1. FTIR Analysis. Figure 1 shows the FTIR spectra for pure CMC, gelatin powder, and herbal extract-loaded hydrogels with different ratios, which were used to identify the bands attributed to the functional groups. The CMC powder characteristic bands at 2698 and 1047 cm^{-1} were assigned to –OH stretching regions from carboxylic acid and –CO stretching regions from vinyl ether stretching and -C-O- in the ether group (–CH-O–CH_2), respectively. The characteristic band at 1410 cm^{-1} corresponds to scissor-like -CH_2 [26]. These absorption bands are in good agreement with reports from a previous paper [27]. The characteristic peaks in the FTIR spectrum for gelatin powder at 3035, 1694, and 1209 cm^{-1} were attributed to –OH, –NH, and –CO functional groups, respectively [26]. The hydrogel (1 : 1) features absorption bands at 2769, 1590, 1454, 1332, 1210, and 1052 cm^{-1} related to the carboxylic acid peak (–OH stretching), the amide peak (–NH bending), alkane from the methyl group (–CH bending), and scissor-like -CH_2, -CO, and –CO functional groups. The absorption bands for hydrogel (1 : 10) at 3209, 1590, 1455, 1383, 1217, and 1031 cm^{-1} corresponded to –OH, –NH, –CH, -CH_2, –CO, and –CO functional groups. The characteristic peaks for hydrogel (10 : 1) at 3061, 2780, 1618, 1454, 1334, 1209, and 1046 cm^{-1} were attributed to –OH, –OH, –NH, –CH, -CH_2, –CO, and –CO functional groups. The nonherbal hydrogel features peaks at 3285, 1627, 1453, 1402, 1337, 1237, and 1053 cm^{-1} attributed to –OH, –NH, –CH, -OH, -CH_2, –CO, and –CO functional groups.

The FTIR spectra of gelatin, CMC, and herbal extract-loaded hydrogels showed that the –CH bending band for the alkane in herbal hydrogels with various ratios at approximately 1450 cm^{-1} was not present in the IR spectra for pure CMC or gelatin powder because the interactions between gelatin and CMC formed a new linkage after cross-linking. The -CH_2 functional group in CMC was shifted to approximately 1335 cm^{-1}, demonstrating that CMC and gelatin were integrated into polymer-based hydrogels and caused conformational changes. According to a previous paper [28], the band at approximately 1651 cm^{-1} attributed to CMC provided information on the helicity of the protein in herbal extract-loaded hydrogels. A broad absorption band at 3300 cm^{-1} for OH groups corresponded to absorbed water, secondary alcohols (CMC), and (intramolecular/intermolecular) hydrogen bonding. The amide I band corresponding to –CO stretching vibration was the best region in the spectrum to show changes in the secondary structure of the protein. In the composite film, the amide I peak shifted from 1589 cm^{-1} to approximately 1615 cm^{-1}. The peaks between 1209 and 1694 cm^{-1} were likely due to CN stretching and NH in-plane deformation vibrations from peptide groups

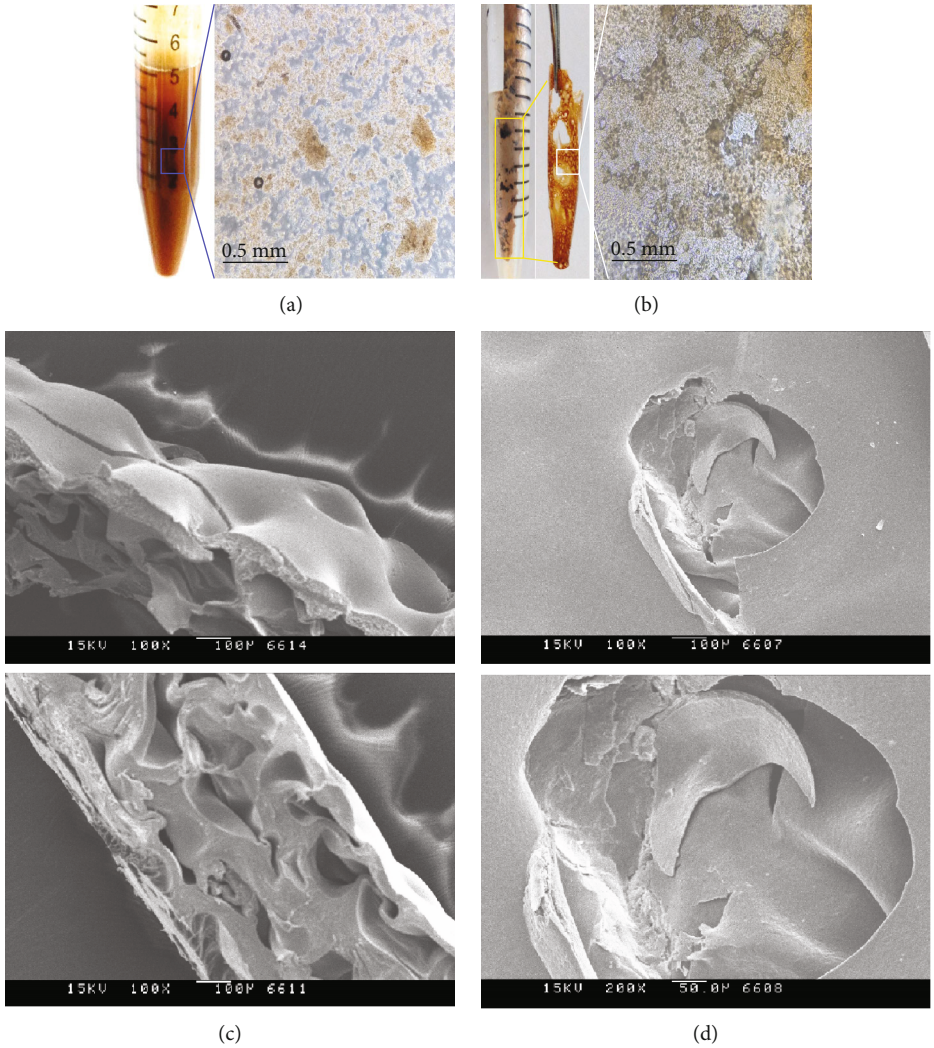

Figure 4: The morphology of the hydrogel (10 : 1), which comprised 9% (*w*/*w*) herbal gelatin mixed with 10% (*w*/*w*) alcohol herbal extract CMC solution: (a) microscopic images of the hydrogel and (b) the freeze-dried sample. The morphology of the hydrogel (10 : 1): (c) the cross-sectional interface and (d) the surface structure scanned by SEM.

in the amide I, amide II, and amide II moieties of gelatin. The absorption bands for different herbal hydrogels at approximately 3000, 1590, 1450, 1350, 1210, and 1050 corresponded to -OH, -NH, -CH, -OH, -CO, and -CO functional groups in CMC and gelatin, respectively. Therefore, the incorporation of CMC and gelatin into herbal extract-loaded hydrogels caused chemical conformational changes.

3.2.2. TGA. TGA in this research helped determine the stability of the biocompatible herbal extract-loaded hydrogel, and the results are shown in Figure 2. All hydrogels underwent two or three major degradation steps, as presented by the TGA curves. Thermal degradation, including water loss, combustion, and hydrogel decomposition, was observed for all samples. No additional thermal event was noted for native and functionalized hydrogels; thus, no impurities or byproducts were observed. Initial weight losses of 14.78%, 12.11%, 15.98%, and 19.44% were observed for the nonherbal hydrogel, hydrogel (10 : 1), hydrogel (1 : 1), and hydrogel (1 : 10), respectively, until 240°C. The decrease in weight was due to the elimination of the moisture retained by the materials and the evaporation of adsorbed water. The significant reduction in moisture content was a result of a strong hydrogen bonding interaction [29]. Weight loss was found to be less than 20% in the hydrogel at 200°C. The weight losses in pure carboxymethyl cellulose (CMC) and pure gelatin were approximately 130°C and 100°C, respectively, suggesting that the hydrogel composed of gelatin, CMC, and herbal extract helped stabilize the hydrogel structure [30, 31].

Strong stretching loss occurred in the nonherbal hydrogel, hydrogel (10 : 1), and hydrogel (1 : 1) between 240 and 380°C, and the values for weight loss were 49.79%, 45.45%, and 53.90%, respectively. Weight loss measurements began at approximately 240°C and ended at approximately 380°C, mainly due to depolymerization of the carbohydrate polymer [26, 29]. The weight loss from 240°C to 380°C was due to the remaining fraction of volatile compounds of herbal extract and nondegraded CMC side branches [30]. At a temperature of less than 700°C, the retained weights of the hydrogel were 9.12%, 13.86%, 10.20%, and 20.78% for

nonherbal hydrogel, hydrogel (10 : 1), hydrogel (1 : 1), and hydrogel (1 : 10), respectively. The weight loss at higher temperatures (approximately 700°C) was sluggish, resulting in no separate or major phase in the composite ingredients pertaining to a specific TGA behavior [30] and thus indicating that some organic materials (CMC and gelatin) were still present in the herbal extract-loaded hydrogels [32].

Two-stage weight loss was observed for the nonherbal hydrogel, hydrogel (10 : 1), and hydrogel (1 : 1), which behaved similarly to the three hydrogels with different blend ratios. Weight loss was slower for the hydrogel containing more gelatin during the first stage of weight loss (to 240°C). Weight loss in hydrogel (1 : 10) decreased faster than that in the other hydrogels at both stages. A volatile decrease in weight loss was observed for hydrogel (1 : 10) from 240 to 600°C. This behavior was different for other hydrogels, possibly because the structure of hydrogel (1 : 10) was incomplete and the components of CMC and gelatin were not mixed well for the various ratios of the hydrogels. The results were similar to the TGA data for pure CMC or pure gelatin (data not shown), which showed incomplete cross-linking between the CMC and gelatin.

Each thermogram exhibited a single exothermic peak at 526°C, 504°C, and 489°C for the nonherbal hydrogel, hydrogel (10 : 1), and hydrogel (1 : 1), respectively. However, no significant exothermic peak was observed in the TGA data for hydrogel (1 : 10), possibly because of the incomplete synthesis of gelatin and CMC at the blend ratio of 10 : 1. More specifically, the addition of CMC to gelatin decreased the melting point of the hydrogel. The interaction between the two macromolecules increased, and CMC plasticized the gelatin for the nonherbal hydrogel and hydrogel (10 : 1). The cross-linked hydrogel was more stable at a blend ratio of 10 : 1 [28]. For both blended gelatin/CMC hydrogels, the glass transition values showed that the cross-linking reaction caused by the addition of CMC affects the thermal properties of the hydrogel. Crosslinking of the gelatin macromolecule and CMC increased the thermal stability of the gelatin hydrogel [33].

3.2.3. Rheological Analysis. The rheological behaviors of the herbal extract-loaded hydrogels were characterized to determine the wound healing properties using a rheometer. The storage modulus was measured using an oscillating strain at a fixed angular frequency (1 rad/s). When the angular frequency changed from 0.1 to 100 strains (%), the hydrogel storage modulus presented no significant change between 0.1 and 10 strains; thus, the hydrogels were stable (Figure 3(a)) [23]. The variation in the storage modulus due to temperature for herbal extract-loaded hydrogels with a blend ratio of 10 : 1 is shown in Figure 3(b). Both hydrogels behaved similarly in that the storage modulus decreased as the temperature increased. Measurement of viscosity as a function of the shear rate showed that the viscosity of the nonherbal hydrogel and hydrogel (10 : 1) decreased as the shear rate increased (Figure 3(c)), which is known as shear-thinning behavior [34]. Shear-thinning behavior resulting in high viscosity at low shear rates has been observed in biological fluids such as biomaterials or gelling

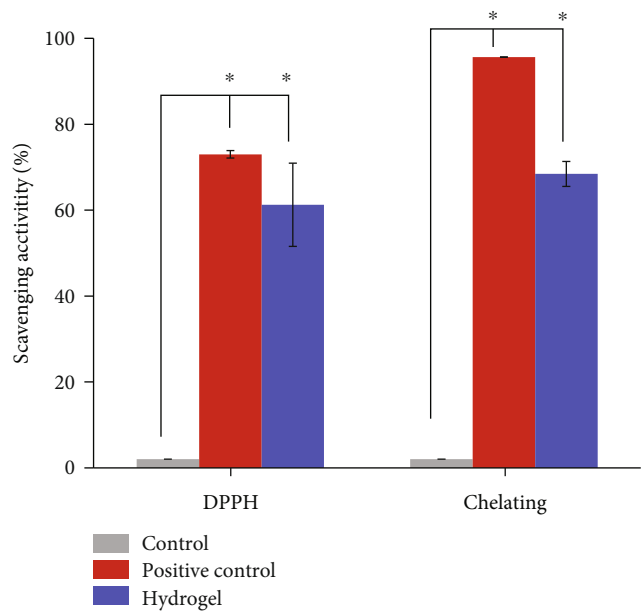

Figure 5: The antioxidant ability in DPPH and the chelating scavenging activity of herbal extract-loaded hydrogels.

products. To increase firmness, stability, and durability, shear-thinning subjects are needed. The shear rate increased as viscosity decreased, and products that exhibited shear-thinning behavior were therefore absorbed easily onto the skin through topical application. Herbal extract-loaded hydrogels are an ideal synthetic film for wound repair applications because they remain on the skin [34].

3.3. Morphology and Antioxidant Ability of Herbal Hydrogels

3.3.1. Morphological Analysis. Herbal water extract with a specific ratio of herbal alcohol extract was stirred at room temperature until it completely dissolved. Both solutions at a specific ratio were dispensed to form an herbal polymer-based gel. Alcohol extraction increased the extraction rate and allowed quick drying of the resultant gel. Figures 4(a) and 4(b) show microscopic images of the morphological features of the CMC/gelatin/herbal extract hydrogel. The microstructure was an interlaced, highly concatenated porous structure, and the surface with multiple apertures was tightly connected after freeze-drying. Figures 4(c) and 4(d) show the SEM images of the nonherbal hydrogel and hydrogel (10 : 1). These SEM images showed that the lyophilized hydrogels were porous and feature an interconnected polymer network with a multilayered structure. Live cells could be incorporated into the hydrogel and stored in multiple layers [35].

3.3.2. Antioxidant Activity. DPPH scavenging capability is a vital element for functional foods and skin care because excessive accumulation of free radicals accelerates the oxidation of lipids in foods and cosmetics [8]. During the reaction for DPPH free radical scavenging, antioxidants inhibit oxidation products. The scavenging value for the DPPH radical was used to determine antioxidant activity. Ferrozine forms

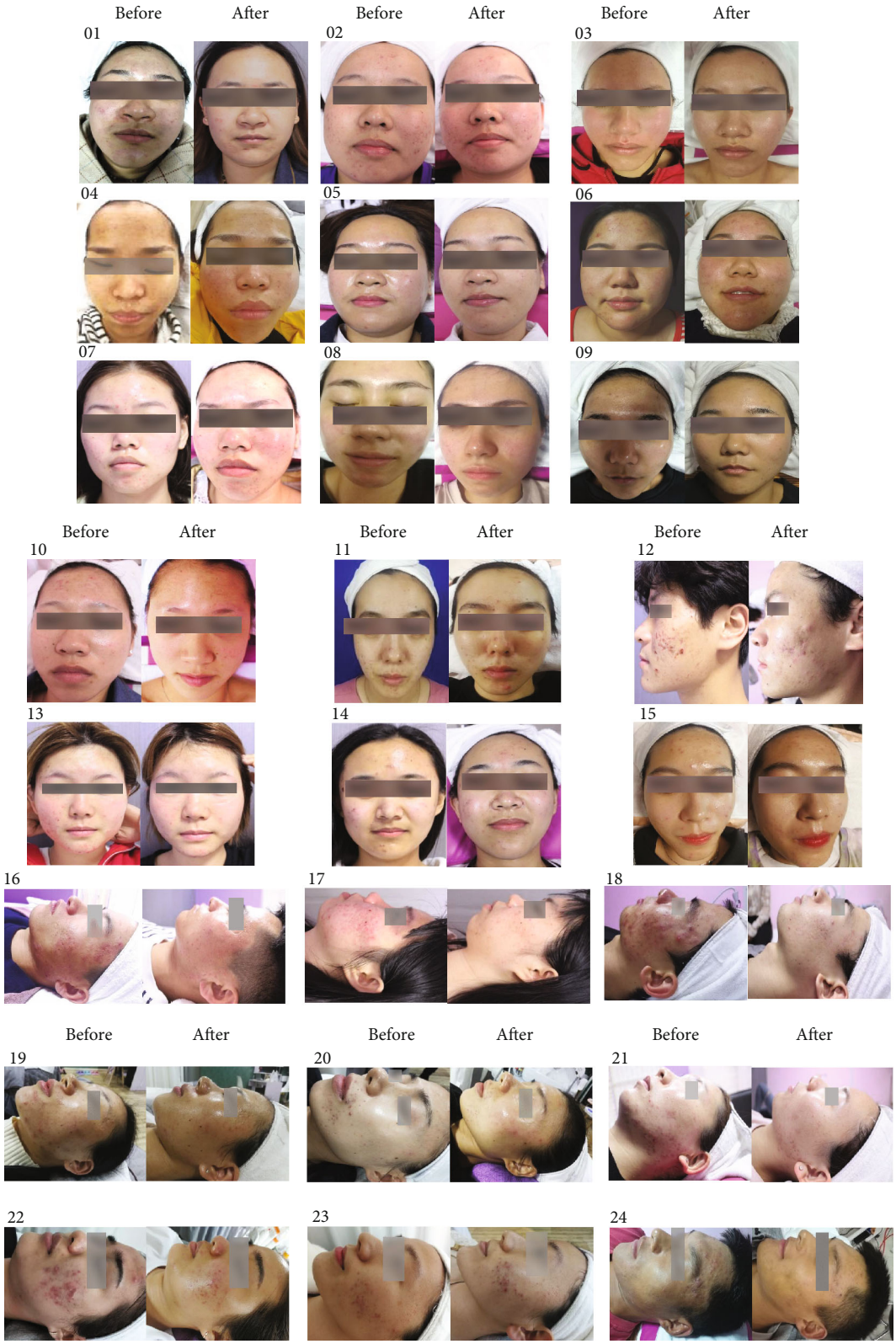

(a)

Figure 6: Continued.

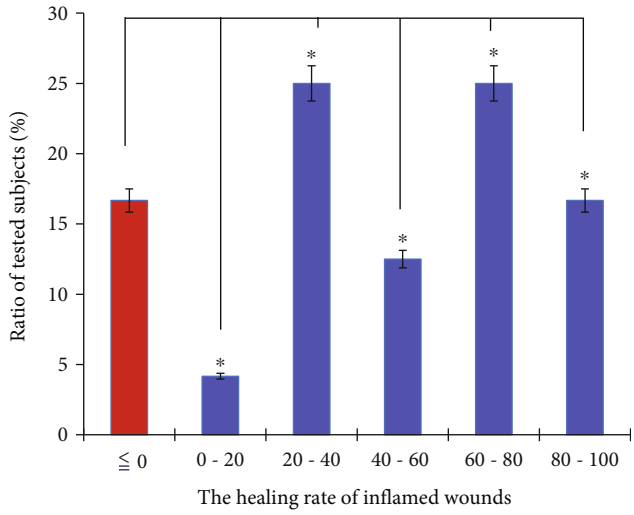

(b)

Figure 6: (a) Images of twenty-four clinical subjects treated with the herbal extract-loaded hydrogel at the beginning and end of 14 days of treatment and (b) the quantitative healing rate for acne with the gel treatments.

complexes with Fe^{2+} quantitatively. The construction of the complex was disrupted by the presence of chelating agents, and the red color of the complex faded. Figure 5 shows the DPPH scavenging activity and metal chelating ability of the herbal extract-loaded hydrogel used in this study. The results showed that the herbal hydrogels increased DPPH scavenging activity and chelating ability by $61.25 \pm 7.07\%$ and $83.93 \pm 9.68\%$, respectively. This figure shows that DPPH scavenging activity was significantly higher in the experimental groups than in the control group. Antioxidants convert the stable radical DPPH into yellow-colored diphenyl-picrylhydrazine. The herbal hydrogel inhibited DPPH more than vitamin C. The chelating value for the herbal extract-loaded hydrogel produced using herbal extract showed a small Fe^{2+} scavenging value because EDTA solution exhibits a moderate-high scavenging capability.

3.4. Case Report. The patients with moderate to severe acne volunteered to accept the whole course of treatment with herbal extract-loaded hydrogels. They were instructed to use the hydrogel to cover acneic areas after cleaning their faces three times per day and to consistently apply this moist wound dressing for 14 days. The results of the human trials are shown in Figure 6. A total of 16.7% of twenty-four individuals showed a recovery area greater than 80%, and 34.28% of the patients experienced a wound healing rate of more than 75%. Seventy-five percent of participants had a repair ratio greater than 30%, and 20.83% of individuals had a recovery ratio of less than 20%. Approximately 54% of the patients had a healing rate greater than 40%. No uncontrollable factors for clinical trials involving human subjects were identified. The volunteers remained at normal temperature and humidity for 14 days, and their daily routine, diet, and intake of liquids were fixed due to their general lifestyles. Some clinical subjects (16.7%) had a specific physiological status or living habits that affected wound healing. The results show that the herbal extract-loaded hydrogel had a positive effect on most clinical subjects, and the biomaterial was effective for curing acne.

4. Discussion

More than 90% of Australian adolescents aged 16–18 years suffer from acne vulgaris, and their self-esteem and emotional state can be affected. Moderate to severe acne can lead to scarring [36]. Many causes of acne vulgaris have been identified, including stress, irregular sleeping habits, lack of sleep, a high-calorie or high-sugar diet, hormonal changes, acne position comparison, improper use of skin care products or cosmetics, a dirty environment, and certain oral medications. Acne is caused by the action of bacteria called *Propionibacterium acnes*, keratinization of follicular keratinocytes, sebum production from sebaceous glands, and the inflammatory response of skin. Acne vulgaris can cause more serious problems, including boils, cellulitis, scars, and keloids, due to bacterial infections and sequelae if treated improperly. The etiology is unclear and probably involves multiple factors; therefore, targeted and low-risk treatments have yet to be developed [36]. Pharmacological therapies, including isotretinoin, benzoyl peroxide, and antibiotics, are often used to treat acne in adolescents [1]. These types of acne medications act by reducing oil production and swelling or by inhibiting bacterial infection. Many months may be necessary to cure acne completely, and some agents heal acne quickly.

This study developed an herbal extract-loaded hydrogel containing green tea extract, ginger, *P. emblica*, and salicylic acid to cure moderate to severe acne completely in two weeks. More than half of the twenty-four test subjects had a 50% healing rate. Current prescription drugs may not produce a change for four to eight weeks, but the herbal extract-loaded hydrogel cured acne rapidly, possibly due to the active ingredients and protection of the skin barrier from outer pathogens. Anti-inflammatory, anti-irritant, and

antibacterial effects are the pharmacological features of natural products such as green tea, *P. emblica*, and ginger extracts and accelerate the wound healing process. Tea polyphenols have been shown to reduce the severity of acne, and green tea extract significantly reduced the number of forehead, cheek, and total lesions after 4 weeks of treatment [4]. The anti-inflammatory and keratolytic effects of salicylic acid have been studied [1]. Salicylates with anti-inflammatory and postinflammatory properties reverse the hypercornification of the follicular canal and facilitate the expulsion of existing comedones by inducing accelerated proliferation of the follicular epithelium [22]. The wound healing effect of gel with natural extracts on full-thickness wounds was reported in one study [20]. This hydrogel achieved water-based transmission to release the active components from the hydrogel. The functional agents achieved the astringent effect of tightening the skin and inhibiting sweat and sebum secretion to temporarily shrink keratin without the problem of drug resistance and sensitization. To enter the cosmetic market, comparative studies with established therapies and combination therapies are necessary. The herbal extract-loaded hydrogel efficiently healed moderate to severe acne. The preliminary clinical trial demonstrated the hydrogel's efficacy in healing acne rapidly and reducing epithelialization.

5. Conclusions

This study mixes herbal extracts, including green tea, *Z. officinale* Rosc., *P. emblica* ingredients, and salicylic acid, with gelatin and CMC to develop an herbal polymer-based hydrogel. The resultant gel was used in an *in vivo* experiment to determine its efficacy in controlling sebum secretion and its anti-inflammatory effect. Polymer-based hydrogels with good mechanical properties, rheological characteristics, and surface morphologies were retained around injured skin, and the microstructure of the gel allowed cells to reside within to support wound repair. The results showed that the addition of herbal extract to the gelatin/CMC gel reduced inflammation and improved the rate of acne closure after 14 days of treatment. More than fifty percent of the twenty-four test subjects showed 50% recovery from moderate-to-severe acne problems. Further study is required to quantify the inflammatory cells and the reduction in sebum production. This preliminary study showed that the proposed hydrogel can heal acne rapidly and reduce epithelialization.

Data Availability

The data that support the findings of this study are available from all authors upon reasonable request.

Conflicts of Interest

The authors declare no conflict of interest.

Authors' Contributions

Y.Y.L. and S.H.L. contributed equally to this work. R.G., S.H.L., and H.M.D.W. conceived and designed the experiments; Y.Y.L., C.H.K., Y.D., W.H.C., and H.M.D.W. performed the experiments; C.C.W. and W.C.L. analyzed the data; Y.Y.L., S.H.L., R.G., C.H.K., C.C.W., W.C.L., Y.D., and H.M.D.W. wrote and edited the paper. Y.D. and H.M.D.W are corresponding.

Acknowledgments

The authors were grateful for the donation of green tea extract by Dr. I-Fan Lin (Challenge Bioproducts Co., Ltd.). This research was funded by the Ministry of Science and Technology (MOST 109-2221-E-005-01), Kaohsiung Armed Forces General Hospital (KAFGH_D_109014), National Chung Hsing University (ENABLE: 108ST001B and 110ST001G), Kasetsart University Joint Research Project (108RA129A), and NCHU-MIRDC Bilateral Joint Research Project (110S0703B).

Supplementary Materials

Figure S1: IRB certificate for human examination (M2019011). Figure S2: images of herbal extract-loaded hydrogels at various mixing ratios of gelatin herbal extract and CMC herbal extract. Table S1: the wound healing areas of the 24 subjects. *(Supplementary Materials)*

References

[1] M. N. Alba, M. Gerenutti, V. M. H. Yoshida, and D. Grotto, "Clinical comparison of salicylic acid peel and LED-laser phototherapy for the treatment of acne vulgaris in teenagers," *Journal of Cosmetic and Laser Therapy*, vol. 19, no. 1, pp. 49–53, 2017.

[2] J. Li, C. Y. Chen, J. Y. Huang et al., "Isokotomolide a from Cinnamomum kotoense induce melanoma autophagy and apoptosis in vivo and in vitro," *Oxidative Medicine and Cellular Longevity*, vol. 2020, 16 pages, 2020.

[3] H.-Y. Haung, Y. C. Wang, Y. C. Cheng et al., "A novel oral astaxanthin nanoemulsion from Haematococcus pluvialis induces apoptosis in lung metastatic melanoma," *Oxidative Medicine and Cellular Longevity*, vol. 2020, 13 pages, 2020.

[4] P.-H. Li, Y. P. Chiu, C. C. Shih et al., "Biofunctional activities of Equisetum ramosissimum extract: protective effects against oxidation, melanoma, and melanogenesis," *Oxidative Medicine and Cellular Longevity*, vol. 2016, 9 pages, 2016.

[5] Y. Chen, J. Y. Huang, Y. Lin et al., "Antioxidative and antimelanoma effects of various tea extracts via a green extraction method," *Journal of Food Quality*, vol. 2018, 6 pages, 2018.

[6] C.-Y. Chen, K. C. Cheng, A. Y. Chang, Y. T. Lin, Y. C. Hseu, and H. M. Wang, "10-Shogaol, an antioxidant from Zingiber officinale for skin cell proliferation and migration enhancer," *International Journal of Molecular Sciences*, vol. 13, no. 2, pp. 1762–1777, 2012.

[7] C.-Y. Chen, C. C. Chiu, C. P. Wu, Y. T. Chou, and H. M. Wang, "Enhancements of skin cell proliferations and migrations via 6-dehydrogingerdione," *Journal of Agricultural and Food Chemistry*, vol. 61, no. 6, pp. 1349–1356, 2013.

[8] H. M. Wang, C. Y. Chen, H. A. Chen et al., "Zingiber officinale (ginger) compounds have tetracycline-resistance modifying effects against clinical extensively drug-resistant Acinetobacter baumannii," *Phytotherapy Research*, vol. 24, no. 12, pp. 1825–1830, 2010.

[9] H. M.-D. Wang, L. Fu, C. C. Cheng et al., "Inhibition of LPS-induced oxidative damages and potential anti-inflammatory effects of Phyllanthus emblica extract via down-regulating NF-κB, COX-2, and iNOS in RAW 264.7 cells," *Antioxidants*, vol. 8, no. 8, p. 270, 2019.

[10] Y.-C. Wang, X. Y. Haung, C. C. Chiu et al., "Inhibitions of melanogenesis via _Phyllanthus emblica_ fruit extract powder in B16F10 cells," *Food Bioscience*, vol. 28, pp. 177–182, 2019.

[11] D. Dhale and U. Mogle, "Phytochemical screening and antibacterial activity of Phyllanthus emblica (L.)," *Science Research Reporter*, vol. 1, no. 3, pp. 138–142, 2011.

[12] W. R. Rolim, M. T. Pelegrino, B. de Araújo Lima et al., "Green tea extract mediated biogenic synthesis of silver nanoparticles: characterization, cytotoxicity evaluation and antibacterial activity," *Applied Surface Science*, vol. 463, pp. 66–74, 2019.

[13] Y. Zu, H. Yu, L. Liang et al., "Activities of ten essential oils towards Propionibacterium acnes and PC-3, A-549 and MCF-7 cancer cells," *Molecules*, vol. 15, no. 5, pp. 3200–3210, 2010.

[14] M. Wang, C. Wang, M. Chen et al., "Efficient angiogenesis-based diabetic wound healing/skin reconstruction through bioactive antibacterial adhesive ultraviolet shielding nanodressing with exosome release," *ACS Nano*, vol. 13, no. 9, pp. 10279–10293, 2019.

[15] H.-M. Wang, Y. T. Chou, Z. H. Wen, Z. R. Wang, C. H. Chen, and M. L. Ho, "Novel biodegradable porous scaffold applied to skin regeneration," *PLoS One*, vol. 8, no. 6, article e56330, 2013.

[16] H.-Y. Chou, C. Lee, J. L. Pan et al., "Enriched astaxanthin extract from Haematococcus pluvialis augments growth factor secretions to increase cell proliferation and induces MMP1 degradation to enhance collagen production in human dermal fibroblasts," *International Journal of Molecular Sciences*, vol. 17, no. 6, p. 955, 2016.

[17] H.-Y. Chou, D. L. Ma, C. H. Leung, C. C. Chiu, T. C. Hour, and H. M. D. Wang, "Purified astaxanthin from Haematococcus pluvialis promotes tissue regeneration by reducing oxidative stress and the secretion of collagen in vitro and in vivo," *Oxidative Medicine and Cellular Longevity*, vol. 2020, 13 pages, 2020.

[18] H. D. López-Calderón, H. Avilés-Arnaut, L. J. Galán-Wong et al., "Electrospun polyvinylpyrrolidone-gelatin and cellulose acetate bi-layer scaffold loaded with gentamicin as possible wound dressing," *Polymers*, vol. 12, no. 10, p. 2311, 2020.

[19] Y.-C. Huang, K. Y. Huang, W. Z. Lew, K. H. Fan, W. J. Chang, and H. M. Huang, "Gamma-irradiation-prepared low molecular weight hyaluronic acid promotes skin wound healing," *Polymers*, vol. 11, no. 7, p. 1214, 2019.

[20] T. Ponrasu, T. H. Cheng, L. Wang, Y. S. Cheng, and H. M. D. Wang, "Natural biocompatible polymer-based polyherbal compound gel for rapid wound contraction and promote re-epithelialization: an _in vivo_ study," *Materials Letters*, vol. 261, p. 126911, 2020.

[21] J. Joy, J. Pereira, R. Aid-Launais et al., "Gelatin – oxidized carboxymethyl cellulose blend based tubular electrospun scaffold for vascular tissue engineering," *International Journal of Biological Macromolecules*, vol. 107, pp. 1922–1935, 2018.

[22] E. Duhoranimana, E. Karangwa, L. Lai et al., "Effect of sodium carboxymethyl cellulose on complex coacervates formation with gelatin: coacervates characterization, stabilization and formation mechanism," *Food Hydrocolloids*, vol. 69, pp. 111–120, 2017.

[23] R. Dong, X. Zhao, B. Guo, and P. X. Ma, "Self-healing conductive injectable hydrogels with antibacterial activity as cell delivery carrier for cardiac cell therapy," *ACS Applied Materials & Interfaces*, vol. 8, no. 27, pp. 17138–17150, 2016.

[24] Z. Naghizadeh, A. Karkhaneh, and A. Khojasteh, "Self-crosslinking effect of chitosan and gelatin on alginate based hydrogels: injectable in situ forming scaffolds," *Materials Science and Engineering: C*, vol. 89, pp. 256–264, 2018.

[25] S. P. Wong, L. P. Leong, and J. H. William Koh, "Antioxidant activities of aqueous extracts of selected plants," *Food Chemistry*, vol. 99, no. 4, pp. 775–783, 2006.

[26] R. Ahmadi, B. Ghanbarzadeh, A. Ayaseh et al., "The antimicrobial bio-nanocomposite containing non-hydrolyzed cellulose nanofiber (CNF) and Miswak (Salvadora persica L.) extract," *Carbohydrate Polymers*, vol. 214, pp. 15–25, 2019.

[27] J.-F. Su, Z. Huang, X. Y. Yuan, X. Y. Wang, and M. Li, "Structure and properties of carboxymethyl cellulose/soy protein isolate blend edible films crosslinked by Maillard reactions," *Carbohydrate Polymers*, vol. 79, no. 1, pp. 145–153, 2010.

[28] C. ASMA, B. MAHMOUD, B. DJAAFER, and B. DJAAFER, "Physicochemical characterization of gelatin-cmc composite edibles films from polyion-complex hydrogels," *Journal of the Chilean Chemical Society*, vol. 59, no. 1, pp. 2279–2283, 2014.

[29] D. Allouss, Y. Essamlali, A. Chakir, S. Khadhar, and M. Zahouily, "Effective removal of Cu (II) from aqueous solution over graphene oxide encapsulated carboxymethylcellulose-alginate hydrogel microspheres: towards real wastewater treatment plants," *Environmental Science and Pollution Research*, vol. 27, no. 7, pp. 7476–7492, 2020.

[30] P. Jantrawut, J. Bunrueangtha, J. Suerthong, and N. Kantrong, "Fabrication and characterization of low methoxyl pectin/gelatin/carboxymethyl cellulose absorbent hydrogel film for wound dressing applications," *Materials*, vol. 12, no. 10, p. 1628, 2019.

[31] S. Esteghlal, M. Niakousari, and S. M. H. Hosseini, "Physical and mechanical properties of gelatin-CMC composite films under the influence of electrostatic interactions," *International Journal of Biological Macromolecules*, vol. 114, pp. 1–9, 2018.

[32] V. Singh and S. Ahmad, "Carboxymethyl cellulose-gelatin-silica nanohybrid: an efficient carrier matrix for alpha amylase," *International Journal of Biological Macromolecules*, vol. 67, pp. 439–445, 2014.

[33] N. Nazmi, M. Isa, and N. Sarbon, "Preparation and characterization of chicken skin gelatin/CMC composite film as compared to bovine gelatin film," *Food Bioscience*, vol. 19, pp. 149–155, 2017.

[34] L. Sun, Y. Huang, Z. Bian et al., "Sundew-inspired adhesive hydrogels combined with adipose-derived stem cells for wound healing," *ACS Applied Materials & Interfaces*, vol. 8, no. 3, pp. 2423–2434, 2016.

[35] L. Zhao, L. Niu, H. Liang, H. Tan, C. Liu, and F. Zhu, "pH and glucose dual-responsive injectable hydrogels with insulin and fibroblasts as bioactive dressings for diabetic wound healing," *ACS Applied Materials & Interfaces*, vol. 9, no. 43, pp. 37563–37574, 2017.

[36] A. K. Clark, K. N. Haas, and R. K. Sivamani, "Edible plants and their influence on the gut microbiome and acne," *International Journal of Molecular Sciences*, vol. 18, no. 5, p. 1070, 2017.

Hindawi
Oxidative Medicine and Cellular Longevity
Volume 2021, Article ID 2060288, 13 pages
https://doi.org/10.1155/2021/2060288

Research Article

Phototoxicity of Ultraviolet-A against the Whitefly *Bemisia tabaci* and Its Compatibility with an Entomopathogenic Fungus and Whitefly Parasitoid

Muhammad Musa Khan,[1,2] **Ze-Yun Fan**,[1,3] **Dylan O'Neill Rothenberg**,[4] **Jing Peng**,[1] **Muhammad Hafeez**,[5] **Xin-Yi Chen**,[1] **Hui-Peng Pan**,[1,2,3] **Jian-Hui Wu**,[1,2,3] **and Bao-Li Qiu**[1,2,3]

[1]*Key Laboratory of Bio-Pesticide Innovation and Application of Guangdong Province, South China Agricultural University, Guangzhou 510642, China*
[2]*Engineering Research Center of Biocontrol, Ministry of Education Guangdong Province, Guangzhou 510640, China*
[3]*Guangdong Laboratory for Lingnan Modern Agriculture, Guangzhou 510640, China*
[4]*College of Horticulture, South China Agricultural University, Guangzhou 510642, China*
[5]*State Key Laboratory Breeding Base for Zhejiang Sustainable Pest and Disease Control, Institute of Plant Protection and Microbiology, Zhejiang Academy of Agricultural Sciences, Hangzhou 310021, China*

Correspondence should be addressed to Muhammad Musa Khan; drmusakhan@outlook.com and Bao-Li Qiu; baileyqiu@scau.edu.cn

Received 20 April 2021; Accepted 9 June 2021; Published 12 July 2021

Academic Editor: Daoud Ali

Ultraviolet (UV) radiation significantly affects insect life and, as a result, has been widely used to control different invertebrate pests. The current results demonstrate that when *Bemisia tabaci* first instar nymphs are exposed to UV-A light for 12, 24, 48, and 72 h, their developmental and biological parameters are negatively affected by UV-A exposure; the effect increased with an increase in exposure time. We hypothesized that UV-A light is compatible with other biological control agents. Results showed that when the entomopathogenic fungus *Cordyceps fumosorosea* was applied to third instar nymphs of *B. tabaci* previously exposed to UV-A light, the LC_{50} was 3.4% lower after 72 h of exposure to UV-A light compared to the control. However, when the fungus was exposed to UV-A light, its virulence decreased with an increase in UV-A exposure time. The parasitism rate of *Encarsia formosa* against 24 h UV-A-exposed third instar nymphs of *B. tabaci* increased while the adult emergence from parasitized nymphs was not affected after UV-A light exposure. Parasitism rate was significantly reduced however following *E. formosa* exposure to UV-A light; but again, adult emergence was not affected from parasitized nymphs. The percentage mortality of *E. formosa* increased with increasing exposure time to UV-A light. The enzyme activity of SOD, CAT, GST, and AChE and the energy reserve contents were negatively affected due to UV-A exposure. Collectively, this study has demonstrated that UV-A light significantly suppresses the immune system of *B. tabaci* and that UV-A light is compatible with other biological control agents if it is applied separately from the biological agent.

1. Introduction

Climate change can have various effects on abiotic stress. As a result, it poses a threat to agricultural systems' long-term viability and productivity. Stress factors, both abiotic and biotic, also play an important role in the life of an insect. There are numerous environmental stresses, such as ozone depletion, increased ultraviolet irradiation, biodiversity destruction, and temperature that impact insects. For many organisms, ultraviolet (UV) radiation is a significant source of stress [1]. UV radiation is currently attracting much attention due to its potentially harmful effects on a variety of species. UV

radiation is generally considered a resilient ecological stressor for biological entities [2]. It may damage nucleic acids, membrane fatty acids, and various amino acids [3, 4], resulting in cell toxicity, genetic modifications, and cell signaling pathway modifications [5]. UV exposure shortens an insects' adult lifespan, increases oviposition rate, and reduces fertility [6, 7]. UV causes the development of reactive oxygen species (ROS), which can damage nucleic acids, membrane lipids, and proteins [4]. These various types of molecule damage have significant biological consequences, such as genetic variation, cytotoxicity, and signaling cell pathway transformation [5].

The whitefly, *Bemisia tabaci*, is a key pest of many greenhouse vegetables, ornamentals, and also field crops worldwide since the midseventies [8]. This whitefly is polyphagous and leads to serious economic losses [9]. The damage to crops is manifold; the feeding of *B. tabaci* causes direct damage to plant foliage. In China, for example, *B. tabaci* MEAM1 is well distributed across 31 provinces or municipalities and causes significant economic losses [10]. Adult and immature whitefly are phloem feeders [11]. Furthermore, *B. tabaci* acts as a vector of around 150 plant viruses [12].

Insecticides have been the mainstay of controlling *B. tabaci* in diverse agricultural production systems. Resistance to insecticides resulting in loss of efficacy of many older insecticides has placed excessive pressure on novel products. Alternative control strategies now have a key role in controlling *B. tabaci* and managing pesticide resistance development. Using biological agents is not only environmentally safe but can also have a significant impact on whitefly management practices. To date, more than 20 species of entomopathogenic fungi are known to infect whitefly. Among these, the entomopathogenic fungus, *Cordyceps fumosorosea* Zare and Gams (Hyphomycetes), formerly known as *Isaria fumosorosea*, designated as Cordyceps clade [13], is a well-known fungal species used for whitefly management and has been widely studied [14–17]. *C. fumosorosea*-based formulations have been commercially available since the 1990s for the management of whitefly [18, 19]. *Encarsia formosa* Gahan (Hymenoptera: Aphelinidae) also plays an important role in managing *B. tabaci* [20, 21]. *E. formosa* is a solitary endoparasitoid that is commercially used as a biocontrol agent for *B. tabaci* [22, 23]. *E. formosa* kills 75% of its whitefly host by probing nymphs with its ovipositor and depositing eggs in their bodies. Larvae of *E. formosa* then feed on the parasitized whitefly internal contents, eating all the organs and leaving only the outer armor in which they pupate from afterwards [24].

UV radiation and other abiotic stressors have a major impact on insect life because they increase the development and accumulation of reactive oxygen species (ROS). These oxygen free radicals increase both the antioxidant potential and oxidant development of cells. They are not harmful at low concentrations and play important roles in cell signaling and defense [25–27]. Multiple biochemical pathways contain carbohydrates, proteins, and lipids as an end product in the energy metabolism of insects [28]. Different physiological processes such as synaptic transmission, morphogenetic behaviors, phospholipid synthesis, sexual maturation, and egg development may be influenced by these carbohydrates, proteins, and lipids (which serve as insect primary energy sources) [29, 30]. As both biological control agents and insect pests share a common habitat [31], it is obvious that the application of UV light has the potential to affect other natural whitefly controlling measures.

The current study was designed to examine the effectiveness of UV-A irradiation against *B. tabaci* by evaluating both biological and physiological parameters. The risks posed to the entomopathogenic fungus and the whitefly parasitoid by UV-A light were also assessed by evaluating the pathogenicity and percentage parasitism, respectively.

2. Materials and Methods

2.1. Insects, Plants, and Entomopathogenic Fungus. *Gossypium hirsutum* L. (cotton plants) were raised under glasshouse conditions at South China Agricultural University (SCAU), Guangzhou, in 15 cm diameter plastic pots containing a mixture of soil consisting of 5% clay, 85% peat, and 10% sand to reach the 7–8 expanding leaf stage. Two symmetrical, completely expanded leaves of identical size were used in all experimental replications.

The silverleaf whitefly, *B. tabaci* Middle East-Asia Minor 1 (formerly known as *B. tabaci* B biotype), was the *B. tabaci* species used in this study. Different cotton leaves were caged, and 60 pairs of the whitefly were released into the cage for egg-laying to occur for 24 hours. The adults of the whitefly were then removed after 24 hours, and the plants were kept at a temperature of $26 \pm 1°C$, relative humidity of 60%, and photoperiod of 14 : 10 (L : D) in an iron-framed and plastic sieve cage ($60 \times 60 \times 60$ cm) to allow for whitefly development as outlined by Ou et al. [32] (Figure S1).

In 2015, *E. formosa* was obtained from the Chinese Academy of Agricultural Sciences, Institute of Plant Protection. Under laboratory conditions at SCAU, the parasitoid population was reared at the temperature of $26 \pm 1°C$, relative humidity of 60%, and a photoperiod of 14 : 10 (L : D) on cotton plants containing third instar whitefly nymphs placed in an iron-framed and plastic sieve cage ($60 \times 60 \times 60$ cm) as outlined by Ou et al. [32].

C. fumosorosea isolate SP535 was originally isolated from soil obtained from the repository of the Key Laboratory of Biopesticides Innovation and Application of Guangdong Province, SCAU. Potato Dextrose Agar (PDA) media was used to maintain the fungal culture (200 g potatoes, 20 g dextrose, and 20 g agar in 1 L of distilled water) in a glass dish (90 mm Ø) for three weeks under dark conditions at $25 \pm 2°C$. The methodology followed for maintaining the experimental materials was as outlined by Ou et al. [32].

2.2. UV-A Irradiation Source. A UV-A irradiation source of 15 W power with 360 nm wavelength was used during the experimentation. The UV-A light source was purchased from

Shenzhen Guanhongya Photoelectronic Technology Co. Ltd. (Shenzhen, China).

2.3. Effect of UV-A Light on Whitefly Development and Biology. To assess the effect of UV-A on the developmental period and other life table parameters of *B. tabaci*, first instar nymphs of *B. tabaci* were used. To obtain a homogeneous first instar nymphal population, cotton plants at the 6-8 expanded leaf stage were used. Leaves were caged, and whitefly adults were released for egg-laying for 24 hours. After removing the adult whiteflies, the plants were kept at 26 ± 1°C and 16 : 8 (L : D) photoperiod for 5-7 days. After the emergence of 80% of first instar nymphs, they were then exposed to UV-A light. A plant containing first instar nymphs was kept under dark conditions before being exposed to UV-A light. The plants containing the first instar nymphs of *B. tabaci* were exposed to UV-A light for 12, 24, 48, and 72 hours. Similar infested plants which were not exposed to UV light acted as controls. The distance between the UV-light source and the leaf containing the first instar nymphs of *B. tabaci* was approximately 50 cm. After exposure of 12, 24, 48, and 72 hours, the plants were exposed to normal light. As nymphs reached the second instar, 90 of them were marked on a leaf with each nymph being given a specific number to aid identification. Each marked nymph was taken as a single replication. Individuals were observed each day, and their current instar was recorded until the nymph either developed into an adult or died. Each emerged female was paired with an emerged male from the same treatment and kept in a small petri dish (3 cm) containing agar gel and a (2 cm) cotton leaf disk. The petri dish was observed daily to calculate fecundity and the number of days of female longevity. A new leaf disk was provided daily to avoid the risk of starvation. The remaining males were kept in a petri dish with agar and cotton leaf disk separately to assess their longevity.

2.4. Effect of UV-A Light on Enzyme Activity and Energy Reserves. *B. tabaci* adults were exposed to UV-A light for 0 (control), 12, 24, 48, and 72 hours. One hundred and fifty adults per treatment per replication were collected. Three technical and three biological replications were established. Collected samples were weighed before homogenization. The total protein content of supernatants from the insect homogenates was determined using bovine albumin serum (BSA) as a norm, as described by Nazir et al. [33].

Adult *B. tabaci* was homogenized with ice-cold 0.05 M sodium phosphate buffer at room temperature (pH 7.3). At 4°C, the homogenized samples were centrifuged for 10 minutes at 12,000 rpm (rotation per minute). The supernatant was collected and moved to new tubes and centrifuged for 15 minutes at 4°C at 12,000 rpm. For the various enzyme assays, the final supernatants were used for enzyme preparation. Antioxidant enzyme (SOD, POD, CAT, and PPO) and detoxification enzyme (AChE, GST, and P450) activity was determined by the commercially available kits purchased from Nanjing Jiancheng Bioengineering Research Institute. The method followed was as per the instructions provided by the manufacturer.

To estimate the whitefly energy reserve contents after exposure to UV-A light, adults were again exposed to UV-A light as outlined above, and samples were collected. The whole bodies of adult *B. tabaci* were homogenized in sodium phosphate buffer pH 7.0. The samples were then centrifuged at 4°C for 10 minutes at 10,000 rpm. The collected supernatants were used in further experimentation. For the estimation of energy reserves, commercially available kits to determine cholesterol, glycogen, and triglyceride were purchased from Solarbio Life Science, Beijing, China. The method followed was as per the instructions provided by the manufacturer.

2.5. Effect of UV-A Light on the Virulence of C. fumosorosea against B. tabaci. To determine the virulence of *C. fumosorosea* against *B. tabaci*, the progressive concentrations were prepared until the mortality ranged between 10 and 95%. The leaf dip application method was used as outlined by Nazir et al. [33]. In a 250 mL reagent container, a stock suspension of conidia was made containing 100 mL distilled water and 0.05% (*v*/*v*) Tween 80® by adding the mass sporulating culture. The mixture was shaken vigorously to isolate spores from the hyphal debris. The conidial concentration was determined using an improved Neubauer hemocytometer (Brand GmbH, Wertheim, Germany). The conidial suspensions were diluted in sterilized water containing 0.05% Tween 80 in five separate suspensions (i.e., 1×10^8, 1×10^7, 1×10^6, 1×10^5, and 1×10^4 conidia mL^{-1}). Distilled water containing Tween 80 at 0.05% was used as control. Plants at 7-8 extended leaf stage containing third instar nymphs were used in this experiment. A germination test was performed on a PDA medium before performing bioassays against the whitefly to determine the percentage of viable conidia [34]. Conidial germination was greater than 95% in all bioassays. Plants containing third instar nymphs were kept in the dark for 2 hours and then exposed for 0 (control), 12, 24, 48, and 72 hours to UV-A light. Leaves were dipped into conidial suspensions for 10 seconds and then air-dried on tissue paper for 15 min at room temperature. Each leaf contained 20 third instar nymphs per treatment per replication. Whitefly mortality was recorded after five days of fungal application. The leaves were plucked and placed on Petri plates containing agar gel to maintain leaf moisture and were kept under dark conditions at relative humidity of 90% to stimulate fungal growth to confirm the whitefly mortality due to fungal infection. Percentage mortality was calculated by using the Abbott formula [35].

To assess the effect of UV-A light on the fungus, the fungal culture was exposed to UV-A light for 12, 24, 48, and 72 h. The fungal culture plates were placed in an environmental chamber under dark conditions, and an external UV-A light source was used to expose the fungi. After exposure, treatment with the conidial suspension was undertaken by the method outlined above.

2.6. Effect of UV-A Light on Parasitism of E. formosa against B. tabaci. To determine the effect of UV-A light on the parasitism of *E. formosa*, cotton plants containing third

Table 1: Effect of UV-A light exposure on the developmental period (mean ± SE) of preadult stages of whitefly *Bemisia tabaci*.

Treatments	The development period of immature stages			
	1st instar (d)	2nd instar (d)	3rd instar (d)	4th instar (d)
Control	5.8 ± 0.1^{a}	2.3 ± 0.1^{a}	3.1 ± 0.1^{a}	2.7 ± 0.1^{a}
12 hours	5.4 ± 0.1^{ab}	2.3 ± 0.1^{ab}	2.9 ± 0.1^{ab}	2.1 ± 0.1^{ab}
24 hours	5.3 ± 0.1^{b}	2.0 ± 0.1^{bc}	2.8 ± 0.1^{ab}	1.9 ± 0.1^{b}
48 hours	5.2 ± 0.1^{bc}	1.9 ± 0.1^{c}	2.6 ± 0.1^{b}	1.8 ± 0.1^{b}
72 hours	4.8 ± 0.1^{c}	1.7 ± 0.1^{c}	2.6 ± 0.1^{b}	1.9 ± 0.1^{b}

The same lowercase letters in the same column are not significantly different based on the paired bootstrap test at the 5% significance level. Ninety nymphs were used for each treatment. d = days.

instar nymphs of *B. tabaci* (<24 h old) were prepared as outlined above. This experiment was divided into two different parts: (1) whitefly was exposed to UV-A light, and then, *E. formosa* was released; and (2) *E. formosa* was exposed to UV-A light and then released onto the whitefly nymphs.

For the first part, cotton plants containing third instar nymphs of whitefly were exposed to UV-A light for 0 (control), 12, 24, 48, and 72 h. Two hundred third instar nymphs (<24 h old) were kept on the leaf, and the remaining nymphs were removed from the leaf using a camel hairbrush. Leaves were caged as shown in Figure S1, and the unexposed parasitoid (<24 h old) with a ratio of 1 : 20 (parasitoid : nymphs) was released into the cages for 24 hours. Each treatment was replicated three times. The number of parasitized nymphs was recorded after ten days. The nymphs that turned brown were considered parasitized. Percentage emergence was then determined by caging the leaves for more than five days. After five days, cages were removed, and the number of emerged adults of *E. formosa* was counted and recorded. Percentage emergence was determined by using the following formula:

$$\text{Percentage Emergence} = \frac{\text{Number of parasitoids emerged from parasitized nymphs}}{\text{Total number of parasitized nymphs}} \times 100. \quad (1)$$

For the second part, the same procedure as outlined above was followed except with the difference that *E. formosa* (<24 h old) were exposed to UV-A light for 0 (control), 12, 24, 48, and 72 h and then released onto third instar nymphs of *B. tabaci*.

2.7. Statistical Analysis. The development time of different stages, the survival rate of different stages, the fecundity off, and female whitefly preoviposition duration and adult longevity were all studied using the age-stage two-sex life table model [36, 37]. TWOSEX-MS Chart program was downloaded from the website http://140.120.197.173/Ecology/prod02.htm [38]. Using 100,000 bootstrap replicates, standard errors (SE) and means were measured [40, 41]. In the TWOSEX-MS Chart, the paired bootstrap method was used to compare all treatments [39].

The software PoloPlus (Version: 1.0 (Pacific Southwest Forest and Range Experiment Station, Berkeley, California, USA)) was used to calculate LC_{50} of *C. fumosorosea* against *B. tabaci*. The data of mortality in replications were subjected to test the hypothesis of equality and parallelism via PoloPlus by following the method described by Chang and He [41]. To analyze the parasitism rate among the treatments and enzymatic activity, one-way ANOVA, along with the Tukey post hoc test at $P < 0.05$, was used to compare the means via SPSS. SigmaPlot 12.0 was used to form graphical work for all parameters. Correlation of enzymatic activity and energy reserves with exposure time to UV-A light was calculated via RStudio v1.3.1056 software with the corrplot package.

3. Results

3.1. Effect of UV-A Light on the Development, Growth, and Dimorphic Parameters of B. tabaci. The effect of UV-A light on the development period of the preadult stages of *B. tabaci* is shown in Table 1. The presented results demonstrate that the developmental period of the first, second, third, and fourth instars was significantly reduced with increasing UV-A exposure time. The male and female longevity was also reduced at 24, 48, and 72 hours of exposure compared to controls. The APOP (adult preoviposition) was not significantly affected by the UV-A light exposure; the TPOP (total preoviposition period) was significantly reduced at 48 and 72 hours of exposure to UV-A light as compared to the control. Following 72 hours of UV-A exposure also significantly reduced the total fecundity of *B. tabaci*.

Similarly, results also showed that the fecundity was significantly reduced with the increasing trend of UV-A light exposure compared to the control (Table 2). The effect of UV-A light on the population growth of *B. tabaci* is given in (Table S1). Results show that r (intrinsic rate of increase) and λ (finite rate of increase) were not affected due to UV-A light exposure. At the same time, R_0 (net reproductive rate) was negatively affected by UV-A light exposure after 48 and 72 h. More exposure time lessened the net reproductive rate as compared to the control. The mean generation time was significantly reduced due to UV-A light exposure after 72 hours compared to the control.

The S_{xj} (survival rate of the specific stage) value was reduced in UV-A-exposed *B. tabaci*. The survival rate of

Table 2: Effect of UV-A light exposure on the life parameters (mean ± SE) of *Bemisia tabaci* adults exposed at the nymphal stage.

Treatments	Female adult longevity (d)	Male adult longevity (d)	APOP (d)	TPOP (d)	Fecundity (eggs/female)
Control	33.0 ± 0.5^{a}	30.4 ± 0.4^{a}	1.7 ± 0.1^{a}	19.6 ± 1.2^{a}	217.0 ± 14.7^{a}
12 hours	31.0 ± 0.4^{a}	29.1 ± 0.4^{a}	1.6 ± 0.1^{a}	17.9 ± 0.4^{b}	180.9 ± 9.3^{b}
24 hours	29.4 ± 0.4^{b}	26.9 ± 0.6^{b}	2.1 ± 0.1^{a}	18.6 ± 0.3^{a}	134.5 ± 9.7^{c}
48 hours	26.8 ± 0.5^{b}	25.7 ± 0.6^{b}	2.1 ± 0.2^{a}	17.4 ± 0.4^{b}	105.5 ± 9.9^{d}
72 hours	23.8 ± 0.6^{c}	23.5 ± 0.4^{c}	1.8 ± 0.2^{a}	16.8 ± 0.3^{c}	87.26 ± 7.2^{e}

The same lowercase letters in the same column are not significantly different based on the paired bootstrap test at the 5% significance level. Ninety nymphs were used for each treatment. d = days.

females and males in controls was observed to be 35 and 33 days, 33 and 36 days after 12 hours of exposure, 34 and 34 days after 24 hours of exposure, 30 and 33 days after 48 hours of exposure, and 27 and 33 days after 72 hours of exposure, respectively. Results showed that UV-A light exposure significantly reduced male and female survival rates (Figure S2).

Results for l_x (survival rate of the specific stage), f_x (fecundity of specific age stage), m_x (overall population fecundity), and $l_x m_x$ (total maternity) are shown in Figure S3. The S_{xj} curves are expressed by l_x, which is a simple form of the S_{xj} curves. The results showed that as UV-A light exposure time increased, the survival rate decreased, affecting other reproductive parameters. As the survival curve started to reduce with time, f_x, m_x, and $l_x m_x$ also reduced. In addition, the fecundity value was also reduced in line with a reducing survival rate.

Results of E_{xj} showed that due to UV-A light exposure, the female life expectancy was significantly reduced compared to male life expectancy. In the controls, the life expectancy of females and males was observed at 36.04 and 34 days, respectively. When nymphs were exposed to UV-A light, the male life expectancy after 12, 24, 48, and 72 hours was 34.00, 32.87, 33.89, and 32.99 days, respectively, which was not significantly altered following UV-A exposure. In comparison, a significant reduction in female life expectancy following 12, 24, 48, and 72 hours of exposure was observed: 35.92, 34.00, 30.06, and 27.01 days, respectively (Figure S4).

Results of V_{xj} (reproduction of a specific stage) show how each individual fits into the next population. Results (Figure S5) showed that on the 25th day, the maximum female reproductive value (106.85) was observed. After exposure to UV-A light for 12, 24, 48, and 72 hours, the reproductive value V_{xj} was 84.39 on the 19th day, 72.43 on the 19th day, 60.99 on the 18th day, and 52.69 on the 15th day, respectively. Results showed that UV-A light exposure not only reduced the duration of reproduction but also reduced age-specific reproduction.

3.2. Effect of UV-A Light Exposure on the Enzyme Activity and Energy Reserve Contents of B. tabaci. The enzymatic analysis showed that following exposure to UV-A light, a significant reduction in enzyme activity was observed in the exposed treatments compared to the control. The activity of SOD, POD, PPO, GST, and cytochrome P450 and contents of glycogen, triglyceride, and total cholesterol were continuously reduced as the UV-A light exposure time increased. At the same time, no significant effect was observed in CAT and AChE enzyme activity (Figures 1).

Results of correlation analysis (Figure 2) of different oxidative and detoxification enzyme activity and energy reserves with UV-A light exposure time demonstrated that, except for PPO, POD, and P450 enzyme activity, all other enzymes had a significant negative correlation with exposure time. These results showed that UV-A light exposure caused depletion of different enzyme activity as the exposure time increased.

3.3. Effect of UV-A Light on the Virulence of C. fumosorosea against B. tabaci. The results of the virulence of *C. fumosorosea* against *B. tabaci* are shown in Table 3. The virulence assessment bioassay showed that LC_{50} in the control (without UV-A exposure) was 2.1×10^5 conidia mL^{-1} (4.5×10^4 -6.7×10^5; $\chi^2 = 1.69$; $P = 0.564$). As the exposure time of UV-A light increased, the LC_{50} concentration decreased. The maximum percentage mortality was recorded in the treatment where 1×10^8 conidial suspension was applied onto 72 hours of UV-A light-exposed nymphs.

When the fungus was exposed to UV-A light for different time periods, the results showed that with an increase in exposure time, the LC_{50} also increased. The virulence assessment showed that LC_{50} in the control (without UV-A exposure) was 2.3×10^6 and after 72 hours of exposure was 5.9×10^8. The maximum percentage mortality was observed where third instar nymphs of *B. tabaci* were treated with 1×10^8 conidial suspension exposed to UV-A light for 12 hours.

3.4. Effect of UV-A Light on Parasitism of E. formosa against B. tabaci. B. tabaci third instar nymphs firstly exposed to UV-A light and then exposed to *E. formosa* to assess percentage parasitism showed (Figure 3) that the nymphs exposed 24 hours to UV-A light were parasitized more than the 12, 48, and 72 hours of exposures ($F_{4,14} = 3.82$; $P < 0.05$). The results showed that UV-A light weakened the nymphs of *B. tabaci* so aiding *E. formosa* to parasitize more. The resulting percentage emergence was not significantly affected. However, when *E. formosa* was exposed to UV-A light, its parasitic ability was significantly reduced compared to the control ($F_{4,14} = 15.2$; $P < 0.01$) (Figure 3(a)). The percentage of adult emergence of *E. formosa* emerging from parasitized nymphs was the same in the control and UV-A light-exposed nymphs ($F_{4,14} = 1.71$; $P > 0.05$). In addition, the percentage of adult emergence was also significantly reduced when the parasitoid was exposed to UV-A light as compared to that in the control ($F_{4,14} = 13.3$; $P > 0.05$) (Figure 3(b)).

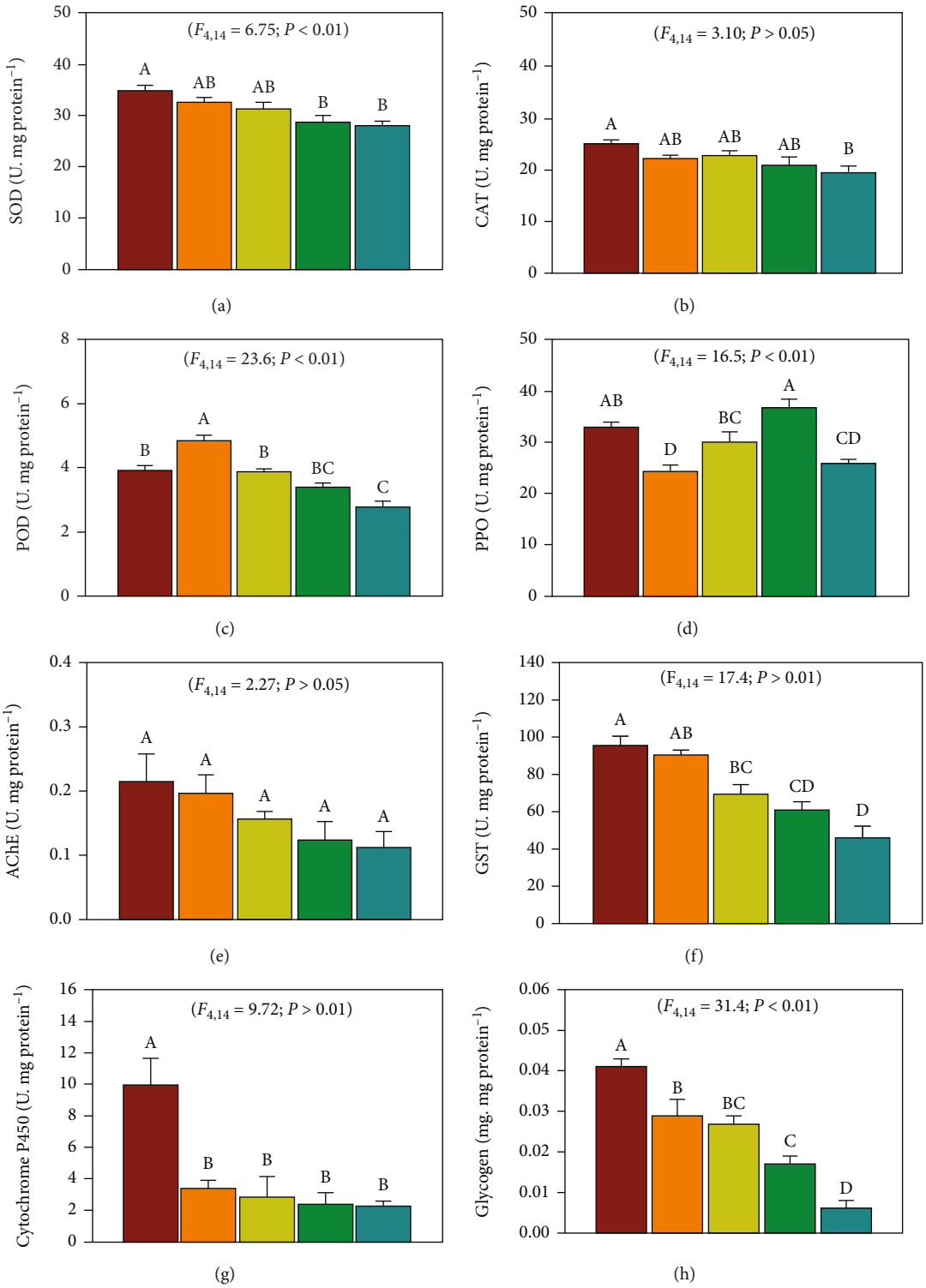

Figure 1: Continued.

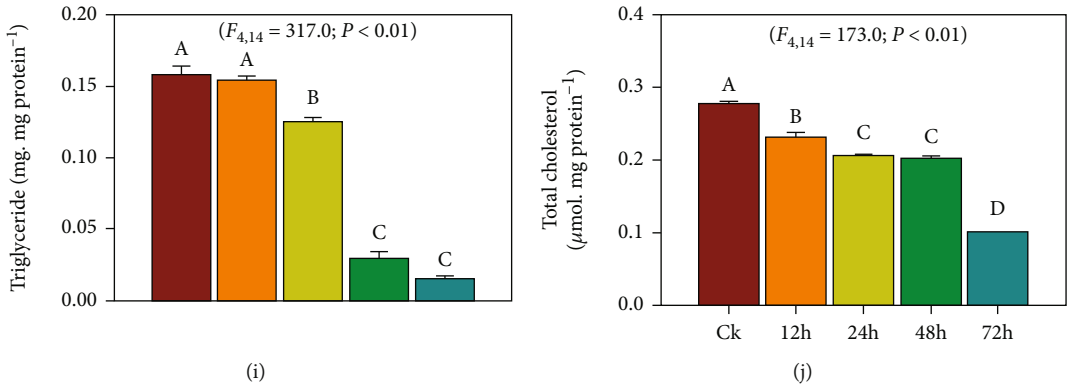

Figure 1: The activity of different enzymes (a) SOD, (b) CAT, (c) POD, (d) PPO, (e) AChE, (f) GST, and (g) cytochrome P450 and contents of different energy reserves (h) glycogen, (i) triglyceride, and (j) total cholesterol of *Bemisia tabaci* exposed to UV-A light for control (0 h), 12 h, 24 h, 48 h, and 72 hours. The bars are showing the mean value of three replications. Standard error bars are showing the standard deviation of the mean. Lowercase lettering is showing the significance among the treatments at $P < 0.05$. Similar letters have no significant difference among the treatments.

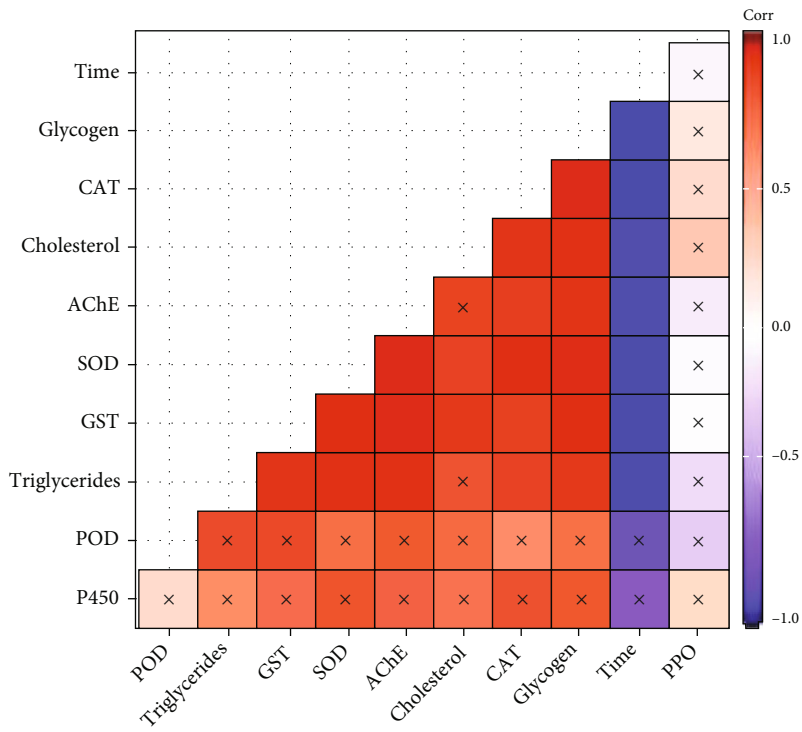

Figure 2: Correlation matrix of UV-A light exposure time and enzyme activity and energy parameters of *Bemisia tabaci*. The intensity of color shows the correlation's strength, while the cross sign shows a nonsignificant correlation at $P < 0.05$.

During the experimentation, it was observed that *E. formosa* is sensitive to UV-A light. A significant number of *E. formosa* adults exposed to UV-A light simply died. So, to assess the survival rate of *E. formosa*, adults were exposed to UV-A light for 12, 24, 48, and 72 hours. Results showed that as the UV-A exposure time increased, the survival percentage significantly decreased, which showed that UV-A light is lethal for *E. formosa* and so both could not be used together to control *B. tabaci* (Figure 3(c)).

All the results provide a model that demonstrates UV-A light can be an effective tool to control *B. tabaci*. UV-A light and biological control agents of *B. tabaci* could be used together if the UV-A light is applied to the whiteflies before applying the biological control agent. Exposure to UV-A light seriously affected the effectiveness of the biological control agents investigated (Figure 4).

4. Discussion

The current study has demonstrated that due to UV-A light exposure, the nymphal developmental period, preoviposition period, fecundity, female longevity, and other dimorphic

Table 3: LC_{50} of *Cordyceps fumosorosea* against *Bemisia tabaci*.

	Treatment	LC_{50}	Limit (95% C.I.)	Slope ± SE	Chi-square	*P* value (df)
B. tabaci exposed to UV-A light	Control	2.1×10^5	4.5×10^4-6.7×10^5	0.302 ± 0.06	1.69	0.56 (3)
	12 hours	3.4×10^4	9.4×10^3-8.4×10^4	0.466 ± 0.06	2.94	0.98 (3)
	24 hours	3.3×10^4	7.7×10^3-8.7×10^4	0.425 ± 0.06	1.67	0.56 (3)
	48 hours	9.4×10^3	1.2×10^3-3.3×10^4	0.410 ± 0.07	0.98	0.34 (3)
	72 hours	7.3×10^3	1.3×10^3-2.1×10^4	0.508 ± 0.08	1.79	0.60 (3)
C. fumosorosea exposed to UV-A light	Control	2.3×10^6	7.6×10^5-6.2×10^6	0.392 ± 0.06	1.43	0.47 (3)
	12 hours	1.2×10^7	4.6×10^6-3.3×10^7	0.371 ± 0.06	0.81	0.27 (3)
	24 hours	5.6×10^6	9.7×10^5-2.5×10^7	0.237 ± 0.05	2.49	0.83 (3)
	48 hours	3.6×10^7	6.8×10^5-4.4×10^8	0.210 ± 0.05	0.43	0.14 (3)
	72 hours	5.9×10^8	9.4×10^7-4.4×10^{10}	0.225 ± 0.06	0.40	0.13 (3)

SE = standard deviation of the slope; df = degree of freedom; C.I. = confidence.

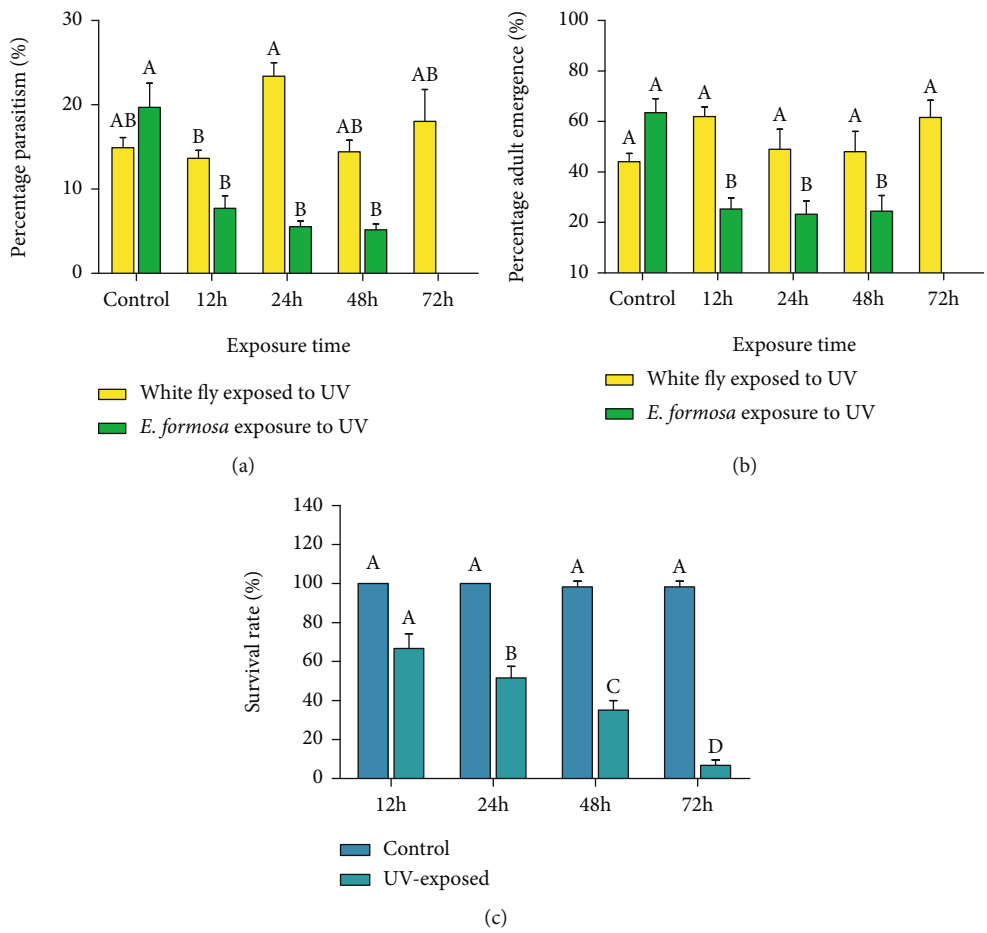

Figure 3: (a) Percentage parasitism, (b) percentage adult emergence, and (c) percentage survival of *Encarsia formosa* exposed to UV-A light for control (0 h), 12 h, 24 h, 48 h, and 72 h. Bars are showing the mean of three replications. Error bars are showing the mean deviation. Lowercase lettering is showing statistically significant differences among different treatments ($P < 0.05$). Similar lettering has no significant difference. Error bars are showing mean deviation.

parameters of *B. tabaci* were significantly affected. Results also showed that survival rate, reproduction rate, and life expectancy also reduced with increased UV-A exposure duration. Our present results coincide with Ali et al. [42] who reported that due to UV-A light exposure, the developmental period of immature stages of *Mythimna separata* (eggs, larvae, and pupa) declined with increased exposure time. The male and female longevity was also reported to

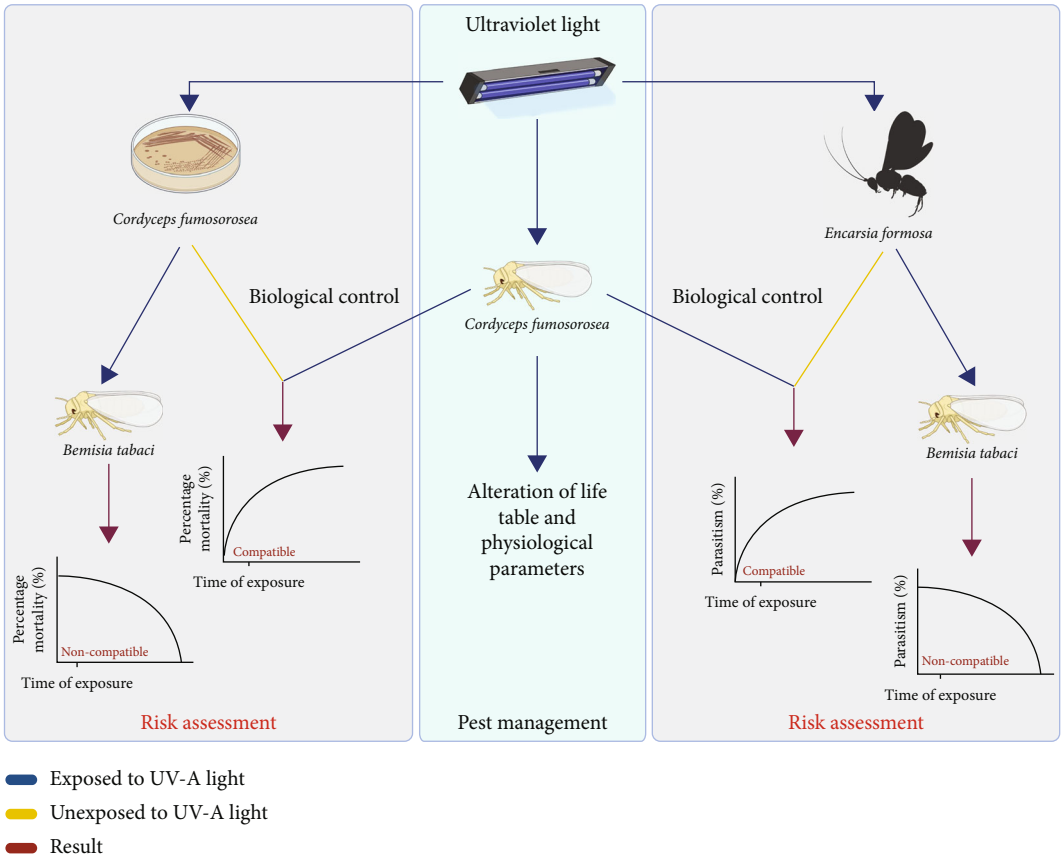

Figure 4: Schematic diagram of a model using UV-A light as a tool to control *Bemisia tabaci* and compatibility with other biological control agents.

decrease with an increase in exposure time. Similarly, Tariq et al. [23] experimented by exposing *Dialeurodes citri* to UV-A light and reported a significantly shorter developmental time of *D. citri* immatures (nymphs and pupa) in the F1 generation after adults were exposed to UV-A light. However, both male and female longevity was significantly reduced with exposure time. Zhang et al. [7] also reported an increase in the immature development period of *Helicoverpa armigera* along with a decrease in male and female longevity as UV exposure time increased. All the stated results confirm that UV-A exposure can significantly affect an insect's developmental period, but the cause of this change in the developmental period is still unknown.

Different antioxidants are in a complex equilibrium state within an insect species in normal circumstances in order to maintain normal physiological activities. Insects have also developed a complex network of antioxidant enzyme systems [43] and detoxification enzymes [44] to fight against the risk of oxidative stress. In the current study, we observed that due to UV-A light exposure, SOD, POD, and PPO activity was significantly affected. Moreover, the activity of detoxification enzymes was also affected due to UV-A exposure. Many previous studies reported the alteration of enzyme activity when exposed to UV irradiation. Ali et al. [45] reported that UV-A exposure caused oxidative stress in *M. separata* and altered antioxidant enzymes' activity. Zhou et al. [46] exposed grain aphid *Sitobion avenae* to UV-B radiation and reported that the antioxidant enzymes SOD, POD, and CAT were significantly affected. UV exposure resulted in more than 90% reduction in PPO activity after 5 minutes of exposure [47]; when *Dendrolimus tabulaeformis* were exposed to UV-A light, elevated oxidative stress and disturbed physiological detoxification were recorded [44]. The current study showed that due to UV-A light exposure, a significant decrease in the contents of energy-providing compounds like glycogen, triglyceride, and total cholesterol was observed. It is a basic life history theory that reproduction always costs survival [48]. These two processes share the energy to maintain normal biological function under UV stress [42]. After exposure to UV light, a reduction in these energy reserves justifies a reduction in reproduction and longevity of *B. tabaci*. However, there is no study available to justify reducing energy reserves due to UV-light exposure; only Ohkawara et al. [49, 50] reported reducing glycogen in humans and minipigs due to UV exposure.

A previous study showed that *C. fumosorosea* (formerly *I. fumosorosea*) is an effective biological control agent against *B. tabaci*, not only being a mycoinsecticide but also in that it exerts oxidative stress in *B. tabaci* [51]. Santos et al., Wang et al., and Zou et al. [52–54] described that *C. fumosorosea* is a very efficient and environmentally safe control agent for *B. tabaci*. However, exposure to solar radiation can strongly

affect conidial development, survival, dispersion, dissemination, germination, pathogenesis, and virulence, although its effects often vary from species to species [55–64].

The current study showed that due to UV-A light exposure to *B. tabaci*, the parasitism rate by *E. formosa* was increased, but the percentage emergence of parasitoids was not affected. Cochard et al. [65] exposed *Aphidius ervi* to UV and reported that due to UV-light exposure, a significant change in parasitism by *A. ervi* was noted, but adult emergence remained unaffected. Our results also showed that UV-A light exposure decreased the parasitism of *E. formosa* and also caused mortality in *E. formosa*. It has been reported that UV-light exposure significantly reduced the parasitism of *Trichogramma cacoeciae*, an egg parasitoid of *Lobesia botrana* [66]. Indeed, many studies report the toxicity of UV light against different insects [67–71]. Due to cascading effects in the food chain, insects higher up in the food chain are thought to be affected more by environmental stress than those at lower levels. As a result, a change in parasitism rate could be described as an instant stress response [72–74]. The factors that influence parasitoid species composition are difficult to identify, and the reasons why some species react to stress more effectively than others have remained unclear [75].

Due to exposure to high-intensity light or UV light, plants usually respond by producing ROS (reactive oxygen species), which has already been reported as a defense against diseases and pests [76]. The abrupt accumulation of hydrogen peroxide on the pathogen target site makes it toxic for pathogens [77]. ROS is also involved in triggering signaling pathways responsible for the activation of defense mechanisms, for example, the production of secondary metabolites, which are defense compounds [77–79]. In addition, Ouhibi et al. [80] has recently shown that after UV-C light exposure against *Botrytis cinerea* and *Sclerotinia minor*, the increased resistance that was observed may include phenolic compounds. It could also be speculated that phytoalexins' biosynthesis can be due to the increased resistance to UV-C treatments [81, 82]. In UV-C-treated tomato fruit, higher glycoalkaloid alpha-tomatine levels, an antifungal compound, showed resistance against *Rhizopus stolonifer* [83]. UV-induced resistance to fungi of the genus Penicillium was associated with the accumulation of scoparone and scopoletin phytoalexins in citrus fruits and structural barriers [84]. However, some studies have reported that UV light has a negative impact on the plant's morphology and physiology; Kakani et al. [85] reported that UV-B light reduced plant height, branch length, leaf area, flower and petal length, petal area, and wax content. However, no reduction in production has been reported regarding exposure to UV light.

5. Conclusion

From the current study, it can be concluded that UV-A light can be used as a *B. tabaci* management tool. UV-A light affects the adults' development duration, longevity, and reproduction as well as affecting its physiology by disrupting the enzymatic balance. The UV-A light exposure exerted stress in the *B. tabaci* and suppressed the immune system, which gave an opportunity to the entomopathogenic fungus to work more efficiently. Therefore, due to the suppression of the immune system, the biological control agent can significantly control *B. tabaci* better. UV-A light can only be applied before the application of the biological control agent. According to the known literature and current experimental trials, both the entomopathogenic fungus and the parasitoid are sensitive to UV-A application. The literature also documents that UV-light exposure helps plants induce resistance, but no effect on productivity has been recorded. This study has laid the basis for conducting investigations on the application of UV-A light for the management of *B. tabaci* under semifield or greenhouse conditions.

Data Availability

All the data has already been given in the manuscript and supplementary material.

Conflicts of Interest

The authors have no conflict of interest to declare.

Acknowledgments

The authors thank Dr. Andrew G. S. Cuthbertson (York, UK) for critical comments on an earlier version of the manuscript. The study was supported by the National Key Research and Development Program of China (2019YFD1002100).

Supplementary Materials

Figure S1: caging of cotton leaves during whitefly rearing and experimentation. Figure S2: graphs show S_{xj} (survival rate of the specific stage) of *Bemisia tabaci* treated at second instar nymph stage exposed to UV-A light. Figure S3: graphs show l_x (survival rate of the specific stage), f_x (fecundity of specific age stage), m_x (overall population fecundity), and $l_x m_x$ (total maternity) values for *Bemisia tabaci* nymphs exposed to UV-A light. Figure S4: graphs show E_{xj} (life expectancy) values of *Bemisia tabaci* nymphs exposed to UV-A light. Figure S5: graphs show V_{xj} (reproduction of a specific stage) values for *B. tabaci* nymphs exposed to UV-A light. Table S1: effect of UV-A light exposure on the population growth parameters (mean ± SE) of *Bemisia tabaci* adults exposed at the nymphal stage. Table S2: percentage mortality of *Bemisia tabaci* exposed to UV-A light for the different durations and treated with different concentrations of *Cordyceps fumosorosea*. *(Supplementary Materials)*

References

[1] V. B. Meyer-Rochow, "Risks, especially for the eye, emanating from the rise of solar UV-radiation in the Arctic and Antarctic regions," *International Journal of Clinical Health*, vol. 59, pp. 38–51, 2000.

[2] M. Schauena, H. T. Hornig-Doa, S. Schomberg, G. Herrmann, and R. J. Wiesner, "Mitochondrial electron transport chain activity is not involved in ultraviolet A (UVA)-induced cell

death," *Free Radical Biology and Medicine*, vol. 42, no. 4, pp. 499–509, 2007.

[3] B. A. Jurkiewicz and G. R. Buettner, "Ultraviolet light-induced free radical formation in skin: an electron paramagnetic resonance study," *Photochemistry and Photobiology*, vol. 59, no. 1, pp. 1–4, 1994.

[4] G. F. Vile and R. M. Tyrrell, "UVA radiation-induced oxidative damage to lipids and proteins in vitro and in human skin fibroblasts is dependent on iron and singlet oxygen," *Free Radical Biology and Medicine*, vol. 18, no. 4, pp. 721–730, 1995.

[5] T. J. McMillan, E. Leatherman, A. Ridley, J. Shorrocks, S. E. Tobi, and J. R. Whiteside, "Cellular effects of long wavelength UV light (UVA) in mammalian cells," *Journal of Pharmacy and Pharmacology*, vol. 60, no. 8, pp. 969–976, 2008.

[6] S. I. Faruki, D. R. Das, and S. Khatun, "Effects of UV-radiation on the larvae of the lesser mealworm, *Alphitobius diaperinus* (Panzer)(Coleoptera: Tenebrionidae) and their progeny," *Journal of Biological Sciences*, vol. 5, no. 4, pp. 444–448, 2005.

[7] C. Y. Zhang, J. Y. Meng, X. P. Wang, F. Zhu, and C. L. Lei, "Effects of UV-A exposures on longevity and reproduction in *Helicoverpa armigera*, and on the development of its F1 generation," *Insect Science*, vol. 18, no. 6, pp. 697–702, 2011.

[8] M. C. Lu, H. R. Chen, and Y. H. Wu, "Current status and future perspectives on natural enemies for pest control in Taiwan," *Biocontrol Science and Technology*, vol. 28, no. 10, pp. 953–960, 2018.

[9] D. Gerling, "Natural enemies of whiteflies: predators and parasitoids," *Whiteflies: Their Bionomics, Pest Status and Management*, pp. 147–185, 1990.

[10] Y. Q. Liu and S. S. Liu, "Species status of Bemisia tabaci complex and their distribution in China," *Journal of Biosafety*, vol. 21, no. 4, pp. 247–255, 2010.

[11] M. T. Islam and S. Ren, "Effect of sweetpotato whitefly, *Bemisia tabaci* (Homoptera: Aleyrodidae) infestation on eggplant (*Solanum melongena* L.) leaf," *Journal of Pest Science*, vol. 82, no. 3, pp. 211–215, 2009.

[12] P. A. Stansly, S. E. Naranjo, J. K. Brown et al., *Bemisia: Bionomics and Management of a Global Pest*, Springer Netherlands, New York, 2010.

[13] R. M. Kepler, J. J. Luangsa-Ard, N. L. Hywel-Jones et al., "A phylogenetically-based nomenclature for Cordycipitaceae (Hypocreales)," *IMA Fungus*, vol. 8, no. 2, pp. 335–353, 2017.

[14] X. Chen, L. Li, Q. Hu et al., "Expression of dsRNA in recombinant *Isaria fumosorosea* strain targets the TLR7 gene in *Bemisia tabaci*," *BMC Biotechnology*, vol. 15, no. 1, p. 64, 2015.

[15] S. Abd-Rabou and A. M. Simmons, "Survey of natural enemies of whiteflies (Hemiptera: Aleyrodidae) in Egypt with new local and world records," *Entomological News*, vol. 124, no. 1, pp. 38–56, 2014.

[16] G. M. Mascarin, N. N. Kobori, E. D. Quintela, and I. Delalibera, "The virulence of entomopathogenic fungi against *Bemisia tabaci* biotype B (Hemiptera: Aleyrodidae) and their conidial production using solid substrate fermentation," *Biological Control*, vol. 66, no. 3, pp. 209–218, 2013.

[17] S. J. Li, X. Xue, M. Z. Ahmed et al., "Host plants and natural enemies of *Bemisia tabaci* (Hemiptera: Aleyrodidae) in China," *Insect Science*, vol. 18, no. 1, pp. 101–120, 2011.

[18] A. G. S. Cuthbertson, L. F. Blackburn, D. P. Eyre, R. J. C. Cannon, J. Miller, and P. Northing, "*Bemisia tabaci*: the current situation in the UK and the prospect of developing strategies for eradication using entomopathogens," *Insect Science*, vol. 18, no. 1, pp. 1–10, 2011.

[19] M. Faria and S. P. Wraight, "Biological control of Bemisia tabaci with fungi," *Crop Protection*, vol. 20, no. 9, pp. 767–778, 2001.

[20] T. Dong, B. Zhang, Y. Jiang, and Q. Hu, "Isolation and classification of fungal whitefly entomopathogens from soils of Qinghai-Tibet Plateau and Gansu Corridor in China," *PLoS One*, vol. 11, no. 5, pp. 1–12, 2016.

[21] Y. Argov, Y. Rössler, D. Rosen, and H. Voet, "Stability in the host-parasitoid relationship of *Dialeurodes citri* and *Encarsia lahorensis* in the citrus orchard," *BioControl*, vol. 48, no. 6, pp. 637–657, 2003.

[22] J. S. Hu, D. B. Gelman, and M. B. Blackburn, "Growth and development of *Encarsia formosa* (Hymenoptera: Aphelinidae) in the greenhouse whitefly, *Trialeurodes vaporariorum* (Homoptera: Aleyrodidae): effect of host age," *Archives of Insect Biochemistry and Physiology*, vol. 49, no. 3, pp. 125–136, 2002.

[23] K. Tariq, M. Noor, S. Saeed, and H. Zhang, "The effect of ultraviolet-a radiation exposure on the reproductive ability, longevity, and development of the *Dialeurodes citri* (Homoptera: Aleyrodidae) F1 generation," *Environmental Entomology*, vol. 44, no. 6, pp. 1614–1618, 2015.

[24] K. Kos, Ž. Tomanović, H. Rojht, V. Matej, and S. Trdan, "First massive occurrence of greenhouse whitefly parasitoid, *Encarsia formosa* Gahan (Hymenoptera: Aphelinidae) on greenhouse whitefly, *Trialeurodes vaporariorum* [Westwood] (Homoptera: Aleyrodidae) in Slovenia," *Acta Agriculturae Slovenica*, vol. 93, no. 3, pp. 285–291, 2009.

[25] Y. Wang, L. W. Oberley, and D. W. Murhammer, "Antioxidant defense systems of two lipidopteran insect cell lines," *Free Radical Biology and Medicine*, vol. 30, no. 11, pp. 1254–1262, 2001.

[26] H. Kamata and H. Hirata, "Redox regulation of cellular signalling," *Cellular Signalling*, vol. 11, no. 1, pp. 1–14, 1999.

[27] L. Lijun, L. Xuemei, G. Yaping, and M. Enbo, "Activity of the enzymes of the antioxidative system in cadmium-treated *Oxya chinensis* (Orthoptera Acridoidae)," *Environmental Toxicology and Pharmacology*, vol. 20, no. 3, pp. 412–416, 2005.

[28] A. Baghban, J. J. Sendi, A. Zibaee, and R. Khosravi, "Effect of heavy metals (Cd, Cu, and Zn) on feeding indices and energy reserves of the cotton boll worm *Helicoverpa armigera* Hübner (Lepidoptera: Noctuidae)," *Journal of Plant Protection Research*, vol. 54, no. 4, pp. 367–373, 2014.

[29] D. M. Olson, H. Fadamiro, J. G. Lundgren, and G. E. Heimpel, "Effects of sugar feeding on carbohydrate and lipid metabolism in a parasitoid wasp," *Physiological Entomology*, vol. 25, no. 1, pp. 17–26, 2000.

[30] P. Hogervorst, F. L. Wäckers, and J. Romeis, "Effects of honeydew sugar composition on the longevity of *Aphidius ervi*," *Entomologia Experimentalis et Applicata*, vol. 122, no. 3, pp. 223–232, 2007.

[31] M. M. Khan, M. Nawaz, H. Hua, W. Cai, and J. Zhao, "Lethal and sublethal effects of emamectin benzoate on the rove beetle, *Paederus fuscipes*, a non-target predator of rice brown planthopper, *Nilaparvata lugens*," *Ecotoxicology and Environmental Safety*, vol. 165, pp. 19–24, 2018.

[32] D. Ou, L. M. Ren, Y. Liu et al., "Compatibility and efficacy of the parasitoid *Eretmocerus hayati* and the entomopathogenic fungus *Cordyceps javanica* for biological control of whitefly *Bemisia tabaci*," *Insects*, vol. 10, no. 12, pp. 1–11, 2019.

[33] T. Nazir, A. Basit, A. Hanan, M. Z. Majeed, and D. Qiu, "In vitro pathogenicity of some entomopathogenic fungal strains against green peach aphid *Myzus persicae* (Homoptera: Aphididae)," *Agronomy*, vol. 9, no. 1, 2019.

[34] M. Barta, "Pathogenicity assessment of entomopathogenic fungi infecting *Leptoglossus occidentalis* (Heteroptera: Coreidae)," *Czech Mycology*, vol. 62, no. 1, pp. 67–78, 2010.

[35] W. S. Abbott, "A method of computing the effectiveness of an insecticide," *Journal of Economic Entomology*, vol. 18, no. 2, pp. 265–267, 1925.

[36] H. Chi and H. Liu, "Two new methods for the study of insect population ecology," *Bulletin of the Institute of Zoology, Academia Sinica*, vol. 24, no. 2, pp. 225–240, 1985.

[37] H. Chi, "Life-table analysis incorporating both sexes and variable development rates among individuals," *Environmental Entomology*, vol. 17, no. 1, pp. 26–34, 1988.

[38] H. Chi, *TWOSEX-MSChart: a computer program for the age-stage, two-sex life table analysis*, vol. 197, 2015http://140.120.

[39] Y. B. Huang and H. Chi, "Age-stage, two-sex life tables of *Bactrocera cucurbitae* (Coquillett) (Diptera: Tephritidae) with a discussion on the problem of applying female age-specific life tables to insect populations," *Insect Science*, vol. 19, no. 2, pp. 263–273, 2012.

[40] I. Akca, T. Ayvaz, E. Yazici, C. L. Smith, and H. Chi, "Demography and population projection of *Aphis fabae* (Hemiptera: Aphididae): with additional comments on life table research criteria," *Journal of Economic Entomology*, vol. 108, no. 4, pp. 1466–1478, 2015.

[41] J. H. Chang and Y. P. He, "The analysis for comparing the pesticide toxicity data using the Polo software," *Acta Agriculturae Zhejiangensis*, vol. 26, no. 6, pp. 1552–1557, 2014.

[42] A. Ali, M. A. Rashid, Q. Y. Huang, and C. L. Lei, "Effect of UV-A radiation as an environmental stress on the development, longevity, and reproduction of the oriental armyworm, *Mythimna separata* (Lepidoptera: Noctuidae)," *Environmental Science and Pollution Research*, vol. 23, no. 17, pp. 17002–17007, 2016.

[43] G. W. Felton and C. B. Summers, "Antioxidant systems in insects," *Archives of Insect Biochemistry and Physiology*, vol. 29, no. 2, pp. 187–197, 1995.

[44] W. Wang, C. Gao, L. Ren, and Y. Luo, "The effect of longwave ultraviolet light radiation on *Dendrolimus tabulaeformis* antioxidant and detoxifying enzymes," *Insects*, vol. 11, no. 1, pp. 1–11, 2020.

[45] A. Ali, M. A. Rashid, Q. Y. Huang, and C. L. Lei, "Influence of UV-A radiation on oxidative stress and antioxidant enzymes in *Mythimna separata* (Lepidoptera: Noctuidae)," *Environmental Science and Pollution Research*, vol. 24, no. 9, pp. 8392–8398, 2017.

[46] D. Zhou, Y. Du, J. Yang et al., "Effect of UV-B radiation in successive generation on the activity og protective enzymes in the grain aphid, *Sitobion avenae* (Hemiptera: Aphididae)," *Acta Entomologica Sinica*, vol. 57, no. 7, pp. 762–768, 2014.

[47] L. Haddouche, A. Phalak, and R. V. Tikekar, "Inactivation of polyphenol oxidase using 254 nm ultraviolet light in a model system," *LWT - Food Science and Technology*, vol. 62, no. 1, pp. 97–103, 2015.

[48] G. C. Williams, "Natural selection, the costs of reproduction, and a refinement of lack's principle," *The American Naturalist*, vol. 100, no. 916, pp. 687–690, 1966.

[49] A. Ohkawara and K. M. Halprin, "Ultraviolet light and glycogen formation in the human epidermis," *Archives of Dermatology*, vol. 95, no. 4, pp. 416–421, 1967.

[50] A. Ohkawara, K. M. Halprin, and V. Levine, "Glycogen metabolism following ultraviolet irradiation," *The Journal of Investigative Dermatology*, vol. 59, no. 3, pp. 264–268, 1972.

[51] J. Tian, H. Diao, L. Liang, C. Hao, S. Arthurs, and R. Ma, "Pathogenicity of *Isaria fumosorosea* to *Bemisia tabaci*, with some observations on the fungal infection process and host immune response," *Journal of Invertebrate Pathology*, vol. 130, pp. 147–153, 2015.

[52] T. T. Santos, E. D. Quintela, G. M. Mascarin, and M. V. Santana, "Enhanced mortality of *Bemisia tabaci* nymphs by *Isaria javanica* combined with sublethal doses of chemical insecticides," *Journal of Applied Entomology*, vol. 142, no. 6, pp. 598–609, 2018.

[53] X. Wang, J. Xu, X. Wang et al., "*Isaria fumosorosea*-based zero-valent iron nanoparticles affect the growth and survival of sweet potato whitefly, Bemisia tabaci (Gennadius)," *Pest Management Science*, vol. 75, no. 8, pp. 2174–2181, 2019.

[54] C. Zou, L. Li, T. Dong, B. Zhang, and Q. Hu, "Joint action of the entomopathogenic fungus *Isaria fumosorosea* and four chemical insecticides against the whitefly *Bemisia tabaci*," *Biocontrol Science and Technology*, vol. 24, no. 3, pp. 315–324, 2014.

[55] J. Rotem, "The role of solar radiation, especially ultraviolet, in the mortality of fungal spores," *Phytopathology*, vol. 75, no. 5, pp. 510–514, 1985.

[56] N. D. Paul, R. J. Jacobson, A. Taylor, J. J. Wargent, and J. P. Moore, "The use of wavelength-selective plastic cladding materials in horticulture: understanding of crop and fungal responses through the assessment of biological spectral weighting functions," *Photochemistry and Photobiology*, vol. 81, no. 5, pp. 1052–1060, 2005.

[57] K. K. Newsham, M. N. R. Low, A. R. McLeod, P. D. Greenslade, and B. A. Emmett, "Ultraviolet-B radiation influences the abundance and distribution of phylloplane fungi on pedunculate oak (*Quercus robur*)," *New Phytologist*, vol. 136, no. 2, pp. 287–297, 1997.

[58] G. U. L. Braga, S. D. Flint, C. D. Miller, A. J. Anderson, and D. W. Roberts, "Both solar UVA and UVB radiation impair conidial culturability and delay germination in the entomopathogenic fungus *Metarhizium anisopliae*," *Photochemistry and Photobiology*, vol. 74, no. 5, p. 734, 2001.

[59] G. U. L. Braga, S. D. Flint, C. L. Messias, A. J. Anderson, and D. W. Roberts, "Effects of UVB irradiance on conidia and germinants of the entomopathogenic hyphomycete *Metarhizium anisopliae*: a study of reciprocity and recovery," *Photochemistry and Photobiology*, vol. 73, no. 2, p. 140, 2001.

[60] L. Englander, M. Browning, and P. W. Tooley, "Growth and sporulation of Phytophthora ramorum in vitro in response to temperature and light," *Mycologia*, vol. 95, no. 3, pp. 365–373, 2006.

[61] A. Fourtouni, Y. Manetas, and C. Christias, "Effects of UV-B radiation on growth, pigmentation, and spore production in the phytopathogenic fungus *Alternaria solani*," *Canadian Journal of Botany*, vol. 76, no. 12, pp. 2093–2099, 1998.

[62] M. P. Santos, L. P. Dias, P. C. Ferreira, L. A. A. P. Pasin, and D. E. N. Rangel, "Cold activity and tolerance of the entomopathogenic fungus Tolypocladium spp. to UV-B irradiation and heat," *Journal of Invertebrate Pathology*, vol. 108, no. 3, pp. 209–213, 2011.

[63] A. Idnurm, "Light sensing in Aspergillus fumigatus highlights the case for establishing new models for fungal photobiology," *mBio*, vol. 4, article e00260, 2013.

[64] P. Cheng, Z. Ma, X. Wang et al., "Impact of UV-B radiation on aspects of germination and epidemiological components of three major physiological races of *Puccinia striiformis* f. sp. tritici," *Crop Protection*, vol. 65, pp. 6–14, 2014.

[65] P. Cochard, T. Galstian, and C. Cloutier, "The proportion of blue light affects parasitoid wasp behavior in LED-extended photoperiod in greenhouses: increased parasitism and offspring sex ratio bias," *Biological Control*, vol. 133, pp. 9–17, 2019.

[66] F. Moreno, I. Pérez-Moreno, and V. Marco, "Effects of *Lobesia botrana* (Lepidoptera: Tortricidae) egg age, density, and UV treatment on parasitism and development of *Trichogramma cacoeciae* (Hymenoptera: Trichogrammatidae)," *Environmental Entomology*, vol. 38, no. 5, pp. 1513–1520, 2009.

[67] M. Nakajima and H. Yoshida, "Studies on ultraviolet sensitivity in silkworm, with special reference to variations in its killing effect during the larval instar stage," *Japanese Journal of Applied Entomology and Zoology*, vol. 15, no. 1, pp. 17–22, 1971.

[68] M. Nakajima and H. Yoshida, "Studies on ultraviolet sensitivity in the silkworm, with special reference to the effect of uv-irradiation on melanin formation in the cuticle of the striped silkworm," *Japanese Journal of Applied Entomology and Zoology*, vol. 15, no. 2, pp. 51–55, 1971.

[69] D. R. A. Wharton, "Ultraviolet repellent and lethal action on the American cockroach," *Journal of Economic Entomology*, vol. 64, no. 1, pp. 252–255, 1971.

[70] S. H. Cohen, J. A. Sousa, and J. F. Roach, "Effects of UV irradiation on nymphs of five species of cockroaches," *Journal of Economic Entomology*, vol. 66, no. 4, pp. 859–862, 1973.

[71] S. H. Cohen, J. A. Saousa, J. F. Roach, and J. B. Gingrich, "Effects of UV irradiation on nymphs of *Blattella germanica* and *Periplaneta americana*," *Journal of Economic Entomology*, vol. 68, no. 5, pp. 687–693, 1975.

[72] C. P. Bonsignore, G. Vono, and U. Bernardo, "Environmental thermal levels affect the phenological relationships between the chestnut gall wasp and its parasitoids," *Physiological Entomology*, vol. 44, no. 2, pp. 87–98, 2019.

[73] W. H. Van Der Putten, M. Macel, and M. E. Visser, "Predicting species distribution and abundance responses to climate change: why it is essential to include biotic interactions across trophic levels," *Philosophical Transactions of the Royal Society B: Biological Sciences*, vol. 365, no. 1549, pp. 2025–2034, 2010.

[74] C. P. Bonsignore and U. Bernardo, "Effects of environmental parameters on the chestnut gall wasp and its complex of indigenous parasitoids," *Science of Nature*, vol. 105, no. 3-4, p. 20, 2018.

[75] C. P. Bonsignore, G. Vizzari, G. Vono, and U. Bernardo, "Short-term cold stress affects parasitism on the asian chestnut gall wasp *Dryocosmus kuriphilus*," *Insects*, vol. 11, no. 12, p. 841, 2020.

[76] X. Liu, C. E. Williams, J. A. Nemacheck et al., "Reactive oxygen species are involved in plant defense against a gall midge," *Plant Physiology*, vol. 152, no. 2, pp. 985–999, 2010.

[77] C. Lamb and R. A. Dixon, "The oxidative burst in plant disease resistance," *Annual Review of Plant Biology*, vol. 48, no. 1, pp. 251–275, 1997.

[78] J. Dat, S. Vandenabeele, E. Vranová, M. Van Montagu, D. Inzé, and F. Van Breusegem, "Dual action of the active oxygen species during plant stress responses," *Cellular and Molecular Life Sciences*, vol. 57, no. 5, pp. 779–795, 2000.

[79] J. J. Grant and G. J. Loake, "Role of reactive oxygen intermediates and cognate redox signaling in disease resistance," *Plant Physiology*, vol. 124, pp. 24–31, 2000.

[80] C. Ouhibi, H. Attia, P. Nicot et al., "Effects of nitrogen supply and of UV-C irradiation on the susceptibility of *Lactuca sativa* L to *Botrytis cinerea* and *Sclerotinia minor*," *Plant and Soil*, vol. 393, no. 1–2, pp. 35–46, 2015.

[81] M. T. Charles, N. Benhamou, and J. Arul, "Physiological basis of UV-C induced resistance to *Botrytis cinerea* in tomato fruit. III. Ultrastructural modifications and their impact on fungal colonization," *Postharvest Biology and Technology*, vol. 47, no. 1, pp. 27–40, 2008.

[82] O. Windram, P. Madhou, S. Mchattie et al., "Arabidopsis defense against *Botrytis cinerea*: chronology and regulation deciphered by high-resolution temporal transcriptomic analysis," *Plant Cell*, vol. 24, no. 9, pp. 3530–3557, 2012.

[83] C. Stevens, V. A. Khan, J. Y. Lu et al., "Induced resistance of sweetpotato to Fusarium root rot by UV-C hormesis," *Crop Protection*, vol. 18, no. 7, pp. 463–470, 1999.

[84] G. D'Hallewin, M. Schirra, M. Pala, and S. Ben-Yehoshua, "Ultraviolet C irradiation at 0.5 kJ·m-2 reduces decay without causing damage or affecting postharvest quality of Star Ruby grapefruit (*C. paradisi* Macf.)," *Journal of Agricultural and Food Chemistry*, vol. 48, no. 10, pp. 4571–4575, 2000.

[85] V. G. Kakani, K. R. Reddy, D. Zhao, and A. R. Mohammed, "Effects of ultraviolet-B radiation on cotton (*Gossypium hirsutum* L.) morphology and anatomy," *Annals of Botany*, vol. 91, no. 7, pp. 817–826, 2003.

Hindawi
Oxidative Medicine and Cellular Longevity
Volume 2021, Article ID 5834418, 8 pages
https://doi.org/10.1155/2021/5834418

Research Article

Poly Lactic-Co-Glycolic Acid- (PLGA-) Loaded Nanoformulation of Cisplatin as a Therapeutic Approach for Breast Cancers

Saad Alkahtani,[1] Saud Alarifi,[1] Gadah Albasher,[1] Mohammed Al-Zharani,[2] Nada H. Aljarba,[3] Mohammed H. Almarzoug,[1] Norah M. Alhoshani,[1] Norah S. AL-Johani,[1] Hani Alothaid,[4] and Abdullah A. Alkahtane[1]

[1]*Department of Zoology, College of Science, King Saud University, Riyadh, Saudi Arabia*
[2]*Department of Biology, College of Science, Imam Muhammad Ibn Saud Islamic University, Riyadh-11432, Saudi Arabia*
[3]*Department of Biology, College of Sciences, Princess Nourah Bint Abdulrahman University, Riyadh, Saudi Arabia*
[4]*Department of Basic Sciences, Faculty of Applied Medical Sciences, Al-Baha University, Al-Baha-65431, Saudi Arabia*

Correspondence should be addressed to Saad Alkahtani; salkahtani@ksu.edu.sa

Received 19 April 2021; Revised 4 June 2021; Accepted 19 June 2021; Published 29 June 2021

Academic Editor: Hui-Min David Wang

Despite recent advancements in cisplatin (*cis*-diamminedichloroplatinum II) and other platinum-based chemotherapeutic drugs for treating solid tumors, their uses are limited by either in terms of toxicity and/or acquired drug resistance. These side effects have a dangerous problem with higher dose for severe patients. To overcome the low therapeutic ratio of the free drug, a polymeric nanoparticle drug delivery system has been explored promoting delivery of cisplatin to tumors. Recently, the applications of nanoparticles (NPs) have been underlined for encouraging the effects of chemotherapeutic drugs in cancerous cells. The intention of this project is to assess the potential of poly lactic-co-glycolic acid (PLGA) nanoparticles (NPs) for enhancing the effects of anticancer drug cisplatin. For the purpose, we have synthesized PLGA-cisplatin nanoparticles for increasing its bioavailability and studied the comparative cytotoxicity of free cisplatin and PLGA-cisplatin against MCF-7 cancer cell lines and HEK-293 normal cell lines. We have also analyzed the hallmarks of PLGA-cisplatin-induced apoptosis. The outcomes of this study may provide the possibility of delivery of anticancer drug to their specific site, which could minimize toxicity and optimize the drug efficacy.

1. Introduction

Cancer has exceeded cardiovascular and cerebrovascular diseases as the foremost cause of death worldwide [1–3]. Thus, the overload of cancer on healthcare systems consistently increases which requires more investigations to further advance an early and rapid recognition of such deadly disease [4, 5]. In particular, breast cancer (BC) is the common diagnosed noncutaneous form of solid tumor among women which is related with larger tumor size, higher grade, and frequent nodal immersion and becomes primary cause of death among women [6–8]. Although, the risk of BC consistently increases with different age groups, due to an elevated level of estrogen metabolite which generates reactive oxygen species (ROS) and prompts uncontrolled DNA production [9]. The incidence of BC is linked to numerous factors, among which the utmost common being its heterogeneous nature [10]. The inter/intratumoral heterogeneity, typically affecting the physical appearance of the breast and molecular variety, shows a pivotal role in its histology and staging [11]. The molecular stratification of BC is primarily based on the expression of hormonal receptors, namely, the estrogen receptor (ER) and progesterone receptor (PR), along with human epidermal growth factor receptor 2 (HER2) [10, 12,

13]. Owing to its heterogeneity, the treatment is complicated and the healing methodologies should be taken carefully [13].

In the last few decades, successful invention for cancer therapy is the use of metal-based pharmaceuticals after the serendipitous discovery of *cis*-Pt $(NH_3)_2Cl_2$ has been extensively studied and remains a front-line treatment against a variety of solid tumors [14–16]. It was regularly accepted that cisplatin is a model chemotherapeutic drug of high proficiency and induces cytotoxicity by interference of transcription and/or the DNA replication mechanisms [17]. The interaction of the cisplatin drug and DNA forming DNA adducts leads to the activation of numerous signal transduction corridors involved in apoptosis [18]. However, there are certain limitations *viz*. severe toxicity, intrinsic and extrinsic resistance, and patient compliance [19, 20]. Additionally, cisplatin retains itself in tumor cell for a short duration due to low molecular weight and it can easily pass into the blood circulation causing damage to normal cells [21]. To conquer such issues, new strategies in the form of combination therapies were employed to improve the drug delivery profile of cisplatin towards the cancer cell line [22, 23]. It provides the possibility of targeted delivery of a certain anticancer drug to the tumor site, which could minimize toxicity and optimize the drug efficacy [24].

To date, various nanocarrier-based delivery systems like liposomes, micelles, and dendrimers have been taken that permit more directed release of the drugs [25–27]. These nanoparticles modify the drug release profile for the purpose of improving drug bioavailability because of their ability for tunable payload release to the specific target domain with minimum toxicity to surrounding healthy tissues. Among numerous biodegradable polymers, poly lactic-co-glycolic acid (PLGA) has been extensively used as drug carriers in clinical medicines as it is an FDA-approved copolymer [24, 28]. PLGA has a promising degradation characteristic that makes it ideal for sustained release for hydrophilic or hydrophobic drug. Furthermore, they can easily conjugate with specific target molecules and have the potential to alter their surface properties and improve interactions to reach specific tissues or cells [29]. Recently, Domínguez-Ríos et al. analyzed the significant improvement in the cytotoxicity along with an enhanced internalization of NPs as compared to free cisplatin for HER2 targeted ovarian cancer [30]. Similarly, Moreno et al. evaluated the *in vivo* efficacy of cisplatin-loaded PLGA nanoparticles administered to tumor-bearing mice, which provide a promising carrier for cisplatin avoiding its side effects without a decline of the efficacy [31].

With this objective to treat breast cancer by utilizing the advantages of PLGA in this study, we chose PLGA nanoparticles as a core for the encapsulation of a cisplatin drug (Figure 1), for the purpose of safe delivery to the target-specific region. *In vitro* anticancer efficacy and cellular localization of this formulation were investigated on MCF-7 cancer cell lines. We assumed that delivery of drug would result in enhanced anticancer efficacy by modulating the tumor microenvironment to increase the penetration of PLGA NPs into the tumor cell.

2. Materials and Methods

2.1. Chemicals. Poly(D, L-lactide-co-glycolide) (PLGA, Resomer® RG 502 H Mw 7–17 kDa lactide: glycolide 50 : 50, acid terminated), cisplatin, dimethylformamide (DMF), polyvinyl alcohol (PVA, 9–10 kDa, 80% hydrolyzed), acetic acid, orthophenylenediamine (OPDA), phosphate buffer saline (PBS), 2-(N-morpholino) ethanesulphonic acid clorhydrate (MES) were purchased from Sigma-Aldrich. Constituents for cell culture media consist of fetal bovine serum (FBS), Dulbecco's modified Eagle medium (DMEM), trypsin, penicillin-streptomycin-neomycin (PSN) antibiotic cocktail, and ethylenediaminetetraacetic acid (EDTA) were procured from Gibco (Grand Island, NY, USA). Antibodies were bought from Santa Cruz Biotechnology, Dallas, Texas, USA, and eBioscience, San Diego, USA. Dyes were acquired from Thermo Fisher Scientific, USA. All other chemicals and solvents (purchased from Sigma-Aldrich) were used as received without further treatment.

2.2. Synthesis of PLGA-Cisplatin NPs. Cisplatin-loaded NPs were obtained by a nanoprecipitation technique in which 27 mg of PLGA was dissolved in minimum amount of DMF (2 mL) by vortexing. To this PLGA solution, cisplatin (10.5 mg) was added. Then, this organic solution was added dropwise to of PVA (20 mL) earlier dissolved in DI water (1% w/v) and stirred for few minutes. The excess amount of PVA and DMF were removed by centrifugation at 10,000 rpm (Thermo Sorvall Legend X1R) for 30 min at 20°C. The final pellet was dispersed in water (8 mL) followed by vortexing at 4°C and kept until apply within 1 h or lyophilized and stored for extended periods of time [31].

2.3. Fourier Transform Infrared (FTIR) Spectroscopy. The FTIR spectroscopy measurements were recorded to characterize the probable participation of the functional groups of cisplatin in synthesized PLGA-cisplatin. The FTIR spectra of PLGA-cisplatin NPs were acquired in an Avatar 330 FTIR spectrometer (Thermo Fisher Scientific, Waltham, MA, USA) over a scale of 4,250–500 cm^{-1} after adding with KBr pellets [32].

2.4. Atomic Force Microscopy (AFM). To observe the surface morphology and measure the size of the resultant PLGA-cisplatin NPs, an AFM was applied. The sample was dropped onto newly cleaved mica slices and dried overnight. An AGILENT-N9445A series 5500 AFM (Agilent Technologies, Santa Clara, CA, USA), which was equipped with Pico View software, was used.

2.5. Cell Culture. The human embryonic kidney cells (HEK293) and breast cancer cell line (MCF-7) were achieved was acquired from ATCC, USA. These cells were culture in DMEM having 10% FBS with 1% antibiotic cocktail in a humidified medium under constant 5% CO_2 at 37°C. Cell seeding was completed with EDTA (0.52 mM) and trypsin (0.25%) in phosphate-buffered saline (PBS) after 70–75% confluence. Later, the cells were plated at an essential concentration to allow them to reequilibrate before performing the experiment [33].

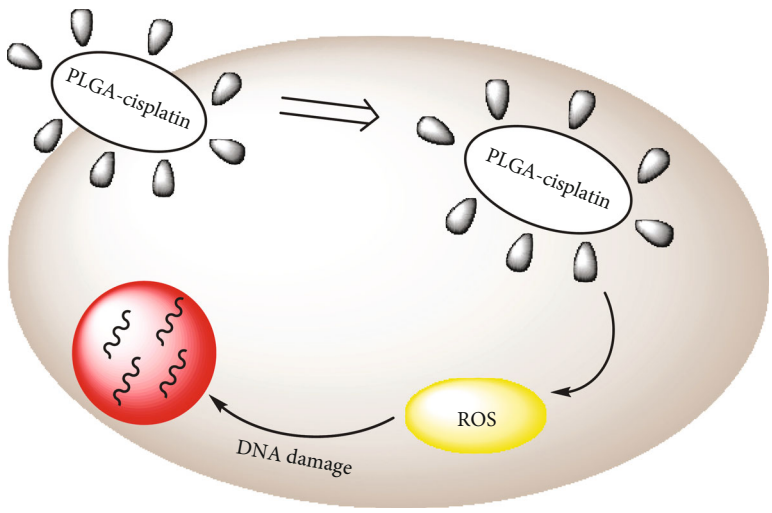

Figure 1: Schematic representation of encapsulation of PLGA-cisplatin NPs and their mode of action.

2.6. Determination of Cell Viability. Determination of cell viability was done by MTT [(4,5- dimethyl-thiazol-2-yl)-2,5-diphenyl-tetrazolium bromide] assay [34]. HEK293 and MCF-7 cells were seeded at a required density (4×10^3 cells/-well) in a 96-well plate from the respective plate. After 18 –24 h of seeding, cells were treated with cisplatin and PLGA-cisplatin at 0-50 (μg/mL) followed by an initial screening for different time duration. After treatment, plates were placed for 24 h in an incubator at 37°C in a humidified CO_2-rich condition (5%). After incubation for 24 h, cells were rinsed from each well of 96-well plates by PBS. Then, the MTT solution was added to each well and reserved in an incubator for 4 h to appear formazan dye. The formazan dye was then solubilized using DMSO, and the absorbance was taken at 595 nm using an ELISA reader (EMax, Molecular Device, USA) [35]. Cell propagation was evaluated from the absorption intensity in terms of cell viability as follows:

$$\text{Cell viability} = \frac{\text{OD of Control} - \text{OD of treated}}{\text{OD of Control}} \times 100. \quad (1)$$

In each case, the PLGA-cisplatin was sonicated before considering in a cell line to obtain homogenized mixtures. Each experiment was repeated thrice to obtain reported biological results.

2.7. Detection of Apoptosis/Necrosis. Necrotic and apoptotic cell death was determined using the Annexin-V FITC/PI apoptosis detection kit (Calbiochem, CA, USA). The MCF-7 cells were plated in six-well plates then treated with PLGA-cisplatin at 23 μg/mL. After 12 and 24 h of incubation, the cells were washed and stained with propidium iodide (PI) and Annexin-V-FITC in the presence of binding buffer as per the manufacturer's protocols [36]. The early and late apoptotic percentages, live, and necrotic cells were analyzed using a flow cytometer (BD LSRFortessa™ San Jose, CA, USA). The acquired data were analyzed using FlowJo (version 10.0) software.

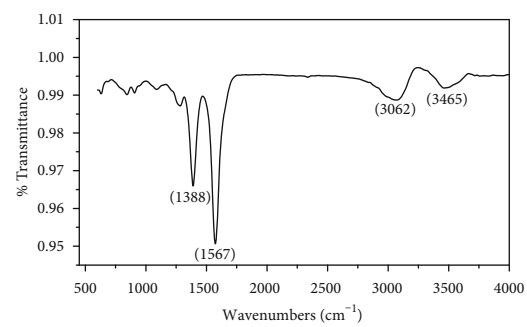

Figure 2: FTIR data of PLGA-cisplatin.

2.8. DNA Fragmentation Assay. Treated cells with the PLGA-cisplatin nanoparticles at different concentrations (0-40 μg/mL) were analyzed for 24 h. Then, the resultant fragmented DNA was calculated using commercially obtainable kits at 405 nm according to the manufacturer's procedure [37].

2.9. Assessment of Intracellular ROS. Intracellular mitochondrial ROS have been calculated following the previously reported protocols [38]. To adopt the intercellular ROS, we incubated the treated MCF-7 cells with 10 μM 2′,7′-dichlorofluorescein diacetate (DCF-DA) for 25 min. The slides were then counterstained with DAPI for 10 min and mounted with the ProLong Antifade Reagent (Molecular Probe, Eugene, OR, USA). Later, the slides were subjected to confocal laser scanning microscope (FV 10i, Olympus, Japan) [39]. The change of DCF-DA fluorescence used as a fluorescent indicator of ROS formation in cell culture-based antioxidant assays.

2.10. In Vitro Cisplatin Release. The *in vitro* cisplatin release experiments were conducted at pH 5.5 with 10 μg/mL of cisplatin containing PLGA. 1 mL of PLGA-cisplatin was loaded into a dialysis bag, then dispersed in a 50 mL of PBS of pH 7.4 at 37°C. Further, the full system was transferred at 130 rpm

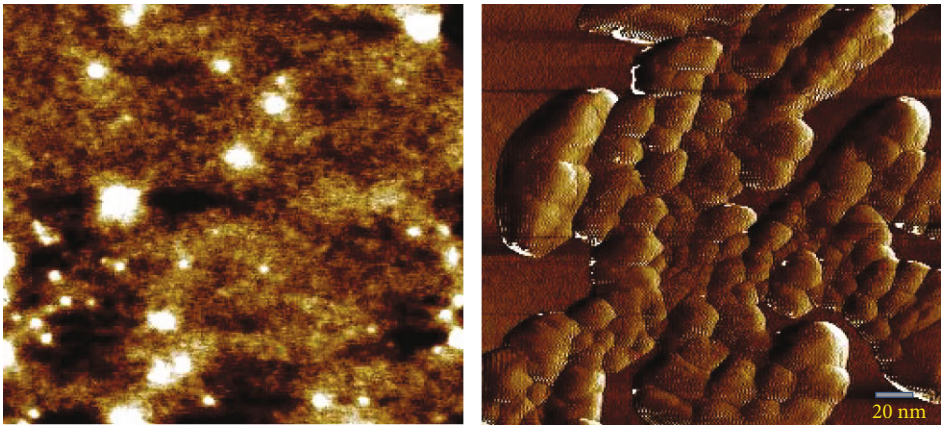

Figure 3: AFM data of PLGA-cisplatin.

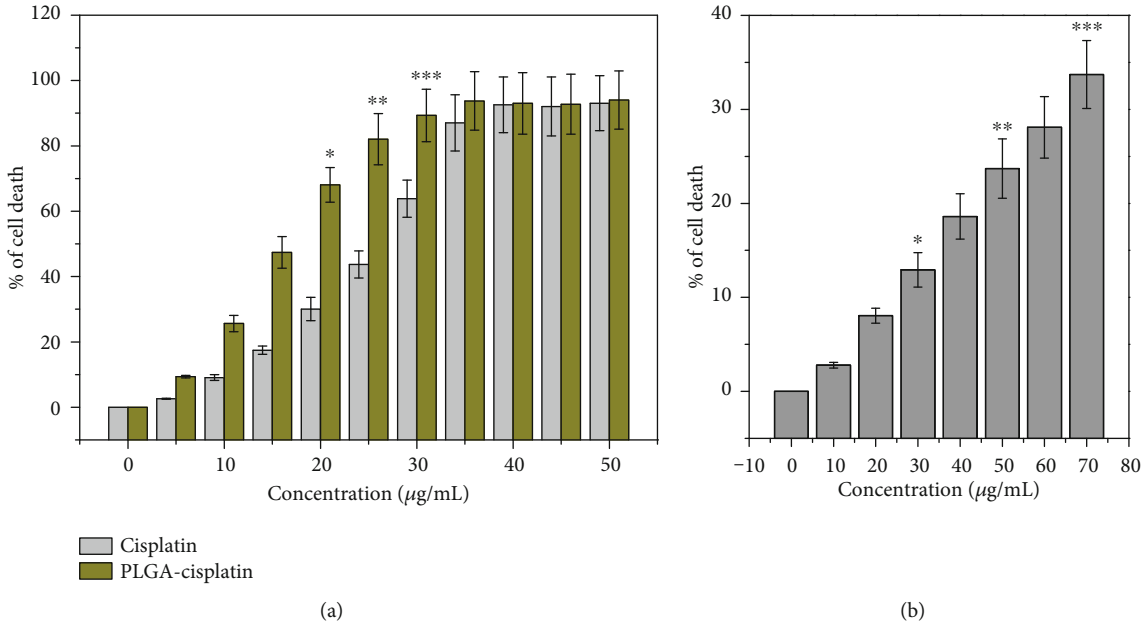

Figure 4: (a) Rate of cell death of MCF-7 cells after treatment with cisplatin only and PLGA-cisplatin for 24 h as evaluated by MTT assay. (b) Rate of cell death of HEK-293 cells after treatment with PLGA-cisplatin NPs. Each value represents the mean ± SE of three experiments. $n = 3$ ($^{*}p < 0.05$, $^{**}p < 0.01$, and $^{***}p < 0.001$), compared with the control.

for 24 h. From the above dispersions after 2 h intervals, 500 μL aliquots were drawn and it was replaced by an equal volume of the fresh PBS solution for retaining the same release medium. The released amount of cisplatin was determined spectrophotometrically at 510 nm [40].

2.11. Statistical Analysis. Data were represented as mean ± SEM of the multiple data points. Statistical significance in the deference was calculated using analysis of variance (ANOVA) using OriginPro (version 8.0) software where $p < 0.05$ was considered significant.

3. Result and Discussion

3.1. Characterization of PLGA-Cisplatin NPs. The encapsulation of weakly soluble and toxic drugs within polymeric NPs increases their therapeutic and pharmacodynamics performance and decreases their side effects [41]. Cisplatin is poor soluble in water (0.23 g/100 mL of water) and organic solvents makes it quite difficult to prepare concentrated solutions necessary to produce NPs. Although DMSO is well known to be a good solvent for cisplatin, it has been reported to compromise the cytotoxic potency of the drug, so DMF was chosen as an organic solvent for the preparation of NPs.

The FTIR spectrum of the sample after the encapsulation of cisplatin is reported (Figure 2). Two peaks were found in the 3062–3465 cm^{-1} (related to asymmetric and symmetric stretching of -NH group) and 1600–1300 cm^{-1} (related to HNH asymmetric and symmetric bending). Some peaks were observed in between 500 and 1300 cm^{-1} (viz. at 956 cm^{-1} for –OH bending), which are the characteristic peaks of PLGA.

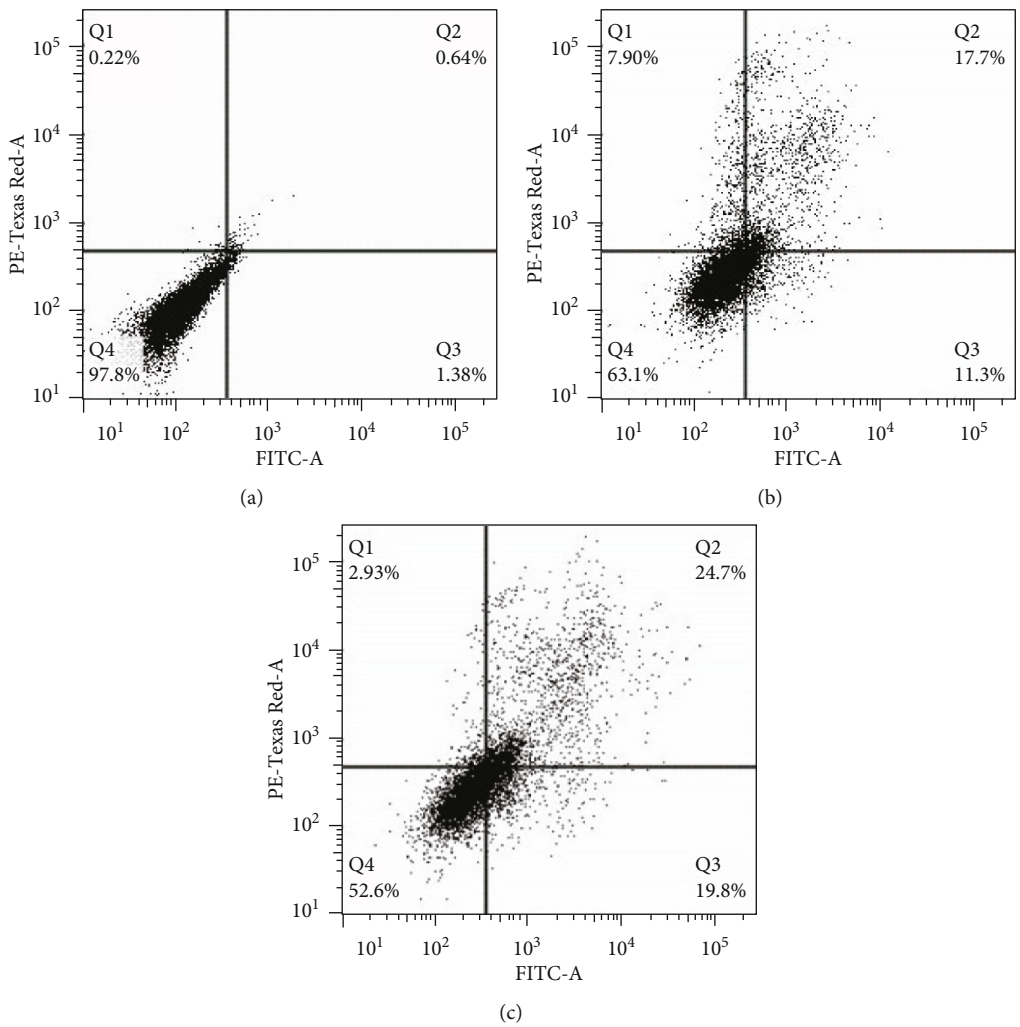

Figure 5: Annexin-V/PI staining to analyze apoptosis/necrosis in MCF-7 cells. Time-dependent study (12 and 24 h) after treatment of cells with 23 μg/mL of PLGA-cisplatin. (a) Untreated cells. (b) Differences in the percentage of cell death in the treated cells for 12 h. (c) Differences in the percentage of cell death in treated cells for 24 h.

Then, we have studied the size and shape of the PLGA-cisplatin NPs by AFM. The AFM data (Figure 3) suggest that PLGA-cisplatin exhibits nanosphere-like shape. We have calculated the size which is around 95.56 ± 7.94 nm from the AFM images.

3.2. PLGA-Cisplatin NPs Induced Cytotoxicity. The cytotoxic effects of PLGA-cisplatin NPs have been tested against the breast cancer cell line (MCF-7) by MTT assay. Based on the values of IC_{50}, different concentrations between 0 and 50 μg/mL of PLGA-cisplatin NPs were selected and the treatment period was for a 24 h period. The MTT assay data cleared that the cell death has been increased with the concentration of PLGA-cisplatin NPs. We have also evaluated the cytotoxicity of cisplatin in the same concentration range. From the MTT assay, we have acquired the IC_{50} value of PLGA-cisplatin NPs is 23 ± 2.80 μg/mL, whereas in case of only cisplatin, the IC_{50} value is 38 ± 3.78 μg/mL. This MTT assay data cleared that PLGA-cisplatin NPs are superior cytotoxic than cisplatin only (Figure 4(a)). We have also checked the cytotoxicity of NPs in the HEK-293 cell line. The data concluded that, after 40 μg/mL, significant cell death was found (Figure 4(b)).

3.3. PLGA-Cisplatin NPs Induced Apoptosis in MCF-7 Cells. To examine whether the PLGA-cisplatin nanosphere was involved in apoptosis/necrosis, flow cytometric assessment was performed using Annexin-V-FITC/PI staining by analyzing the elevated level of serine phosphatidyl in the outer membrane of cells. As shown in (Figure 5), it was evident that the percentages of apoptotic (early and late) cells have been enhanced in a time-dependent manner (11.3% EA/17.7% LA for 12 h and 19.8% EA/24.7% in LA for 24 h) after treatment of 23 μg/mL of PLGA-cisplatin NPs, with respect to the control cells (1.38% EA and 0.64% LA). These results suggested that PLGA-cisplatin NPs-induced cell death was directly correlated with cytotoxicity followed by apoptosis.

3.4. Assessment of Intracellular ROS Generation. Cisplatin is a well-known ROS inducer [42]. So, we have established the

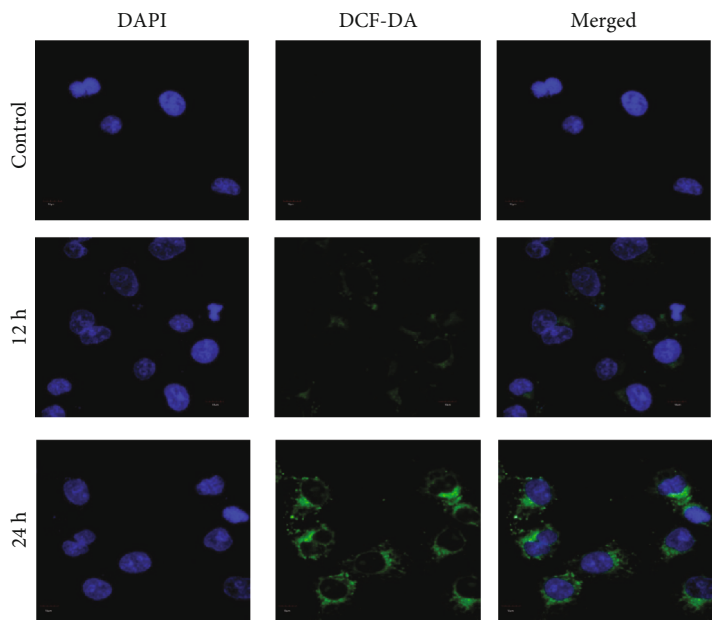

Figure 6: Measurement of ROS generation after a time-dependent treatment (12 and 24 h) of 23 μg/mL PLGA-cisplatin (DAPI-nuclear stainer).

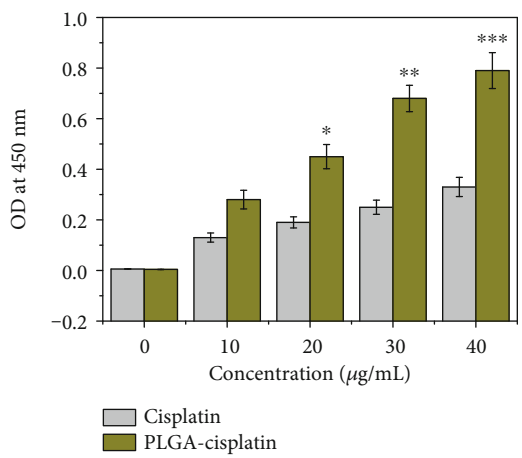

Figure 7: DNA fragmentation assay: cisplatin- and PLGA-cisplatin- (0-40 μg/mL) treated MCF-7 cells. Each value represents the mean ± SE of three experiments, $n = 3$ ($^{*}p < 0.05$, $^{**}p < 0.01$, and $^{***}p < 0.001$), compared with control.

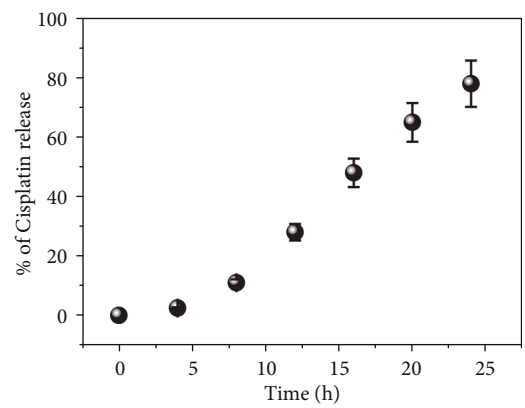

Figure 8: Time-dependent cisplatin release from PLGA-cisplatin at pH -5.5 (UV-Vis spectroscopic data). Each value represents the mean ± SE of three experiments ($n = 3$).

ROS generation by confocal microscopy after PLGA-cisplatin NP treatment (23 μg/mL) in a time-dependent manner (12 and 24 h) using the DCF-DA dye as an indicator of ROS. Increase in DCF-DA fluorescence emission (595 nm) is the indication of increase in ROS (Figure 6). Here, DAPI has been taken as a nuclear stainer. As shown in Figure 5, the microscopic images showed that the green emission has been increased in a time-dependent manner after treatment of 23 μg/mL of PLGA-cisplatin NPs. This above data confirmed that PLGA-cisplatin NPs are increasing ROS in theMCF-7 cell line.

3.5. Detection of DNA Damage. ROS overload also prompts oxidative damage to the cell's biomacromolecules, which culminates in the cell dysfunction and death. At high levels, ROS can lead to impaired physiological function through cellular damage of DNA. Hence, the DNA fragmentation assay was accomplished for both cisplatin and PLGA-cisplatin NPs, respectively, at 0-40 μg/mL concentrations. For the purpose, we have selected the OD value after treatment at 405 nm (Figure 7). The OD value suggests that the DNA fragmentation has been increased with the concentration of cisplatin and PLGA-cisplatin NPs. However, in case of PLGA-cisplatin NPs, the DNA fragmentation was found to be higher. This observation cleared that the elevated amount of ROS is damaging the DNA. These data showed that ROS-mediated DNA damage is correlated with PLGA-cisplatin NP-induced apoptosis in MCF-7 cancer cells.

3.6. Drug Release of Cisplatin from PLGA-Cisplatin NPs. We have also checked the delivery of cisplatin from PLGA-

cisplatin NPs at buffer of pH -5.5 by dialysis membrane technique. The measured the OD value at 4 h interval and extended up to further 24 h. It has been perceived that after 16 h almost 50% of cisplatin has been released, which confirmed that the bioavailability of PLGA-cisplatin NPs is more superior than only cisplatin (Figure 8).

4. Conclusions

In this study, cisplatin-loaded PLGA NPs possessing chemotherapy properties were obtained by a multistep process. PLGA-cisplatin NPs were characterized by AFM and FTIR techniques. The cytotoxicity data of the nanoparticles along with only cisplatin into MCF-7 have been evaluated by MTT Assay. A colorimetric UV–Vis method was adapted to quantify cisplatin in buffer samples. The pH-dependent drug release profile of NPs was observed on the surrounding medium, favoring the release of cisplatin under an acidic environment. In this way, we confirmed that the bioavailability of PLGA-cisplatin NPs has been increased. As in case of PLGA-cisplatin, the anticancer efficacy is higher compared to only cisplatin, so the risk of severe physiological disorders will be reduced. We have also established that the ROS generation into MCF-7 has been increased after PLGA-cisplatin nanoparticle treatment in a time-dependent manner. After that, we have checked the DNA damage which is following ROS generation data so we can say ROS generation is the cause of DNA damage in PLGA-cisplatin-induced apoptosis. Thus, PLGA-cisplatin NPs has huge potential to be employed as an anticancer agent to overcome the epidemiology of cancer in future.

Abbreviations

PLGA: Poly lactic-co-glycolic acid
BC: Breast cancer
ROS: Reactive oxygen species
ER: Estrogen receptor
PR: Progesterone receptor;
HER2: Human epidermal growth factor receptor
DMF: Dimethylformamide
PVA: Polyvinyl alcohol
OPDA: Orthophenylenediamine
OD: Optical density
MES: Ethanesulphonic acid clorhydrate
FTIR: Fourier transforms infrared
AFM: Atomic force microscopy
PSN: Penicillin-streptomycin-neomycin
DCF-DA: $2'$,$7'$-Dichlorofluorescein diacetate.

Data Availability

The data generated or analyzed in this article are publicly available online without request.

Conflicts of Interest

The authors have declared that no competing interest exists.

Authors' Contributions

Mohammed Al-Zharani, Gadah Albasher, and Hani Alothaid performed cell culture and treatments. Norah Saad AL-Johani evaluated the cytotoxicity. Nada H. Aljarba, Mohammed H. Almarzoug, and Norah M. Alhoshani detected the apoptosis and necrosis. Mohammed Al-Zharani and Abdullah A. Alkahtane determined the oxidative stress and performed statistical analysis. Saad Alkahtani and Saud Alarifi were involved in the conception and design of the study, data interpretation, and critical revision of the manuscript. All authors read and approved the final manuscript.

Acknowledgments

The authors extend their appreciation to the Deanship of Scientific Research at King Saud University for funding this work through research group no (RG-1441-018).

References

[1] J. Ferlay, M. Colombet, I. Soerjomataram et al., "Estimating the global cancer incidence and mortality in 2018: GLOBOCAN sources and methods," *International Journal of Cancer*, vol. 144, no. 8, pp. 1941–1953, 2019.

[2] H. Brody, "Cancer prevention," *Nature*, vol. 471, no. 7339, p. S1, 2011.

[3] T. A. Gaziano, A. Bitton, S. Anand, S. Abrahams-Gessel, and A. Murphy, "Growing epidemic of coronary heart disease in low- and middle-income countries," *Current Problems in Cardiology*, vol. 35, no. 2, pp. 72–115, 2010.

[4] P. Anand, A. B. Kunnumakara, C. Sundaram et al., "Cancer is a preventable disease that requires major lifestyle changes," *Pharmaceutical Research*, vol. 25, no. 9, pp. 2097–2116, 2008.

[5] B. Han, L. Sha, X. Yu, M. Yang, Y. Cao, and J. Zhao, "Identification of dual therapeutic targets assisted by _in situ_ automatous DNA assembly for combined therapy in breast cancer," *Biosensors and Bioelectronics*, vol. 176, article 112913, 2021.

[6] X. Wang, Y. Shi, D. Huang, and X. Guan, "Emerging therapeutic modalities of PARP inhibitors in breast cancer," *Cancer Treatment Reviews*, vol. 68, pp. 62–68, 2018.

[7] S. Al-Othman, A. Haoudi, S. Alhomoud, A. Alkhenizan, T. Khoja, and A. Al-Zahrani, "Tackling cancer control in the Gulf Cooperation Council Countries," *The Lancet Oncology*, vol. 16, no. 5, pp. e246–e257, 2015.

[8] B. Cánovas, A. Igea, A. A. Sartori et al., "Targeting p38α Increases DNA Damage, Chromosome Instability, and the Anti- tumoral Response to Taxanes in Breast Cancer Cells," *Cancer Cell*, vol. 33, no. 6, pp. 1094–1110.e8, 2018.

[9] S. Modi, C. Saura, C. Henderson et al., "A multicenter trial evaluating retaspimycin HCL (IPI-504) plus trastuzumab in patients with advanced or metastatic HER2-positive breast cancer," *Breast Cancer Research and Treatment*, vol. 139, no. 1, pp. 107–113, 2013.

[10] S. Al-Bahlani, B. Al-Dhahli, K. Al-Adawi, A. Al-Nabhani, and M. Al-Kindi, "Platinum-based drugs differentially affect the ultrastructure of breast cancer cell types," *BioMed Research International*, vol. 2017, Article ID 3178794, 13 pages, 2017.

[11] A. Sartaj, S. Baboota, and J. Ali, "Exploring the therapeutic potential of nanostructured lipid carrier approaches to

tackling the inherent lacuna of chemotherapeutics and herbal drugs against breast cancer," *Journal of Drug Delivery Science and Technology*, vol. 63, article 102451, 2021.

[12] T. Sorlie, C. M. Perou, R. Tibshirani et al., "Gene expression patterns of breast carcinomas distinguish tumor subclasses with clinical implications," *Proceedings of the National Academy of Sciences of the United States of America*, vol. 98, no. 19, pp. 10869–10874, 2001.

[13] G. Turashvili and E. Brogi, "Tumor heterogeneity in breast cancer," *Frontiers in Medicine*, vol. 4, 2017.

[14] P. ter Brugge, P. Kristel, E. van der Burg et al., "Mechanisms of therapy resistance in patient-derived xenograft models of BRCA1-deficient breast cancer," *Journal of the National Cancer Institute*, vol. 108, no. 11, article djw148, 2016.

[15] D. P. Silver, A. L. Richardson, A. C. Eklund et al., "Efficacy of neoadjuvant cisplatin in triple-negative breast cancer," *Journal of Clinical Oncology*, vol. 28, no. 7, pp. 1145–1153, 2010.

[16] M. P. Decatris, S. Sundar, and K. J. O'Byrne, "Platinum-based chemotherapy in metastatic breast cancer: current status," *Cancer Treatment Reviews*, vol. 30, no. 1, pp. 53–81, 2004.

[17] A.-M. Florea and D. Büsselberg, "Cisplatin as an anti-tumor drug: cellular mechanisms of activity, drug resistance and induced side effects," *Cancers*, vol. 3, no. 1, pp. 1351–1371, 2011.

[18] Z. H. Siddik, "Cisplatin: mode of cytotoxic action and molecular basis of resistance," *Oncogene*, vol. 22, no. 47, pp. 7265–7279, 2003.

[19] L. R. Kelland, "Preclinical perspectives on platinum resistance," *Drugs*, vol. 59, Supplement 4, pp. 1–8, 2000.

[20] J. Reedijk, "New clues for platinum antitumor chemistry: kinetically controlled metal binding to DNA," *Proceedings of the National Academy of Sciences of the United States of America*, vol. 100, no. 7, pp. 3611–3616, 2003.

[21] M. Konishi, Y. Tabata, M. Kariya et al., "In vivo anti-tumor effect through the controlled release of cisplatin from biodegradable gelatin hydrogel," *Journal of Controlled Release*, vol. 92, no. 3, pp. 301–313, 2003.

[22] S. Rezvantalab, N. I. Drude, M. K. Moraveji et al., "PLGA-based nanoparticles in cancer treatment," *Frontiers in Pharmacology*, vol. 9, p. 1260, 2018.

[23] W. Zhang, J. Shen, H. Su et al., "Co-delivery of cisplatin prodrug and chlorin e6 by mesoporous silica nanoparticles for chemo-photodynamic combination therapy to combat drug resistance," *ACS Applied Materials & Interfaces*, vol. 8, no. 21, pp. 13332–13340, 2016.

[24] P. Dana, S. Bunthot, K. Suktham et al., "Active targeting liposome-PLGA composite for cisplatin delivery against cervical cancer," *Colloids and Surfaces B: Biointerfaces*, vol. 196, article 111270, 2020.

[25] V. V. Ranade, M. A. Hollinger, and J. B. Cannon, *Drug Delivery Systems*, CRC Press, 1995.

[26] G. Prencipe, S. M. Tabakman, K. Welsher et al., "PEG branched polymer for functionalization of nanomaterials with ultralong blood circulation," *Journal of the American Chemical Society*, vol. 131, no. 13, pp. 4783–4787, 2009.

[27] R. Mout, D. F. Moyano, S. Rana, and V. M. Rotello, "Surface functionalization of nanoparticles for nanomedicine," *Chemical Society Reviews*, vol. 41, no. 7, pp. 2539–2544, 2012.

[28] H. K. Makadia and S. J. Siegel, "Poly lactic-co-glycolic acid (PLGA) as biodegradable controlled drug delivery carrier," *Polymers*, vol. 3, no. 3, pp. 1377–1397, 2011.

[29] J. A. Loureiro and M. C. Pereira, "PLGA based drug carrier and pharmaceutical applications: the most recent advances," *Pharmaceutics*, vol. 12, no. 9, p. 903, 2020.

[30] R. Domínguez-Ríos, D. R. Sánchez-Ramírez, K. Ruiz-Saray et al., "Cisplatin-loaded PLGA nanoparticles for HER2 targeted ovarian cancer therapy," *Colloids and Surfaces B: Biointerfaces*, vol. 178, pp. 199–207, 2019.

[31] D. Moreno, S. Zalba, I. Navarro, C. Tros de Ilarduya, and M. J. Garrido, "Pharmacodynamics of cisplatin-loaded PLGA nanoparticles administered to tumor- bearing mice," *European Journal of Pharmaceutics and Biopharmaceutics*, vol. 74, no. 2, pp. 265–274, 2010.

[32] G. M. Severini, L. Pascolo, B. Bortot et al., "Detection of PLGA-based nanoparticles at a single-cell level by synchrotron radiation FTIR spectromicroscopy and correlation with X-ray fluorescence microscopy," *International Journal of Nanomedicine*, vol. 9, pp. 2791–2801, 2014.

[33] P. K. Das, F. Islam, and A. K. Lam, "The roles of cancer stem cells and therapy resistance in colorectal carcinoma," *Cells*, vol. 9, no. 6, p. 1392, 2020.

[34] C. Pathak, F. U. Vaidya, and S. M. Pandey, "Mechanism for development of nanobased drug delivery system," *Applications of Targeted Nano Drugs and Delivery Systems*, pp. 35–67, 2019.

[35] A. V. Tonder, A. M. Joubert, and A. D. Cromarty, "Limitations of the 3-(4, 5-dimethylthiazol-2-yl)-2, 5-diphenyl-2H-tetrazolium bromide (MTT) assay when compared to three commonly used cell enumeration assays," *BMC Research Notes*, vol. 8, pp. 1–10, 2015.

[36] P. C. Wever, J. Aten, R. J. Rentenaar et al., "Apoptotic tubular cell death during acute renal allograft rejection," *Clinical Nephrology*, vol. 49, no. 1, pp. 28–34, 1998.

[37] P. Bhanja, S. Mishra, K. Manna, A. Mallick, K. Das Saha, and A. Bhaumik, "Covalent organic framework material bearing phloroglucinol building units as a potent anticancer agent," *ACS Applied Materials & Interfaces*, vol. 9, no. 37, pp. 31411–31423, 2017.

[38] B. Perillo, M. D. Donato, A. Pezone et al., "ROS in cancer therapy: the bright side of the moon," *Experimental & Molecular Medicine*, vol. 52, no. 2, pp. 192–203, 2020.

[39] R. Nandi, S. Mishra, T. K. Maji et al., "A novel nanohybrid for cancer theranostics: folate sensitized Fe_2O_3 nanoparticles for colorectal cancer diagnosis and photodynamic therapy," *Journal of Materials Chemistry B*, vol. 5, no. 21, pp. 3927–3939, 2017.

[40] N. Deirram, C. Zhang, S. S. Kermaniyan, A. P. R. Johnston, and G. K. Such, "pH-responsive polymer nanoparticles for drug delivery," *Macromolecular Rapid Communications*, vol. 40, no. 10, article 1800917, 2019.

[41] N. Kamaly, B. Yameen, J. Wu, and O. C. Farokhzad, "Degradable controlled-release polymers and polymeric nanoparticles: mechanisms of controlling drug release," *Chemical Reviews*, vol. 116, no. 4, pp. 2602–2663, 2016.

[42] R. Marullo, E. Werner, N. Degtyareva et al., "Cisplatin induces a mitochondrial-ROS response that contributes to cytotoxicity depending on mitochondrial redox status and bioenergetic functions," *PLoS One*, vol. 8, no. 11, article e81162, 2013.

Hindawi
Oxidative Medicine and Cellular Longevity
Volume 2021, Article ID 5511523, 12 pages
https://doi.org/10.1155/2021/5511523

Research Article

Ameliorative Effect of Thymoquinone-Loaded PLGA Nanoparticles on Chronic Lung Injury Induced by Repetitive Intratracheal Instillation of Lipopolysaccharide in Rats

Sultan A. M. Saghir,[1] Naif A. Al-Gabri,[2,3,4] Abdelmoniem A. Ali,[3] Al-Sayed R. Al-Attar,[3] Mosa'd Al-Sobarry,[5] Omar Y. A. Al-shargi,[6] Amal Alotaibi,[7] Mohammed Al-zharani,[8] Fahd A. Nasr,[9] Nader Al-Balagi,[10] Mahfoudh A. M. Abdulghani,[11] Sulaiman M. Alnaimat,[1] Osama Y. Althunibat,[1] and Ayman M. Mahmoud[12,13]

[1]*Department of Medical Analysis, Princess Aisha Bint Al-Hussein College of Nursing and Medical Sciences, Al-Hussein Bin Talal University, Ma'an 71111, Jordan*
[2]*Department of Pathology, Faculty of Veterinary Medicine, Thamar University, Dhamar 87246, Yemen*
[3]*Department of Pathology, Faculty of Veterinary Medicine, Zagazig University, Zagazig, Egypt*
[4]*Laboratory of Djibouti Regional livestock Quarantine, Abu Yasser International Est., Djibouti*
[5]*Department of Pharmacology, College of Pharmacy, Ittihad Private University, Al-Raqqah, Syria*
[6]*College of Pharmacy, Riyadh Elm University, Riyadh, Saudi Arabia*
[7]*Basic Science Department, College of Medicine, Princess Nourah bint Abdulrahman University, Riyadh 11671, Saudi Arabia*
[8]*Biology Department, College of Science, Imam Mohammad ibn Saud Islamic University, Riyadh 11623, Saudi Arabia*
[9]*Medicinal, Aromatic and Poisonous Plants Research Center, College of Pharmacy, King Saud University, Riyadh 11451, Saudi Arabia*
[10]*Ministry of Health, Riyadh, Saudi Arabia*
[11]*Department of Pharmacology & Toxicology, Unaizah College of Pharmacy, Qassim University, Al Qassim 51911, Saudi Arabia*
[12]*Biotechnology Department, Research Institute of Medicinal and Aromatic Plants, Beni-Suef University, Beni-Suef, Egypt*
[13]*Physiology Division, Zoology Department, Faculty of Science, Beni-Suef University, Beni-Suef, Egypt*

Correspondence should be addressed to Naif A. Al-Gabri; naifaljabry2014@gmail.com
and Ayman M. Mahmoud; ayman.mahmoud@science.bsu.edu.eg

Received 30 January 2021; Revised 22 February 2021; Accepted 10 May 2021; Published 28 May 2021

Academic Editor: Daniele Vergara

Thymoquinone (TQ), the active constituent of *Nigella sativa*, possesses several benefits in traditional and modern medicines. This study examined the effect of a single dose of Nano-TQ on chronic lung injury induced by repetitive intratracheal installation of lipopolysaccharide (LPS). Rats received LPS twice weekly for 8 weeks via intratracheal installation and a single dose of TQ-PLGA NPs on the day after the last dose of LPS. Six rats from each group were sacrificed after 8 and 10 weeks, and samples were collected for analysis. Repetitive intratracheal installation of LPS caused histopathological alterations, including partial or complete obstruction of the alveoli, interstitial edema, mild fibroblastic proliferation, fibrous strands besides lymphocytes and plasma infiltrations, suffered fetalization, bronchiectasis, hypertrophied arterioles, and others. Investigation of the ultrastructure revealed prominent necrotic pneumocytes with destructed chromatin and remnant of necrotic debris in the narrowing alveolar lumen in LPS-induced rats. TQ-PLGA NPs effectively ameliorated LPS-induced histopathological and ultrastructural alterations in the lung of rats. In addition, TQ-PLGA NPs significantly alleviated serum levels of IL-10 and TGF-β1 in LPS-induced rats. In conclusion, TQ-PLGA NPs prevented inflammation and tissue injury in the lungs of rats challenged with repetitive intratracheal installation of LPS. Therefore, TQ-PLGA NPs represent a promising candidate for the prevention of lung injury induced by LPS, pending further studies to determine its safety and exact protective mechanism.

1. Introduction

Chronic airway inflammation leads to respiratory diseases such as chronic obstructive pulmonary disease (COPD), resulting in a significant economic and social burden [1, 2]. Chronic airway inflammation provokes persistent lung injury (PLI) caused by bacterial infection [3, 4]. A large number of virulent microbes requires the activation of innate immune system, mainly neutrophils and macrophages. In PLI, multiple inflammatory cells and mediators are activated, and the mechanisms for resolving inflammation are impaired [1, 5–7]. In response to microbial infection, Toll-like receptors (TLRs) mediate the activation of macrophages. TLRs are pattern recognition receptors (PRRs) and fundamental regulators of both innate and adaptive immunity [8, 9]. Lipopolysaccharide (LPS), the main component of the bacterial cell wall [10, 11], stimulates TLR-4 and promotes the activation of nuclear factor κB (NF-κB) and subsequent release of proinflammatory cytokines [12]. Thus, suppressing the NF-κB signaling pathway can represent a strategy to downregulate excessive inflammatory responses. In pulmonary disease, cytokines and inflammatory factors, such as transforming growth factor-beta (TGF-β1) and interleukin- (IL-) 10, are released from the injured tissues and promote lung fibrosis [13, 14]. TGF-β1 is considered the key factor behind pulmonary fibrosis [15]. Besides its effect in the transdifferentiation of quiescent fibroblasts into myofibroblasts, it is the basic inducer of alveolar epithelial–mesenchymal transformation [16]. Interestingly, the activation of TGF-β1 is regulated by IL-10, which can play a part in attenuating the fibrosis [17].

Thymoquinone (TQ) is the primary active chemical component of the *Nigella sativa* essential oil. TQ is a potent antioxidant and anti-inflammatory agent [18–20] and a potential therapeutic effect in respiratory diseases [21–23]. TQ protects against toxic medications such as bleomycin-induced lung fibrosis [24, 25], gentamicin-induced kidney and liver injury [19, 20], and titanium dioxide nanoparticle-induced toxicity [26]. However, it has limitations in effectiveness due to its narrow therapeutic window and poor oral bioavailability [27, 28]. TQ is a hydrophobic molecule and has poor water solubility and poor formulation. TQ-nanoparticles (TQ NPs) revealed potential antioxidant and anti-inflammatory effects [29, 30] and improved oral bioavailability and formulation [21, 31]. Poly lactic-co-glycolic acid (PLGA) improved the pharmacokinetics and pharmacodynamics properties of TQ NP intranasal administration [32]. In addition, a prior study reported that TQ-PLGA NPs possess the capability to attenuate bleomycin-induced pulmonary fibrosis through suppression of oxidative stress and inflammation [33]. Accordingly, this study was established to explore the ameliorative effects of TQ-PLGA-PVA NPs on chronic lung injury induced by repetitive intratracheal (i.t.) instillation of LPS in rats and its effects on regulation of serum TGF-β1 and IL-10 levels.

2. Materials and Methods

2.1. Designing TQ-PLGA Nanoemulsion. Nanoparticles were prepared with PLGA using the solid/oil/water (S/O/W) solvent evaporation method as previously described [21, 34] with some modifications (Figure 1). Briefly, PLGA (Sigma, USA) was dissolved in HPLC-grade dichloromethane (DCM) as an oil phase for 12 h to obtain uniform solution followed by the addition 5 mg TQ (Sigma, USA). The suspension was sonicated for 2 min to generate S/O primary emulsion that was emulsified with an aqueous phase of 20 ml saline with polyvinyl alcohol (1% w/v) to form S/O/W emulsion using a magnetic stirrer at 400 rpm. The mixture was vortexed for 10 sec at a high setting followed by ultrasonication (20 KH2) for 3 min to generate the final S/O/W emulsion. The organic solvent was evaporated using a rotary evaporator at 50°C. Following centrifugation at 10,000 rpm for 20 min at 4°C, the synthesized material was collected and resuspended in 2% sucrose. The shape and size of the particles were confirmed using transmission electron microscope (TEM) [35]. The characteristics of TQ-PLGA NPs were reported in our previous work [33]. The suspension of TQ-PLGA NPs exhibited turbid white color, and the nanoparticles were spherical in shape and 20 nm (10-30 nm) sized with 80% encapsulation efficiency.

2.2. Encapsulation Efficiency (EE) of TQ-PLGA NPs. Nanoparticles suspension was subjected to centrifugation at 30,000 rpm for 15 min. The supernatant was removed, and 1 ml of methanol was added to the sediment which was treated with sonication for 5 min and then injected to HPLC to measure the amount of TQ. The EE was 80% as calculated using the following equation [21]:

$$\text{EE\%} = \frac{\text{Total TQ} - \text{Nonencapsulated TQ}}{\text{Total TQ}} \times 100 \quad (1)$$

2.3. Animals and Treatments. Forty-eight male healthy albino rats weighing 250 ± 50 g, obtained from the animal house of Zagazig University, were used in this investigation. The animals were housed under standard conditions and given a free access to water and a standard diet (El-Nasr Chemical Company, Egypt). The study was conducted according to the guidelines of the National Institutes of Health (NIH publication No. 85-23, revised 2011) and were approved by the local animal care review committee of Zagazig University (Ethical approval number: ZU-IACUC/2/F/71/2020).

The animals were acclimatized for one week and allocated into 4 groups as follows: Group I (control): received i.t. instillation of saline twice weekly for 8 weeks. Group II (TQ-PLGA NPs): received i.t. instillation of saline twice weekly for 8 weeks and a single i.t. dose of TQ-PLGA NPs on the day after the final dose of saline. Group III (LPS): received i.t. instillation of LPS dissolved in saline twice weekly for 8 weeks. Group IV (LPS + TQ-PLGA NPs): received i.t. instillation of LPS dissolved in saline twice weekly for 8 weeks and a single i.t. dose of TQ-PLGA NPs on the day after the final dose of LPS.

LPS and TQ-PLGA NPs were i.t. instilled as previously described [36, 37] with slight modifications. In brief, ketamine/xylazine-anesthetized rats were fixed on their back at an angle of 70 degrees on a glass board. LPS (*Escherichia coli* 055: B5; Sigma, USA) and TQ-PLGA NPs were dissolved in

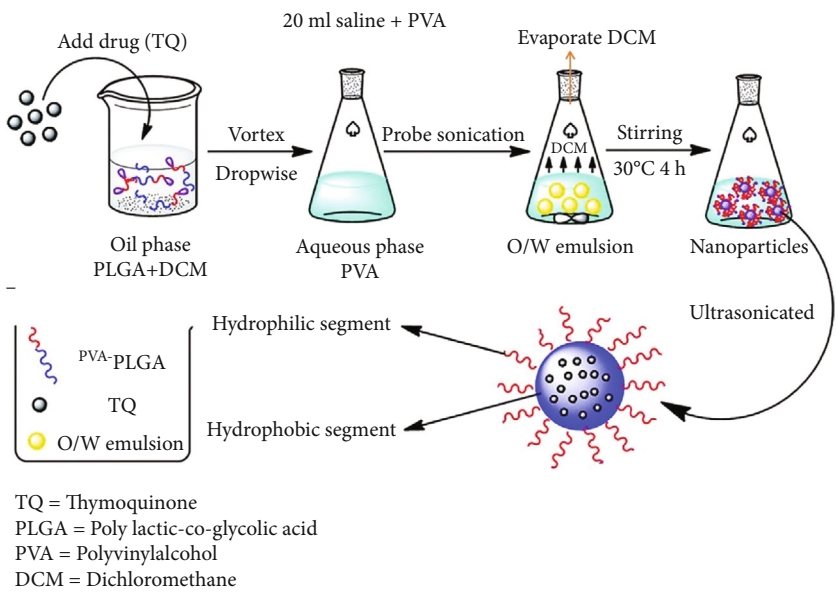

Figure 1: A schematic illustration of TQ-PLGA NP synthesis method.

saline and instilled into the trachea at a dose level of 2 mg/kg body weight [33]. i.t. instillation was performed using a 3-gauge intravenous plastic needle connected to a syringe followed by 0.3 ml air. The rats were then placed in a vertical position and rotated for 1 min to distribute the instillation evenly within the lungs.

Six rats from each group were sacrificed under ketamine/xylazine anesthesia 24 h after the instillation of TQ-PLGA NPs (8 weeks point) and at the end of week 10 (10 weeks point) from the beginning of the experiment. The gross lesions were recorded, and blood samples were collected via cardiac puncture, left to coagulate for 30 min, and centrifuged at 3000 rpm for 10 min, and serum was separated. Specimens from lungs were fixed in 10% neutral buffered formalin for histopathology, and other specimens were rapidly kept in 2.5% glutaraldehyde for TEM.

2.4. Histopathology. The examined tissue specimens were fixed in 10% buffered formalin for 24 h. Preserved tissues were processed routinely by the paraffin embedding technique [38]. Histopathological changes were evaluated by light microscopy by semiquantitative lesion score system. Lesion score represented by -, normal; +, mild; ++, moderate; and +++, severe as previously described [39].

2.5. Ultrastructure Assessment. To examine the ultrastructure, the lung samples were rapidly trimmed into fine sections by sharp blade and fixed in 2.5% glutaraldehyde (pH 7.2) for 4 h then put in 1.33% osmium tetroxide overnight at 4°C followed by dehydration and clearance. The samples were embedded in epoxy resin, and sem-thin sections were obtained by ultramicrotome and stained by toluidine blue and evaluated by light microscopy to detect lesions [40]. The sections were processed for the detection of lesions after the tissue up-load on the grid and stained by lead citrate and uranium. Finally, the ultrasections were evaluated by TEM (JEOL JEM-1230).

2.6. Assessment of TGF-β1 and IL-10. Sera levels of IL-10 were assayed using a specific ELISA kit (Cat. No. ELR-IL-10, RayBiotech, USA), and TGF-β1 was measured by the ELISA kit (Cat. No. K4344, BioVision, USA) according to the manufacturers' instructions. The sensitivity of TGF-β1 ELISA kit is <1 pg/ml, whereas the sensitivity of IL-10 kit is 10 pg/ml.

2.7. Statistical Analysis. The results of IL-10 and TGF-β1 were statistically analyzed using two-way ANOVA on GraphPad Prism 7 followed by Tukey's test. The results are presented as means ± standard error of the mean (SEM), and $P < 0.05$ was considered statistically significant.

3. Results

3.1. Clinical Signs and Gross Findings. The rats did not suffer any clinical signs or mortality throughout the experiment. The control group showed normal morphology of pulmonary tissues at 8 and 10 weeks. Supplementation of TQ-PLGA NPs to normal rats exerted no alterations, and only the focal mild apical hepatized area was observed. The gross pictures showed the effect of repetitive i.t. instillation of LPS at 8 and 10 weeks that revealed consolidations as a depressed area and in general small-size lobules. Moreover, TQ-PLGA NPs restored the normal size of lobules with still small red foci in the lung of LPS-challenged rats (Figure 2).

3.2. Histopathological Findings. Examined sections from sacrificed rats received repetitive i.t. saline revealed normal histomorphology architectures of both alveoli and airways with mild edema and congestions at week 8. After 10 weeks, all structures were normal without any alterations except slight individual congested blood vessels and limitation emphysema (Figures 3–5). Sections from sacrificed rats treated with TQ-PLGA NPs at 8 weeks revealed activated alveolar macrophages which contain NPs and nearly normal

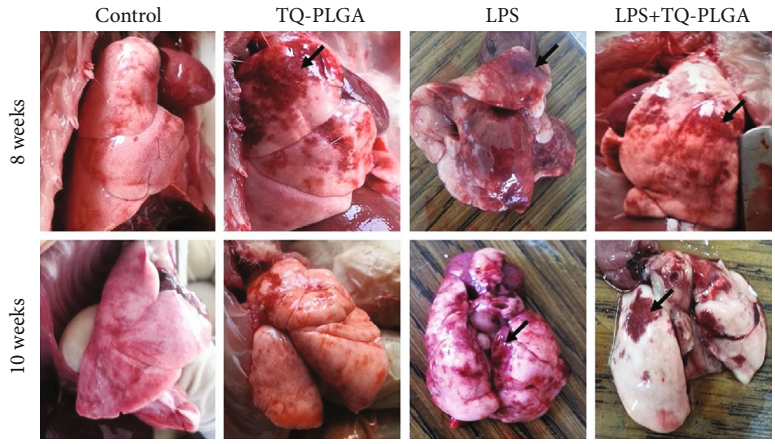

Figure 2: The gross pictures from control rats showing normal morphology of pulmonary tissues, TQ-PLGA NP group showing mild apical hepatized area (arrow), LPS-challenged rats showing consolidations as a depressed area and in small-size lobules (arrows), and LPS + TQ-PLGA NPs showing restoration of the normal size of the lobules with still small red foci (arrows).

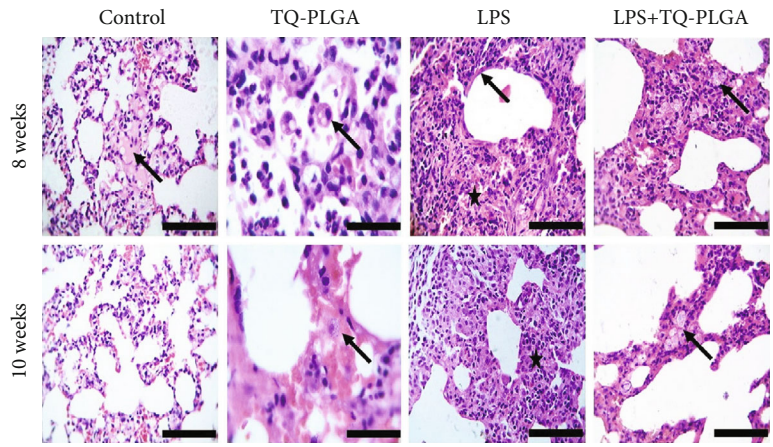

Figure 3: Representative photomicrograph of the control rats showing normal histomorphology architectures with mild edema and congested blood vessels at 8 weeks (arrow) and normal pulmonary alveoli and septa with minute congested blood vessels at 10 weeks, TQ-PLGA NP group showing activated alveolar macrophages (arrow) besides little acute inflammatory cells in the alveolar lumen at 8 weeks and hemorrhages with congested blood capillary (arrow), LPS-challenged rats showing marked obstructions of pulmonary alveoli due to fibroblastic proliferations and chronic inflammatory cells (star) with hyaline wall (arrow) at 8 weeks, and alveolar obstruction with moderate thickening septa (star) at 10 weeks, and LPS + TQ-PLGA NPs showing severe thickening of alveolar septa characterized by proliferated pneumocytes admixed with chronic inflammatory cells which contain granular nanoparticles (arrow) at 8 weeks, remodeling the pulmonary tissues characterized with clear lumen and nearly thinning alveolar septa which contain nanomaterials (arrow) (H&E, scale bar 100 μm).

airways except a few exfoliated little mucosa inside the lumen. Moreover, nearly normal blood vessels and capillaries with mild vacuolated media followed by edema were observed in few rats. After 10 weeks, the sections revealed congested blood capillary with few pulmonary foamy cells containing NPs, whereas airways contained small vacuoles and blood vessels appeared normal (Figures 3 and 4).

The examined sections from rats received with repetitive i.t. LPS twice weekly for 8 weeks revealed chronic pneumonia represented by chronic exudate within the alveoli and complete or partial obstruction due to interstitial edema and mild fibroblastic proliferation. These alterations along with little fibrous strands beside lymphocytes and plasma infiltrations were observed in the majority of sections. Some alveoli suffered hyperplasia of the alveolar epithelium, and the pulmonary airways showed partial obstructions of the bronchioles (bronchiectasis) due to thick mucus materials admixed with inflammatory cells. Hypertrophied arteriole wall was noticed, and some emphysematous alveoli showed partial hyalinization of their wall. After 10 weeks (two weeks post the last LPS dose), the lesion in the majority of sacrificed rats is still intense and pronounced and represented by diffuse and large chronic active pneumonic areas consisted of necrotic alveolar tissues invaded by proliferated and hyperplastic pneumocytes type II and alveolar macrophages (foamy cells). The airways suffered narrowing due to goblet cells metaplasia (Figures 3 and 4).

Sections from rats treated with TQ-PLGA NPs after LPS and sacrificed 24 h after treatment revealed amelioration of

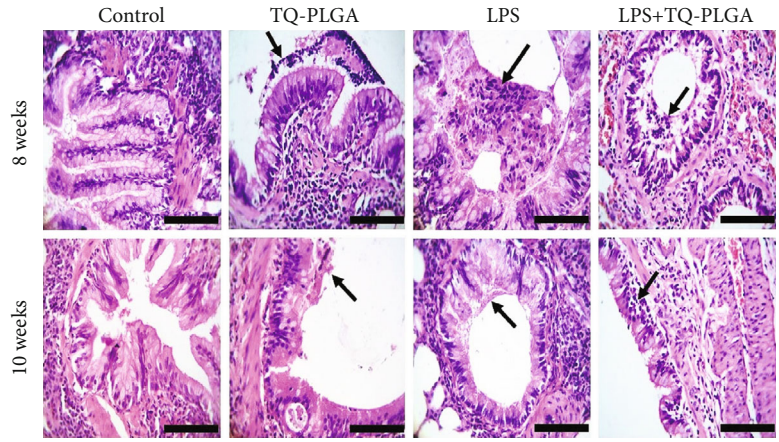

Figure 4: Representative photomicrograph of the pulmonary airways of the control rats showing normal columnar epithelium with mild goblet cell metaplasia and normal pulmonary airways, TQ-PLGA NP group showing clear mucous inflammatory exudate intact to the bronchial mucosa (arrow) at 8 weeks and submucosal vacuoles with few desquamated cells (arrow) at 10 weeks, LPS-challenged rats showing partial obstructions of the bronchioles due to thick mucus materials admixed with inflammatory cells (arrow) at 8 weeks and narrow airways due to narrow airways due to mucous secretions pavementing on the surface of normal epithelium lining (arrow) at 10 weeks, and LPS + TQ-PLGA NPs showing little mucus with inflammatory cells (arrow) and still peribronchial hemorrhages at 8 weeks and nearly normal pulmonary airways with clear lumen and still slight submucosal edema and a few lymphocytes (arrow) (H&E, scale bar 100 μm).

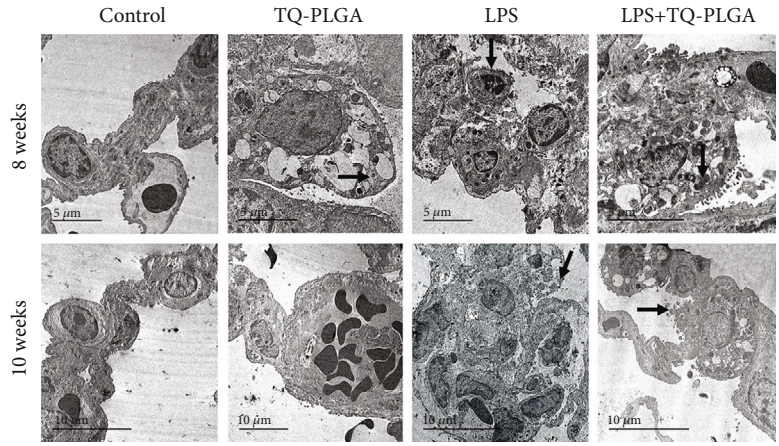

Figure 5: Representative electron micrograph of the lung of control rats showing normal ultrastructure (arrow) at 8 weeks and 10 weeks, TQ-PLGA NP group showing nearly normal pneumocytes nuclei with prominent vacuolated cytoplasm with a little lamellar material as well as nanomaterials (arrow) at 8 weeks and normal air-blood barrier with widening of blood capillary lumen which contain numerous erythrocytes (arrow) at 10 weeks, LPS-challenged rats showing diffuse loss of rough endoplasmic reticulum, mitochondria, blebbing of the nuclear membrane and glycogen lysis with destructed chromatin (arrows) at 8 and 10 weeks, and LPS + TQ-PLGA NPs showing some collagen fibers deposits besides vacuolated pneumocytes which contain nanomaterials (arrow) at 8 weeks, and prominent restoration of the ultrastructural features of the pneumocytes ultrastructure (arrow) at 10 weeks.

the lung lesions with still thickening of alveolar septa characterized by large foamy cells which contain dark bluish granular nanoparticles besides the absence of exudate in the majority of alveoli lumen. Numerous active macrophages (foamy cells) with vacuolated cytoplasm with tendency to form syncytial giant cells were predominant in interalveolar tissue. The airways still show a little mucous with inflammatory cells on the mucosa and goblet cells metaplasia (Figures 3 and 4).

The histopathological alterations caused by repetitive LPS i.t. instillation and the ameliorative effect of TQ-PLGA NPs are summarized in Table 1.

3.3. Ultrastructure Findings. The ultrastructure of the lungs of control and TQ-PLGA NP groups appeared normal with no alterations (Figure 5). Lesion scores of ultrastructure findings of pulmonary airways, blood vessels, alveoli, and pulmonary septa in LPS-treated rats are shown in Table 2. Examination of ultrastructures of lung tissues from rats which received repetitive i.t. LPS revealed prominent necrotic pneumocytes with destructed chromatin and remnant of necrotic debris from the cytoplasmic organelles which extend to the narrow alveolar lumen. After 10 weeks, LPS-challenged rats showed prominent destructed and necrotic pneumocytes without any cytoplasmic organelles with

Table 1: Severity of histopathologic lesions recorded in pulmonary airways, blood vessels, and alveoli in LPS-challeneged rats and the ameliorative effect of TQ-PLGA NPs.

		Control	TQ-PLGA	LPS	LPS + TQ-PLGA	Control	TQ-PLGA	LPS	LPS + TQ-PLGA
		8 weeks				10 weeks			
Airways (bronchi and bronchioles)	Submucosal inflammatory cells infiltrations	-	+	++ +	++	-	-	++ +	++
	Proliferated epithelium and goblet cells metaplasia	-	+	++ +	++	-	-	++ +	++
	Bronchostenosis	-	-	++ +	++	-	-	++ +	++
	Peribronchial plasma and fibroblast proliferation	-	+	++ +	++	-	-	++ +	++
	Hyperplasia and apoptosis of bronchial associated lymphoid tissues (BALT)	-	-	++ +	+++	-	-	++ +	+
Pulmonary blood vessels	Endotheliosis	-	-	++ +	+	-	-	++ +	+
	Perivascular edema	-	-	++ +	++	-	-	++ +	++
	Hyperplasia of smooth muscles	-	-	++ +	++	-	-	++ +	+
Alveolar tissue (alveoli and blood-air barrier)	Hyperplasia and hypertrophy of pneumocytes I and II	-	+	++ +	++	-	+	++ +	++
	Activated alveolar macrophage	-	+	++ +	++	-	+	++ +	++
	Thickening of alveoli septal	-	+	++ +	++	-	+	++ +	+
	Atelectasis	-	-	++ +	++	-	-	++ +	+
	Chronic pneumonia	-	-	++ +	+	-	-	++ +	+
	Compensatory emphysema	-	+	++ +	++	-	+	++ +	++

No. of examined fields (5 fields/rat). The severity of lesion was graded by estimating the percentage area affected in the entire section. -: absence of lesion, +: 5–25%, ++: 26–50%, and +++: ≥51%.

destructed chromatins and microvilli in the pneumocytes surfaces. In contrast, rats that received TQ-PLGA NPs showed few collagen fiber deposits besides vacuolated pneumocytes with empty lamellar bodies which sometimes contain nanomaterials at 8 weeks, and nearly normal pneumocytes nuclei and its chromatin with prominent vacuolated cytoplasm with a little lamellar material as well as nanomaterials as well as prominent restoration of the ultrastructural features of the pneumocytes after 10 weeks (Figure 5).

3.4. TQ-PLGA NPs Ameliorate Serum Levels of IL-10 and TGF-β1 in LPS-Challenged rats. Rats of the LPS group showed a significant increase in serum IL-10 (Figure 6) and TGF-β1 (Figure 7) levels when compared with the control rats ($P < 0.001$). Administration of TQ-PLGA NPs ameliorated serum IL-10 and TGF-β1 levels in LPS-challenged rats with no effect in normal rats.

4. Discussion

Thymoquinone is a promising compound possesses a strong antioxidant and anti-inflammatory activities both *in vitro* and in *vivo*. In the present study, we used a rat model of LPS-induced chronic lung injury to investigate the potential effects of Nano-TQ. Crude TQ could be toxic at high doses and causes allergic dermatitis and has poor water solubility. To overcome these disadvantages, biodegradable and biocompatible polymeric nanoparticles would be attractive alternatives for TQ delivery. The route of administration of Nano-TQ was instillation into the trachea to enhance local TQ effect on pulmonary immune system and avoid systematic injection because it is hydrophobic and should be slowly disseminated [41, 42].

In our experiment, the pulmonary tissue of rats that received repeated doses for LPS was characterized by many chronic alterations, including severe narrowing (bronchostenosis) due to active chronic bronchiolitis with mucous exudates and goblet cell metaplasia. Our results partially agreed with Harkema and Hotchkiss who noticed mucous cell metaplasia in the trachea and bronchial airways of rats exposed to repeated doses of LPS [43]. Similar findings were added by Stolk et al. who described bronchial mucus cell hyperplasia in lungs of hamster due to repetitive i.t. installation of LPS for 5 weeks [44]. Moreover, other researchers noticed thickened airway wall with patchy actin staining after long-term exposure to corn dust extract in mice [45]. On the other

Table 2: Lesion scores of ultrastructure findings of pulmonary airways, blood vessels and alveoli in LPS-challenged rats and the ameliorative effect of TQ-PLGA NPs.

		Control	TQ-PLGA	LPS	LPS + TQ-PLGA	Control	TQ-PLGA	LPS	LPS + TQ-PLGA
		8 weeks				10 weeks			
Airways (bronchi and bronchioles)	Submucosal inflammatory cells infiltrations	-	+	++ +	++	-	-	++ +	++
	Proliferated epithelium and goblet cells metaplasia	-	+	++ +	++	-	-	++ +	++
	Bronchostenosis	-	-	++ +	++	-	-	++ +	++
	Peribronchial plasma and fibroblast proliferation	-	+	++ +	++	-	-	++ +	++
	Hyperplasia and apoptosis of bronchial associated lymphoid tissues (BALT)	-	-	++ +	++	-	-	++ +	+
Pulmonary blood vessels	Endotheliosis	-	-	++ +	+	-	-	++ +	+
	Perivascular edema	-	-	++ +	++	-	-	++ +	++
	Hyperplasia of smooth muscles	-	-	++ +	++	-	-	++ +	+
Alveolar tissue (alveoli and blood-air barrier)	Hyperplasia and hypertrophy of pneumocytes I and II	-	+	++ +	++	-	+	++ +	++
	Activated alveolar macrophage	-	+	++ +	++	-	+	++ +	++
	Thickening of alveoli septal	-	+	++ +	++	-	+	++ +	+
	Atelectasis	-	-	++ +	++	-	-	++ +	+
	Chronic pneumonia	-	-	++ +	+	-	-	++ +	+
	Compensatory emphysema	-	+	++ +	++	-	+	++ +	++
Pulmonary septa	Thickening (inflammatory edema)	-	-	++ +	++	-	-	++ +	+

No. of examined fields (5 fields/rat). The severity of lesion was graded by estimating the percentage area affected in the entire section. -: absence of lesion, +: 5–25%, ++: 26–50%, and +++: ≥50%.

hand, our findings included BALT hyperplasia with prominent mitotic and karyorrhexis activities in its germinal center. These findings disagree with Kaneko et al. who attributed thickened airways due to infiltration of leukocytes into BALT [46]. Moreover, the later authors noticed inflammatory cells infiltrations within emphysematous alveoli, swelling of the alveolar walls besides goblet cell hyperplasia in the airways, and a large number of inflammatory cells infiltrations mainly macrophages and neutrophils after 15 min from LPS exposure by nebulizer [46].

The lesions in our work also included emphysema and bronchial mucus cell hyperplasia. Prior study noticed that PMNs recruitment and the neutrophil-derived elastase can induce pulmonary emphysema and bronchial mucus cell hyperplasia [44], findings that are consistent with the current study. Additionally, inhibition of elastase resulted in protection against LPS-induced emphysema and to a lesser extent bronchial mucus cell hyperplasia [44]. Furthermore, Khedoe et al. found emphysema and increased number of macrophages, alveolar destruction, and neutrophils infiltrations in sacrificed mice after LPS administration (twice weekly for 20 weeks) [47]. The findings of this study stated the presence of prominent pulmonary emphysema in rats sacrificed after 8 and 10 weeks which are in agreement with findings of Finlay and his colleges who considered that the presence of emphysema could be due to COPD [48]. They also demonstrated an increase in BALT concentrations and macrophage expression of matrix metalloproteinase-1 (MMP-1) and MMP-9 [48].

Similar conclusions were reported previously indicating that the mechanisms of emphysema include activation of macrophages by LPS release and elastolytic enzymes (proteinase), mainly MMP-2, MMP-9, MMP-12, and cytokines from chemotactic neutrophils [49–51]. Also, emphysema could be responsible for destruction of lung parenchyma, including alveolar wall and capillary beds [51].

Partial or complete obstruction of the alveoli (chronic alveolitis) accompanied with interstitial proliferated and activated pneumocytes together with alveolar macrophages were common in LPS-challenged rats. Similar results were reported by previous investigations showing that chronic alveolitis could be attributed to numerous mononuclear leukocytes infiltrations mainly macrophages in the pulmonary

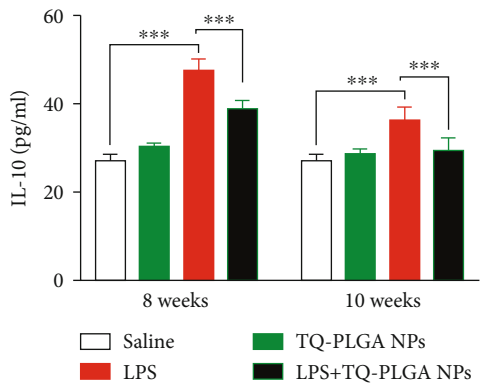

Figure 6: TQ-PLGA NPs ameliorate serum IL-10 in LPS-challenged rats. Data are mean ± SEM, $n = 6$. $^{***}P < 0.001$.

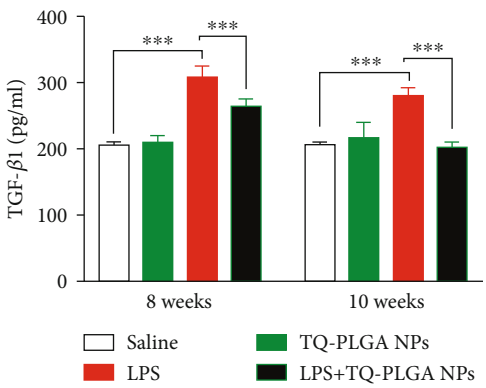

Figure 7: TQ-PLGA NPs ameliorate serum TGF-β1 in LPS-challenged rats. Data are mean ± SEM, $n = 6$. $^{***}P < 0.001$.

parenchyma and mucus cell metaplasia in airways [52, 53]. Our results pointed out that LPS was a strong activator of macrophages. Moreover, resident macrophages were activated by lymphokines to induce a second burst of cytokines mainly via NF-κB activation [53]. The pulmonary septa had variable degrees of thickness due to fibroblast proliferation besides airways fibrosis. The airway fibrosis was explained by consistent and repetitive LPS administration which led to continuous infiltration and activation of neutrophils which followed by increased expression of TGF-1 in the conducting airways [54].

The current study showed an increase in TGF-β1 level in agreement with prior reports showing that cytokines in chronic obstruction diseases are involved in tissue remodeling and increased expression of TGF-β1 that activates proliferation of fibroblasts [55, 56]. Also, Savov et al. noticed inflammatory cell infiltration and deposits of fibrin in subepithelial airways and high levels of MMP-9 in the lung tissue post daily exposure of LPS 4 h/day for 8 weeks [57].

The lung of LPS-challenged rats treated with a single dose of TQ-PLGA NPs revealed many ameliorative events and regenerative attempts which remodeled the majority of pulmonary architectures. A few apoptosis of some BALT and lung epithelium was encountered and could be attributed to the antiproliferative effects of TQ via induction of p53-independent apoptosis and through activation of caspase-8, caspase-9, and caspase-3 in the caspase cascade [58]. Moreover, it was reported that TQ could act as an activator for p53 gene and its downstream effecter p21WAFI and ultimately reduced the antiapoptotic protein Bcl-2 [59, 60]. TQ-PLGA NPs' role in the amelioration of chronic lesions, mainly fibrosis, emphysema, and thickened alveolar and pulmonary septa was demonstrated. Our results fully matched with the findings of El-Khouly et al. who reported that TQ alleviated the progression of pulmonary fibrosis induced by bleomycin in rats [61].

TQ counteracted emphysema of alveoli, inflammatory cell infiltration, hyperplastic lymphoid cells in the surrounding bronchioles, and the overexpression of NF-κB in lung tissue in bleomycin-induced rats [61]. The ameliorative benefits of TQ-PLGA NPs recorded in this study were in accordance with Kanter who noticed possible beneficial effects of *N. sativa* seeds on the experimental lung injury of male rats after pulmonary aspirations of different materials [62]. The same study showed that *N. sativa* treatment significantly reduced peribronchial inflammatory cell infiltration, alveolar septal inflammatory cells infiltration, edema, alveolar exudation, interstitial fibrosis, granuloma, and pulmonary necrosis [62].

The ultrastructural changes due to LPS included severe thickening of blood-air barriers, proliferated pneumocytes, fibroblasts, macrophages, and excess collagen fibrils. Pneumocyte type II exhibited apoptotic changes characterized by condensed nuclear chromatin, distorted nuclear membrane, partial loss of cytoplasmic organelles, and shrunken cell membrane. Pneumocyte type II contained cytoplasmic vacuolation with abnormality or empty lamellar bodies, megamitochondria, and partial loss of surface microvilli. Normally, pneumocyte type II covers 5% of the internal surface area of the lung while pneumocyte type I cells cover the remaining surface [63]. Their distribution was defective in chronic lung injury. The findings of this study were in agreement with Chattopadhyay et al. who reported that the surfactant was increased after platelets derived activated factor (strongly stimulator for the surfactant secretion) released by macrophages challenged by LPS [64]. In addition, LPS can also stimulate surfactant secretion by acting directly on pneumocytes type II cells [65].

In this investigation, the activated and proliferated macrophages were prominent due to monocyte differentiation into macrophages inside the alveoli which comes in line with the observation of Domenici-Lombardo et al. who noticed hyperplasia of pneumocytes type II and hypertrophy of interstitial fibroblasts at 48 h post 5 mg/kg LPS instillation in rats [66]. The monocytes appeared inside blood capillaries and interstitium at 12 h then migrated from alveoli and differentiation into macrophages 24 h [66]. The aforementioned results disagreed with Vernooy et al. who reported that macrophages' number was reduced after 1 week recovery from LPS administration (twice weekly for 8 weeks) [52]. However, Ofulue et al. demonstrated that long-term exposure (up to 6 months) to cigarette smoke resulted in increased intra-alveolar macrophages [67]. LPS-challenged rats that received TQ-PLGA NPs revealed normal blood-air barrier, numerous exuded interalveolar macrophages enclosing

multiple intracytoplasmic electron-dense bodies (nanoparticles) besides persistence of little collagen fibrils deposits. The majority of collagen deposits suffered from collagenolysis together with a few degenerated pneumocytes type II containing electron-dense bodies and free nanoparticles in the interstitium. The rats sacrificed after 10 weeks showed normal blood-air barrier, normal alveolar pneumocyte I, and pneumocyte type II containing intracytoplasmic vacuoles and condensed mitochondria.

TQ-PLGA NPs used in this study that are characterized by around 20 nm size and spherical shape were observed inside bronchial epithelium, pneumocytes, macrophages, and interstitium. These results were in a partial agreement with previous report by Hara et al. who noticed fluorescein isothiocyanate- (FITC-) conjugated PLGA nanoparticles inside all pneumocytes and endothelium after i.t. installation of rat lung [68]. Moreover, Kapp et al. [69] and Geiser et al. [70] confirmed that ultrafine particles were detected after ultrafine particles are inhaled. Ultrafine particles can cross cellular membranes by nonphagocytic mechanisms of lungs and culture cells and may appear in many compartments of the body, including the liver, heart, and nervous system [70]. In addition, Geiser et al. detected 20 nm titanium dioxide (TiO_2) nanoparticles in a bronchial associated macrophages phagolysosomes of rats at 24 h post inhalation [71]. They also detected inhaled ultrafine TiO_2 particles on the luminal side of airways and alveoli, and within capillaries [71]. The rats that received TQ-PLGA NPs only had mild ultrastructure changes represented by vacuolation of mitochondria and appeared denser along with phagocytic vacuoles which contain dense materials in pneumocyte type II, macrophages, and airways epithelium. Our results partially agreed with Geiser who mentioned that the alveolar macrophages have role in the clearance of inhaled micro- and nanoparticles [72]. In addition, similar findings were reported by Penberthy et al. who demonstrated the phagocytic capacity of bronchial epithelial cells in allergic air ways [73].

The ameliorative effect of TQ-PLGA NPs on LPS-induced lung injury was supported by the significant reduction in serum IL-10 and TGF-β1. These results are closely linked to the improvement of alveolar macrophages proliferation and activation. In this context, Yanagawa et al. have reported that macrophages secrete IL-10 in human lung cancer patients [74]. An increase in the expression of TGF-β which induced proliferation of fibroblasts in lung of rats exposed to LPS for 8 weeks was noted previously [57]. The ameliorative effect of TQ has also been supported by a previous study showing its ameliorative effect on the pulmonary blood vessels damage in LPS-induced acute injury [23]. The effects of TQ were mediated via modulating proinflammatory cytokines [23].

5. Conclusions

This study introduces information on the ameliorative effect of TQ-PLGA NPs on chronic lung injury induced by repetitive i.t. instillation of LPS in rats. The administration of a single dose of TQ-PLGA NPs following the 8-week challenge with LPS significantly ameliorated the histological and ultrastructural alterations in the alveoli, airways and pulmonary blood vessels, and decreased serum levels of IL-10 and TGF-β1. Given the well-documented beneficial pharmacological activities of TQ, TQ-PLGA NPs can represent a better alternative to overcome the poor solubility and other factors limiting its therapeutic applications.

Data Availability

Data analyzed or generated during this study are included in this manuscript.

Conflicts of Interest

The authors declare that they have no competing interest.

Acknowledgments

This research was funded by the Deanship of Scientific Research at Princess Nourah bint Abdulrahman University through the Fast-track Research Funding Program.

References

[1] C. Robb, K. Regan, D. Dorward, and A. G. Rossi, "Key mechanisms governing resolution of lung inflammation," *Seminars in Immunopathology*, vol. 38, no. 4, pp. 425–448, 2016.

[2] C. Nathan and A. Ding, "Nonresolving inflammation," *Cell*, vol. 140, no. 6, pp. 871–882, 2010.

[3] K. Chakraborty, M. Raundhal, B. B. Chen et al., "The mito-DAMP cardiolipin blocks IL-10 production causing persistent inflammation during bacterial pneumonia," *Nature Communications*, vol. 8, no. 1, pp. 1–15, 2017.

[4] J. Balany and V. Bhandari, "Understanding the impact of infection, inflammation, and their persistence in the pathogenesis of bronchopulmonary dysplasia," *Frontiers in Medicine*, vol. 2, p. 90, 2015.

[5] S. Herold, T. S. Tabar, H. Janßen et al., "Exudate macrophages attenuate lung injury by the release of IL-1 receptor antagonist in gram-negative pneumonia," *American Journal of Respiratory and Critical Care Medicine*, vol. 183, no. 10, pp. 1380–1390, 2011.

[6] B. N. Porto and R. T. Stein, "Neutrophil extracellular traps in pulmonary diseases: too much of a good thing?," *Frontiers in Immunology*, vol. 7, p. 311, 2016.

[7] W. Xu, Y. Zhu, Y. Ning et al., "Nogo-B protects mice against lipopolysaccharide-induced acute lung injury," *Scientific Reports*, vol. 5, no. 1, article 12061, 2015.

[8] M. J. Jiménez-Dalmaroni, M. E. Gerswhin, and I. E. Adamopoulos, "The critical role of toll-like receptors – From microbial recognition to autoimmunity: a comprehensive review," *Autoimmunity Reviews*, vol. 15, no. 1, pp. 1–8, 2016.

[9] C. W. Wieland, M. H. van Lieshout, A. J. Hoogendijk, and T. van der Poll, "Host defence during Klebsiella pneumonia relies on haematopoietic-expressed Toll-like receptors 4 and 2," *European Respiratory Journal*, vol. 37, no. 4, pp. 848–857, 2011.

[10] S. Liu, X. Su, P. Pan et al., "Neutrophil extracellular traps are indirectly triggered by lipopolysaccharide and contribute to acute lung injury," *Scientific Reports*, vol. 6, no. 1, article 37252, 2016.

[11] G. Ramachandran, "Gram-positive and gram-negative bacterial toxins in sepsis: a brief review," *Virulence*, vol. 5, no. 1, pp. 213–218, 2014.

[12] Y. Zhang and O. J. Igwe, "Exogenous oxidants activate nuclear factor kappa B through Toll-like receptor 4 stimulation to maintain inflammatory phenotype in macrophage," *Biochemical Pharmacology*, vol. 147, pp. 104–118, 2018.

[13] P. A. Baeuerle and T. Henkel, "Function and activation of NF-kappaB in the immune system," *Annual Review of Immunology*, vol. 12, no. 1, pp. 141–179, 1994.

[14] L. Sun, M. C. Louie, K. M. Vannella et al., "New concepts of IL-10-induced lung fibrosis: fibrocyte recruitment and M2 activation in a CCL2/CCR2 axis," *American Journal of Physiology. Lung Cellular and Molecular Physiology*, vol. 300, no. 3, pp. L341–L353, 2011.

[15] A. Biernacka, M. Dobaczewski, and N. G. Frangogiannis, "TGF-β signaling in fibrosis," *Growth Factors*, vol. 29, no. 5, pp. 196–202, 2011.

[16] H. Kasai, J. T. Allen, R. M. Mason, T. Kamimura, and Z. Zhang, "TGF-β1 induces human alveolar epithelial to mesenchymal cell transition (EMT)," *Respiratory Research*, vol. 6, no. 1, p. 56, 2005.

[17] K. Nakagome, M. Dohi, K. Okunishi, R. Tanaka, J. Miyazaki, and K. Yamamoto, "In vivo IL-10 gene delivery attenuates bleomycin induced pulmonary fibrosis by inhibiting the production and activation of TGF-beta in the lung," *Thorax*, vol. 61, no. 10, pp. 886–894, 2006.

[18] S. Darakhshan, A. Bidmeshki Pour, A. Hosseinzadeh Colagar, and S. Sisakhtnezhad, "Thymoquinone and its therapeutic potentials," *Pharmacological Research*, vol. 95-96, pp. 138–158, 2015.

[19] A. M. Mahmoud, O. M. Ahmed, and S. R. Galaly, "Thymoquinone and curcumin attenuate gentamicin-induced renal oxidative stress, inflammation and apoptosis in rats," *EXCLI Journal*, vol. 13, pp. 98–110, 2014.

[20] S. R. Galaly, O. M. Ahmed, and A. M. Mahmoud, "Thymoquinone and curcumin prevent gentamicin-induced liver injury by attenuating oxidative stress, inflammation and apoptosis," *Journal of Physiology and Pharmacology*, vol. 65, no. 6, pp. 823–832, 2014.

[21] I. Nallamuthu, A. Parthasarathi, and F. Khanum, "Thymoquinone-loaded PLGA nanoparticles: antioxidant and antimicrobial properties," *International Current Pharmaceutical Journal*, vol. 2, no. 12, pp. 202–207, 2013.

[22] E.-S. M. Ammar, N. M. Gameil, N. M. Shawky, and M. A. Nader, "Comparative evaluation of anti-inflammatory properties of thymoquinone and curcumin using an asthmatic murine model," *International Immunopharmacology*, vol. 11, no. 12, pp. 2232–2236, 2011.

[23] N. A. al-Gabri, M. M. Qaid, N. H. el-shaer, M. H. Ali, and A. M. Abudabos, "Thymoquinone ameliorates pulmonary vascular damage induced byEscherichia coli–derived lipopolysaccharide via cytokine downregulation in rats," *Environmental Science and Pollution Research*, vol. 26, no. 18, pp. 18465–18469, 2019.

[24] A. Ahmad, K. M. Alkharfy, B. L. Jan et al., "Thymoquinone treatment modulates the Nrf2/HO-1 signaling pathway and abrogates the inflammatory response in an animal model of lung fibrosis," *Experimental Lung Research*, vol. 46, no. 3-4, pp. 53–63, 2020.

[25] X. Su, Y. Ren, N. Yu, L. Kong, and J. Kang, "Thymoquinone inhibits inflammation, neoangiogenesis and vascular remodeling in asthma mice," *International Immunopharmacology*, vol. 38, pp. 70–80, 2016.

[26] K. M. A. Hassanein and Y. O. El-Amir, "Protective effects of thymoquinone and avenanthramides on titanium dioxide nanoparticles induced toxicity in Sprague-Dawley rats," *Pathology, Research and Practice*, vol. 213, no. 1, pp. 13–22, 2017.

[27] C. Rathore, M. J. Rathbone, D. K. Chellappan et al., "Nanocarriers: more than tour de force for thymoquinone," *Expert Opinion on Drug Delivery*, vol. 17, no. 4, pp. 479–494, 2020.

[28] C. Rathore, N. K. Upadhyay, A. Sharma, U. R. Lal, K. Raza, and P. Negi, "Phospholipid nanoformulation of thymoquinone with enhanced bioavailability: development, characterization and anti-inflammatory activity," *Journal of Drug Delivery Science and Technology*, vol. 52, pp. 316–324, 2019.

[29] G. M. Ganea, S. O. Fakayode, J. N. Losso, C. F. van Nostrum, C. M. Sabliov, and I. M. Warner, "Delivery of phytochemical thymoquinone using molecular micelle modified poly (D, L lactide-co-glycolide)(PLGA) nanoparticles," *Nanotechnology*, vol. 21, no. 28, article 285104, 2010.

[30] P. Negi, C. Rathore, G. Sharma, B. Singh, and O. P. Katare, "Thymoquinone a potential therapeutic molecule from the plant Nigella sativa: role of colloidal carriers in its effective delivery," *Recent Patents on Drug Delivery & Formulation*, vol. 12, no. 1, pp. 3–22, 2018.

[31] M. A. Kalam, M. Raish, A. Ahmed et al., "Oral bioavailability enhancement and hepatoprotective effects of thymoquinone by self-nanoemulsifying drug delivery system," *Materials Science and Engineering: C*, vol. 76, pp. 319–329, 2017.

[32] N. Ahmad, R. Ahmad, S. al Qatifi, M. Alessa, H. al Hajji, and M. Sarafroz, "A bioanalytical UHPLC based method used for the quantification of Thymoquinone-loaded-PLGA-nanoparticles in the treatment of epilepsy," *BMC Chemistry*, vol. 14, no. 1, pp. 10–15, 2020.

[33] S. A. Saghir, N. A. al-Gabri, A. F. Khafaga et al., "Thymoquinone-PLGA-PVA nanoparticles ameliorate bleomycin-induced pulmonary fibrosis in rats via regulation of inflammatory cytokines and iNOS signaling," *Animals*, vol. 9, no. 11, p. 951, 2019.

[34] X. Xie, Q. Tao, Y. Zou et al., "PLGA nanoparticles improve the oral bioavailability of curcumin in rats: characterizations and mechanisms," *Journal of Agricultural and Food Chemistry*, vol. 59, no. 17, pp. 9280–9289, 2011.

[35] N. Vij, T. Min, R. Marasigan et al., "Development of PEGylated PLGA nanoparticle for controlled and sustained drug delivery in cystic fibrosis," *Journal of Nanobiotechnology*, vol. 8, no. 1, p. 22, 2010.

[36] B. Rivera, S. R. Miller, E. M. Brown, and R. E. Price, "A novel method for endotracheal intubation of mice and rats used in imaging studies," *Journal of the American Association for Laboratory Animal Science*, vol. 44, no. 2, pp. 52–55, 2005.

[37] S. Hou, H. Ding, Q. Lv et al., "Therapeutic effect of intravenous infusion of perfluorocarbon emulsion on LPS-induced acute lung injury in rats," *PLoS One*, vol. 9, no. 1, p. e87826, 2014.

[38] K. S. Suvarna, C. Layton, and J. D. Bancroft, *Bancroft's Theory and Practice of Histological Techniques E-Book*, Elsevier Health Sciences, 2018.

[39] K. N. Gibson-Corley, A. K. Olivier, and D. K. Meyerholz, "Principles for valid histopathologic scoring in research," *Veterinary Pathology*, vol. 50, no. 6, pp. 1007–1015, 2013.

[40] N. Cheville and J. Stasko, "Techniques in electron microscopy of animal tissue," *Veterinary Pathology*, vol. 51, no. 1, pp. 28–41, 2014.

[41] M. Erdurmus, R. Yagci, B. Yilmaz et al., "Inhibitory effects of topical thymoquinone on corneal neovascularization," *Cornea*, vol. 26, no. 6, pp. 715–719, 2007.

[42] C. Cingi, G. Eskiizmir, D. Burukoğlu, N. Erdoğmuş, A. Ural, and H. Ünlü, "The histopathological effect of thymoquinone on experimentally induced rhinosinusitis in rats," *American Journal of Rhinology & Allergy*, vol. 25, no. 6, pp. e268–e272, 2011.

[43] J. R. Harkema and J. A. Hotchkiss, "Ozone- and endotoxin-induced mucous cell metaplasias in rat airway epithelium: Novel animal models to study toxicant-induced epithelial transformation in airways," *Toxicology Letters*, vol. 68, no. 1-2, pp. 251–263, 1993.

[44] J. Stolk, A. Rudolphus, P. Davies et al., "Induction of emphysema and bronchial mucus cell hyperplasia by intratracheal instillation of lipopolysaccharide in the hamster," *The Journal of Pathology*, vol. 167, no. 3, pp. 349–356, 1992.

[45] C. L. George, H. Jin, C. L. Wohlford-Lenane et al., "Endotoxin responsiveness and subchronic grain dust-induced airway disease," *American Journal of Physiology. Lung Cellular and Molecular Physiology*, vol. 280, no. 2, pp. L203–L213, 2001.

[46] Y. Kaneko, K. Takashima, N. Suzuki, and K. Yamana, "Effects of theophylline on chronic inflammatory lung injury induced by LPS exposure in Guinea pigs," *Allergology International*, vol. 56, no. 4, pp. 445–456, 2007.

[47] P. P. S. Khedoe, M. C. Wong, G. T. Wagenaar et al., "The effect of PPE-induced emphysema and chronic LPS-induced pulmonary inflammation on atherosclerosis development in APOE∗3-LEIDEN mice," *PLoS One*, vol. 8, no. 11, article e80196, 2013.

[48] G. A. Finlay, L. R. O'Driscoll, K. J. Russell et al., "Matrix metalloproteinase expression and production by alveolar macrophages in emphysema," *American Journal of Respiratory and Critical Care Medicine*, vol. 156, no. 1, pp. 240–247, 1997.

[49] S. D. Shapiro, "The macrophage in chronic obstructive pulmonary disease," *American Journal of Respiratory and Critical Care Medicine*, vol. 160, supplement_1, pp. S29–S32, 1999.

[50] P. J. Barnes, S. D. Shapiro, and R. Pauwels, "Chronic obstructive pulmonary disease: molecular and cellularmechanisms," *European Respiratory Journal*, vol. 22, no. 4, pp. 672–688, 2003.

[51] R. Vlahos and S. Bozinovski, "Role of alveolar macrophages in chronic obstructive pulmonary disease," *Frontiers in Immunology*, vol. 5, p. 435, 2014.

[52] J. H. Vernooy, M. A. Dentener, R. J. van Suylen, W. A. Buurman, and E. F. M. Wouters, "Long-term intratracheal lipopolysaccharide exposure in mice results in chronic lung inflammation and persistent pathology," *American Journal of Respiratory Cell and Molecular Biology*, vol. 26, no. 1, pp. 152–159, 2002.

[53] T. S. Hallstrand, T. L. Hackett, W. A. Altemeier, G. Matute-Bello, P. M. Hansbro, and D. A. Knight, "Airway epithelial regulation of pulmonary immune homeostasis and inflammation," *Clinical Immunology*, vol. 151, no. 1, pp. 1–15, 2014.

[54] N. al-Gabri, A.-M. Ali, E. S. al-Attar, and M. Hamed, "Pathological study on the role of thymoquinone in experimentally induced acute lung injury in rats," *Zagazig Veterinary Journal*, vol. 45, no. 3, pp. 228–237, 2017.

[55] J. D. Savov, S. H. Gavett, D. M. Brass, D. L. Costa, and D. A. Schwartz, "Neutrophils play a critical role in development of LPS-induced airway disease," *American Journal of Physiology. Lung Cellular and Molecular Physiology*, vol. 283, no. 5, pp. L952–L962, 2002.

[56] K. Chung, "Cytokines in chronic obstructive pulmonary disease," *European Respiratory Journal*, vol. 18, no. 1, pp. 50–59, 2001.

[57] J. D. Savov, D. M. Brass, K. G. Berman, E. McElvania, and D. A. Schwartz, "Fibrinolysis in LPS-induced chronic airway disease," *American Journal of Physiology. Lung Cellular and Molecular Physiology*, vol. 285, no. 4, pp. L940–L948, 2003.

[58] M. A. el-Mahdy, Q. Zhu, Q. E. Wang, G. Wani, and A. A. Wani, "Thymoquinone induces apoptosis through activation of caspase-8 and mitochondrial events in p53-null myeloblastic leukemia HL-60 cells," *International Journal of Cancer*, vol. 117, no. 3, pp. 409–417, 2005.

[59] H. Gali-Muhtasib, M. Diab-Assaf, C. Boltze et al., "Thymoquinone extracted from black seed triggers apoptotic cell death in human colorectal cancer cells via a p53-dependent mechanism," *International Journal of Oncology*, vol. 25, no. 4, pp. 857–866, 2004.

[60] H. Gali-Muhtasib, A. Roessner, and R. Schneider-Stock, "Thymoquinone: a promising anti-cancer drug from natural sources," *The International Journal of Biochemistry & Cell Biology*, vol. 38, no. 8, pp. 1249–1253, 2006.

[61] D. el-Khouly, W. M. el-Bakly, A. S. Awad, H. O. el-Mesallamy, and E. el-Demerdash, "Thymoquinone blocks lung injury and fibrosis by attenuating bleomycin-induced oxidative stress and activation of nuclear factor kappa-B in rats," *Toxicology*, vol. 302, no. 2-3, pp. 106–113, 2012.

[62] M. Kanter, "Thymoquinone attenuates lung injury induced by chronic toluene exposure in rats," *Toxicology and Industrial Health*, vol. 27, no. 5, pp. 387–395, 2011.

[63] K. C. Stone, R. R. Mercer, B. A. Freeman, L. Y. Chang, and J. D. Crapo, "Distribution of lung cell numbers and volumes between alveolar and nonalveolar tissue," *American Review of Respiratory Disease*, vol. 146, no. 2, pp. 454–456, 1992.

[64] S. Chattopadhyay, P. Sun, P. Wang, B. Abonyo, N. L. Cross, and L. Liu, "Fusion of lamellar body with plasma membrane is driven by the dual action of Annexin II tetramer and arachidonic acid∗," *Journal of Biological Chemistry*, vol. 278, no. 41, pp. 39675–39683, 2003.

[65] R. Chaby, I. Garcia-Verdugo, Q. Espinassous, and L. A. Augusto, "Interactions between LPS and lung surfactant proteins," *Journal of Endotoxin Research*, vol. 11, no. 3, pp. 181–185, 2005.

[66] L. Domenici-Lombardo, C. Adembri, M. Consalvo et al., "Evolution of endotoxin induced acute lung injury in the rat," *International Journal of Experimental Pathology*, vol. 76, no. 5, pp. 381–390, 1995.

[67] A. F. Ofulue, M. Ko, and R. T. Abboud, "Time course of neutrophil and macrophage elastinolytic activities in cigarette smoke-induced emphysema," *American Journal of Physiology. Lung Cellular and Molecular Physiology*, vol. 275, no. 6, pp. L1134–L1144, 1998.

[68] K. Hara, H. Tsujimoto, C. C. Huang et al., "Ultrastructural and immunohistochemical studies on uptake and distribution of FITC-conjugated PLGA nanoparticles administered intratracheally in rats," *Journal of Toxicologic Pathology*, vol. 25, no. 1, pp. 19–26, 2012.

[69] N. Kapp, W. Kreyling, H. Schulz et al., "Electron energy loss spectroscopy for analysis of inhaled ultrafine particles in rat lungs," *Microscopy Research and Technique*, vol. 63, no. 5, pp. 298–305, 2004.

[70] M. Geiser, B. Rothen-Rutishauser, N. Kapp et al., "Ultrafine particles cross cellular membranes by nonphagocytic mechanisms in lungs and in cultured cells," *Environmental Health Perspectives*, vol. 113, no. 11, pp. 1555–1560, 2005.

[71] M. Geiser, M. Casaulta, B. Kupferschmid, H. Schulz, M. Semmler-Behnke, and W. Kreyling, "The role of macrophages in the clearance of inhaled ultrafine titanium dioxide particles," *American Journal of Respiratory Cell and Molecular Biology*, vol. 38, no. 3, pp. 371–376, 2008.

[72] M. Geiser, "Update on macrophage clearance of inhaled micro- and nanoparticles," *Journal of Aerosol Medicine and Pulmonary Drug Delivery*, vol. 23, no. 4, pp. 207–217, 2010.

[73] K. K. Penberthy, I. J. Juncadella, and K. S. Ravichandran, "Apoptosis and engulfment by bronchial epithelial cells. Implications for allergic airway inflammation," *Annals of the American Thoracic Society*, vol. 11, Supplement 5, pp. S259–S262, 2014.

[74] H. Yanagawa, E. Takeuchi, Y. Suzuki et al., "Production of interleukin-10 by alveolar macrophages from lung cancer patients," *Respiratory Medicine*, vol. 93, no. 9, pp. 666–671, 1999.

Hindawi
Oxidative Medicine and Cellular Longevity
Volume 2021, Article ID 9996503, 8 pages
https://doi.org/10.1155/2021/9996503

Review Article

The Mechanism Underlying the Extreme Sensitivity of Duck to Aflatoxin B_1

Kuntan Wu, Minjie Liu, Huanbin Wang, Shahid Ali Rajput, Yajing Shan, Desheng Qi, and Shuai Wang

Department of Animal Nutrition and Feed Science, College of Animal Science and Technology, Huazhong Agricultural University, Wuhan 430070, China

Correspondence should be addressed to Desheng Qi; qds@mail.hzau.edu.cn and Shuai Wang; wangshuai@mail.hzau.edu.cn

Received 7 March 2021; Revised 1 April 2021; Accepted 18 April 2021; Published 17 May 2021

Academic Editor: Daoud Ali

Most metabolites of aflatoxin B_1 (AFB_1), especially exo-AFB_1-8,9-epoxide (AFBO), can induce the production of reactive oxygen species (ROS) to vary degrees, causing oxidative stress and liver damage, and ultimately induce liver cancer in humans and animals. Duck is one of the most sensitive animals to AFB_1, and severe economic losses are caused by duck AFB_1 poisoning every year, but the exact mechanism of this high sensitivity is still unclear. This review highlights significant advances in our understanding of the AFB_1 metabolic activation, like cytochrome P450s (CYPs), and AFB_1 metabolic detoxification, like glutathione S-transferases (GSTs) in poultry. In addition, AFB_1 may have other metabolic pathways in poultry, such as the mutual conversion of AFB_1 and aflatoxicol (AFL) and the process of AFBO to produce AFB_1-8,9-dihydrodiol (AFB_1-dhd) and further metabolize it into detoxification substances. This review also summarized some exogenous regulatory substances that can alleviate AFB_1-induced oxidative stress.

1. Introduction

Aflatoxins are secondary metabolites produced by *Aspergillus flavus* and *Aspergillus parasiticus*, including aflatoxin B_1 (AFB_1), aflatoxin B_2, aflatoxin G_1, and aflatoxin G_2. AFB_1 is extremely toxic and carcinogenic, as classified by the International Agency for Research on Cancer (IARC), as a class 1A carcinogen [1]. AFB_1 generates a large amount of ROS during metabolism, which can cause oxidative damage [2] and reduce the level of antioxidant enzymes in animals [3] that eventually cause AFB_1's toxic effects such as cell damage, DNA damage, protein damage, and lipid peroxidation [4]. AFB_1 has the strong liver toxicity and can reduce production performance, feed utilization [3], egg production, and immunosuppression in poultry [5]. Young ducks and turkeys are extremely susceptible to AFB_1 [5]. 3 μg/(kg·BW) of AFB_1 can cause significant damage to the DNA of duckling liver cells (Wang et al., 2009). 10-40 μg/(kg·BW) of AFB_1 can cause significant changes in the expression of many genes related to the oxidation-reduction process, metabolic toxins and detoxification process, and carcinogenesis in duck [6]. However, chickens (500 μg/kg AFB_1) and rats (100–1,000 μg/kg AFB_1) are relatively insensitive [5]. In China's national feed hygiene standard "GB 13078-2017," the concentration limit of AFB_1 in feed for meat ducks and laying ducks is ≤15 μg/kg, and the concentration limit of AFB_1 in feed for ducklings is ≤10 μg/kg.

Duck is one of the most important poultry for humans. Asia is the most important region for duck meat production (the ratio is 82.2%), followed by Europe with 12.4% [7]. In 2016, there were 1.24 billion ducks in the world and 1.1 billion (the ratio is 89.0%) in Asia. China raises more than 70% of the world's ducks, the annual production of meat ducks is maintained at more than 2 billion, and the stock of laying ducks is about 250 million. The consumption of duck eggs accounts for 10–30% of the total consumption of eggs in China and Southeast Asia. Notably, most areas of China and Southeast Asian countries are located in tropical and temperate zones, and the warm and humid summers cause widespread moldy feed. AFB_1 widely contaminates grain and

animal feed worldwide [8, 9]. Of feed ingredients and compound feeds, 1,569 in different China provinces were checked in 2016–2017. The pollution rate of AFB_1 is as high as 83.3% [10]. As the pollution of AFB_1 in feed is difficult to avoid, ducks have biological defects susceptible to AFB_1, causing countless economic losses due to duck AFB_1 poisoning each year. This review summarizes and discusses the possible mechanisms of ducks' high sensitivity to AFB_1 and the feasibility of regulating ducks' AFB_1 metabolism through exogenous substances, thereby enhancing ducks' tolerance to AFB_1. This article is aimed at providing a theoretical basis for the research of exogenous substances to prevent and regulate duck aflatoxin poisoning.

2. Metabolic Process of AFB_1

After AFB_1 is absorbed in the intestine, it is converted into various metabolites by many cytochrome oxidase P450 family members (CYP 450 s, CYPs) in the liver. Aflatoxins M_1 (AFM_1) and aflatoxin P_1 (AFP_1) can be excreted directly through urine or milk [11]. The unabsorbed AFB_1 and part of its metabolites are excreted through feces. As the liver's dominant enzyme to metabolize AFB_1, CYP1A2 can metabolize AFB_1 into AFM_1 and aflatoxin Q_1 (AFQ_1). CYP3A4 can metabolize AFB_1 into AFQ_1 and exo-AFB_1-8,9-epoxide (AFBO). Primates mainly produce AFQ_1 and AFP_1, while poultry mainly produces aflatoxicol (AFL) [12]. CYP450 participates in AFB_1 activation into AFBO; so, it is closely related to the occurrence of liver cancer. AFBO has oxidative activity and can induce excessive ROS formation, leading to DNA bases' damage and inducing lipid peroxidation [13]. AFBO and ROS are then combined and metabolized and detoxified by some antioxidant enzymes and substances, such as GSTs, SOD, and GSH. AFBO can (1) combine with glutathione (GSH) under the activity of the body's phase II metabolic enzymes, such as glutathione S-transferases (GSTs), to form AFB_1-mercaptutic acid (AFB_1-NAC) and be excreted through urine [14]; (2) combined with glucuronic acid and excreted through feces [15]; (3) combined with DNA to form AFB_1-N^7-guanine adduct and undergo the DNA repair process to quickly remove most of the AFB_1-N^7-GUA adducts and excrete them through urine; and (4) after binding to serum albumin, AFB_1 mainly remains in the blood by the form of AFB_1-lysine adduct [11]. The transformation process in animals is summarized in Figure 1.

The order of the sensitivity of different poultries to AFB_1 from high to low is ducklings > turkey > gosling > quail > chicks [16]. The 400 μg/kg AFB_1 in the diet seriously affected turkeys' growth performance and relative liver index. Chickens were not affected by this concentration, and their body weight increased by 3.3% [17]. Similarly, 220–400 μg/kg of AFB_1 significantly reduced ducks' performance but had a weak effect on chickens [18]. What causes different sensitivity of poultry to AFB_1? A study of perfusion of isolated organs proved that poultry's sensitivity to AFB_1 is related to cell specificity (different species) but not to extracellular factors, such as the digestion and absorption process [19]. After AFB_1 enters the liver, it undergoes two processes: metabolic activation and metabolic detoxification. AFB_1 is metabolically activated by phase I metabolic enzymes, such as CYPs, to produce highly toxic AFBO and other metabolites. AFBO can be metabolized by phase II metabolic enzymes, such as GSTs, into low-toxic conjugates, and excreted from the body [11]. When the amount of AFBO produced exceeds the detoxification ability of phase II metabolic enzymes, AFBO will react or combine with DNA and proteins, resulting in cytotoxicity and genetic toxicity. Therefore, ducks' high sensitivity to AFB_1 may be related to excessive activation into harmful substances or insufficient detoxification of the harmful metabolites.

3. Metabolic Activation and Detoxification of AFB_1 in Poultry

3.1. Metabolic Activation of AFB_1 in Poultry. AFBO can cause oxidative stress, and AFBO is produced after AFB_1 is activated by phase I enzyme metabolism. Therefore, reducing phase I metabolic enzyme activity can reduce the AFBO produced by metabolism and alleviate oxidative stress and other toxicities. Western countries raise and consume a large number of turkeys, while ducks are relatively few. Therefore, western countries have carried out a lot of research work on the metabolic mechanism of AFB_1 in turkeys, but there are few studies on ducks. Turkeys are susceptible to AFB_1 because their phase I enzymes can efficiently activate AFB_1 [20]. An earlier study found that duck liver microsomes only need 50 seconds to metabolize AFB_1 with LD_{50} concentration, while chickens need 32–100 minutes [21].

Interestingly, the content and activity of CYPs in the liver decrease with age in poultry. Young turkeys (9 d) activate AFB_1 to AFBO more effectively than old turkeys (65 d) [22]. The same situation occurs in Ross broilers [23] and AA broilers [24]. The content and activity of liver CYPs on the first day after hatching were more than twice that of other ages, especially CYP1A, CYP3A, CYP2C, CYP2D, and CYP2H. It dropped rapidly to 28 days in the first week after hatching and then rose slightly to 56 days [23]. These studies indicate that the increase in age will affect phase I metabolic enzyme activity, affecting the toxicity and metabolic activation of AFB_1 in animals.

Different CYPs metabolize AFB_1 at different concentrations. CYP1A2 metabolizes human hepatocytes at lower concentrations (0.133 μM AFB_1), and at higher concentrations (256 μM AFB_1), they are metabolized by CYP3A4 [25]. Some enzymes are orthologous to human CYP1A2 and CYP3A4 in the turkey liver, CYP1A5 [26], and CYP3A37, respectively [27]. CYP1A5 metabolizes AFB_1 into AFM_1 and AFBO, and CYP3A37 metabolizes AFB_1 into AFQ_1 and AFBO. When 0.1–20 μM AFB_1 is added to turkeys' liver microsomes, it is mainly metabolized by CYP1A5 to produce AFBO. When 50 μM AFB_1 is added, the proportion of AFBO produced by CYP1A5 and CYP3A37 is nearly equal, and 100–1,000 μM AFB_1 is metabolized by CYP3A37 into AFBO [28]. Because the concentration of environmentally relevant AFB_1 is mostly low-dose levels, CYP1A5 is an important enzyme involved in biological activation in turkeys and can regulate the production of AFBO. After ducklings were exposed to AFB_1, the expression of *CYP46A1*, *CYP3A9*, and

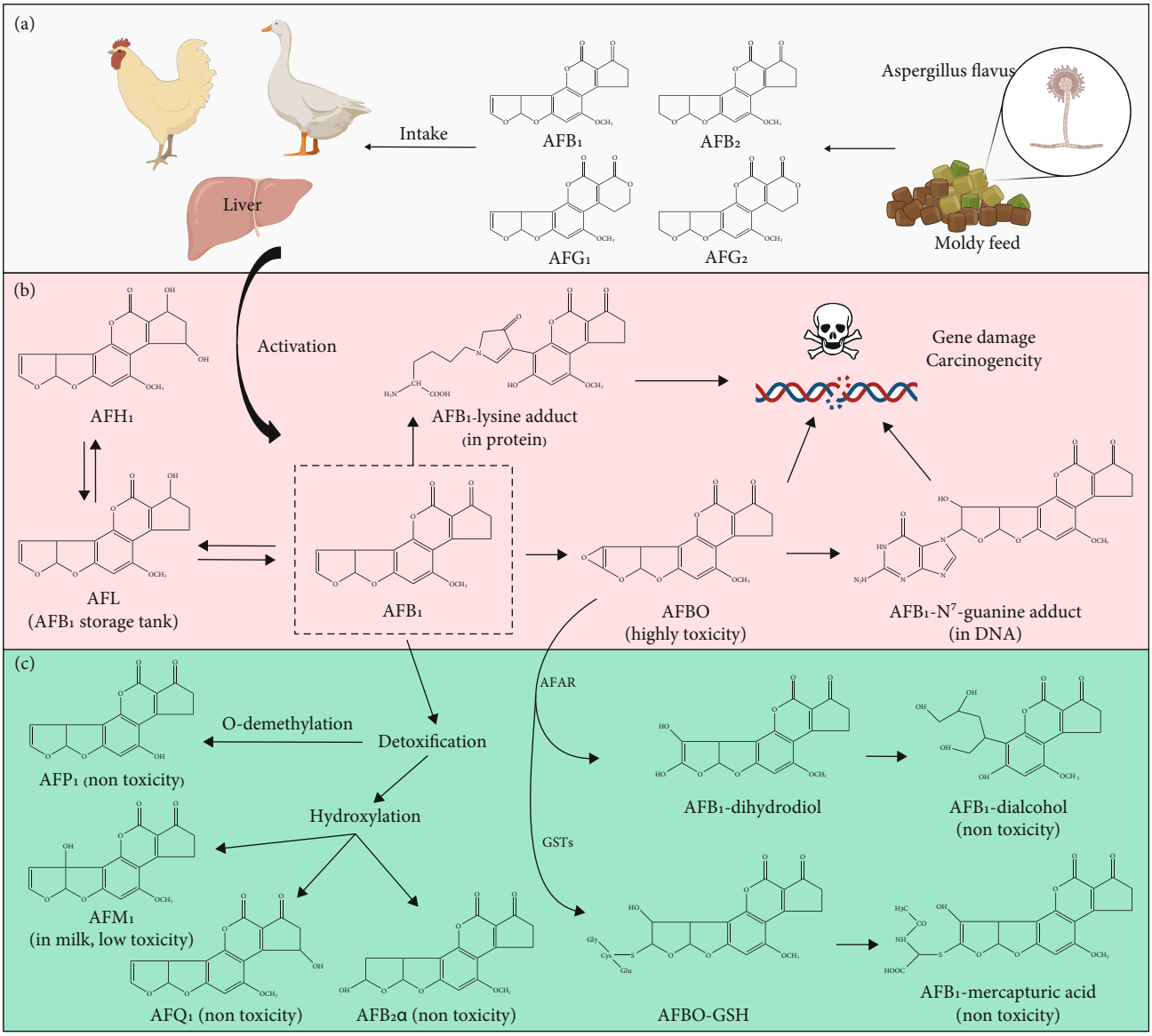

Figure 1: Metabolic process of aflatoxin B_1 (AFB_1) in the animal liver. (a) *Aspergillus flavus* grows in moldy feed, producing toxic metabolites, like AFB_1. Poultry consume feed contaminated with AFB_1. (b) In the liver, AFB_1 produces exo-AFB_1-8,9-epoxide (AFBO) under the action of phase I metabolic activating enzymes, such as cytochrome oxidase P450 (CYP 450), and binds to DNA and protein, causing gene damage and cytotoxicity and is potently carcinogenic. (c) At the same time, some phase I metabolic activating enzymes also convert AFB_1 into low-toxic metabolites; or under the action of phase II metabolic detoxification enzymes, such as glutathione S-transferases (GSTs), AFB_1 combines with antioxidants into nontoxic conjugates and is then excreted from the body to alleviate the toxicity of AFB_1.

CYP4B1 in the liver was upregulated, while the expression of *CYP2H1*, *CYP1A5*, *CYP27A1*, *CYP2K1*, and *CYP2F3* was downregulated [6].

Studies have found that the activation of AFB_1 in turkeys [29] and broiler chickens [30] is mainly due to the role of CYP2A6 orthologues. CYP1A1 orthologues also participate in the formation of AFBO to a certain extent, but the effect of CYP3A4 on the formation of AFBO can be ignored. In the duck liver, CYP2A6 and CYP3A4 orthologues are the most important CYPs responsible for the activation of AFB_1, and CYP1A1/2 orthologues are also involved in the formation of AFBO to a certain extent. The four CYP enzymes have differences in the activation of AFB_1 and their enzyme activities, which may be one reason for the differences in poultry sensitivity to AFB_1 [31]. In addition, it has been reported that fumonisin B1 (FB1) exposure significantly increased the activity of CYP1A1/2 and CYP3A4 orthologues in the duck liver, so that FB1 may cause more biological activation of AFB_1 [32]. FB1 and AFB_1 are often cocontaminated in feed; so, the combined toxicity to ducks may increase [33]. Although the difference in CYPs (type and activity) can partially explain turkeys' high sensitivity to AFB_1, it is inconsistent with the apparent sensitivity of chickens, ducks, quail, and turkeys. Thus, it is not sufficient to fully explain the high sensitivity of ducks [34]. Therefore, it is necessary to continue investigating the biochemical and molecular biological

mechanisms of duck and turkey's high sensitivity to AFB_1, which is of great significance to the development of technologies to prevent and control the hazards of AFB_1 [5].

3.2. Metabolic Detoxification of AFB_1 in Poultry. Enhancing the activity of phase II enzymes can remove harmful AFBO and ROS faster, thereby alleviating oxidative stress and other toxicities. The high sensitivity of ducks to AFB_1 may also be related to the lack of effective phase II detoxification enzymes, especially GSTs. The expression level of α-GST in the mouse liver is very high; so, it has a high tolerance to AFB_1 [35]. Among the five GSTs in rats, α-GST and μ-GST can bind AFBO very effectively [36]. Poultry GSTs received less attention in the early stage [37] and gradually began to receive attention after 2000. At present, some GSTs found in poultry have been reported [11]. Compared with wild turkeys, commercial turkeys lack functional GST that has a sufficient affinity for AFBO, especially GSTA3 [38]. The process of domestication may lead to the loss of important detoxification GSTs genes, silence, or downregulation of expression, which may be an important reason for the sensitivity of commercial turkeys [39]. Interestingly, transcriptomic results showed that other organs and tissues, such as the cecal tonsil [40] and spleen [41], also helped enhance the tolerance of wild turkeys to AFB_1. The modern poultry industry continuously selects and improves varieties, intensively breeds poultry, and shortens the breeding time. Since 1980, the sensitivity of poultry to AFB_1 and external adverse factors has increased. This phenomenon suggests that we should reduce the adverse effects of mycotoxins and external diseases on poultry, while cultivating poultry with high feed conversion efficiency.

The activities of phase II metabolic enzymes, such as GSTs and AFB_1 aldehyde reductase (AFAR), increase with the age of poultry, such as GSTA3, GSTA4, and EPHX1 in the liver of broilers [24]. Turkeys of all ages have low GST activity [22]. The lack of effective phase II enzyme detoxification may be another important reason why turkeys are susceptible to AFB_1 [20]. AFB_1 treatment increased the protein expression levels of GST Yc and Yc2 in turkeys' liver [22]. A study amplified and identified the *tGST* genes (*tGSTA1.1*, *tGSTA1.2*, *tGSTA1.3*, *tGSTA2*, *tGSTA3*, and *tGSTA4*) in the turkey liver [42]. The expression of *GST1*, *GST3,* and *GSTK1* genes in the liver of ducklings increased after exposure to AFB_1 [6]. Recombined tGSTA can detoxify AFBO, but its liver form cannot, indicating that it can affect the affinity of tGSTA and AFBO by adjusting the modification of tGSTA [43]. It shows that it is feasible to modify and adjust the activity of GSTs by exogenous substances, thereby enhancing the tolerance of poultry to AFB_1. Therefore, the low activity of metabolic detoxification enzymes, like GSTs, may be a critical factor in ducks' high sensitivity to AFB_1. GSTs play an essential role in the metabolic detoxification of AFB_1. However, current research reports mostly identify the types of GSTs in poultry [42] or analyze GSTs that are significantly changed after AFB_1 treatment [6]. There is a lack of further research on the specific detoxification effect of a certain GST in the process of duck metabolism AFB_1.

3.3. Mutual Transformation of AFL and AFB_1. Lozano and Diaz (2006) found that turkey and duck produced AFB_1-GSH levels 3.25 times and 1.54 times that of chickens, respectively. This shows that the detoxification ability of GSTs in turkeys and ducks is not lower than that of chickens, and the differences in the types and activities of CYPs and GSTs cannot completely explain the reasons for the high sensitivity of ducks to AFB_1. Therefore, there may be other toxicological mechanisms. AFL is one of the metabolites of AFB_1, which can be converted to AFB_1. AFB_1 reductase is mainly responsible for converting AFB_1 to AFL, while AFL dehydrogenase is mainly responsible for converting AFL to AFB_1. Since the production of AFL may have a dual effect, it is controversial whether it can be used as a detoxification product. AFL is considered a form of detoxification in fish, combined with glucuronic acid for excretion through bile and feces [44]. Unfortunately, as a storage form of AFB_1, AFL can be converted back to AFB_1 and continue to be metabolized into AFBO, prolonging the half-life of AFB_1 and causing chronic toxicity in AFB_1 sensitive animals [45]. Lozano and Diaz (2006) and Murcia and Diaz (2020) also seem to have reached conflicting conclusions. Lozano and Diaz (2006) found that the levels of AFL and AFB_1-8,9-dihydrodiol (AFB_1-dhd) produced by turkeys and ducks were 1.97–4.09 times and 1.77–3.15 times, respectively, that of chickens. Because turkeys and ducks are more sensitive to AFB_1 than chickens, the author believes that AFL and AFB_1-dhd may also have certain toxicity. The large amount of AFL is one reason for the high sensitivity of ducks to AFB_1 [46]. Murcia and Diaz (2020) found that chicken AFB_1 reductase had the greatest activity, while AFL dehydrogenase showed only minor differences among four poultry (chicken, quail, turkey, and duck). The order of the AFB_1 reductase/AFL dehydrogenase ratio from high to low is chicken > turkey > quail > duck [47]. This is inversely proportional to the known sensitivity of poultry to AFB_1. Therefore, Murcia and Diaz (2020) believe that AFL is not a toxic metabolite but a detoxified form of AFB_1 in poultry. Chickens can convert more AFB_1 into AFL, thereby reducing the production of AFBO, which is one of the reasons why chickens are relatively insensitive to AFB_1.

Comparing the two studies, we found that there may be two reasons for the cognitive differences in the effects of AFL: the specific content and level of doses were different. First, Lozano and Diaz (2006) measured AFB_1-dhd and AFL levels in microsomes and the cytoplasm. They found that although ducks are very sensitive to AFB_1, the amount of AFBO produced by their liver microsomes is not high. Murcia and Diaz (2020) studied the kinetic parameters (V_{max}, K_M, and CL_{int}) of AFB_1 reductase and AFL dehydrogenase. The article stated that "chicken AFB_1 reductase has the greatest activity so that it can produce most efficiently." AFL is the only speculation and has not been verified by further experiments. Another difference is the dose of AFB_1. Lozano and Diaz (2006) used 128 μM AFB_1 for processing. Murcia and Diaz (2020) found that when 0–9 μM AFB_1 was used to treat chicken liver microsomes, AFB_1 reductase had the greatest activity, while the difference in AFL dehydrogenase was small. When AFB_1 is greater than 30 μM, the

AFB_1 reductase and AFL dehydrogenase activities of ducks and turkeys are much higher than those of chickens, indicating that the mutual transformation of AFL and AFB_1 in ducks and turkeys is more active than that of chickens. This can be partially corroborated by the results of Lozano and Diaz (2006), who found that turkeys and ducks produce higher AFL levels than chickens. Based on the possible dual effects of AFL production and previous studies, we speculate that poultry can tolerate a certain concentration of AFL, so converting AFB_1 to AFL within a certain level can prevent the epoxidation of AFB_1 into toxic AFBO, thereby alleviating the toxicity of AFB_1. Due to the high activity of AFB_1 reductase and AFL dehydrogenase in ducks and turkeys, when too much AFL is transformed and stored, its toxicity will also be toxic to tissues and cells. In past studies, on the metabolic activation and metabolic detoxification of AFB_1, the function and dual effects of AFL were often overlooked. Therefore, future research on the role of AFL in the metabolic process of AFB_1 is a potential breakthrough point.

3.4. Role of AFB_1-dhd in the Toxic Effect of AFB_1. AFL plays the role of storage and buffering. The more AFB_1 converted to AFL, the less AFB_1 will be epoxidized to AFBO. But AFL is not a complete detoxification product. AFBO can be hydrolyzed spontaneously or converted into AFB_1-dhd under the metabolism of epoxide hydrolase (EPHX). AFB_1-dhd can interconvert with AFB_1-dialdehyde under different pH conditions. Unfortunately, as a toxic metabolite of AFB_1, AFB_1-dialdehyde and AFB_1-dhd both cause oxidative stress and react with lysine residues in proteins [35], resulting in cytotoxicity [48]. The study sorted the ratios of AFB_1-dhd/AFB_1-monoalcohol produced in the order of duck > quail > turkey > broiler. Ducks can produce large amounts of AFB_1-dhd, and the ratio of AFB_1-dhd/AFB_1-dialcohol is more than 100 times higher than that of broilers. Ducks may not be able to metabolize AFB_1-dhd into nontoxic AFB_1-diethanol efficiently; so, AFB_1-dhd may cause protein damage through conversion to AFB_1-dialdehyde (see Figure 2). AFAR can continue to convert AFB_1-dhd into AFB_1-C_6-monoalcohol and AFB_1-C_8-monoalcohol [49]. AFAR can continue to catalyze them to form the final AFB_1-diethanol (see Figure 2). AFB_1-diethanol cannot bind to proteins; so, it is a complete detoxification product. AFAR has been shown to play an important role in alleviating the toxicity of AFB_1 in poultry [50]. The low activity of AFAR may be an important reason for the high sensitivity of ducks to AFB_1 [35]. If individuals with high AFAR activity can be genetically selected from ducks and turkeys, it may be possible to improve the tolerance of ducks and turkeys to AFB_1 to a certain extent through genetic breeding. AFAR activity in liver microsomes increases with age in turkeys [22]. Notably, AFAR enzyme activity is not the only thing that affects the production of AFB_1-dhd. GSTs can reduce the production of AFB_1-dhd by combining with AFBO and further affect the production of AFB_1-dialdehyde (see Figure 2). In pigs and rats, the AFAR enzyme's inhibitory effect on AFB_1 toxicity is far less than that of GSTs, and no relationship between AFAR and mammalian tolerance to AFB_1 has been found [51]. Therefore, mammals may mainly have a detoxification effect on AFB_1 by GSTs. In short, ducks may metabolize to produce and store AFL, but they cannot bear and convert more AFB_1 into AFBO and AFB_1-dhd, resulting in their high sensitivity to AFB_1. However, more research is needed to determine the metabolic fate of AFL and AFB_1-dhd in ducks.

Different aquatic animals have different sensitivity to AFB_1. Rainbow trout are very sensitive to AFB_1, while catfish are less sensitive to AFB_1. The liver microsomes of rainbow trout have the highest affinity for AFB_1. CYP2K1 can quickly and efficiently produce a large amount of AFBO, and the enzyme content is more than five times that of catfish [52]. The activity of AFB_1 reductase and the binding efficiency of GST and AFBO are also very low [51]. In contrast, the study found that due to the low content of CYPs in the catfish liver, the efficiency of CYPs in catalyzing the epoxidation of AFB_1 is lower than that of rainbow trout. Moreover, AFB_1 reductase uses AFB_1 to produce AFL faster than CYPs metabolize AFB_1 to produce AFBO. Catfish quickly excrete AFL for detoxification [44]. The process of aquatic animals' metabolism of AFB_1 and the reasons for the differences in sensitivity can help us understand the mechanism of differences in the sensitivity of different animals to AFB_1 and inspire us to explore the reasons for the high sensitivity of ducks to AFB_1. This section further supplements and discusses possible other toxicological mechanisms of poultry to AFB_1. The possible key metabolic pathways of AFB_1 in poultry are shown in Figure 2. Based on previous studies on the sensitivity of different poultries to AFB_1, there is still a lack of research on the relationship between mutual transformation products (like AFB_1 and AFL and AFB_1-dhd and AFB_1-dialdehyde) and metabolic detoxification enzymes (like GSTs and AFAR) in different poultries.

4. Exogenous Substances Alleviate the Toxicity of AFB_1

Many methods have been used to reduce the damage of AFB_1 to animals. We can control the level of AFB_1 in the feed from the source by cultivating crops resistant to *Aspergillus* and taking appropriate transportation and storage measures [53]. Controlling the quality of feed and storage conditions can effectively reduce AFB_1 ingested by animals. If aflatoxins already exist in feed, physical, chemical, and biological detoxification can remove or reduce toxicity [11]. Vitamin E and yeast selenium can reduce the adverse effects of AFB_1 on duck growth performance, immune function, and tissue structure [54]. Grape seed proanthocyanidin extract has protective effects against aflatoxicosis caused by 1 mg/kg AFB_1 in broiler chickens [55]. It is an effective strategy to reduce the toxicity of AFB_1 by inhibiting the activity of CYPs and/or enhancing the activity of GSTs. Isoimperatorin can inhibit the activity of some CYPs and induce the activity of some GSTs on rat liver cancer cells, thereby reducing the cytotoxic effect of AFB_1 [56]. Oltipraz can inhibit the activity of CYP1A2 and CYP3A4, leading to the reduction of AFB_1 metabolites in human primary hepatocytes [57]. Butylated hydroxytoluene (BHT) mainly reduces the production of AFBO by regulating phase I related to AFB_1 metabolism in the liver of turkeys, such as competitively inhibiting the effect

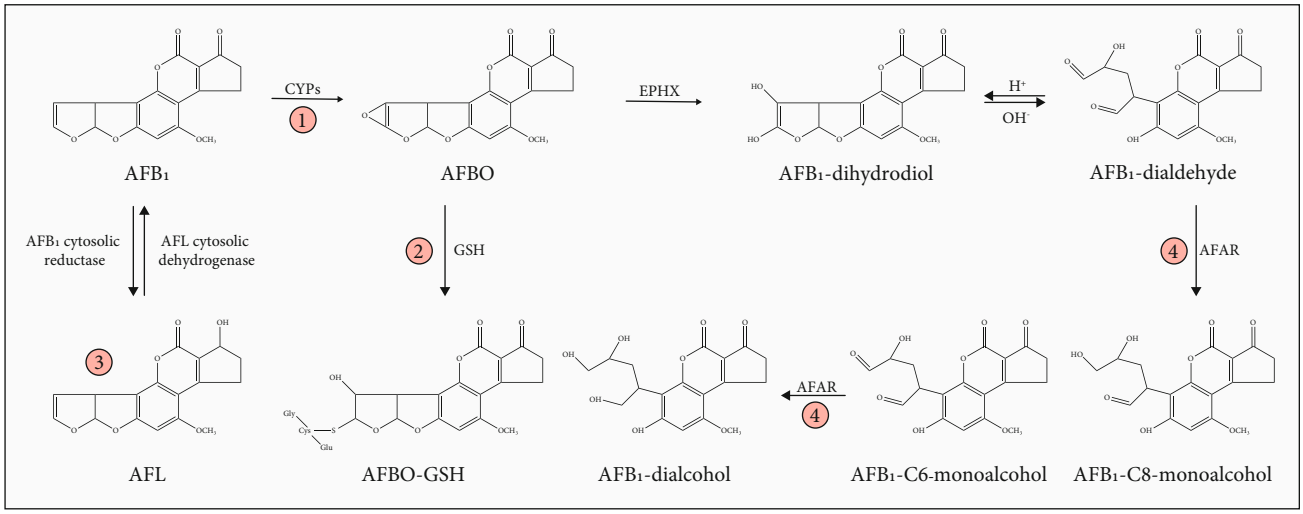

Figure 2: The possible key metabolic pathways and potential regulatory points of aflatoxin B_1 (AFB_1) in poultry (four points), modified from Murcia and Diaz (2020). ① AFB_1 is metabolized by CYPs into AFBO. ② AFBO combines with GSH to form a detoxification compound. ③ As the storage form of AFB_1, AFL can be transformed with AFB_1. ④ AFBO removes epoxidation and initially forms AFB_1-dhd, which is finally reduced to AFB_1-dialcohol under the action of AFAR.

of CYP1A5 and inducing CYP3A4 to metabolize AFB_1 into AFQ_1 for detoxification [58, 59]. Curcumin has vast therapeutic potential because of its antioxidant, anti-inflammatory, and antiproliferative properties [60]. Curcumin reduces the toxicity of AFB_1 to chicks by inhibiting the gene expression of *CYP1A1*, *CYP1A2*, *CYP2A6*, and *CYP3A4* [3]. Suforaphane can inhibit the activity of CYPs in the human liver, thereby reducing the formation of AFBO in liver cells and preventing AFB_1-induced cancer [61]. Marine algal polysaccharides can upregulate the gene expression of *GSTA3*, *GPx1*, *CAT1*, and *GSTT1* in the bursa of fabric in broilers [62]. Fisetin can enhance various antioxidant enzymes, attenuate the oxidative stress-inflammatory pathway induced by AFB_1, and reduce the risk of liver cancer [63]. Fucoidan relieves liver and kidney damage caused by AFB_1 by reducing oxidative stress, DNA damage, and inflammation [64].

These studies indicate that exogenous substances can inhibit or induce metabolic enzyme activity in the body, change the metabolic rate and metabolic pathways of exogenous toxins, and alleviate the animal's oxidative stress state, reducing the harmful effects of AFB_1. Nevertheless, most of the research model is "exogenous material effect test ⟶ mechanism analysis", which causes blindness in selecting effective exogenous regulators. Therefore, studying the mechanism of ducks' high sensitivity to AFB_1 can guide the selection of exogenous regulators and reduce blindness. This has important theoretical significance and good economic value.

5. Summary

The activation and detoxification of AFB_1 in poultry involve multiple metabolic pathways. In addition to the activation of CYPs in phase I and the detoxification of GSTs in phase II, there may be other metabolic pathways of AFB_1, such as the mutual conversion of AFB_1 and AFL, the production of AFB_1-dhd, and the enzymatic activity of EPHX and/or AFAR. In summary, the high sensitivity of ducks to AFB_1 may be caused by CYPs producing too much AFBO and AFL and lack of effective GSTs and AFAR to further metabolize harmful AFBO and AFB_1-dhd. In the future, the key control points of AFB_1 metabolism in ducks should be clarified, such as enhancing the activity of GSTs and AFAR, to guide the selection of exogenous regulators.

Conflicts of Interest

The authors declare that they have no competing interests.

Authors' Contributions

Kuntan Wu contributed to the writing—reviewing, editing, and investigation. Minjie Liu contributed to the writing—original draft preparation and conceptualization. Huanbin Wang performed the data curation. Shahid Ali Rajput performed the methodology. Yajing Shan performed the visualization and software. Desheng Qi and Shuai Wang contributed to the supervision. All authors read and approved the final manuscript.

Acknowledgments

This research was funded by the National Key Research and Development Program of China (project no. 2016YFD0501207) and the National Natural Science Foundation of China (project no. 31772635).

References

[1] K. Wu, S. Jia, J. Zhang et al., "Transcriptomics and flow cytometry reveals the cytotoxicity of aflatoxin B_1 and aflatoxin M_1 in bovine mammary epithelial cells," *Ecotoxicology and Environmental Safety*, vol. 209, p. 111823, 2021.

[2] D. E. Marin and I. Taranu, "Overview on aflatoxins and oxidative stress," *Toxin Reviews*, vol. 31, no. 3-4, pp. 32–43, 2012.

[3] N.-Y. Zhang, M. Qi, L. Zhao et al., "Curcumin prevents aflatoxin B_1 hepatoxicity by inhibition of cytochrome P 450 isozymes in chick liver," *Toxins*, vol. 8, no. 11, p. 327, 2016.

[4] H. M. Shen, C. Y. Shi, H. P. Lee, and C. N. Ong, "Aflatoxin B_1-induced lipid peroxidation in rat liver," *Toxicology and Applied Pharmacology*, vol. 127, no. 1, pp. 145–150, 1994.

[5] S. Rawal, J. E. Kim, and R. J. Coulombe, "Aflatoxin B_1 in poultry: toxicology, metabolism and prevention," *Research in Veterinary Science*, vol. 89, no. 3, pp. 325–331, 2010.

[6] N.-Y. Zhang, M. Qi, X. Gao et al., "Response of the hepatic transcriptome to aflatoxin B_1 in ducklings," *Toxicon*, vol. 111, pp. 69–76, 2016.

[7] J. S. Ismoyowati, "Duck production for food security," *IOP Conference Series: Earth and Environmental Science*, vol. 372, 2019.

[8] E. Streit, G. Schatzmayr, P. Tassis et al., "Current situation of mycotoxin contamination and co-occurrence in animal feed–focus on Europe," *Toxins*, vol. 4, no. 10, pp. 788–809, 2012.

[9] S. Monbaliu, C. Van Poucke, C. Detavernier et al., "Occurrence of mycotoxins in feed as analyzed by a multi-mycotoxin LC-MS/MS method," *Journal of Agricultural and Food Chemistry*, vol. 58, no. 1, pp. 66–71, 2010.

[10] R. Ma, L. Zhang, M. Liu et al., "Individual and combined occurrence of mycotoxins in feed ingredients and complete feeds in China," *Toxins*, vol. 10, no. 3, p. 113, 2018.

[11] J. Deng, L. Zhao, N.-Y. Zhang et al., "Aflatoxin B_1 metabolism: regulation by phase I and II metabolizing enzymes and chemoprotective agents," *Mutation research*, vol. 778, pp. 79–89, 2018.

[12] B. D. Roebuck and G. N. Wogan, "Species comparison of in vitro metabolism of aflatoxin B_1," *Cancer Research*, vol. 37, no. 6, pp. 1649–1656, 1977.

[13] A. M. Alzahrani and P. Rajendran, "The multifarious link between cytochrome P450s and cancer," *Oxidative Medicine and Cellular Longevity*, vol. 2020, Article ID 3028387, 18 pages, 2020.

[14] D. H. Swenson, J. K. Lin, E. C. Miller, and J. A. Miller, "Aflatoxin B_1-2, 3-oxide as a probable intermediate in the covalent binding of aflatoxins B_1 and B_2 to rat liver DNA and ribosomal RNA in vivo," *Cancer Research*, vol. 37, no. 1, pp. 172–181, 1977.

[15] V. Dohnal, Q. Wu, and K. Kuca, "Metabolism of aflatoxins: key enzymes and interindividual as well as interspecies differences," *Archives of Toxicology*, vol. 88, no. 9, pp. 1635–1644, 2014.

[16] A. S. Arafa, R. J. Bloomer, H. R. Wilson, C. F. Simpson, and R. H. Harms, "Susceptibility of various poultry species to dietary aflatoxin," *British Poultry Science*, vol. 22, no. 5, pp. 431–436, 1981.

[17] W. E. Huff, "Evaluation of tibial dyschondroplasia during aflatoxicosis and feed restriction in young broiler chickens," *Poultry Science*, vol. 59, no. 5, pp. 991–995, 1980.

[18] H. T. Ostrowski-Meissner, "Biochemical and physiological responses of growing chickens and ducklings to dietary aflatoxins," *Comparative biochemistry and physiology. C, Comparative pharmacology*, vol. 79, no. 1, pp. 193–204, 1984.

[19] W. M. Colwell, R. C. Ashley, D. G. Simmons, and P. B. Hamilton, "The relative in vitro sensitivity to aflatoxin B_1 of tracheal organ cultures prepared from day-old chickens, ducks, Japanese quail, and turkeys," *Avian Diseases*, vol. 17, no. 1, pp. 166–172, 1973.

[20] M. Melissa, C. Roger, and R. Kent, "Aflatoxicosis: lessons from toxicity and responses to aflatoxin B_1 in poultry," *Agriculture*, vol. 5, no. 3, pp. 742–777, 2015.

[21] D. S. Patterson, "Metabolism as a factor in determining the toxic action of the aflatoxins in different animal species," *Food and cosmetics toxicology*, vol. 11, no. 2, pp. 287–294, 1973.

[22] P. J. Klein, T. R. Van Vleet, J. O. Hall, and R. J. Coulombe, "Biochemical factors underlying the age-related sensitivity of turkeys to aflatoxin B_1," *Comparative Biochemistry and Physiology. Toxicology & Pharmacology*, vol. 132, no. 2, pp. 193–201, 2002.

[23] S. X. Hu, "Effect of age on hepatic cytochrome P450 of Ross 708 broiler chickens," *Poultry Science*, vol. 92, no. 5, pp. 1283–1291, 2013.

[24] H. Wang, W. Li, I. Muhammad et al., "Biochemical basis for the age-related sensitivity of broilers to aflatoxin B_1," *Toxicology Mechanisms and Methods*, vol. 28, no. 5, pp. 361–368, 2018.

[25] E. P. Gallagher, K. L. Kunze, P. L. Stapleton, and D. L. Eaton, "The kinetics of aflatoxin B_1oxidation by human cDNA-expressed and human liver microsomal cytochromes P450 1A2 and 3A4," *Toxicology and Applied Pharmacology*, vol. 141, no. 2, pp. 595–606, 1996.

[26] S. S. Yip and R. J. Coulombe, "Molecular cloning and expression of a novel cytochrome P450 from turkey liver with aflatoxin B_1 oxidizing activity," *Chemical Research in Toxicology*, vol. 19, no. 1, pp. 30–37, 2006.

[27] S. Rawal, K. M. Mendoza, K. M. Reed, and R. J. Coulombe, "Structure, genetic mapping, and function of the cytochrome P450 3A37 gene in the turkey (Meleagris gallopavo)," *Cytogenetic and Genome Research*, vol. 125, no. 1, pp. 67–73, 2009.

[28] S. Rawal and R. A. Coulombe, "Metabolism of aflatoxin B_1 in Turkey liver microsomes: the relative roles of cytochromes P450 1A5 and 3A37," *Toxicology and Applied Pharmacology*, vol. 254, no. 3, pp. 349–354, 2011.

[29] G. J. Diaz, H. W. Murcia, and S. M. Cepeda, "Bioactivation of aflatoxin B_1 by turkey liver microsomes: responsible cytochrome P450 enzymes," *British Poultry Science*, vol. 51, no. 6, pp. 828–837, 2010.

[30] G. J. Diaz, H. W. Murcia, and S. M. Cepeda, "Cytochrome P450 enzymes involved in the metabolism of aflatoxin B_1 in chickens and quail," *Poultry Science*, vol. 89, no. 11, pp. 2461–2469, 2010.

[31] G. J. Diaz, H. W. Murcia, S. M. Cepeda, and H. J. Boermans, "The role of selected cytochrome P450 enzymes on the bioactivation of aflatoxin B_1 by duck liver microsomes," *Avian Pathology*, vol. 39, no. 4, pp. 279–285, 2010.

[32] M. Raynal, J. D. Bailly, G. Benard, and P. Guerre, "Effects of fumonisin B1 present in _Fusarium moniliforme_ culture material on drug metabolising enzyme activities in ducks," *Toxicology Letters*, vol. 121, no. 3, pp. 179–190, 2001.

[33] S. Leeson, G. J. Diaz, and J. D. Summers, "Publication announcement: poultry metabolic disorders and mycotoxins," *Journal of Applied Poultry Research*, vol. 4, no. 2, 1995.

[34] G. J. Diaz and H. W. Murcia, "Biotransformation of aflatoxin B_1 and its relationship with the differential toxicological response to aflatoxin in commercial poultry species," *Aflatoxins-Biochemistry and Molecular Biology*, vol. 1, 2011.

[35] G. J. Diaz and H. W. Murcia, "An unusually high production of hepatic aflatoxin B_1-dihydrodiol, the possible explanation

for the high susceptibility of ducks to aflatoxin B_1," *Scientific Reports*, vol. 9, no. 1, p. 8010, 2019.

[36] C. Wang, T. K. Bammler, Y. Guo, E. J. Kelly, and D. L. Eaton, "Mu-class GSTs are responsible for aflatoxin B_1-8, 9-epoxide-conjugating activity in the nonhuman primate macaca fascicularis liver," *Toxicological Sciences*, vol. 56, no. 1, pp. 26–36, 2000.

[37] T. C. Yeung and A. S. Gidari, "Purification and properties of a chicken liver glutathione _S_ -transferase," *Archives of Biochemistry and Biophysics*, vol. 205, no. 2, pp. 404–411, 1980.

[38] K. M. Reed, K. M. Mendoza, J. E. Abrahante, and R. A. Coulombe, "Comparative response of the hepatic transcriptomes of domesticated and wild turkey to aflatoxin B_1," *Toxins*, vol. 10, no. 1, p. 42, 2018.

[39] P. J. Klein, R. Buckner, J. Kelly, and R. A. Coulombe, "Biochemical basis for the extreme sensitivity of turkeys to aflatoxin B_1," *Toxicology and Applied Pharmacology*, vol. 165, no. 1, pp. 45–52, 2000.

[40] K. M. Reed, K. M. Mendoza, and R. J. Coulombe, "Differential transcriptome responses to aflatoxin B_1 in the cecal tonsil of susceptible and resistant turkeys," *Toxins*, vol. 11, no. 1, 2019.

[41] K. M. Reed, K. M. Mendoza, and R. J. Coulombe, "Altered gene response to aflatoxin B_1 in the spleens of susceptible and resistant turkeys," *Toxins*, vol. 11, no. 5, p. 242, 2019.

[42] J. E. Kim, M. M. Bauer, K. M. Mendoza, K. M. Reed, and R. J. Coulombe, "Comparative genomics identifies new alpha class genes within the avian glutathione _S_ -transferase gene cluster," *Gene*, vol. 452, no. 2, pp. 45–53, 2010.

[43] J. E. Kim, B. R. Bunderson, A. Croasdell, K. M. Reed, and R. J. Coulombe, "Alpha-class glutathione S-transferases in wild turkeys (Meleagris gallopavo): characterization and role in resistance to the carcinogenic mycotoxin aflatoxin B_1," *Plos One*, vol. 8, no. 4, 2013.

[44] E. P. Gallagher and D. L. Eaton, "_In Vitro_ Biotransformation of Aflatoxin B_1 (AFB_1) in Channel Catfish Liver," *Toxicology and Applied Pharmacology*, vol. 132, no. 1, pp. 82–90, 1995.

[45] G. S. Bailey, P. M. Loveland, C. Pereira, D. Pierce, J. D. Hendricks, and J. D. Groopman, "Quantitative carcinogenesis and dosimetry in rainbow trout for aflatoxin B_1 and aflatoxicol, two aflatoxins that form the same DNA adduct," *Mutation research*, vol. 313, no. 1, pp. 25–38, 1994.

[46] M. C. Lozano and G. J. Diaz, "Microsomal and cytosolic biotransformation of aflatoxin B_1 in four poultry species," *British Poultry Science*, vol. 47, no. 6, pp. 734–741, 2006.

[47] H. W. Murcia and G. J. Diaz, "_In vitro_ hepatic aflatoxicol production is related to a higher resistance to aflatoxin B1 in poultry," *Scientific Reports*, vol. 10, no. 1, p. 5508, 2020.

[48] G. E. Neal, S. A. Metcalfe, R. F. Legg, D. H. Judah, and J. A. Green, "Mechanism of the resistance to cytotoxicity which precedes aflatoxin B_1 hepatocarcinogenesis," *Carcinogenesis*, vol. 2, no. 5, pp. 457–461, 1981.

[49] H. W. Murcia and G. J. Diaz, "Dealing with aflatoxin B_1 dihydrodiol acute effects: impact of aflatoxin B_1-aldehyde reductase enzyme activity in poultry species tolerant to AFB_1 toxic effects,," *Plos One*, vol. 15, no. 6, p. e0235061, 2020.

[50] D. J. Judah, J. D. Hayes, J. C. Yang et al., "A novel aldehyde reductase with activity towards a metabolite of aflatoxin B_1 is expressed in rat liver during carcinogenesis and following the administration of an antioxidant," *The Biochemical journal*, vol. 292, no. 1, pp. 13–18, 1993.

[51] P. Tulayakul, S. Sakuda, K. S. Dong, and S. Kumagai, "Comparative activities of glutathione- _S_ -transferase and dialdehyde reductase toward aflatoxin B1 in livers of experimental and farm animals," *Toxicon*, vol. 46, no. 2, pp. 204–209, 2005.

[52] G. S. Bailey, D. E. Williams, J. S. Wilcox, P. M. Loveland, R. A. Coulombe, and J. D. Hendricks, "Aflatoxin B_1 carcinogenesis and its relation to DNA adduct formation and adduct persistence in sensitive and resistant salmonid fish," *Carcinogenesis*, vol. 9, no. 11, pp. 1919–1926, 1988.

[53] W. L. Bryden, "Mycotoxin contamination of the feed supply chain: Implications for animal productivity and feed security," *Animal Feed Science and Technology*, vol. 173, no. 1-2, pp. 134–158, 2012.

[54] J. He, K. Y. Zhang, D. W. Chen, X. M. Ding, G. D. Feng, and X. Ao, "Effects of vitamin E and selenium yeast on growth performance and immune function in ducks fed maize naturally contaminated with aflatoxin B_1," *Livestock Science*, vol. 152, no. 2-3, pp. 200–207, 2013.

[55] R. S. Ali, L. H. Sun, and N. Y. Zhang, "Ameliorative effects of grape seed proanthocyanidin extract on growth performance, immune function, antioxidant capacity, biochemical constituents, liver histopathology and aflatoxin residues in broilers exposed to aflatoxin B_1," *Toxins*, vol. 9, no. 11, 2017.

[56] Y. R. Pokharel, E. H. Han, J. Y. Kim et al., "Potent protective effect of isoimperatorin against aflatoxin B_1-inducible cytotoxicity in H4IIE cells: bifunctional effects on glutathione S-transferase and CYP1A," *Carcinogenesis*, vol. 27, no. 12, pp. 2483–2490, 2006.

[57] S. Langouët, B. Coles, F. Morel et al., "Inhibition of CYP1A2 and CYP3A4 by oltipraz results in reduction of aflatoxin B_1 metabolism in human hepatocytes in primary culture," *Cancer Research*, vol. 55, no. 23, pp. 5574–5579, 1995.

[58] J. A. Guarisco, J. O. Hall, and R. A. Coulombe, "Mechanisms of butylated hydroxytoluene chemoprevention of aflatoxicosis–inhibition of aflatoxin B_1 metabolism," *Toxicology and Applied Pharmacology*, vol. 227, no. 3, pp. 339–346, 2008.

[59] P. J. Klein, T. R. Van Vleet, J. O. Hall, and R. J. Coulombe, "Effects of dietary butylated hydroxytoluene on aflatoxin B_1-relevant metabolic enzymes in turkeys," *Food and Chemical Toxicology*, vol. 41, no. 5, pp. 671–678, 2003.

[60] N. E. Rainey, A. Moustapha, and P. X. Petit, "Curcumin, a multifaceted hormetic agent, mediates an intricate crosstalk between mitochondrial turnover, autophagy, and apoptosis," *Oxidative Medicine and Cellular Longevity*, vol. 2020, Article ID 3656419, 23 pages, 2020.

[61] K. Gross-Steinmeyer and D. L. Eaton, "Dietary modulation of the biotransformation and genotoxicity of aflatoxin B_1," *Toxicology*, vol. 299, no. 2-3, pp. 69–79, 2012.

[62] Y. Guo, B. Balasubramanian, Z. Zhao, and W. Liu, "Marine algal polysaccharides alleviate aflatoxin B1-induced bursa of Fabricius injury by regulating redox and apoptotic signaling pathway in broilers," *Poultry Science*, vol. 100, no. 2, pp. 844–857, 2021.

[63] B. K. Maurya and S. K. Trigun, "Fisetin modulates antioxidant enzymes and inflammatory factors to inhibit aflatoxin-B1 induced hepatocellular carcinoma in rats," *Oxidative Medicine and Cellular Longevity*, vol. 2016, Article ID 1972793, 2016.

[64] M. S. Aleissa, S. Alkahtani, M. A. A. Eldaim et al., "Fucoidan ameliorates oxidative stress, inflammation, DNA damage, and hepatorenal injuries in diabetic rats intoxicated with aflatoxin B1," *Oxidative Medicine and Cellular Longevity*, vol. 2020, Article ID 9316751, 10 pages, 2020.

Hindawi
Oxidative Medicine and Cellular Longevity
Volume 2021, Article ID 6670135, 12 pages
https://doi.org/10.1155/2021/6670135

Research Article

The Beneficial Role of *Filipendula ulmaria* Extract in Prevention of Prodepressant Effect and Cognitive Impairment Induced by Nanoparticles of Calcium Phosphates in Rats

Natalija Arsenijevic,[1] Dragica Selakovic,[2] Jelena S. Katanic Stankovic,[3] Vladimir Mihailovic,[4] Slobodanka Mitrovic,[5] Jovana Milenkovic,[1] Pavle Milanovic,[1] Miroslav Vasovic,[1] Snezana D. Markovic,[6] Marko Zivanovic,[3,7] Jelena Grujic,[3] Nemanja Jovicic,[8] and Gvozden Rosic[2]

[1]*Department of Dentistry, Faculty of Medical Sciences, University of Kragujevac, 34000 Kragujevac, Serbia*
[2]*Department of Physiology, Faculty of Medical Sciences, University of Kragujevac, 34000 Kragujevac, Serbia*
[3]*Department of Science, Institute for Information Technologies Kragujevac, University of Kragujevac, 34000 Kragujevac, Serbia*
[4]*Department of Chemistry, Faculty of Science, University of Kragujevac, 34000 Kragujevac, Serbia*
[5]*Department of Pathology, Faculty of Medical Sciences, University of Kragujevac, 34000 Kragujevac, Serbia*
[6]*Department for Biology and Ecology, Faculty of Science, University of Kragujevac, 34000 Kragujevac, Serbia*
[7]*BioIRC, Bioengineering R&D Center, 34000 Kragujevac, Serbia*
[8]*Department of Histology and Embryology, Faculty of Medical Sciences, University of Kragujevac, 34000 Kragujevac, Serbia*

Correspondence should be addressed to Nemanja Jovicic; nemanjajovicic.kg@gmail.com and Gvozden Rosic; grosic@medf.kg.ac.rs

Received 4 January 2021; Revised 30 January 2021; Accepted 2 February 2021; Published 12 February 2021

Academic Editor: Madhukar Saxena

Mineral components of dental composites are used in many medical and dental applications, including preventive, restorative, and regenerative dentistry. To evaluate the behavioural alterations induced by nanosized particles of novel dental composites, by means of depressive level and cognitive functions, experimental groups of rats were chronically administered with nanosized hydroxyapatite (HA), tricalcium phosphate (TCP), and amorphous calcium phosphate (ACP) with or without simultaneous application of *Filipendula ulmaria* L. (FU) methanolic extract. The significant prodepressant action was observed in groups solely treated with HA and ACP. Besides, prolonged treatment with ACP also resulted in a significant decline in cognitive functions estimated in the novel object recognition test. The adverse impact of calcium phosphates on estimated behavioural functions was accompanied by increased oxidative damage and apoptotic markers in the prefrontal cortex, as well as diminished specific neurotrophin (BDNF) and gabaergic expression. The results of our investigation showed that simultaneous antioxidant supplementation with FU extract prevented calcium phosphate-induced behavioural disturbances, as well as prooxidative and apoptotic actions, with the simultaneous restoration of BDNF and GABA-A receptors in the prefrontal cortex. These findings suggest that FU may be useful in the prevention of prodepressant impact and cognitive decline as early as the manifestation of calcium phosphate-induced neurotoxicity.

1. Introduction

Calcium phosphate (CaP) compounds are widely used in preventive, restorative, and regenerative treatments in various fields of medicine [1]. The use of CaP compounds, naturally present in the process of bone maturation [2], has primarily shown importance in areas of the medical treatment and rehabilitation of bone tissues and, further, in the prevention and therapy of dental diseases.

Calcium phosphates are progressively used in restorative dentistry. The widespread clinical application of dental composites has indicated significant shortcomings of these

materials. The most common cause for decay of modern composite fillings is the formation of secondary caries, followed by further loss of tooth tissue and the need for filling replacement [3]. Although secondary caries develops as a consequence of the imperfection of composite materials, the impact of the filling to the solid dental tissues is the most often passive. One way to prevent the recurrence of caries is to provide a high concentration of Ca^{2+} and PO_4^{3-} dissolved in saliva. These ions originate from the mineral component of dental composites, which creates conditions for the remineralization of tissues that directly surround the filling [4]. There are only a few commercial preparations of dental composites with the ability to remineralize dental tissues. However, numerous studies are investigating different forms of CaPs (hydroxyapatite (HA), monocalcium phosphates, dicalcium phosphates, tricalcium phosphate (TCP), tetracalcium phosphate, and amorphous calcium phosphate (ACP)), as a bioactive component of composites [5]. The amorphous structure and chemical composition of ACP, the direct precursor of HA [6], cause the formation of high concentrations of ions in aqueous solutions [7]. In order to increase the remineralization potential, bioactive dental composites usually contain CaPs in the form of nanoparticles [8].

Although previous studies have confirmed the biocompatibility of these compounds, studies of nanosized CaP toxicity have yielded conflicting results [9]. Thus, Liu and colleagues indicated that systemic administration of nano-HA (in rabbits) caused liver function alterations manifested by increasing AST, ALT, and ALP levels [10]. Also, it was noted that the main mechanism of the nano-HA-induced osteoblast demise is apoptosis associated with ROS hyperproduction and mitochondrial, lysosome, and DNA damage [11]. Furthermore, the nano-TCP particles incorporated into rabbit tibial defects elicited an excessive and prolonged inflammatory response associated with decreased bone regeneration [12]. *In vitro* studies revealed that nano-TCP induced dose-dependent cytotoxicity, while nanoparticle transport via endocytosis was accompanied by an intracellular increase in calcium and phosphate ions, increased ROS production, and both external and internal pathway-mediated apoptosis [13]. Li and colleagues showed that ACP nanoparticles induced leukemia cell apoptosis by affecting the G1 phase of the cell cycle in particular, where the cytotoxic effect was directly dependent on ACP exposure interval [14].

On the other hand, literature data confirmed that the natural products with antioxidant effects, such as curcumin [15] and chicory extract [16], reduced the harmful effects of chronic CaP intake [17]. Among the natural products with a confirmed antioxidant action is the extract of *Filipendula ulmaria* [18]. *Filipendula ulmaria* (L.) Maxim. (*Rosaceae*) (FU), known as meadowsweet, is a perennial plant found in wild and cultivated habitats in Europe and Asia [19]. All parts of the plant are traditionally used for medical purposes, with the most beneficial effects observed from aerial parts [20]. FU has been used in the treatment of various inflammatory processes, rheumatism, neuralgia, diarrhea, and urinary tract infections [21]. A plethora of evidence of the numerous beneficial effects of FU is directly attributed to its specific polyphenolic content, rich in anti-inflammatory [20, 22], antioxidant [23, 24], and antimicrobial [24] compounds. Previous phytochemical investigations of *F. ulmaria* by our team [18] lead to a conclusion that some specific bioactive compounds determined in this extract, such as catechin, rutin, and spiraeoside [24], may be also responsible for antioxidant actions in the nervous system. Analyzing data concerning the distribution and mechanism of action for nano-CaPs after systemic application [25], the neurotoxic effects of CaP nanoparticles following this route of the administration still appear to be insufficiently elucidated. Although it has been reported that these particles cross the blood-brain barrier [26], their effect on the central nervous system is not fully investigated.

The use of nanosized CaP particles in medical practice, as the most potent in the prevention of damage and in regeneration of mineralized tissue, implicates the necessity to clarify the system toxicity, including neurotoxicity, as well as the potential ways to reduce their side effects. Following the findings that the principle mechanism of CaP toxicity involves oxidative imbalance, it seems reasonable to examine the antioxidant effect of FU, following experimental nanosized CaP prolonged load. Therefore, the aim of this study was to examine the beneficial effects of FU on changes in the cognitive functions and depressive behaviour, as the functional manifestations of nano-CaP-induced neurotoxicity.

2. Materials and Methods

2.1. Animals and Treatment. Two-month-old male Wistar rats, with b.w. range of 180–220 g, were obtained from the Military Medical Academy, Belgrade, Serbia. The animals were kept in the translucent cages in the groups of three under the standard conditions (temperature $23 \pm 1^{\circ}$C, humidity $50 \pm 5\%$) with light/dark cycle (12/12 h) and were provided standard chow and water *ad libitum* for the duration of the study.

The animals were randomised into seven equal groups (6 rats per group): control group; groups that orally received CaP nanoparticles in a daily dose of hydroxyapatite (17.8 mg/kg b.w.)—HA, tricalcium phosphate hydrate (11 mg/kg b.w.)—TCP, amorphous calcium phosphate (9.65 mg/kg b.w.)—ACP, solely, or simultaneously with *F. ulmaria* extract (100 mg/kg b.w.)—HA+FU, TCP+FU, and ACP+FU group. All protocols continuously lasted for 30 days, as presented in Figure 1.

The mineral components of dental composites in the nanoparticles were obtained from Sigma-Aldrich, Germany: hydroxyapatite nanopowder, <200 nm particle size (BET), ≥97%, synthetic; tricalcium phosphate hydrate nanopowder, <200 nm particle size (BET); calcium phosphate, amorphous nanopowder, <150 nm particle size (BET). The applied doses of mineral components were selected to be equimolar levelling the lowest dose of HA that showed toxic effects in the previously published study performed *in vivo* with nanoparticles in the rodents [27]. Also, the doses of CaPs in this study were chosen according to the reported release of mineral components from dental composites obtained *in vitro* [28]. The oral administration was chosen in order to mimic the

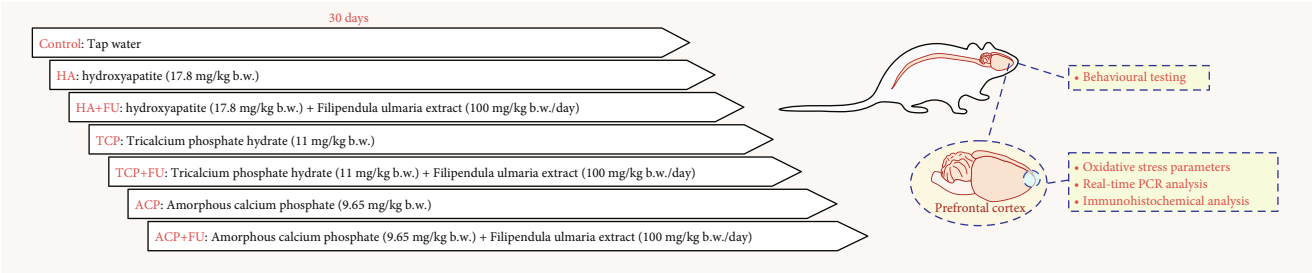

Figure 1: Experimental design.

authentic application route of investigated materials in the human population. The plant material (from the aerial part) and preparation of the extract as well as the content identification was performed using the previously described procedure [18]. FU extract dose was selected on the basis of our previous study that confirmed biological activity of this medicinal plant [18], reaching the optimal effective concentration at 100 mg/kg b.w. daily. The final concentration of all applied substances was calculated on the basis of an average water intake in the previous 24 h and dissolved in tap water.

All research procedures were carried out in accordance with the European Directive for the welfare of laboratory animals no. 86/609/EEC and the principles of Good Laboratory Practice and in accordance with the ARRIVE guidelines. All experiments were approved by the Ethical Committee of the Faculty of Medical Sciences, University of Kragujevac, Kragujevac, Serbia.

2.2. Behavioural Testing. Twenty-four hours after completing protocols, the animals were placed in the testing room for 1–2 h prior to the initiation of each test (approximately at 8 a.m.). All tests were performed under proper conditions of silence and illumination. During the trials, the experimenters were not present in the testing room. At the end of each trial, the experimental fields were cleaned in order to remove possible interfering scents. All tests were recorded by digital video camera mounted above the mazes at appropriate heights. Video files from the novel object recognition test were analyzed using EthoVision software (XT 12), an integrating video tracking system for automatic recording of activity movement and interactions of animals (Noldus Information Technology, the Netherlands).

2.2.1. Tail Suspension Test. For the evaluation of depressive state level, we used the tail suspension test (TST). This test has been successfully used for that purpose for decades and was performed on the previously standardized procedure with described apparatus [29]. In TST, we determined the latency to the first immobility (s), the number of immobility episodes, the total duration of immobility (s), and an average duration of an immobility episode (s).

2.2.2. Novel Object Recognition Test. Testing for the estimation of cognitive functions, the novel object recognition (NOR) test was performed according to the methods presented by Bevins and Besheer [30], with modification by Mumby and coworkers [31]. Testing involved three phases (performed in square arena $60 \times 60 \times 30$ cm): phase 1—familiarization with the empty testing arena, phase 2—the introduction of two identical objects in the same arena placed on a fixed position, and phase 3—the replacement of one familiar object (from phase 2) with the new one (novel object). All phases lasted for five minutes, with intersession interval of 45 minutes. The following parameters were estimated (using EthoVision software XT12) in the NOR test: the frequency to novel object zone, the cumulative duration in novel object zone (s), and the time interval while head directed to novel object (s).

2.3. Determination of Tissue Oxidative Stress Parameters. Prefrontal cortex (PFC) homogenates were prepared according to the standard procedure previously established in our lab, as reported by Kumburovic and coworkers [32] and Vukovic and colleagues [33], with the chemicals listed in Supplementary file 2. Principally, phosphate-buffered saline (PBS, pH 7.4) was used for PFC tissue homogenization, and after centrifugation at 4000 rpm for 15 min at 4°C, the supernatant was separated and used for further analyses. For all spectrophotometric analyses, a UV-Vis double beam spectrophotometer (model Halo DB-20S, with a temperature controller, Dynamica GmbH, Dietikon, Switzerland) was used. Lowry's method was used for the evaluation of protein content in the homogenates, and bovine serum albumin was used as a standard [34]. The oxidative stress parameters tested in this study were the activities of superoxide dismutase (SOD) and catalase (CAT) as well as the levels of reduced glutathione (GSH) and thiobarbituric acid reactive substance (TBARS). The activity of SOD was determined according to the spectrophotometric method reported by Misra and Fridovich [35] where the inhibition of epinephrine transformation to adrenochrome was monitored. The CAT is known for its ability to catalyze the decomposition of hydrogen peroxide to water and oxygen which is, therefore, used in the method of Beers and Sizer [36] based on the rate of hydrogen peroxide degradation. The activities of both tested enzymes were expressed as units per milligram of proteins (U/mg). The level of GSH in tested samples was monitored according to Ellman's method [37] using 5,5-dithio-bis-(2-nitrobenzoic acid). The concentration of GSH in samples was expressed in milligrams GSH per gram of proteins (mg GSH/g). The products of lipid oxidation in tissue samples were estimated as the levels of thiobarbituric acid reactive substance

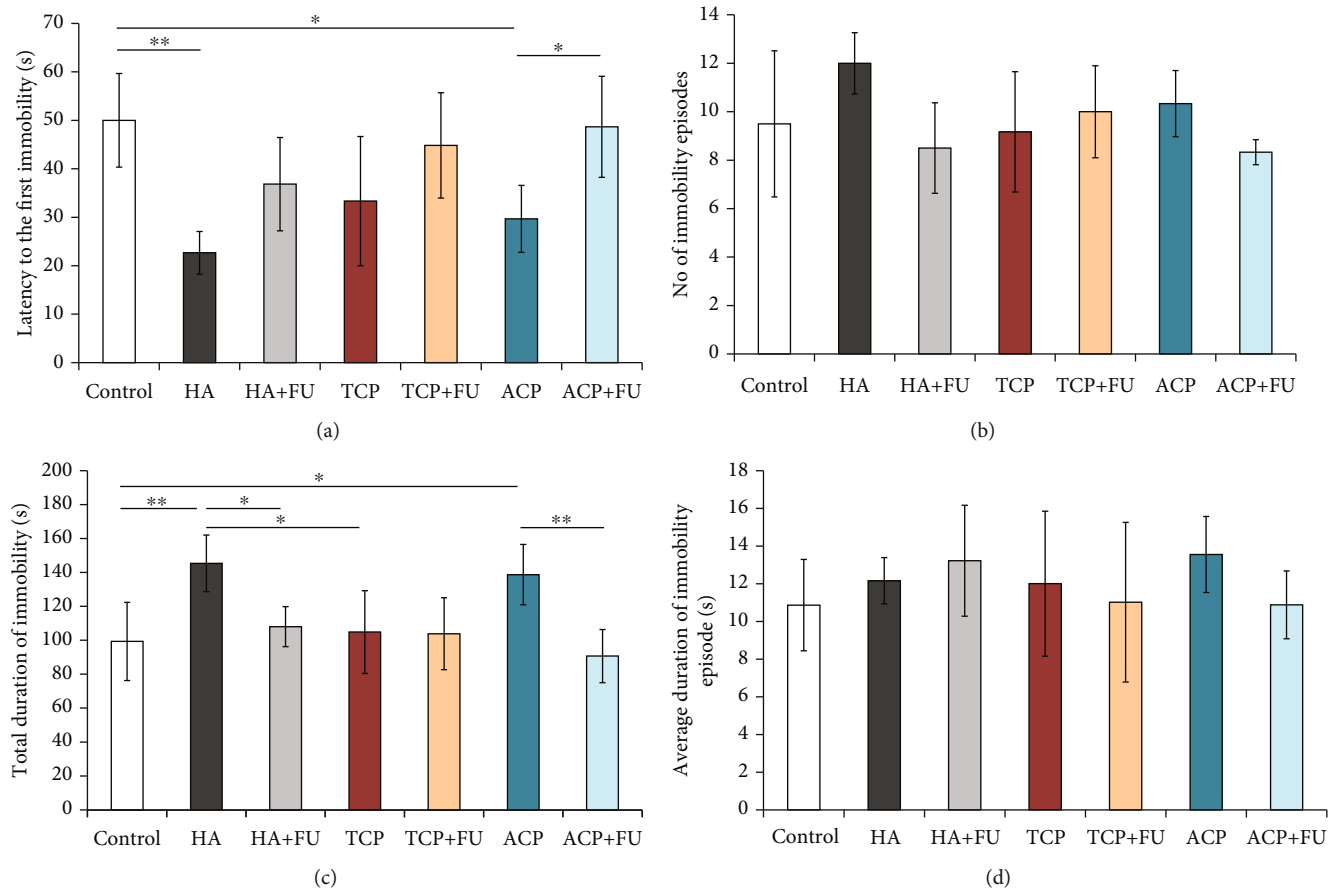

Figure 2: Parameters obtained in the tail suspension test: (a) the latency to the first immobility, (b) the number of immobility episodes, (c) the total duration of immobility, and (d) the average duration of immobility. The values are mean ± SD; *a significant difference $p < 0.05$, **a significant difference $p < 0.01$.

(TBARS) and expressed as nmol of malondialdehyde (MDA) per milligram of proteins (nmol MDA/mg) [38].

2.4. Prefrontal Cortex RNA Isolation and Real-Time PCR Analysis. Total RNA was extracted from PFC tissue using PureZOL reagent (Bio-Rad, USA) according to the manufacturer's instructions. Reverse transcription was done using iScript Reverse Transcription Mastermix (Bio-Rad, USA). Quantitative RT-PCR was performed using SsoAdvanced Universal SYBR Green Supermix (Bio-Rad, USA). mRNA specific primers for Bax, Bcl-2, BDNF, anti-GABA A receptor alpha 5/GABRA5, and β-actin as a housekeeping gene were used (Supplementary file (available here)). Quantitative RT-PCR reactions were done in Applied Biosystems 7500 (Applied Biosystems, USA), and after data analysis, the relative gene expression was calculated according to Livak and Schmittgen [39].

2.5. Immunohistochemical Analysis. The prefrontal tissue specimens were fixed in 4% formaldehyde solution and embedded in paraffin. Coronal brain sections, 5 μm thick, were dewaxed, rehydrated, and treated with citrate buffer (pH 6.0) in the microwave for antigen retrieval. Staining was visualized by using the EXPOSE Rabbit Specific HRP/DAB Detection IHC Kit (ab80437, Abcam, UK), and sections were counterstained with Mayer's hematoxylin. The slices were incubated with GABRA5 antibody (PA5-77413, Thermo Fisher Scientific, USA) and recombinant anti-BDNF antibody (EPR1292) (ab108319, Abcam, UK) overnight at room temperature. Sections were photomicrographed with a digital camera mounted on a light microscope (Olympus BX51, Japan), digitized and analyzed. The analyses were made by independent experimenters who were blind to the experimental protocol.

2.6. Statistical Analysis. Statistical analysis was performed with SPSS version 20.0 statistical package (IBM SPSS Statistics 20). The results are expressed as the means ± standard errors of the mean (S.E.M.). The parameters were initially submitted to Levene's test for homogeneity of variance and to Shapiro-Wilk test of normality. One-way ANOVA, followed by Bonferroni test, was used for comparisons between the groups. The significance was determined at $p < 0.05$ for all tests.

3. Results

The results obtained in the tail suspension test confirmed that the applied protocols significantly altered depressive levels by means of the latency to the first immobility (Figure 2(a), df = 6, $F = 6.731$). The chronic oral intake of

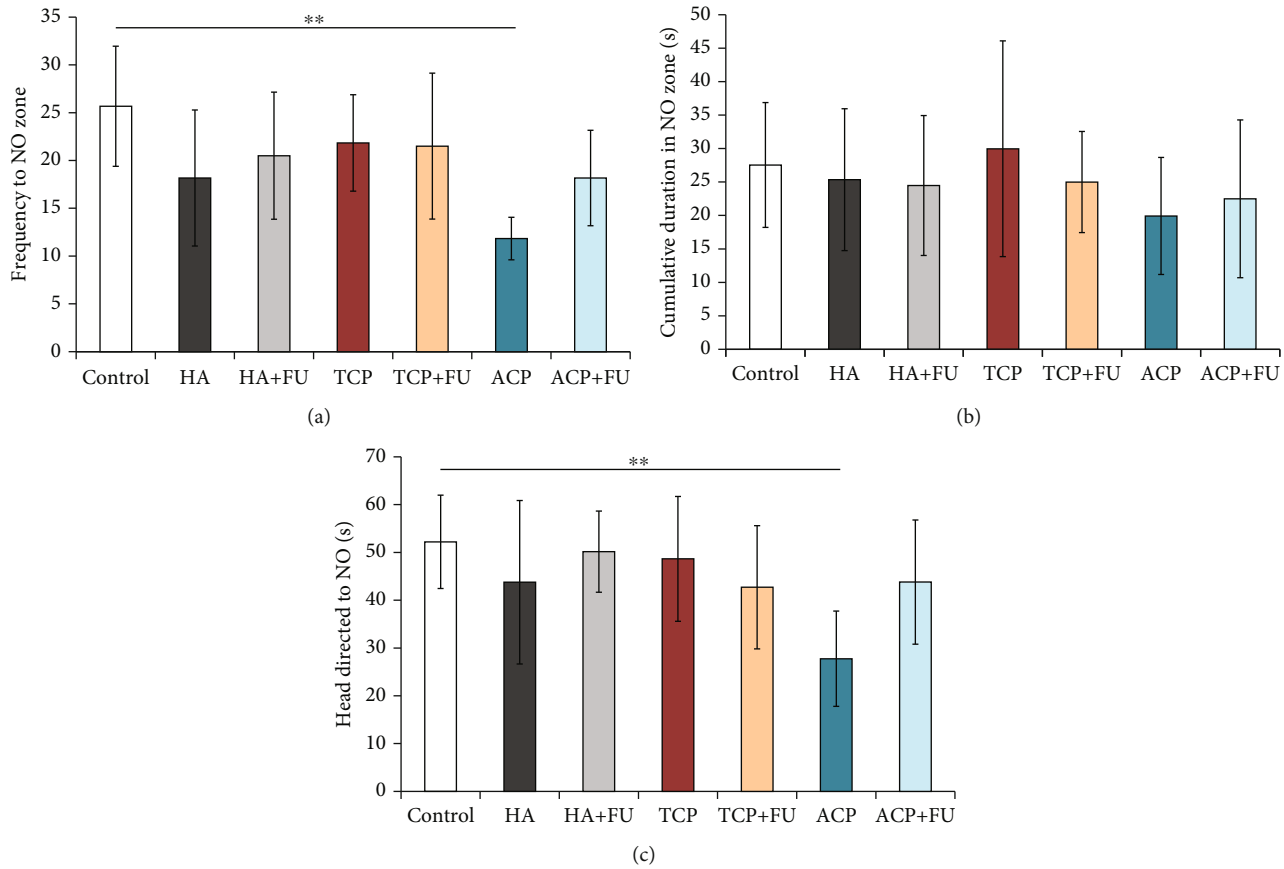

Figure 3: Parameters obtained in the novel object recognition test: (a) the frequency to the NO zone, (b) the cumulative duration in the NO zone, and (c) the head directed to NO. The values are mean ± SD; **a significant difference $p < 0.01$.

nano-HA and nano-ACP significantly reduced the latency to the first immobility ($p < 0.01$ and $p < 0.05$, respectively). However, this prodepressant action of both nano-CaPs was successfully prevented by the antioxidant supplementation with FU extract that diminished the decline in the latency to the first immobility for both nano-HA and nano-ACP compared to control and even (for nano-ACP) when compared to the group where CaP was administered solely ($p < 0.05$). At the same time, neither of the applied protocols had significantly influenced the number of immobility episodes ($F = 2.524$, Figure 2(b)). As shown in Figure 2(c), the individual application of nano-CaPs produced a different impact on the total duration of immobility ($F = 7.031$). While nano-HA and nano-ACP significantly increased this main marker of depression in TST, compared to control ($p < 0.01$ and $p < 0.05$, respectively) and even to nano-TCP (for nano-HA, $p < 0.05$), this prodepressant action was not observed in the nano-TCP group. At the same time, the restoration of the total duration of immobility was observed following simultaneous administration of FU extract in both nano-HA and nano-ACP that resulted in significant increase of this parameter ($p < 0.05$ and $p < 0.01$, respectively). Finally, the applied protocols produced no significant alterations in the average duration of immobility episodes ($F = 0.925$, Figure 2(d)).

Unlike the depressive level estimation, the results of the novel object recognition test showed that long-term application of nano-CaPs led to changes in the frequency to the NO zone (df = 6, $F = 3.123$) strongly depending on nano-CaP particle structure. Thus, in the ACP group, the frequency was reduced compared to the control group ($p < 0.01$), with no changes in other groups (Figure 3(a)). As shown in Figure 3(b), none of the applied protocols significantly altered the cumulative duration in the NO zone ($F = 0.529$). However, the prolonged administration of nano-ACP significantly decreased the time interval with head directed to NO ($F = 2.578$, $p < 0.01$), with no difference observed following other protocols (Figure 3(c)). The beneficial effect of antioxidant supplementation with FU extract in the prevention of nano-ACP-induced cognitive impairment was manifested by reversing the values of spatial memory markers (Figures 3(a) and 3(c)) back to control.

As shown in Figure 4, the prolonged intake of nano-CaPs had a significant impact on oxidative stress markers in the rat PFC. All three nanosized CaPs applied in this study significantly increased the index of lipid peroxidation (Figure 4(a)), expressed as TBARS ($F = 14.283$, $p < 0.01$). Although the administration of FU extract along with CaPs reduced lipid peroxidation when compared to the groups with individual CaP intake (significant only for nano-ACP,

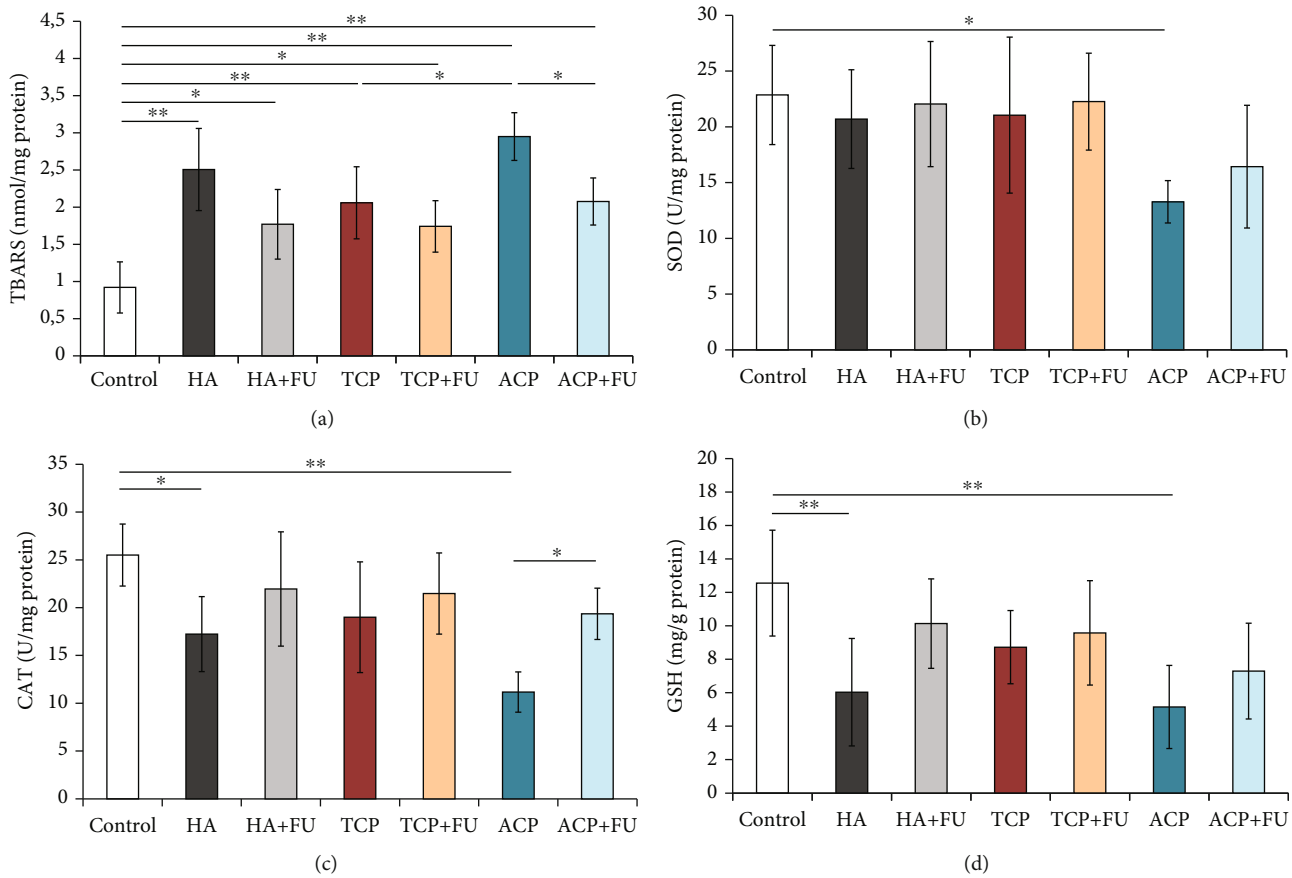

Figure 4: Oxidative stress parameters in rat PFC: (a) thiobarbituric acid reactive substances (TBARS), (b) superoxide dismutase (SOD), (c) catalase (CAT), and (d) glutathione (GSH). The values are mean ± SD; *a significant difference $p < 0.05$, **a significant difference $p < 0.01$.

$p < 0.05$), the TBARS values remained significantly above the control values ($p < 0.05$ for nano-HA and TCP, $p < 0.01$ for nano-ACP). The activity of antioxidant enzymes, expressed by means of SOD (Figure 4(b)) and CAT (Figure 4(c)), was significantly diminished following prolonged nano-CaP intake ($F = 3.115$ and 6.777, respectively). While the SOD activity in PFC was significantly reduced ($p < 0.05$) only in the nano-ACP group and successfully reversed with the simultaneous FU extract administration, the decline in CAT activity was observed in both nano-HA and ACP groups ($p < 0.05$ and $p < 0.01$, respectively). Again, the antioxidant supplementation restored CAT activity ($p < 0.05$). The nonenzymatic antioxidant capacity, expressed by means of GSH, in PFC (Figure 4(d)) was also diminished by nano-HA and ACP particle intake ($F = 4.853$, $p < 0.01$). The simultaneous administration of FU extract levelled GSH content up to control values.

The evaluation of apoptotic markers (Figure 5) showed the significant alterations in both proapoptotic and antiapoptotic indicators in the rat PFC following the applied protocols. Bax relative mRNA expression was significantly enhanced by all three applied nano-CaPs ($F = 20.963$, $p < 0.01$). However, the strongest proapoptotic effect was observed in the ACP group resulting in Bax relative mRNA expression that was even significantly above the values observed in the TCP group ($p < 0.05$). On the other hand, the antioxidant supplementation with FU extract failed to prevent the proapoptotic action of the applied CaPs. The antiapoptotic mechanism, expressed by Bcl-2 relative mRNA expression, was also significantly affected by the applied protocols ($F = 17.234$). Again, all three applied CaPs significantly reduced relative Bcl-2 expression ($p < 0.01$), with the most prominent response to ACP (significant decline even when compared to the TCP group, $p < 0.01$). Like for Bax, FU extract was insufficient to prevent the diminishing effect of the applied CaPs on Bcl-2. Finally, the analysis of the Bax/Bcl-2 ratio confirmed the strong proapoptotic impact of the applied CaPs ($F = 16.939$), although not significant in the TCP group. Evidently, the strongest proapoptotic action was observed in the ACP group, but also successfully prevented by the simultaneous administration of FU extract ($p < 0.01$).

The RT-PCR analysis of PFC tissue homogenate (Figure 6) showed the significant alterations in BDNF mRNA relative expression ($F = 13.246$), manifested by significant decline achieved only in the ACP groups ($p < 0.01$), while the other two nanosized CaPs did not induce significant decrease. Although the simultaneous administration of FU extract resulted in a significant increase in BDNF expression, compared with the group where ACP was applied solely ($p < 0.05$), the BDNF levels in the combined group remained significantly below the control values ($p < 0.05$).

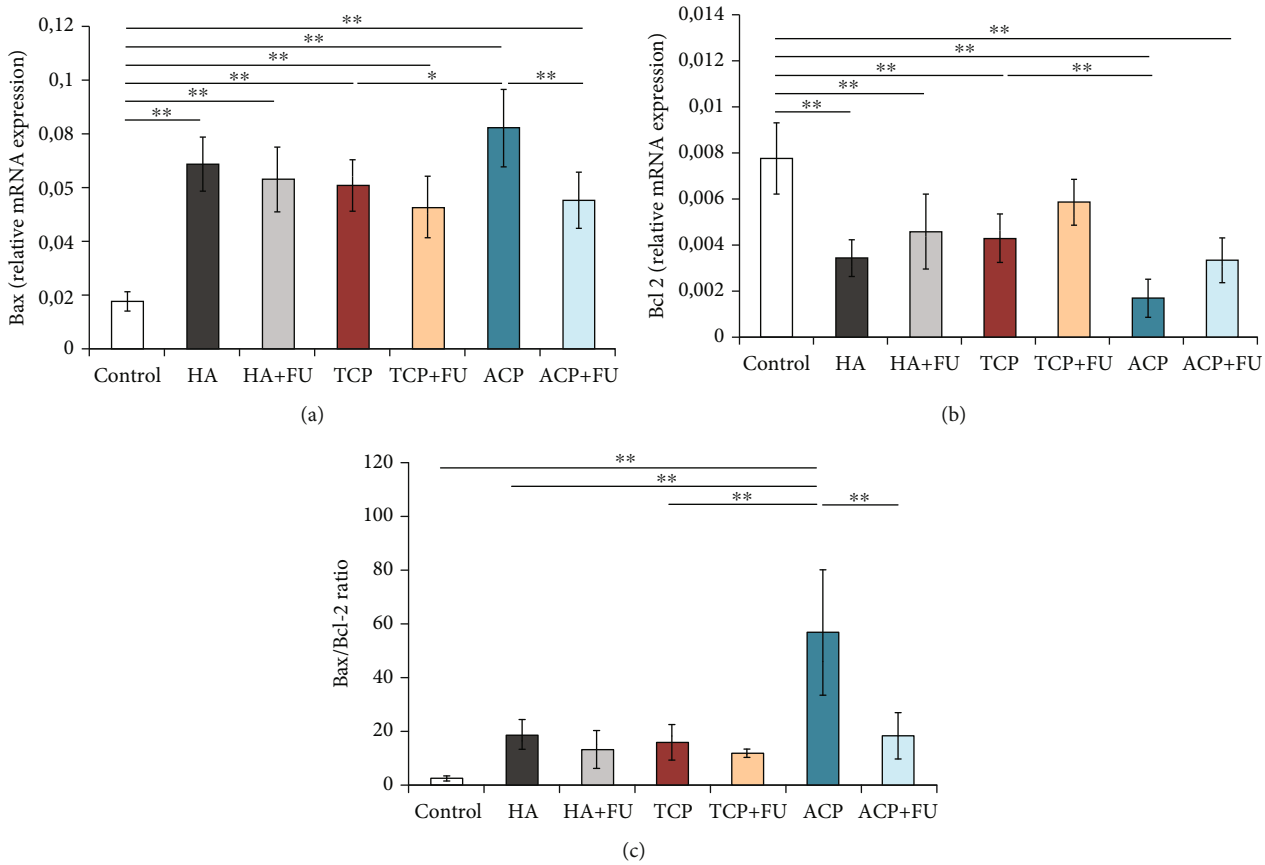

Figure 5: The relative gene expression of the pro- and antiapoptotic genes in the rat PFC: (a) Bax, (b) Bcl-2, and (c) Bax/Bcl-2 ratio. The values are mean ± SD; *a significant difference $p < 0.05$, ** a significant difference $p < 0.01$.

The expression of GABA-A receptors in PFC, estimated by means of subunit 5 relative mRNA expression, as shown in Figure 7, was also significantly altered by the applied protocols ($F = 14.471$). Nano-HA and ACP particles significantly decreased GABA-AR expression ($p < 0.01$), while TCP-induced decline was not significant. Interestingly, the reduction of GABA-AR5S observed in the HA and ACP groups was significant even when compared to the TCP group ($p < 0.05$ and $p < 0.01$, respectively). The antioxidant supplementation with FU extract significantly restored GABA-AR5S expression in the HA group ($p < 0.05$) but failed to restore GABA-AR expression in the ACP group that remained significantly below the control values ($p < 0.01$).

4. Discussion

Increasing interest in the application of bone replacement materials, as expected, is accompanied by the necessity for the estimation of the adverse effects of such a therapeutic approach in a broad field of medical disciplines, most frequently in dentistry. However, since there is evidence that CaPs, as main dental tissue remineralizing agents, are found to cross the blood-brain barrier as nanoparticles [26], there is still a need to evaluate the impact of those compounds on the central nervous system following prolonged systemic administration, in order to mimic clinical conditions for their usage. It should be emphasized that this study was performed with the minimal doses of nano-CaPs, corresponding to the previous investigations that analyzed the expected release of CaPs [28], and also to the minimal doses for the systemic application that was reported to produce toxic effects in other organ systems [27]. Furthermore, the individual doses for nano-Ca compounds applied in this study were set to be equimolar in order to allow the comparison of the observed outcome, based on predefined nano-HA dose for parenteral usage [27] and nano-ACP dose for the release capacity from dental composites [28], as referent values. Also, the daily dose of FU extract was chosen, by means of optimal biological effectiveness, according to our previous findings [18, 20].

The results of our study strongly confirmed the oxidative damage induced by nanosized CaP particles. However, the response in the oxidative stress markers significantly differed depending on the composite type. While the lipid peroxidation was enhanced by all three applied CaPs, the antioxidant system, expressed by means of both enzymatic and nonenzymatic capacity, was not disturbed by all applied substances. Thus, with no significant effect of nano-TCP, nano-HA mostly affected CAT and GSH, but nano-ACP induced the total reduction of the evaluated antioxidant mechanisms (SOD, CAT, and GSH, Figure 4). Our results are in line with the reported prooxidative action of HA nanoparticles *in vitro*, where their application increased ROS levels and

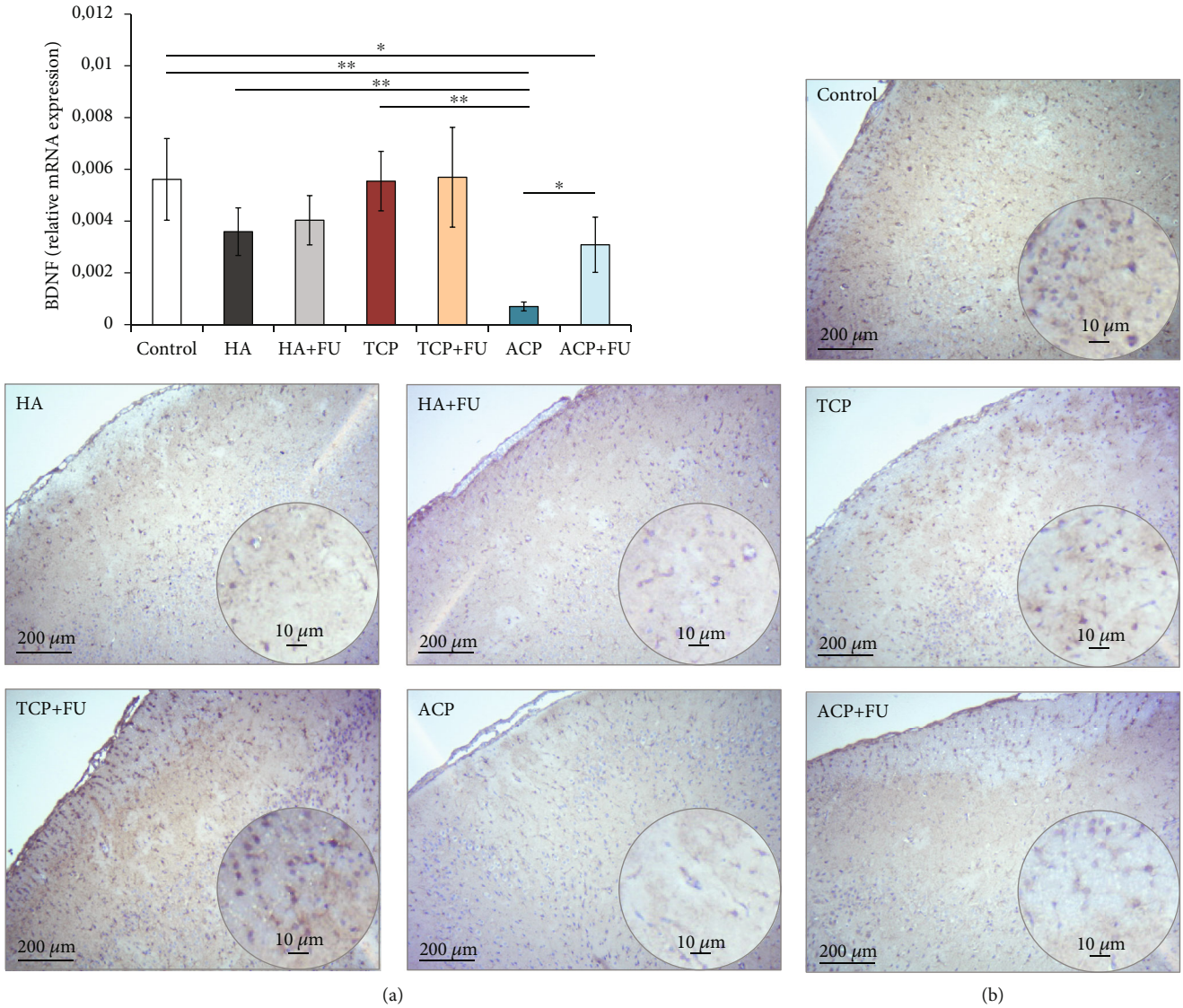

Figure 6: The relative gene expression and the immunohistochemical expression of BDNF in rat PFC: (a) the relative BDNF gene expression and (b) representative images of BDNF IHC staining on paraffin-embedded PFC sections (original magnification 10x and 40x; scale bar = 200 and 10 μm). The values are mean ± SD; *a significant difference $p < 0.05$, **a significant difference $p < 0.01$.

decreased SOD and GSH in the osteoblastic MC3T3-E1 [11] and C6 cells [40]. However, there is no data considering the effects of TCP and ACP. Since there is no literature data for the impact of CaPs (in nanoparticles) on the oxidative stress markers *in vivo*, we can only compare the observed alterations with other nanosized metallic particles. Thus, the results of our study are in line to previously reported oxidative damage in the brain (with no focus on PFC) following ZnO [41], CuO [42], Ag [43], and TiO_2 [44] administration.

The CaP-induced oxidative damage was significantly attenuated with the simultaneous administration of FU extract. Thus, the antioxidant supplementation along with CaP particles prevented the decline in the activity of the antioxidant enzymes, as well as GSH content in PFC. At the same time, FU extract decreased lipid peroxidation, but the values remained above control (Figure 4). Again, due to the lack of literature data, we cannot compare our results with the estimation of the antioxidant supplementation impact on CaP nanoparticle-induced oxidative damage. Instead, we can only comment that amelioration of metallic nanoparticles (ZnO, CuO, and Ag) prooxidative action in the brain tissue was achieved with different phytochemical compounds such as flavonoid glucosides hesperidin [45] and rutin [43], as well as crocetin [46], a diterpenoid from saffron spice.

As numerous literature data stated that the oxidative imbalance may often be accompanied by the apoptosis-mediating pathways [47], we also estimated the impact of the prolonged nanosized CaP intake on the apoptotic markers in PFC. Indeed, the results obtained in this study confirmed the proapoptotic action of all investigated nanosized CaPs that was manifested by both upregulation of the proapoptotic (Bax) and downregulation of the antiapoptotic (Bcl-2) markers (Figure 5). However, it should be noticed that the proapoptotic impact in the nano-ACP-treated group

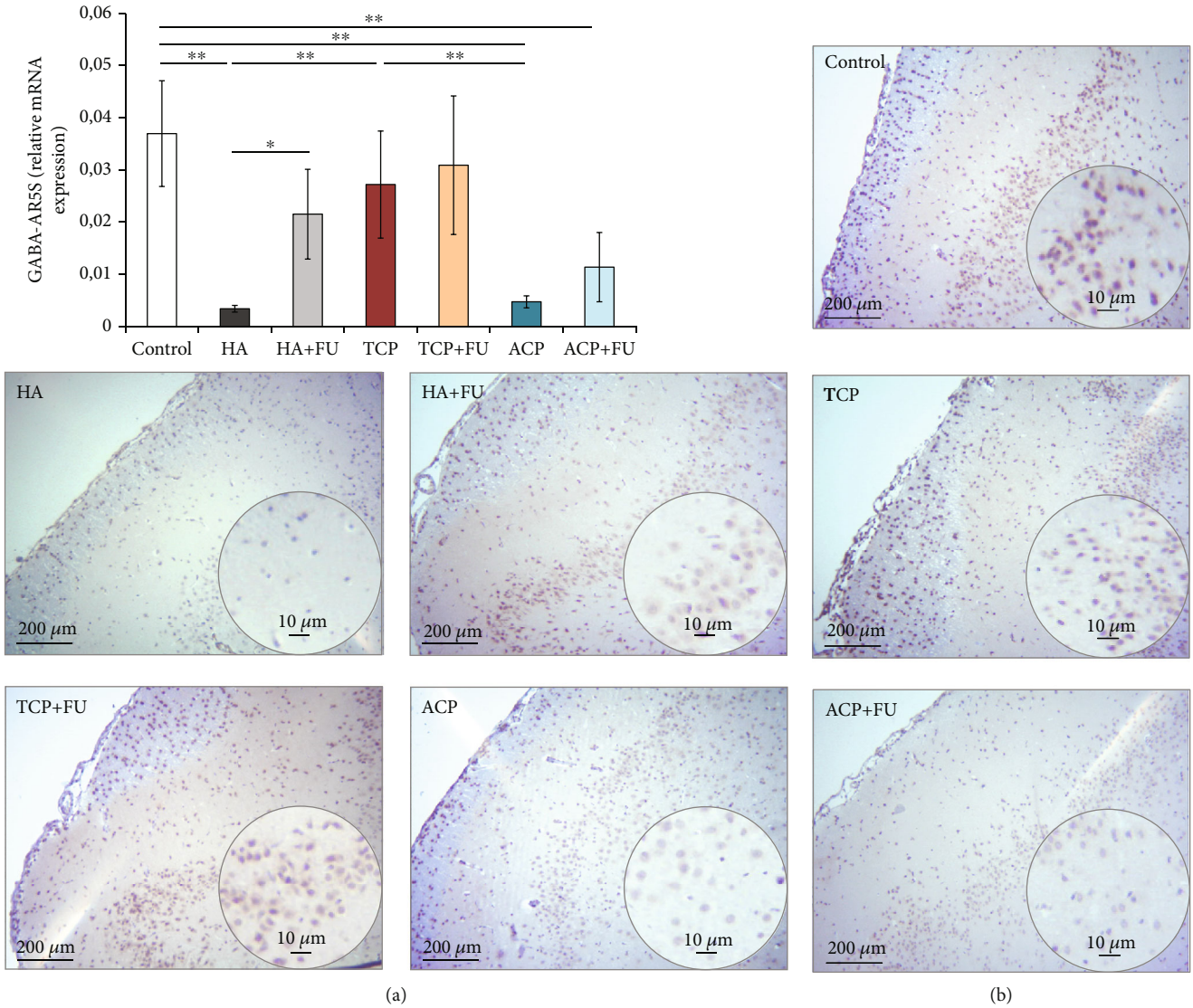

Figure 7: The relative gene expression and the immunohistochemical expression of the GABA-AR5S in rat PFC: (a) the relative GABA-AR5S gene expression and (b) representative images of GABA-AR5S IHC staining on paraffin-embedded PFC sections (original magnification 10x and 40x; scale bar = 200 and 10 μm). The values are mean ± SD; *a significant difference $p < 0.05$, **a significant difference $p < 0.01$.

was more pronounced than for HA and TCP, and this proapoptotic action of ACP, although significantly reduced by FU extract, remained markedly above the control values. The results obtained in both *in vitro* and *in vivo* studies also confirmed the stimulation of proapoptotic mechanisms following the nanosized CaP administration. It has been reported that HA nanoparticles increased apoptosis in osteoblasts and macrophages [48, 49] by the mechanism that involves increased p53 expression and caspase family activity with the simultaneous downregulation of Bcl-2, while ACP nanoparticles induced apoptosis of leukemia cells by selective effect in G1 phase [14]. In order to compare the proapoptotic action of nanosized CaPs as observed in this study, it should be mentioned that the other metallic nanosized compounds such as CuO [46] also enhanced apoptosis in hippocampal HT22 cells by Bax upregulation and Bcl-2 downregulation. Furthermore, *in vivo* studies that evaluated the influence of the nanosized CaPs on apoptosis were conducted only with HA and TCP, but with no specific data for the brain tissue. Nano-HA particles induced morphologically verified apoptosis in the rat liver and kidney [27], and this proapoptotic action of nano-HA was accompanied by an increase of Bax expression [50]. Nano-β-TCP induced apoptosis of tumor cells by the apoptotic signalling that resulted in overexpression of Bax, caspase-3, and caspase-9 [13]. Like for the oxidative damage, the beneficial effects of antioxidant supplementation on the nanosized CaP-induced apoptosis were not evaluated in the brain tissue, but were confirmed with medicinal plant chicory (*Cichorium intybus*) [50] and pure compounds curcumin and chitosan [17] in the rat kidney.

The analysis of the relative mRNA expression in PFC showed a significant decline for both BDNF and GABA-AR, expressed by subunit 5, following the prolonged intake of HA and ACP, with no significant alterations observed in the TCP group (Figures 6 and 7, respectively). Also, our

results showed that simultaneous antioxidant supplementation with FU extract attenuated the decline in BDNF and GABA-AR5S expression, although the values in the ACP +FU group remained significantly below the values observed in the control group. Since there is no literature data for the influence of nanosized CaP particles on BDNF and gabaergic system in the brain tissue, we can only compare our results with the influence of silver nanoparticles. Thus, it was shown that the silver nanoparticles produced a significant decrease in various monoamine neurotransmitters, including GABA, levels in the rat brain homogenate [43] and also inhibited BDNF signalling in the human neuroblastoma cell line SH-SY5Y [51]. It is worth to notice that the antioxidant supplementation with rutin prevented the decline in monoamine neurotransmitter levels [43].

Taking into account previously commented results, it is not surprising that both depressive state levels and cognitive functions estimated in this study were significantly affected by the chronic CaP nanoparticles intake (Figures 2 and 3). Interestingly, the prodepressant action was observed within both HA and ACP groups, while a significant cognitive impairment was noticed only in the ACP group. However, it seems important to underlie that both investigated behavioural patterns were successfully prevented by the simultaneous antioxidant supplementation with FU extract. As already declared, due to the lack of data for nano-CaP particles' impact on those specific behavioural patterns, we can only compare the behavioural alterations observed in this study with the behavioural impact of some other nanosized metallic compounds. Therefore, the most frequently investigated metallic compound, nano-TiO_2, produced an adverse effect on rodent behaviour by means of both prodepressant action [52, 53] and cognitive impairment [52, 54]. The prodepressant action of nanosized metallic compounds was also observed with ZnO nanoparticles [55], while the disruption of learning and memory was also reported following CuO nanoparticle application [56]. However, none of the mentioned investigations employed the antioxidant supplementation to estimate the potential role of oxidative stress in the mediation of metallic nanoparticle-induced behavioural disturbances.

Finally, the observed differences between the individual CaPs applied in this study may be addressed to different Ca/P ratio [57] and compound structure—crystallization [58], which still have to be evaluated in our future investigations. However, it seems that the antioxidant supplementation (with FU extract) in this study may be useful in the prevention of the behavioural manifestations of nano-CaP-induced neurotoxicity.

5. Conclusions

In summary, the widespread medical use of nano-CaPs is accompanied by the confirmed toxicities, so it requires further elucidation of a general mechanism that may compromise the efficiency and safety. According to the results obtained in this study, it appears that the antioxidant supplementation may prevent the processes underlying the side effects of nano-CaPs, including the neurotoxicity manifested through the specific behavioural alterations.

Data Availability

Data are available upon request.

Conflicts of Interest

The authors declare no conflict of interest.

Authors' Contributions

Natalija Arsenijevic and Dragica Selakovic contributed equally to this work.

Acknowledgments

This work was supported by the Faculty of Medical Sciences, University of Kragujevac, Serbia (JP 01/19), and Ministry of Education, Science and Technological Development of the Republic of Serbia 451-03-68/2020-14/200107 (Faculty of Engineering, University of Kragujevac), 451-03-68/2020-14/200378 (Institute for Information Technologies Kragujevac, University of Kragujevac), and 451-03-68/2020-14/200122 (Faculty of Science).

Supplementary Materials

Supplementary file 1: list of chemicals for oxidative stress determination. Supplementary file 2: list of primers used for RT-PCR analysis. *(Supplementary Materials)*

References

[1] M. Canillas, P. Pena, A. H. de Aza, and M. A. Rodríguez, "Calcium phosphates for biomedical applications," *Boletín de la Sociedad Española de Cerámica y Vidrio*, vol. 56, no. 3, pp. 91–112, 2017.

[2] Z. Tarle and M. Par, "Bioactive dental composite materials," *Medical Science*, vol. 45, pp. 83–100, 2018.

[3] I. Nedeljkovic, J. De Munck, A. Vanloy et al., "Secondary caries: prevalence, characteristics, and approach," *Clinical oral investigations*, vol. 24, no. 2, pp. 683–691, 2020.

[4] H. H. Xu, J. L. Moreau, L. Sun, and L. C. Chow, "Nanocomposite containing amorphous calcium phosphate nanoparticles for caries inhibition," *Dental Materials*, vol. 27, no. 8, pp. 762–769, 2011.

[5] A. A. Balhaddad, A. A. Kansara, D. Hidan, M. D. Weir, H. H. K. Xu, and M. A. S. Melo, "Toward dental caries: exploring nanoparticle-based platforms and calcium phosphate compounds for dental restorative materials," *Bioactive materials*, vol. 4, pp. 43–55, 2018.

[6] M. Yu, L. Wang, W. Zhang, and B. Ganss, "An evolutionarily conserved subdomain in amelotin promotes amorphous calcium phosphate-to-hydroxyapatite phase transition," *Crystal Growth & Design*, vol. 19, no. 4, pp. 2104–2113, 2019.

[7] S. V. Dorozhkin, "Amorphous calcium (ortho)phosphates," *Acta Biomaterialia*, vol. 6, no. 12, pp. 4457–4475, 2010.

[8] R. N. Jardim, A. A. Rocha, A. M. Rossi et al., "Fabrication and characterization of remineralizing dental composites

containing hydroxyapatite nanoparticles," *Journal of the Mechanical Behavior of Biomedical Materials*, vol. 109, article 103817, 2020.

[9] T. Ding, Y. Xue, H. Lu, Z. Huang, and J. Sun, "Effect of particle size of hydroxyapatite nanoparticles on its biocompatibility," *IEEE Transactions on Nanobioscience*, vol. 11, no. 4, pp. 336–340, 2012.

[10] L. P. Liu, Y. B. Xiao, Z. W. Xiao, Z. B. Wang, C. Li, and X. Gong, "Toxicity of hydroxyapatite nanoparticles on rabbits," *Journal of hygiene research*, vol. 34, pp. 474–476, 2005.

[11] Y. Jin, X. Liu, H. Liu et al., "Oxidative stress-induced apoptosis of osteoblastic MC3T3-E1 cells by hydroxyapatite nanoparticles through lysosomal and mitochondrial pathways," *RSC advances*, vol. 7, pp. 13010–13018, 2017.

[12] J. P. Ooi, S. R. Kasim, R. B. Shaari, and N. A. Saidin, "In vivo efficacy and toxicity of synthesized nano-β-tricalcium phosphate in a rabbit tibial defect model," *Toxicology Research and Application*, vol. 2, pp. 1–9, 2018.

[13] L. Liu, H. Dai, Y. Wu et al., "In vitro and in vivo mechanism of hepatocellular carcinoma inhibition by β-TCP nanoparticles," *International Journal of Nanomedicine*, vol. Volume 14, pp. 3491–3502, 2019.

[14] G. Li, J. Huang, Y. Li, R. Zhang, J. Zhang, and H. Aoki, "In vitro study on influence of a discrete nano-hydroxyapatite on leukemia P388 cell behavior," *Bio-medical Materials and Engineering*, vol. 17, no. 5, pp. 321–327, 2007.

[15] V. P. Menon and A. R. Sudheer, "Antioxidant and anti-inflammatory properties of curcumin," *The molecular targets and therapeutic uses of curcumin in health and disease*, vol. 595, pp. 105–125, 2007.

[16] L. Sinkovič, P. Jamnik, M. Korošec, R. Vidrih, and V. Meglič, "In-vitro and in-vivo antioxidant assays of chicory plants (Cichorium intybus L.) as influenced by organic and conventional fertilisers," *BMC plant biology*, vol. 20, pp. 1–10, 2020.

[17] I. F. Mosa, M. Youssef, M. Kamel, O. F. Mosa, and Y. Helmy, "Synergistic antioxidant capacity of CsNPs and CurNPs against cytotoxicity, genotoxicity and pro-inflammatory mediators induced by hydroxyapatite nanoparticles in male rats," *Toxicology Research*, vol. 8, no. 6, pp. 939–952, 2019.

[18] J. Katanić, S. Matić, E. M. Pferschy-Wenzig et al., "Filipendula ulmaria extracts attenuate cisplatin-induced liver and kidney oxidative stress in rats: in vivo investigation and LC-MS analysis," *Food and Chemical Toxicology*, vol. 99, pp. 86–102, 2017.

[19] L. Barros, L. Cabrita, M. V. Boas, A. M. Carvalho, and I. C. F. R. Ferreira, "Chemical, biochemical and electrochemical assays to evaluate phytochemicals and antioxidant activity of wild plants," *Food Chemistry*, vol. 127, no. 4, pp. 1600–1608, 2011.

[20] J. Katanić, T. Boroja, V. Mihailović et al., "In vitro and in vivo assessment of meadowsweet (Filipendula ulmaria) as anti-inflammatory agent," *Journal of Ethnopharmacology*, vol. 193, pp. 627–636, 2016.

[21] S. Matić, J. Katanić, S. Stanić et al., "In vitro and in vivo assessment of the genotoxicity and antigenotoxicity of the Filipendula hexapetala and Filipendula ulmaria methanol extracts," *Journal of Ethnopharmacology*, vol. 174, pp. 287–292, 2015.

[22] S. Samardžić, J. Arsenijević, D. Božić, M. Milenković, V. Tešević, and Z. Maksimović, "Antioxidant, anti-inflammatory and gastroprotective activity of Filipendula ulmaria (L.) Maxim. and Filipendula vulgaris Moench," *Ethnopharmacology*, vol. 213, pp. 132–137, 2018.

[23] M. Pukalskienė, R. Venskutonis, and A. Pukalskas, "Phytochemical characterization of Filipendula ulmaria by UPLC/Q-TOF-MS and evaluation of antioxidant activity," *Records of natural products*, vol. 9, pp. 451–455, 2015.

[24] J. Katanić, T. Boroja, N. Stanković et al., "Bioactivity, stability and phenolic characterization of Filipendula ulmaria (L.) Maxim," *Food & Function*, vol. 6, no. 4, pp. 1164–1175, 2015.

[25] S. A. Kollenda, J. Klose, T. Knuschke et al., "In vivo biodistribution of calcium phosphate nanoparticles after intravascular, intramuscular, intratumoral, and soft tissue administration in mice investigated by small animal PET/CT," *Acta Biomaterialia*, vol. 109, pp. 244–253, 2020.

[26] O. A. Abbas, I. G. Ibrahim, and A. E. Ismail, "Therapeutic effects of Nano-HAp in a rat model of $AlCl_3$ induced neurotoxicity," *Iranian Journal of Pharmaceutical Research: IJPR*, vol. 18, no. 3, pp. 1309–1322, 2019.

[27] L. Wang, G. Zhou, H. Liu et al., "Nano-hydroxyapatite particles induce apoptosis on MC3T3-E1 cells and tissue cells in SD rats," *Nanoscale*, vol. 4, no. 9, pp. 2894–2899, 2012.

[28] K. Zhang, L. Cheng, M. D. Weir, Y. X. Bai, and H. H. Xu, "Effects of quaternary ammonium chain length on the antibacterial and remineralizing effects of a calcium phosphate nanocomposite," *International journal of oral science*, vol. 8, no. 1, pp. 45–53, 2016.

[29] J. Joksimovic, D. Selakovic, M. Matovic, I. Zaletel, N. Puskas, and G. Rosic, "The role of neuropeptide-Y in nandrolone decanoate-induced attenuation of antidepressant effect of exercise," *PLoS One*, vol. 12, no. 6, article e0178922, 2017.

[30] R. A. Bevins and J. Besheer, "Object recognition in rats and mice: a one-trial non-matching-to-sample learning task to study 'recognition memory'," *Nature Protocols*, vol. 1, no. 3, pp. 1306–1311, 2006.

[31] D. G. Mumby, S. Gaskin, M. J. Glenn, T. E. Schramek, and H. Lehmann, "Hippocampal damage and exploratory preferences in rats: memory for objects, places, and contexts," *Learning & Memory*, vol. 9, no. 2, pp. 49–57, 2002.

[32] I. Kumburovic, D. Selakovic, T. Juric et al., "Antioxidant effects of Satureja hortensis L. attenuate the anxiogenic effect of cisplatin in rats," *Oxidative Medicine and Cellular Longevity*, vol. 2019, Article ID 8307196, 15 pages, 2019.

[33] R. Vukovic, I. Kumburovic, J. Joksimovic Jovic et al., "N-Acetylcysteine protects against the anxiogenic response to cisplatin in rats," *Biomolecules*, vol. 9, no. 12, p. 892, 2019.

[34] O. H. Lowry, N. J. Rosebrough, A. L. Farr, and R. J. Randall, "Protein measurement with the Folin phenol reagent," *The Journal of Biological Chemistry*, vol. 193, no. 1, pp. 265–275, 1951.

[35] H. P. Misra and I. Fridovich, "The role of superoxide anion in the autoxidation of epinephrine and a simple assay for superoxide dismutase," *The Journal of Biological Chemistry*, vol. 247, no. 10, pp. 3170–3175, 1972.

[36] R. F. Beers and I. W. Sizer, "A spectrophotometric method for measuring the breakdown of hydrogen peroxide by catalase," *The Journal of Biological Chemistry*, vol. 195, no. 1, pp. 133–140, 1952.

[37] G. L. Ellman, "Tissue sulfhydryl groups," *Archives of Biochemistry and Biophysics*, vol. 82, no. 1, pp. 70–77, 1959.

[38] H. Ohkawa, N. Ohishi, and K. Yagi, "Assay for lipid peroxides in animal tissues by thiobarbituric acid reaction," *Analytical Biochemistry*, vol. 95, no. 2, pp. 351–358, 1979.

[39] K. J. Livak and T. D. Schmittgen, "Analysis of relative gene expression data using real-time quantitative PCR and the 2(-delta delta C(T)) method," *Methods*, vol. 25, no. 4, pp. 402–408, 2001.

[40] J. Xu, P. Xu, Z. Li, J. Huang, and Z. Yang, "Oxidative stress and apoptosis induced by hydroxyapatite nanoparticles in C6 cells," *Journal of Biomedical Materials Research Part A*, vol. 100, no. 3, pp. 738–745, 2012.

[41] A. Rahdar, M. R. Hajinezhad, M. Bilal, F. Askari, and G. Z. Kyzas, "Behavioral effects of zinc oxide nanoparticles on the brain of rats," *Inorganic Chemistry Communications*, vol. 119, p. 108131, 2020.

[42] S. Ouni, D. Askri, M. Jeljeli, H. Abdelmalek, M. Sakly, and S. Amara, "Toxicity and effects of copper oxide nanoparticles on cognitive performances in rats," *Archives of Environmental & Occupational Health*, vol. 75, no. 7, pp. 384–394, 2020.

[43] M. M. Ahmed and M. M. A. Hussein, "Neurotoxic effects of silver nanoparticles and the protective role of rutin," *Biomedicine & Pharmacotherapy*, vol. 90, pp. 731–739, 2017.

[44] I. Grissa, J. ElGhoul, R. Mrimi, L. E. Mir, H. B. Cheikh, and P. Horcajada, "In deep evaluation of the neurotoxicity of orally administered TiO_2 nanoparticles," *Brain Research Bulletin*, vol. 155, pp. 119–128, 2020.

[45] S. Ansar, M. Abudawood, S. S. Hamed, and M. M. Aleem, "Exposure to zinc oxide nanoparticles induces neurotoxicity and proinflammatory response: amelioration by hesperidin," *Biological Trace Element Research*, vol. 175, no. 2, pp. 360–366, 2017.

[46] K. Niska, M. J. Santos-Martinez, M. W. Radomski, and I. Inkielewicz-Stepniak, "CuO nanoparticles induce apoptosis by impairing the antioxidant defense and detoxification systems in the mouse hippocampal HT22 cell line: protective effect of crocetin," *Toxicology In Vitro*, vol. 29, no. 4, pp. 663–671, 2015.

[47] K. Poh Loh, S. Hong Huang, R. De Silva, B. K. H. Tan, and Y. Zhun Zhu, "Oxidative stress: apoptosis in neuronal injury," *Current Alzheimer Research*, vol. 3, no. 4, pp. 327–337, 2006.

[48] Z. Xu, C. Liu, J. Wei, and J. Sun, "Effects of four types of hydroxyapatite nanoparticles with different nanocrystal morphologies and sizes on apoptosis in rat osteoblasts," *Journal of Applied Toxicology*, vol. 32, no. 6, pp. 429–435, 2012.

[49] J. Sun and T. Ding, "p53 reaction to apoptosis induced by hydroxyapatite nanoparticles in rat macrophages," *Journal of Biomedical Materials Research Part A*, vol. 88, no. 3, pp. 673–679, 2009.

[50] T. El-Masry, N. Altwaijry, B. Alotaibi, E. Tousson, A. Saleh, and A. Alboghdadly, "Chicory (Cichorium intybus L.) extract ameliorates hydroxyapatite nanoparticles induced kidney damage in rats," *Nano*, vol. 33, pp. 1251–1260, 2020.

[51] J. H. Park, S. Gurunathan, Y. J. Choi, J. W. Han, H. Song, and J. H. Kim, "Silver nanoparticles suppresses brain-derived neurotrophic factor-induced cell survival in the human neuroblastoma cell line SH-SY5Y," *Journal of Industrial and Engineering Chemistry*, vol. 47, pp. 62–73, 2017.

[52] Y. Cui, X. Chen, Z. Zhou et al., "Prenatal exposure to nanoparticulate titanium dioxide enhances depressive-like behaviors in adult rats," *Chemosphere*, vol. 96, pp. 99–104, 2014.

[53] M. Tarlan, J. Sajedianfard, and M. Fathi, "Effect of titanium dioxide nanoparticles administered during pregnancy on depression-like behavior in forced swimming and tail suspension tests in offspring mice," *Toxicology and Industrial Health*, vol. 36, no. 4, pp. 297–304, 2020.

[54] F. Hong, Y. Zhou, J. Ji, J. Zhuang, L. Sheng, and L. Wang, "Nano-TiO_2 inhibits development of the central nervous system and its mechanism in offspring mice," *Journal of Agricultural and Food Chemistry*, vol. 66, no. 44, pp. 11767–11774, 2018.

[55] S. Alimohammadi, M. S. Hosseini, and L. Behbood, "Prenatal exposure to zinc oxide nanoparticles can induce depressive-like behaviors in mice offspring," *International Journal of Peptide Research and Therapeutics*, vol. 25, no. 1, pp. 401–409, 2019.

[56] L. An, S. Liu, Z. Yang, and T. Zhang, "Cognitive impairment in rats induced by nano-CuO and its possible mechanisms," *Toxicology Letters*, vol. 213, no. 2, pp. 220–227, 2012.

[57] H. Liu, H. Yazici, C. Ergun, T. J. Webster, and H. Bermek, "An in vitro evaluation of the Ca/P ratio for the cytocompatibility of nano-to-micron particulate calcium phosphates, for bone regeneration," *Acta Biomaterialia*, vol. 4, no. 5, pp. 1472–1479, 2008.

[58] X. Liu, M. Zhao, J. Lu, J. Ma, J. Wei, and S. Wei, "Cell responses to two kinds of nanohydroxyapatite with different sizes and crystallinities," *International Journal of Nanomedicine*, vol. 7, pp. 1239–1250, 2012.

Hindawi
Oxidative Medicine and Cellular Longevity
Volume 2021, Article ID 6672525, 15 pages
https://doi.org/10.1155/2021/6672525

Research Article

Different Doses of β-Cryptoxanthin May Secure the Retina from Photooxidative Injury Resulted from Common LED Sources

Cemal Orhan,[1] Mehmet Tuzcu,[2] Hasan Gencoglu,[2] Emre Sahin,[1] Nurhan Sahin,[1] Ibrahim Hanifi Ozercan,[3] Tejas Namjoshi,[4] Vandita Srivastava,[4] Abhijeet Morde,[5] Deshanie Rai,[6] Muralidhara Padigaru,[5] and Kazim Sahin[1]

[1]*Department of Animal Nutrition, Faculty of Veterinary Science, Firat University, Elazig 23119, Turkey*
[2]*Division of Biology, Faculty of Science, Firat University, Elazig 23119, Turkey*
[3]*Department of Pathology, Faculty of Medicine, Firat University, Elazig 23119, Turkey*
[4]*OmniActive Health Technologies, Biotechnology Park, Pune 411057, India*
[5]*OmniActive Health Technologies, Wagle Estate, Thane 400604, India*
[6]*OmniActive Health Technologies Inc, Morristown, NJ 07960, USA*

Correspondence should be addressed to Kazim Sahin; nsahinkm@yahoo.com

Received 9 October 2020; Revised 27 January 2021; Accepted 1 February 2021; Published 10 February 2021

Academic Editor: Daoud Ali

Retinal damage associated with loss of photoreceptors is a hallmark of eye diseases such as age-related macular degeneration (AMD) and diabetic retinopathy. Potent nutritional antioxidants were previously shown to abate the degenerative process in AMD. β-Cryptoxanthin (BCX) is an essential dietary carotenoid with antioxidant, anti-inflammatory, and provitamin A activity. It is a potential candidate for developing intervention strategies to delay the development/progression of AMD. In the current study, the effect of a novel, highly purified BCX oral formulation on the rat retinal damage model was evaluated. Rats were fed with BCX for four weeks at the doses of 2 and 4 mg/kg body weight in the form of highly bioavailable oil suspension, followed by retinal damage by exposing to the bright light-emitting diode (LED) light (750 lux) for 48 hrs. Animals were sacrificed after 48 hours, and eyes and blood samples were collected and analyzed. BCX supplementations (2 and 4 mg/kg) showed improvements in the visual condition as demonstrated by histopathology of the retina and measured parameters such as total retinal thickness and outer nuclear layer thickness. BCX supplementation helped reduce the burden of oxidative stress as seen by decreased serum and retinal tissue levels of malondialdehyde (MDA) and restored the antioxidant enzyme activities in BCX groups. Further, BCX supplementation modulated inflammatory markers (IL-1β, IL-6, and NF-κB), apoptotic proteins (Bax, Bcl-2, caspase 3), growth proteins and factors (GAP43, VEGF), glial and neuronal proteins (GFAP, NCAM), and heme oxygenase-1 (HO-1), along with the mitochondrial stress markers (ATF4, ATF6, Grp78, Grp94) in the rat retinal tissue. This study indicates that oral supplementation of BCX exerts a protective effect on light-induced retinal damage in the rats via reducing oxidative stress and inflammation, also protected against mitochondrial DNA damage and cellular death.

1. Introduction

Light-induced degeneration of photoreceptor cells and the disease's progression in the age-related macular degeneration (AMD) comprise the oxidative damage and, eventually, visual cell loss, which can be inhibited or decelerated by the contribution of antioxidants [1, 2]. Accumulation of drusen and β-amyloid peptides in the subretinal space resulting in inflammation and photoreceptor degeneration is observed in early AMD [3]. Further, oxidative stress, inflammation, cell damage leading to cell death, and mitochondrial DNA damage are cellular processes associated with AMD [4]. However, the crucial photobiological role of ultraviolet lights (UVB and UVA) induced apoptosis and cytotoxic damage in DNA prevention was documented in earlier reports [5, 6]. The retina is one of the tissues that consume the most oxygen in the human body [7]. Oxidative stress and inflammation governed by the activation of nuclear factor kappa B (NF-

κB) have been suggested to mediate crucial parts in retinopathy's pathogenesis [8]. Even though light-emitting diode (LED) usage has advantages like low energy expenditure and longer lifetime, concerns have been raised due to the harmful blue region of the light spectrum from white LEDs, which can cause eventual retinal damage and toxicity because of their intense emission [9].

It has been shown that some carotenoids, such as lutein and zeaxanthin that are located in the macula and retina, have useful properties against oxidative stress and are also protect against photooxidative damage [10–13]. To protect the retinal pigment epithelium against the photooxidative damage, carotenoids are proposed to act through two primary mechanisms: firstly, carotenoids help to filter harmful blue light and, secondly, remove the triple-state molecules, singlet molecular oxygen, and reactive oxygen species such as lipid peroxides and superoxide radical anions [13, 14].

Humans and animals cannot synthesize carotenoids, and they have to get them from dietary origins like fruits and vegetables [15]. Many findings from the various studies have shown that β-cryptoxanthin (BCX) has reasonably high bioavailability from its mutual nutritive origins, to the extent that some foods rich in BCX might be equal to or better than β-carotene-rich foods as retinol sources [16]. BCX is a provitamin A polar carotenoid (xanthophyll), and its selective uptake and deposition as a macular xanthophyll in the retina and brain are enhanced by specific xanthophyll-binding proteins [17]. Carotenoid oxygenases are suggested to be used by mammals for the retinoid synthesis from provitamin A carotenoids [18]. BCX is thought to be cleaved in the metabolism via the provitamin A-converting enzymes, involving both cytosolic β-carotene oxygenase 1 (BCO1) and mitochondrial BCO2, through a multistep process [18, 19].

Comprehending the molecular mechanisms of retinal light injury in the animal models can yield vital information concerning the effects of light in clinical diseases and can be the basis for future treatments to inhibit or delay visual cell loss [20, 21], impaired vision performance, and eye diseases such as AMD. Given that BCX is an efficient provitamin A carotenoid with potent antioxidant effects [16, 22] and in light of the role of vitamin A in eye health and vision performance, including dark adaptation. Hence, it was our main interest to understand if and how BCX can play a role in limiting the mechanistic pathways mediating light-induced retinal injury and photooxidative stress. Therefore, our study measured the effectiveness of BCX using the damaged retinal model on a variety of oxidant and antioxidant biochemical and inflammatory markers. These included interleukin-1β (IL-1β), interleukin-6 (IL-6), NF-κB; apoptotic proteins; B-cell lymphoma 2 (Bcl-2), Bcl-2-associated X protein (Bax), cysteine-aspartic acid protease-3 (caspase-3); notable proteins and molecules like growth-associated protein 43 (GAP43), glial fibrillary acidic protein (GFAP), neural cell adhesion molecule (NCAM), heme oxygenase-1 (HO-1), vascular endothelial growth factor (VEGF) and the endoplasmic reticulum/mitochondrial stress markers such as activating transcription factor 4 and 6 (ATF4, ATF6), and glucose-regulated proteins 78 and 94 (Grp78, Grp94). Furthermore, we have also evaluated the effects of BCX on the retinal layer pathology, BCX, and retinol changes in the serum and retina of the rats exposed to intense LED illuminance.

2. Materials and Methods

2.1. Animals and Diets. Twenty-eight Wistar Albino male rats, age: 8 weeks, weight: 180 ± 20 g, were housed in a controlled environment with a 12 : 12-h light-dark cycle at 22°C and were provided with standard rat chow (Table 1) and tap water *ad libitum*. All the experiments were conducted under the National Institutes of Health's Guidelines for the Care and Use of Laboratory Animals and approved by the Firat University Ethics Committee, Elazig (2019-94-143). After providing compliance with the laboratory conditions, rats were randomly divided into four treatment groups, each containing seven animals.

Animals were orally administered with BCX for four weeks followed by 48 hrs (12 hours light/12 hours dark periods) to induce retinal degeneration (RD) with LED light illumination (750 lux), and animals were continued on BCX supplementation during these two days of light exposure. Before intense light exposure, pupils of the animals were dilated with 1% tropicamide, and after exposure, animals were kept in the dark until evaluation. BCX (BCXcel™) was supplied by OmniActive Health Technologies Pvt. Ltd., Mumbai, India (B.No:141025). BCX concentrate was derived from Paprika oleoresin by solvent extraction and column chromatography. BCX concentrate, which contained about 10–80% by weight total xanthophyll, of which about 75–98% by weight was trans-beta-cryptoxanthin, the remaining including zeaxanthin, trans-capsanthin, beta-carotene, and trace amounts of other carotenoids, derived from oleoresin. The active ingredient (β-cryptoxanthin) was analyzed by UV spectrophotometer (Shimadzu UV-1800) and Agilent 1200 HPLC System (Agilent Technologies, Santa Clara, CA, USA). For sample preparation, 100 mg sample was weighed, 30 mL of tetrahydrofuran was added in 100-mL amber-colored volumetric flask and sonicated till sample is dissolved with intermediate shaking. After cooling, a volume of up to 100 mL was made with ethyl acetate (sample stock solution A). Next, the extract was pipetted with 5.0 mL of sample stock solution A into a 25-mL volumetric flask, diluted with the mobile phase, and filtered through a 0.45-micron filter. The sample was then run with an HPLC system using YMC- Carotenoid S5 micron (250 mm x 4.6 mm) column and mobile phase methanol: chloroform 900 : 100 at a flow rate of 1.5 mL/min. Chromatograms were examined at 451 nm, and the injection volume was 20 μl. Mixed tocopherol (0.3%) was added to the oil suspension as an antioxidant.

2.2. Experimental Design. The experimental design of the groups is summarized in Table 2. The rats were divided into four groups: (i) standard control: these animals only received standard rat chow and tap water ad until the end of the study; (ii) retinal degeneration (RD): fed as the control group, but remained under intense LED lighting for 48 hours after four weeks of the study; (iii) β-cryptoxanthin 1 (BCX1): fed as the control group and given BCX intragastrically by oral gavage

Table 1: Ingredients and chemical analysis of the standard diet.

Ingredients	Quantity (%)
Maize	30.22
Barley	10.07
Soybean meal	38.28
Sunflower seed meal	6.04
Wheat bran	10.08
Molasses	3.02
Limestone	1.51
Salt	0.08
DL-Methionine	0.30
Dicalcium phosphate	0.20
Vitamin-mineral premix *	0.20
Chemical analysis	
Crude protein %	24.00
Metabolizable energy (kcal/kg**)	3100
Ether extract %	3.40
Crude cellulose %	6.90
Ash %	8.10
Calcium %	1.30
Phosphorus %	0.90

*In per kilogram of vitamin-mineral mixture: 1.8 mg all-trans retinyl acetate (vitamin A), 0.025 mg cholecalciferol (vitamin D), 12.5 mg whole rac-alpha-tocopherol acetate (vitamin E), 1.1 mg menadione sodium bisulfite (vitamin K3), 1.1 mg thiamine (vitamin B1), 4.4 mg riboflavin (vitamin B2), 35 mg niacin (vitamin B3), 10 mg calcium pantothenate (vitamin B5), 2.2 mg vitamin B6, 0.02 vitamin B12, 0.55 mg folic acid, 0.1 mg d-biotin, 40 mg Mn (MnO), 12.5 mg Fe (FeSO4), 25 mg Zn (ZnO), 3.5 mg Cu (CuSO4), 0.3 mg I (KI), 0.15 mg Se (Na2SeO3), 175 mg choline chlorite (C5H14ClNO). **Metabolic energy was calculated according to the National Research Council [71].

(2 mg/kg BW/day) then remained under intense LED lighting for 48 hours after the four weeks of the study; (iv) β-cryptoxanthin 2 (BCX2): fed as the control group and given BCX intragastrically by oral gavage (4 mg/kg BW/day) then remained under intense LED lighting for 48 hours after the four weeks of the study. The doses of BCX were chosen from a previous study (Sahin et al. 2017). BCX application was also continued during the 48 hours with intensive lighting. Oral gavage is commonly used to deliver substances to animals in pharmacological and toxicological studies [23]. To ensure standardized dosage and to prevent inadvertent oxidation, delivery of the treatment (BCX or corn oil) was administered by oral gavage. Oral gavage was carried out by using a curved metal needle with a bulbed tip. All gavage procedures were carried out once per day at a similar time of day without administering any anesthesia (between 8.30 a.m. and 10 : 30 a.m.) for 6 d per week over four consecutive weeks. BCX was dissolved in corn oil. The control group received corn oil in a similar condition to the treatment of other experimental groups.

For an intense light exposure experiment, each rat was kept in an isolated cage. White light-emitting diodes were placed on the top of the shelves and were measured at a distance of 20 cm from the remote source to achieve 750 lux standard indoor lighting levels for all groups [24]. To allow retinal degeneration to occur, animals were placed in an environmentally organized light stress box equipped with 750 lux of diffuse white LEDs fixed on the inner upper surface, which lightened the inner walls. Animals were sacrificed by cervical dislocation under xylazine (10 mg/kg, i.m.) and ketamine (50 mg/kg, i.m.) anesthesia immediately following the light and dark exposures; eyes were removed and blood tissue collected.

2.3. Biochemical Analysis. Immediately after collecting the target samples, blood tissue was centrifuged at 5000 rpm for obtaining the serum. Serum biochemical parameters (glucose, BUN, and ALT and AST) were examined with a biochemistry analyzer (Samsung Co., Suwon, Korea). Tissues were rinsed with 0.5 mL of a phosphate buffer saline solution (pH 7.4). Tissues were then homogenized in 5-10 mL of cold buffer [20 mM HEPES buffer, pH 7.2 containing 1 mM EGTA, 210 mM mannitol and 70 mM sucrose for superoxide dismutase (SOD), 50 nM potassium phosphate, pH 7.0, containing 1 mM EDTA for catalase (CAT), and 50 mM Tris-HCI, pH 7.5, 5 mM EDTA, and 1 mM DTT for glutathione peroxidase (GSH-Px)] per gram tissue for each enzyme assay. Homogenates were centrifuged at 10,000 × g at 4°C for 15 min for CAT and GSHPx and centrifuged at 1,500 × g for 5 min at 4°C for SOD. Supernatants were then removed and assayed for enzyme activities using the commercial kits (Cayman Chemical, Ann Arbor, MI, USA) depending on the colorimetric methods, which were then measured with a highly sensitive Enzyme-Linked Immunosorbent Assay (ELISA) spectrophotometry reader (ELx800 ™ Absorbance Microplate Reader (BioTek Instruments Winooski VT) according to the manufacturer's procedure (Cayman Chemical, Ann Arbor, MI, USA). The protein concentrations were indicated by the Bradford method using Bradford reagent (Sigma Aldrich, Bradford reagent-B6916-1KT, USA). The intra- and interassay coefficients of variation (CV) for SOD, CAT, and GSH-Px were 3.2% and 3.7%, 3.8% and 9.9%, and 5.7% and 7.2%, respectively.

For MDA analyses, samples were homogenized in a mixture of 0.5 mL of $HClO_4$ (0.5 M), 2.5 mL distilled water, and 2[6]-di-tert-butyl-p-cresol (BHT) for precipitating proteins and releasing the MDA bound to the amino groups of proteins and other amino compounds. The samples were then centrifuged at 4500 rpm for 5 min, and supernatants were injected into the HPLC system. For this purpose, an HPLC apparatus of Shimadzu UV–vis SPD-10 AVP detector, a CTO-10 AS VP column, and 30 mM KH_2PO_4 and methanol (82.5: 17.5, v/v, pH 3.6) at a flow rate of 1 mL/min were used (Shimadzu, Kyoto Japan). Chromatograms were monitored at 250 nm, and the injection volume was 20 μl [25, 26].

Serum and retinal tissue BCX and retinol levels were also analyzed by using HPLC. Samples were homogenized in 1 mL of cold acetone. Homogenized samples were transferred into polyethylene tubes, and 2 mL ethanol was added to the tubes. After 0.3 mL n-hexane was filled into tubes for extractions, they were centrifuged. This step was repeated three times. N-hexane in tubes was evaporated, and the residues were solved in the mobile phase (methanol : acetonitrile : -chloroform; 47 : 42 : 11, *v*/*v*) [25].

Table 2: Experimental design of the study.

Groups	Standard control $n = 7$	RD control $n = 7$	RD+BCX1 Dose level 1 $n = 7$	RD+BCX2 Dose level 2 $n = 7$
Dose	—	—	2 mg/kg BW of active β-cryptoxanthin	4 mg/kg BW of active β-cryptoxanthin
LED illumination	—	Intense LED light (750 lux) Exposure for 48 hours after four weeks	Intense LED light (750 lux) Exposure for 48 hours after four weeks	Intense LED light (750 lux) Exposure for 48 hours after four weeks

BCX: β-cryptoxanthin; BW: Body Weight; LED: Light Emitting Diode; RD: Retinal Degeneration.

2.4. Histopathological Analysis. After the eye removal of each rat, the retinas were examined grossly. The tissue was then removed for histological study, washed with plain ordinary saline, immersion-fixed (4% paraformaldehyde and then paraffin), and sectioned into 5-μm thick slices using a microtome. Retinal tissues were stained with hematoxylin and eosin (H&E) and examined using light microscopy. The retinal histology was performed for all the groups with slight modifications as defined earlier [27]. The tissue's midsuperior aspect was examined for all histological analyses through a light microscope at 100x (Olympus, BX51, Japan). Retinal edema damage caused by an intense LED light is graded as follows: (+) mild, (++) moderate, and (+++) rated as severe edema.

2.5. Western Blot Analysis. Target proteins were detected via western blotting with slight modifications as previously described in detail [28, 29]. The retinal interleukin-1β (IL-1β), interleukin-6 (IL-6), NF-κB; apoptotic proteins; B-cell lymphoma 2 (Bcl-2), Bcl-2-associated X protein (Bax), cysteine-aspartic acid protease-3 (caspase-3); notable proteins and molecules like growth-associated protein 43 (GAP43), glial fibrillary acidic protein (GFAP), neural cell adhesion molecule (NCAM), heme oxygenase-1 (HO-1), vascular endothelial growth factor (VEGF) and the endoplasmic reticulum/mitochondrial stress markers such as activating transcription factor 4 and 6 (ATF4, ATF6), and glucose-regulated proteins 78 and 94 (Grp78, Grp94), and actin (as a reference protein to control protein loading) were targeted. Briefly, after the homogenization, each group of animals was examined in triplicates for each experimental situation. 20-50 μg of total proteins was transferred to a nitrocellulose membrane (Schleicher and Schuell Inc., Keene, NH, USA) via immunoblotting after the electrophoresis using Bio-Rad Mini-Protean Tetra electrophoresis "wet-transfer" system (Bio-Rad, California, USA). The phosphorylated form of antibodies against IL-1β, IL-6, NF-κB, VEGF, Bax, Bcl2, Caspase-3, GAP43, GFAP, NCAM, HO-1, ATF4, ATF6, Grp78, and Grp94 (Abcam, Cambridge, UK) was diluted in a concentration of (1 : 1000-1 : 2000) in a PBS buffer which contains 0.05% of tween20. The loading of proteins was checked by a monoclonal mouse antibody against β-actin (A5316; Sigma). Blots were performed at least three times to confirm the reproducibility of the results. Bands were analyzed densitometrically using an image analysis system (Image J; National Institute of Health, Bethesda, USA).

2.6. Statistical Analysis. The sample size of the study was determined as 28 rats for all groups (7 animals per group) with the help of the G $*$ Power package program (Version 3.1.9.2) with alpha error 0.05 and 85% power with an effect size of 0.69 [30]. Conformity to the normality assumption from the prerequisites of the parametric tests was performed using the "Shapiro-Wilk" test. The homogeneity of the variances was checked with the "Levene" test. Analysis of variance (ANOVA) test was performed to determine the differences between the groups, and *post hoc* Tukey test was used for multiple comparisons of the groups. All analyzes performed using the SPSS statistical program (IBM, SPPS Version 21). p values < 0.05 were considered significant. Data is presented as mean and standard deviation.

3. Results

The effects of BCX1 and BCX2 supplementation on the serum biochemical parameters are presented in Table 3. BCXcel™ supplementation did not change the serum levels of glucose ($p = 0.890$), creatinine ($p = 0.953$), blood urea nitrogen (BUN) ($p = 0.654$), total protein (TP) ($p = 0.661$), albumin (ALB) ($p = 0.725$), globulin (GLOB) ($p = 0.955$), and activities of alanine aminotransferase (ALT) ($p = 0.698$), aspartate aminotransferase (AST) ($p = 0.866$), alkaline phosphatase (ALP) ($p = 0.892$), and total bilirubin (TBIL) level ($p = 0.101$), in all the groups of rats ($p > 0.05$). Changes in serum and retina activities of SOD, GSH-Px, CAT, and MDA, BCX, and retinol levels during intense LED light-induced retinal degeneration between the groups are presented in Table 4. Accordingly, serum and retina MDA levels were the highest in the RD group, while BCX1 and BCX2 administration significantly decreased serum and retinal tissue MDA levels ($p < 0.0001$). Retina SOD, GSHPx, and CAT activities were measured at the highest levels in the control group, while the lowest values were determined in the RD group ($p < 0.05$). However, BCX administration significantly increased antioxidant enzymes' retinal activities, especially the BCX2 dose, which was more effective ($p < 0.001$). Serum and retina BCX levels were not detected in the control and RD groups, while in the BCX2 group, serum levels were 2.3 times, and retinal levels were 2.8 times higher than the BCX1 group ($p < 0.05$). Serum and retina retinol levels were found in the lowest number in the RD groups, whereas BCX2, BCX1, and control groups were found in higher amounts, respectively ($p < 0.05$).

Table 3: Effects of BCX supplementation on serum biochemical parameters in rats exposed to LED light.

Items	Groups				p^*
	Control	RD	RD+BCX1	RD+BCX2	
Glucose, mg/dL	119.71 ± 8.12	120.43 ± 8.08	117.71 ± 13.62	122.06 ± 10.92	0.890
Creatinine, mg/dL	0.41 ± 0.11	0.42 ± 0.12	0.39 ± 0.09	0.41 ± 0.14	0.953
BUN, mg/dL	21.96 ± 1.89	22.91 ± 1.38	23.04 ± 2.66	22.34 ± 0.75	0.654
TP, g/dL	7.47 ± 0.77	7.01 ± 0.51	7.30 ± 1.00	7.41 ± 0.55	0.661
ALB, g/dL	3.57 ± 0.34	3.39 ± 0.46	3.49 ± 0.30	3.57 ± 0.28	0.725
GLOB, g/dL	3.76 ± 0.46	3.83 ± 0.47	3.71 ± 0.68	3.69 ± 0.32	0.955
ALT, U/L	71.14 ± 5.64	68.71 ± 4.61	67.86 ± 5.64	72.43 ± 13.25	0.698
AST, U/L	91.29 ± 7.06	96.43 ± 16.30	92.29 ± 9.89	95.71 ± 17.95	0.866
ALP, U/L	132.57 ± 9.50	130.29 ± 14.50	135.57 ± 21.03	137 ± 22.35	0.892
TBIL, mg/dL	0.21 ± 0.02	0.22 ± 0.02	0.23 ± 0.02	0.24 ± 0.03	0.101

BCX: β-cryptoxanthin; BUN: blood urea nitrogen; TP: total protein; ALB: albumin; GLOB: globulin; ALT: alanine aminotransferase; AST: aspartate aminotransferase; ALP: alkaline phosphatase; TBIL: total bilirubin; RD: retinal degeneration. Data are presented as means and standard deviations. Means in the same line without a common superscript differ significantly ($p < .05$; *ANOVA and Tukey's *post hoc* test).

Table 4: Effects of BCX supplementation on MDA, BCX, retinol levels, and antioxidant enzyme activities in rats exposed to LED light.

Markers	Groups			
	Control	RD	RD+BCX1	RD+BCX2
Serum MDA, nmol/mL	0.45 ± 0.08^{c}	1.19 ± 0.17^{a}	0.79 ± 0.12^{b}	0.64 ± 0.07^{b}
Retina MDA, nmol/mg	0.8 ± 0.11^{d}	1.81 ± 0.12^{a}	1.51 ± 0.08^{b}	1.12 ± 0.15^{c}
Retina SOD, U/mg protein	85.34 ± 6.57^{a}	56.71 ± 7.11^{c}	65.9 ± 4.77^{bc}	75.13 ± 6.74^{b}
Retina GSH-Px, U/mg protein	29.48 ± 1.83^{a}	14.29 ± 1.78^{d}	19.16 ± 1.62^{c}	23.74 ± 2.23^{b}
Retina CAT, U/mg protein	33.96 ± 3.9^{a}	13.88 ± 1.5^{c}	20.84 ± 3.15^{b}	25.2 ± 3.39^{b}
Serum BCX, nmol/L	—	—	6.86 ± 1.35^{b}	15.83 ± 1.83^{a}
Retina BCX, nmol/g	—	—	0.2 ± 0.08^{b}	0.56 ± 0.11^{a}
Serum retinol, ng/mL	275.49 ± 27.91^{ab}	240.43 ± 20.61^{b}	282.87 ± 19.57^{a}	288.3 ± 27.9^{a}
Retina retinol, μg/g	5.69 ± 0.97	4.75 ± 0.81	5.87 ± 1.07	5.92 ± 1.34

The data are presented as means ± standard deviations. Mean values in the same row without a common superscript (a–d) differ significantly ($p < .05$). BCX: β-cryptoxanthin; MDA: malondialdehyde; RD: retinal degeneration; SOD: superoxide dismutase; GSH-Px: glutathione peroxidase; CAT: catalase.

A representative image showing the histopathological effect of both doses of BCXcel™ supplementation on intense LED light-induced retinal degeneration is presented in Figure 1. The retina had a normal histological appearance in the control group. In the RD group, severe edema (+++) was observed in the ganglion layer of the retina, and significant thickening was observed in the outer plexiform layer of the retina. In the RD+BCX1 group, edema decreased in the ganglion layer (++), and there was a slight decrease in the thickening of the outer plexiform layer of the retina. In the RD+BCX2 group, very mild edema (+) near the normal was observed in the ganglion layer, and a marked decrease in the thickening of the outer plexiform layer of the retina was observed. Figure 2 demonstrates that four weeks of BCXcel™ supplementation significantly preserved the quantifications of both retinal thickness and the ONL thickness of the intense LED light-exposed rats, compared with the control and RD groups ($p < .05$).

The effects of both doses of BCXcel™ supplementation on the levels of inflammatory genes, IL-1β, IL-6, and NF-κB along with VEGF, are shown in Figure 3. RD group showed significantly more IL-1β, IL-6, NF-κB levels in all groups compared to other groups ($p < 0.001$); however, BCXcel™ supplementation significantly decreased these levels while bringing them closer to control levels, especially in the group administered with BCX ($p < 0.001$). Also, retina VEGF levels were found higher in control, while the RD and BCX1/BCX2 groups decreased significantly ($p < 0.0001$). Figure 4 shows the effects of two doses of BCXcel™ on Bax, Bcl-2, Caspase-3, Gap43, GFAP, NCAM, and HO-1 retinal protein levels in rats. Proapoptotic proteins Bax and Caspase-3 retina levels were upregulated depending on the amount of BCXcel™ supplement ($p < 0.001$), whereas the antiapoptotic Bcl-2 levels were found to be downregulated ($p < 0.0001$). While GAP43 levels decreased significantly in all groups compared to the control group ($p < 0.01$), it was significantly lower in the BCX2 group compared to the RD group ($p < 0.05$). GFAP levels showed the most significant increase in the RD group compared to all groups ($p < 0.001$), while BCX application decreased these levels significantly ($p < 0.001$), and there

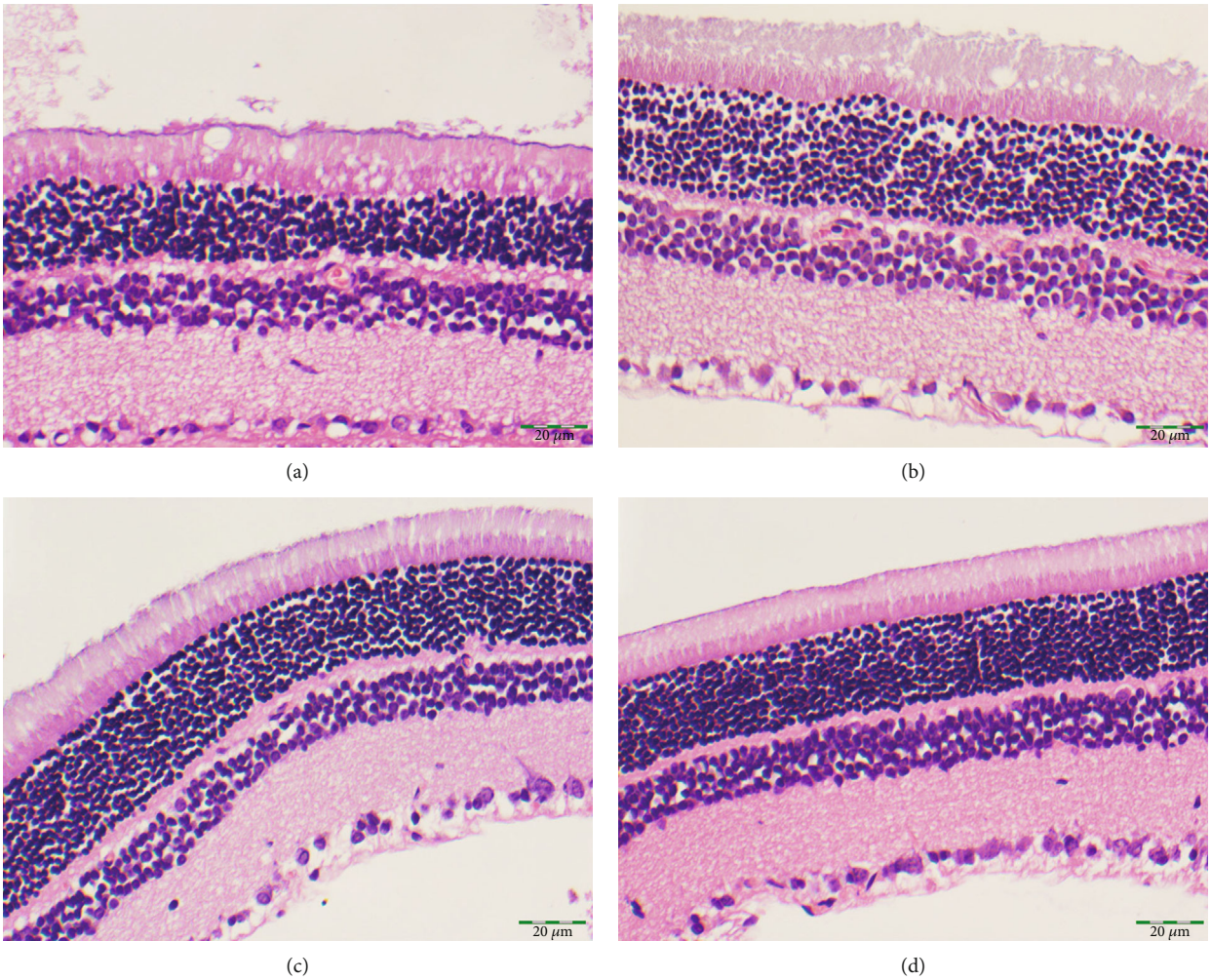

Figure 1: The histopathological appearance of the rat retinas exposed to the intense LED light-induced retinal degeneration between the groups. (a) Control. (b) RD. (c) RD+BCX1. (d) RD+BCX2. (H&E X400), (Bar = 20 μm). BCX: β-cryptoxanthin; LED: light-emitting diode; RD: retinal degeneration.

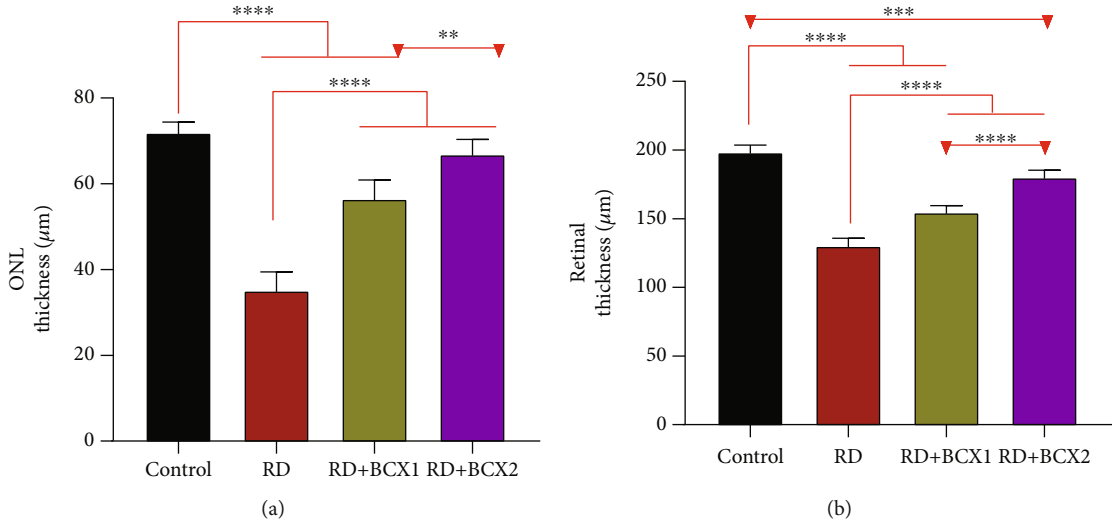

Figure 2: Treatment with β-cryptoxanthin (BCX) altered retinal morphology under intense LED light-exposed rats. (a) Quantification of the ONL thickness compared with the control. (b) Quantification of the Retinal thickness compared with the control ($n = 7$; $P < .05$). BCX: β-cryptoxanthin; LED: light-emitting diode; ONL: outer nuclear layer; RD: retinal degeneration.

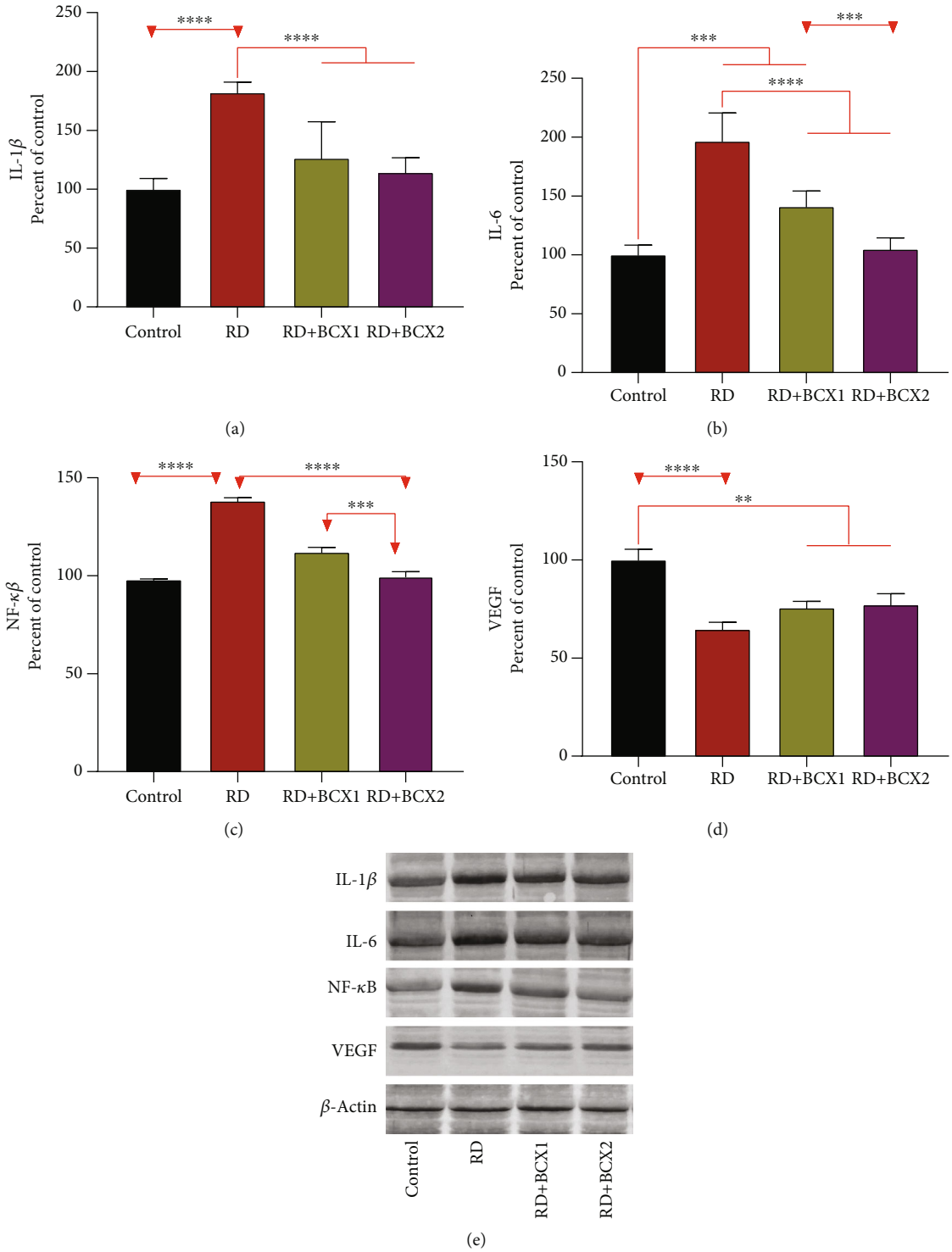

Figure 3: Effects of BCX on retinal protein levels of IL-1β (a), IL-6 (b), NF-κB (c), and VEGF (d) levels in rats with RD. The intensity of the western blot bands (e) was quantified by densitometric analysis, and β-actin was included to ensure equal protein loading. Data are expressed as a ratio of the control value (set to 100%). The bar represents the standard error of the mean. Blots were repeated at least three times ($n = 3$) and a representative blot is shown. Asterisks indicate statistical differences among groups ($^{**}p < .01$; $^{***}p < .001$; $^{****}p < .0001$). BCX: β-Cryptoxanthin; IL-1β: interleukin-1β; IL-6: interleukin-6; NF-κB: nuclear factor kappa B; RD: retinal degeneration; VEGF: vascular endothelial growth factor.

was no difference between BCX and control ($p > 0.05$). NCAM levels decreased in all groups compared to control ($p < 0.001$), while both BCX doses significantly increased NCAM compared to the RD group ($p < 0.001$). While HO1 levels decreased in all groups compared to control ($p < 0.001$), BCX1 ($p < 0.05$), and BCX2 ($p < 0.001$)

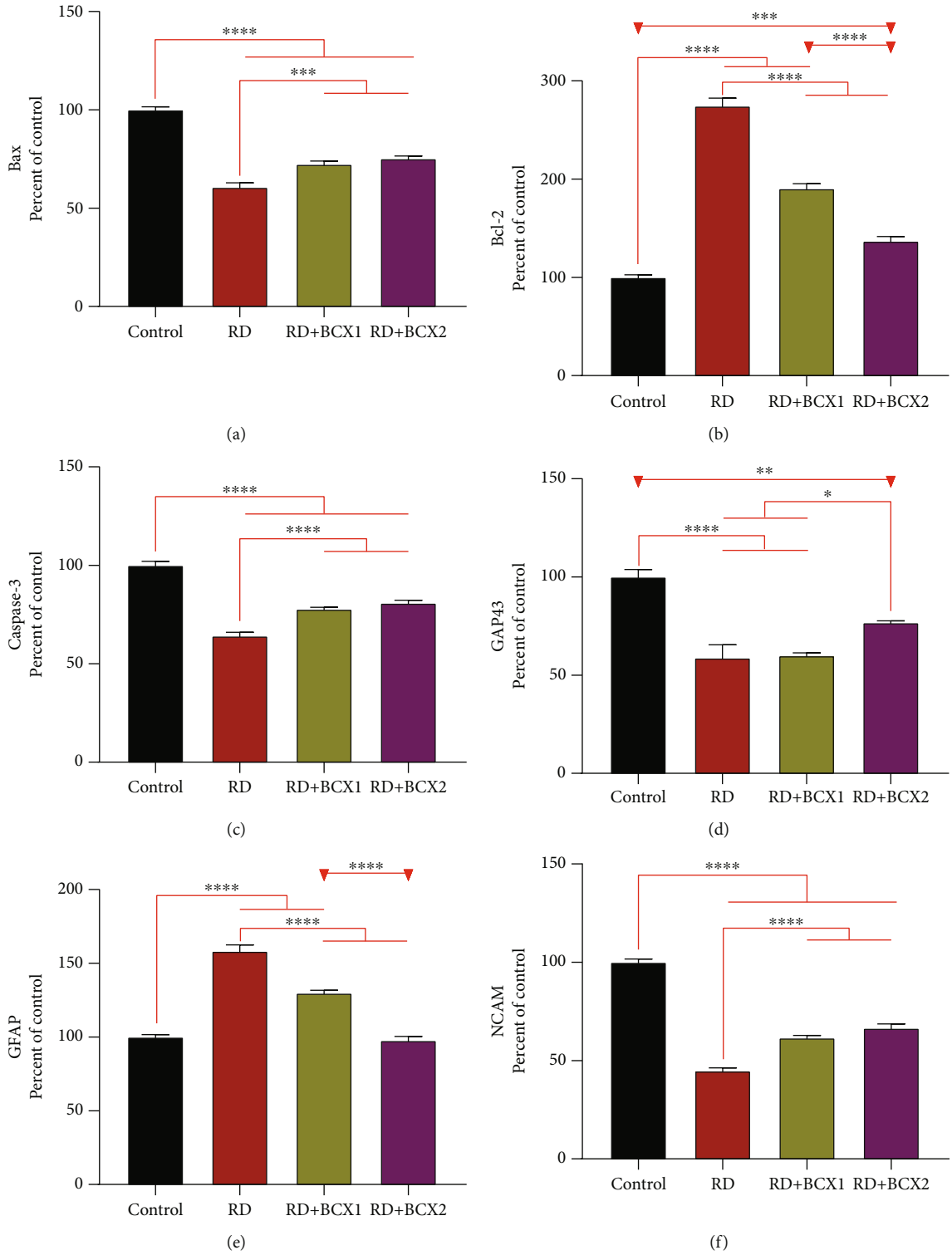

Figure 4: Continued.

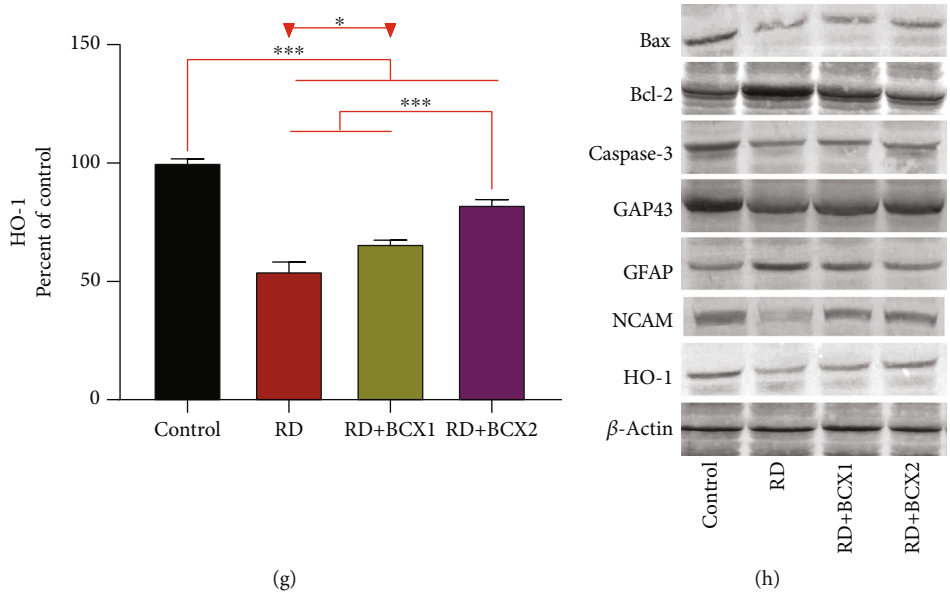

Figure 4: Effects of BCX on retinal protein levels of Bax (a), Bcl-2 (b), Caspase-3 (c), Gap43 (d), GFAP (e), NCAM (f) and HO-1 (g) levels in rats with RD. The intensity of the western blot bands (h) was quantified by densitometric analysis, and β-actin was included to ensure equal protein loading. Data are expressed as a ratio of the control value (set to 100%). The bar represents the standard error of the mean. Blots were repeated at least three times ($n = 3$) and a representative blot is shown. Asterisks indicate statistical differences among groups ($^{*}p < .05$; $^{**}p < .01$; $^{***}p < .001$; $***\,*p < .0001$). BCX: β-cryptoxanthin; Bax: Bcl-2-associated X; Bcl-2: B-cell lymphoma 2; Caspase-3: cysteine-aspartic acid protease-3; GAP43: growth-associated protein 43; GFAP: glial fibrillary acidic protein; HO-1: heme oxygenase-1; NCAM: neural cell adhesion molecule; NF-κB: nuclear factor kappa B; RD: retinal degeneration.

significantly increased HO1 levels compared to RD group. The effects of two doses of BCXcel™ on ATF4, ATF6, and Grp78, Grp94 protein levels in rat retinas are shown in Figure 5. Accordingly, ATF4 and ATF6 levels significantly increased in all groups compared to the control group ($p < 0.001$). While this increase was reduced with BCXcel™ supplementation for both proteins, the lowest level was found in the BCX2 group, which was very close to the control ($p < 0.05$). In contrast, Grp78 levels increased in all groups compared to control ($p < 0.001$), and a significant decrease was observed in the BCX2 group when compared to the RD group and even BCX1 group ($p < 0.001$). In contrast, while Grp94 levels decreased significantly compared to control ($p < 0.001$), this decrease was found in the BCX2 group at the lowest level and close to control ($p < 0.05$).

4. Discussion

This study aimed to investigate the well-established provitamin A carotenoid, BCX, to limit LED-induced retinal damage, including its adverse consequences on metabolic markers and histopathological changes within the retina.

Reactive oxygen species (ROS) have been reported to cause cellular damage by attacking macromolecules in the visual cells when the intense light exposure time exceeds the threshold [31]. Two types of damage caused by light have earlier been proposed: the first contains rhodopsin and affects the photoreceptors; the second concerns retinal pigment epithelium (RPE), which is selectively vulnerable to high-energy blue light [21]. Excessive LED light exposure could lead to phototoxic effects because of the potent blue light hazard; accordingly, it can damage the macula [9, 32]. However, macular degeneration is the primary cause of blindness and severe visual deterioration of older people over 65 [33].

MDA is a well-established marker of light-induced oxidative stress that is easily detectable in the retina. MDA is produced by photoreactive lipofuscin granules, which generate H_2O_2 and other potentially cytotoxic molecules in response to light in RPE [34, 35]. Our study showed similar outcomes to long time constant (200 lux, 2 to 8 days) [36], or short time-intense (3,000 lux, 2 hours) [37], exposure to LED light both showed similar results such as photoreceptor cell deaths, remodeling of the retina and its cellular layers. In the RD group, the serum and retina lipid peroxidation marker, MDA, significantly increased, while the BCXcel™ consumption significantly reversed this effect of lipid peroxidation. This result parallels the findings of a recent study that showed LED exposure critically increases lipid peroxidation and 4-HNE production at the anterior segment level [38].

Our study has also clearly demonstrated that retina SOD, CAT, and GSH-Px activities and serum and retina retinol levels increased with BCXcel™ supplementation. Significant protective effects have also been characterized by both the increase of these BCX levels and the regulation of prominent protein levels as a result of the one-month BCX supplementations to the usual diet, which continued for 48 hours (12 h light/12 h dark) of intense LED light retinal degeneration. Using histopathological measurements, we also determined that retinal thickness, outer nuclear layer (ONL) thickness, and damaged retinal ganglion cell layers, which were

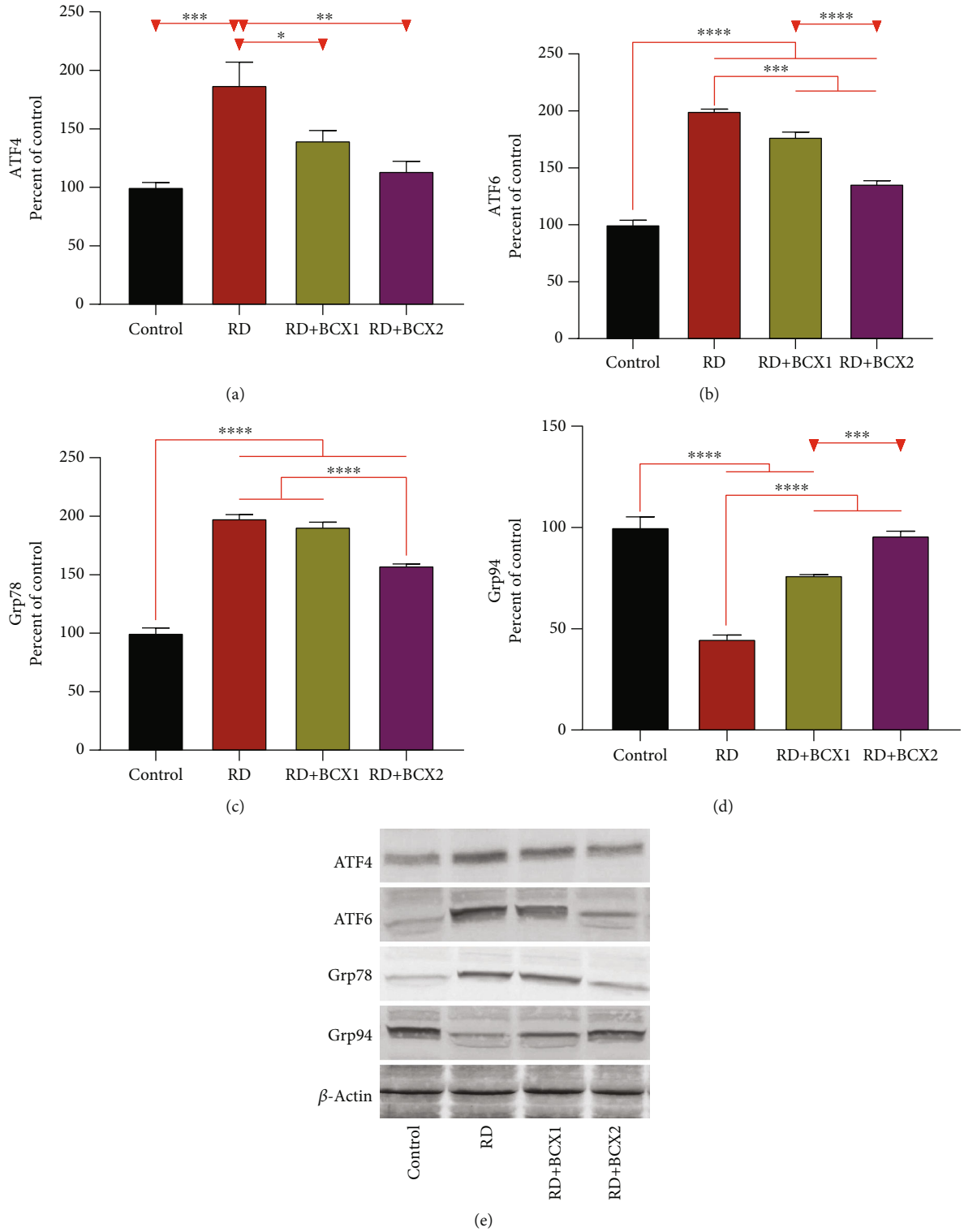

Figure 5: Effects of BCX on retinal protein expression of ATF4 (a), ATF6 (b), Grp78 (c), and Grp94 (d) levels in rats with RD. The intensity of the western blot bands (e) was quantified by densitometric analysis, and β-actin was included to ensure equal protein loading. Data are expressed as a ratio of the control value (set to 100%). The bar represents the standard error of the mean. Blots were repeated at least three times ($n = 3$) and a representative blot is shown. Asterisks indicate statistical differences among groups ($^{*}p < .05$; $^{**}p < .01$; $^{***}p < .001$; $^{****}p < .0001$). ATF4: activating transcription factor 4; ATF6: activating transcription factor 4; BCX: β-cryptoxanthin; Grp78: glucose-regulated protein 78; Grp94: glucose-regulated protein 94; RD: retinal degeneration.

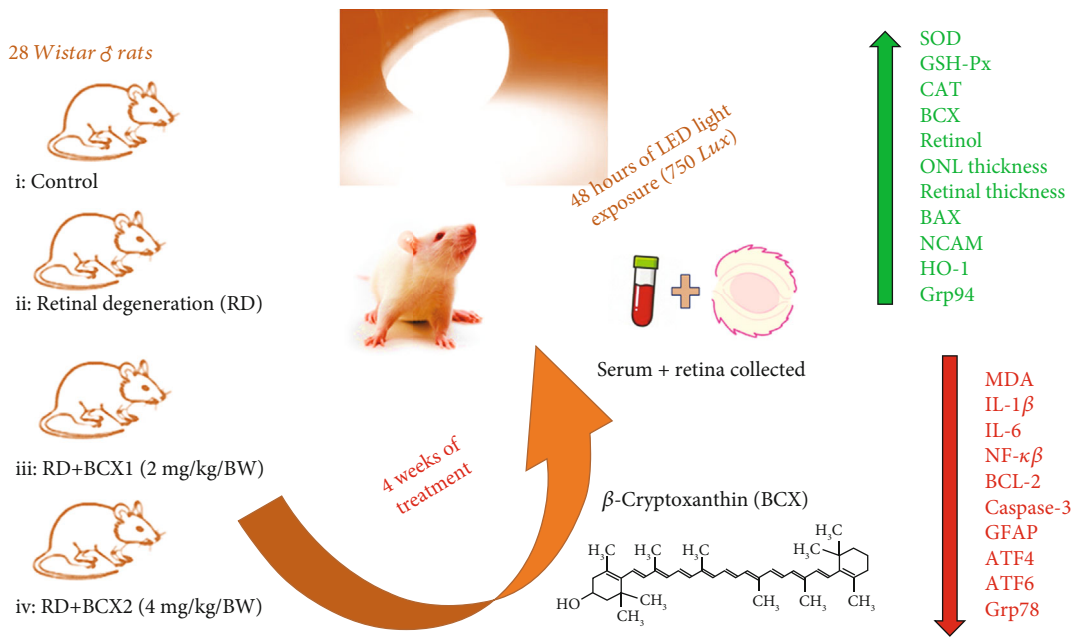

Figure 6: Study overview.

degenerated due to exposure to LED light, were preserved through BCXcel™ supplementation at both doses of BCX.

Inhibition of NF-κB activation and downregulation of cellular inflammatory genes such as IL-1 family and IL-6 were proposed as unique retinal protection mechanisms during antioxidant treatments like curcumin [39]. NF-κB is a transcription factor found in all cell types found inactive in the cytoplasm and can move to the nucleus when activated [40]. The IL-1 family is a cluster of 11 cytokines that induce a complex proinflammatory cytokine linkage plus control and initiate inflammatory responses over and done with the expression of integrins on leukocytes and endothelial cells [41]. IL-6 is an interleukin that functions as a proinflammatory cytokine and an anti-inflammatory myokine [42]. Contributors of the IL-1 family facilitate the photoreceptor cell death, inflammation, and angiogenesis in retinal degenerative diseases [41, 43], their reduction besides NF-κB in the retina has been significantly observed in the present study as the BCX supplement increased.

Vascular endothelial growth factor (VEGF) is a signal protein produced by cells that stimulate vasculogenesis and angiogenesis [44]. In this study, VEGF levels decreased in the RD group and did not statistically change with the addition of BCX. However, blue light is known to trigger inflammatory and angiogenic gene expressions in the early stages and has been reported to increase vascular endothelial growth factor (VEGF) secretion in A2E-loaded RPE cells [45]. In our study, if exposure to LED light was prolonged, BCX efficacy at these levels would be more noticeable as a ROS scavenger [46, 47].

We also observed that proapoptotic Bax and caspase-3 levels were decreased significantly in the RD group compared to control, which was reversed by BCX supplementation at both doses. The adverse effects of excessive LED damage on the antiapoptotic marker, Bcl-2, were evident in the RD group but were reversed positively by BCXcel™ supplementation. Photoreceptor cells were found to show intense light-induced apoptosis in chicks and albino fishes' retinas under constant intense light [20, 48]. Similarly to our results, in a recent study in which ganglion cell injury was induced through experimental ocular glaucoma model in rats, it was shown that ocular hypertension provoked apoptosis via the intrinsic pathway, owing to Bax and caspase-3 activation, in both retina and cornea, which also found to led DNA damage due to p53 activation [49]. As a result of antioxidant therapy, there was a suppression of proapoptotic markers and stimulation of antiapoptotic markers of ganglion cell damage, supporting antioxidants' role in reducing retinal damage [49, 50]. Contrary to the findings in the present study, the proapoptotic marker Bax was upregulated in the retina for up to 24 hours after a blast retinal damage study, whereas cytosolic Bax is shown to decrease 3 and 6 hours after retinal artery occlusion injury, while mitochondrial Bax levels rise at 3, 6, and 24 hours, indicating that Bax was settled in the mitochondria [51, 52]. It was shown that degeneration of retinal capillaries under disease conditions could be reduced by antioxidant therapy through caspase-3 and nuclear factor-κB (NF-κB) activation, which plays a vital role in retinal capillary apoptosis [43, 53].

BCX supplementation was able to reverse the 1.5-fold increase in retina GFAP levels measured in the RD group. Indeed, increased GFAP levels have also been reported by de Raad and colleagues [54], who showed that GFAP accumulated in Müller cells in response to photoreceptor damage in the rat retina [54]. GFAP is upregulated during the light stress and blue light exposure, which leads to a nonspecific reactive change of Müller cells known as gliosis [55, 56]. However, GFAP accumulation in Müller cells was reported as an essential photoreceptor stress parameter in retinopathy induced rats, in accordance with our findings [57]. In a recent

study, a pattern of GFAP ADPase staining also suggested a robust Müller cells/astrocytes reactivity in the Goto-Kakizaki rat retina [58]. In another novel study, a Chinese traditional antioxidant composition FSR prevented retinal thickness, including the ONL and retinal thickness in the diabetic rat retina, and similarly reduced the GFAP expressions in retinal tissues [59].

In the present study, retinal HO-1 levels decreased in the RD group, while the addition of BCXcel™ to the diet increased the levels similar to the control group. It is inversely proportional to an earlier report that created retinal damage via LED lights of different wavelengths and claimed that the iron ion load increased retinal damage in addition to oxidative stress and accordingly raised HO-1 levels [60]. In other studies similar to ours, HO-1 levels were found to be increased and protected light degeneration in the retina, while the antioxidant phytochemicals supported increased protection of the retina [39, 61].

Activating transcription factor 4 (ATF4) is the main component that encodes the cAMP response element-binding transcription factor, stimulating cell survival via modulation of redox reactions, stress response, protein synthesis, and secretion [62, 63]. ATF4 is triggered by stress signals such as anoxia/hypoxia, amino acid abstinence, endoplasmic reticulum stress, and oxidative stress [62]. Activating transcription factor 6 (ATF6) is a transmembrane protein located in the unfolded protein response in mammals and serves as a sensor for the endoplasmic reticulum homeostasis [64, 65]. ATF6 is necessary to optimize protein folding, secretion, and degradation throughout the ER stress and, therefore, ease the improvement of acute stress and indulgence for chronic stress [66]. In our study, both ATF4 and ATF6 levels increased up to 2 times in the RD group compared to the control, and these levels decreased with BCXcel™ supplementation primarily via the higher dose. These data allude to one of the mechanisms by which BCXcel™ can protect against increased light stress, a commonly described mechanism of light-induced retinal damage [67, 68]. Our findings also support that BCXcel™ supplementation normalized GRP78 and GRP94 levels to similar levels compared to the control group. It is proposed that ATF6 acts in synchronization with GRP78 and affects the response to stress, which is in line with the results obtained in our previous study (S. X. [69]). We also observed the increased levels of ER chaperone GRP94 via higher doses of BCXcel™ supplementation. This finding supported a previous report that BCX could positively modulate the stress response and was consistent with the requirement of maintaining hematopoietic stem cell interactions [70]. BCX has been revealed the upregulation of the energy metabolism, response to stress, reducing inflammation, and protein homeostasis as the primary metabolic objectives of this xanthophyll carotenoid [46].

5. Conclusion

In conclusion, oral supplementation of BCX has effectively demonstrated in our four weeks study that in a rat model, and BCXcel™ has a protective effect on high-intensity light-induced retinal damage by reducing oxidative stress and inflammation as well as protecting against mitochondrial DNA damage and cellular death (Figure 6). Present findings of this study on BCX doses have provided new in vivo evidence of the potential medicinal utilization of BCX in the suppression of diseases connected to intense LED toxicity on the retina and in those in which light has been considered a potential pathological inducer (e.g., AMD). Although MDA is an important oxidative stress marker, measuring MDA alone limits this study. In addition to MDA, measuring 8-isoprostane and 4-hydroxynonenal (4-HNE) for protein oxidation and 8-hydroxy-2′-deoxyguanosine (8-OHdG) levels for DNA/RNA oxidation would further strengthen similar studies. Another limitation is that the animal data cannot be extrapolated directly to humans due to differences between nutrient requirements and the severity and duration of metabolism and dietary therapy. In conclusion, considering that LED lighting has been widely used, it is recommended to conduct more molecular studies using carotenoids as protective agents against the adverse effects of LED.

Data Availability

The data used to support the findings of this study are included within the article and the supplementary information files.

Conflicts of Interest

T. Namjoshi, V. Srivastava, A. Morde, M. Padigaru, and D. Rai are employed by OmniActive Health Technologies (Morristown, NJ, USA and Thane, India) company. The remaining authors declare no competing interests.

Authors' Contributions

K. Sahin and C. Orhan designed the research project. M. Tuzcu, H. Gencoglu, E. Sahin, and N. Sahin conducted the experiments. M. Tuzcu, H. Gencoglu, E. Sahin, N. Sahin, and I.H. Ozercan analyzed the experimental data. T. Namjoshi, V. Srivastava, and A. Morde involved in the design and optimization protocols for β-cryptoxanthin extraction followed by formulation strategy to ensure optimal bioavailability and efficacy. A Morde, M. Padigaru, and D. Rai were involved in the scientific evaluation of β-cryptoxanthin and identified biological relevance. H.Gencoglu, K. Sahin, M. Padigaru, and D. Rai wrote and edited the manuscript. All the authors read and approved the final manuscript.

Acknowledgments

The authors thank OmniActive Health Technologies (Morristown, NJ, USA and Thane, India) and the Turkish Academy of Science (in part, KS, Turkey). This work was supported by OmniActive Health Technologies (Morristown, NJ, USA, and Thane, India) and in part by the Turkish Academy of Science (Turkey). The funders had no role in the

project design, data collection, data analyses, and interpretation.

Supplementary Materials

Figure 3 S1: (A-E) shows the full immunoblots related to Figure 3. Figure 3 S1: (A-H) shows the full immunoblots related to Figure 3. Figure 3 S1: (A-E) shows the full immunoblots related to Figure 5. *(Supplementary Materials)*

References

[1] I. Bellezza, "Oxidative stress in age-related macular degeneration: Nrf2 as therapeutic target," *Frontiers in Pharmacology*, vol. 9, p. 1280, 2018.

[2] P. Wong, M. Markey, C. M. Rapp, R. M. Darrow, A. Ziesel, and D. T. Organisciak, "Enhancing the efficacy of AREDS antioxidants in light-induced retinal degeneration," *Molecular Vision*, vol. 23, pp. 718–739, 2017.

[3] C. A. Curcio, "Soft drusen in age-related macular degeneration: biology and targeting via the oil spill strategies," *Investigative Ophthalmology & Visual Science*, vol. 59, no. 4, pp. AMD160–AMD181, 2018.

[4] K. Kaarniranta, E. Pawlowska, J. Szczepanska, A. Jablkowska, and J. Blasiak, "Role of mitochondrial DNA damage in ROS-mediated pathogenesis of age-related macular degeneration (AMD)," *International Journal of Molecular Sciences*, vol. 20, no. 10, p. 2374, 2019.

[5] D. Ali, R. S. Ray, and R. K. Hans, "UVA-induced cyototoxicity and DNA damaging potential of benz (e) acephenanthrylene," *Toxicology Letters*, vol. 199, no. 2, pp. 193–200, 2010.

[6] D. Ali, A. Verma, F. Mujtaba, A. Dwivedi, R. K. Hans, and R. S. Ray, "UVB-induced apoptosis and DNA damaging potential of chrysene via reactive oxygen species in human keratinocytes," *Toxicology Letters*, vol. 204, no. 2-3, pp. 199–207, 2011.

[7] M. Wong-Riley, "Energy metabolism of the visual system," *Eye and Brain*, vol. 2, no. 7, pp. 99–116, 2010.

[8] R. A. Kowluru and P.-S. Chan, "Oxidative stress and diabetic retinopathy," *Experimental Diabetes Research*, vol. 2007, Article ID 43603, 12 pages, 2007.

[9] I. Jaadane, G. E. V. Rodriguez, P. Boulenguez et al., "Effects of white light-emitting diode (LED) exposure on retinal pigment epithelium in vivo," *Journal of Cellular and Molecular Medicine*, vol. 21, no. 12, pp. 3453–3466, 2017.

[10] X. Gong, C. S. Draper, G. S. Allison, R. Marisiddaiah, and L. P. Rubin, "Effects of the macular carotenoid lutein in human retinal pigment epithelial cells," *Antioxidants*, vol. 6, no. 4, p. 100, 2017.

[11] K. J. McClinton, M. Aliani, S. Kuny, Y. Sauvé, and M. Suh, "Differential effect of a carotenoid-rich diet on retina function in non-diabetic and diabetic rats," *Nutritional Neuroscience*, vol. 23, no. 11, pp. 838–848, 2020.

[12] K. Sahin, F. Akdemir, C. Orhan et al., "(3R, 3'R)-zeaxanthin protects the retina from photo-oxidative damage via modulating the inflammation and visual health molecular markers," *Cutaneous and Ocular Toxicology*, vol. 38, no. 2, pp. 161–168, 2019.

[13] W. Stahl, "Macular carotenoids: lutein and zeaxanthin," *Developments in Ophthalmology*, vol. 38, pp. 70–88, 2005.

[14] A. Junghans, H. Sies, and W. Stahl, "Macular pigments lutein and zeaxanthin as blue light filters studied in liposomes," *Archives of Biochemistry and Biophysics*, vol. 391, no. 2, pp. 160–164, 2001.

[15] M. Eggersdorfer and A. Wyss, "Carotenoids in human nutrition and health," *Archives of Biochemistry and Biophysics*, vol. 652, pp. 18–26, 2018.

[16] B. J. Burri, M. R. La Frano, and C. Zhu, "Absorption, metabolism, and functions of β-Cryptoxanthin," *Nutrition Reviews*, vol. 74, no. 2, pp. 69–82, 2016.

[17] J. Widomska, M. Zareba, and W. K. Subczynski, "Can xanthophyll-membrane interactions explain their selective presence in the retina and brain?," *Foods (Basel, Switzerland)*, vol. 5, no. 4, p. 7, 2016.

[18] J. Amengual, M. Airanthi, K. Widjaja-Adhi et al., "Two Carotenoid Oxygenases Contribute to Mammalian Provitamin A Metabolism," *The Journal of Biological Chemistry*, vol. 288, no. 47, pp. 34081–34096, 2013.

[19] J. Coronel, I. Pinos, and J. Amengual, "β-carotene in obesity research: technical considerations and current status of the field," *Nutrients*, vol. 11, no. 4, p. 842, 2019.

[20] K. A. Jha, T. C. Nag, V. Kumar et al., "Differential expression of AQP1 and AQP4 in avascular chick retina exposed to moderate light of variable photoperiods," *Neurochemical Research*, vol. 40, no. 11, pp. 2153–2166, 2015.

[21] D. T. Organisciak and D. K. Vaughan, "Retinal light damage: mechanisms and protection," *Progress in Retinal and Eye Research*, vol. 29, no. 2, pp. 113–134, 2010.

[22] B. J. Burri, "Beta-cryptoxanthin as a source of vitamin A," *Journal of the Science of Food and Agriculture*, vol. 95, no. 9, pp. 1786–1794, 2015.

[23] R. Arantes-Rodrigues, A. Henriques, R. Pinto-Leite et al., "The effects of repeated oral gavage on the health of male CD-1 mice," *Lab Animal*, vol. 41, no. 5, pp. 129–134, 2012.

[24] K. Sahin, H. Gencoglu, F. Akdemir et al., "Lutein and zeaxanthin isomers may attenuate photo-oxidative retinal damage via modulation of G protein-coupled receptors and growth factors in rats," *Biochemical and Biophysical Research Communications*, vol. 516, no. 1, pp. 163–170, 2019.

[25] O. Barim and M. Karatepe, "The effects of pollution on the vitamins A, E, C, beta-carotene contents and oxidative stress of the freshwater crayfish, Astacus leptodactylus," *Ecotoxicology and Environmental Safety*, vol. 73, no. 2, pp. 138–142, 2010.

[26] M. Karatepe, "Simultaneous determination of ascorbic acid and free malondialdehyde in human serum by HPLC-UV," *LC-GC North America*, vol. 22, no. 4, pp. 362–365, 2004.

[27] R. J. Collier, W. Yu, S. S. Smith et al., "Complement deposition and microglial activation in the outer retina in light-induced retinopathy: inhibition by a 5-HT1AAgonist," *Investigative Ophthalmology & Visual Science*, vol. 52, no. 11, pp. 8108–8116, 2011.

[28] C. Orhan, F. Akdemir, M. Tuzcu et al., "Mesozeaxanthin protects retina from oxidative stress in a rat model," *Journal of Ocular Pharmacology and Therapeutics*, vol. 32, no. 9, pp. 631–637, 2016.

[29] M. Ulas, C. Orhan, M. Tuzcu et al., "Anti-diabetic potential of chromium histidinate in diabetic retinopathy rats," *BMC Complementary and Alternative Medicine*, vol. 15, no. 1, p. 16, 2015.

[30] F. Faul, E. Erdfelder, A.-G. Lang, and A. Buchner, "G∗Power 3: a flexible statistical power analysis program for the social, behavioral, and biomedical sciences," *Behavior Research Methods*, vol. 39, no. 2, pp. 175–191, 2007.

[31] B. Aydin, D. Erdem, S. Necat Yilmaz et al., "Retinal endoilluminator toxicity of xenon and light-emitting diode (LED) light source: rabbit model," *Cutaneous and Ocular Toxicology*, vol. 33, no. 3, pp. 192–196, 2013.

[32] P. N. Youssef, N. Sheibani, and D. M. Albert, "Retinal light toxicity," *Eye*, vol. 25, no. 1, pp. 1–14, 2011.

[33] S. B. Bressler and N. M. Bressler, "Chapter 65 - age-related macular degeneration: non-neovascular early AMD, intermediate AMD, and geographic atrophy," in *Retina (Fifth Edition)*, S. J. Ryan, S. V. R. Sadda, D. R. Hinton, A. P. Schachat, S. V. R. Sadda, C. P. Wilkinson, P. Wiedemann, and A. P. Schachat, Eds., pp. 1150–1182, W.B. Saunders, London, 2013.

[34] V. E. Baksheeva, V. V. Tiulina, N. K. Tikhomirova et al., "Suppression of light-induced oxidative stress in the retina by mitochondria-targeted antioxidant," *Antioxidants*, vol. 8, no. 1, p. 3, 2019.

[35] M. Rózanowska, J. Jarvis-Evans, W. Korytowski, M. E. Boulton, J. M. Burke, and T. Sarna, "Blue light-induced reactivity of retinal age pigment. In vitro generation of oxygen-reactive species," *The Journal of Biological Chemistry*, vol. 270, no. 32, pp. 18825–18830, 1995.

[36] Q. Wei, X. Liang, Y. Peng et al., "17β-estradiol ameliorates oxidative stress and blue light-emitting diode-induced retinal degeneration by decreasing apoptosis and enhancing autophagy," *Drug Design, Development and Therapy*, vol. 12, pp. 2715–2730, 2018.

[37] M. M. Benedetto, M. E. Guido, and M. A. Contin, "Non-visual photopigments effects of constant light-emitting diode light exposure on the inner retina of Wistar rats," *Frontiers in Neurology*, vol. 8, p. 417, 2017.

[38] I. Jun, S. J. Han, H.-S. Shin et al., "Comparison of ophthalmic toxicity of light-emitting diode and organic light-emitting diode light sources," *Scientific Reports*, vol. 10, no. 1, p. 11582, 2020.

[39] M. N. A. Mandal, J. M. R. Patlolla, L. Zheng et al., "Curcumin protects retinal cells from light-and oxidant stress-induced cell death," *Free Radical Biology & Medicine*, vol. 46, no. 5, pp. 672–679, 2009.

[40] A. Oeckinghaus and S. Ghosh, "The NF-κB family of transcription factors and its regulation," *Cold Spring Harbor Perspectives in Biology*, vol. 1, no. 4, article a000034, 2009.

[41] C. A. Dinarello, "Overview of the IL-1 family in innate inflammation and acquired immunity," *Immunological Reviews*, vol. 281, no. 1, pp. 8–27, 2018.

[42] J. J. Fuster and K. Walsh, "The good, the bad, and the ugly of Interleukin-6 signaling," *The EMBO Journal*, vol. 33, no. 13, pp. 1425–1427, 2014.

[43] C. Li, X. Miao, F. Li et al., "Oxidative stress-related mechanisms and antioxidant therapy in diabetic retinopathy," *Oxidative Medicine and Cellular Longevity*, vol. 2017, Article ID 9702820, 15 pages, 2017.

[44] C. J. Peach, V. W. Mignone, M. A. Arruda et al., "Molecular pharmacology of VEGF-A isoforms: binding and signalling at VEGFR2," *International Journal of Molecular Sciences*, vol. 19, no. 4, p. 1264, 2018.

[45] C.-H. Lin, M.-R. Wu, W.-J. Huang, D. S.-L. Chow, G. Hsiao, and Y.-W. Cheng, "Low-luminance blue light-enhanced phototoxicity in A2E-laden RPE cell cultures and rats," *International Journal of Molecular Sciences*, vol. 20, no. 7, p. 1799, 2019.

[46] S. Llopis, M. J. Rodrigo, N. González et al., "β-Cryptoxanthin reduces body fat and increases oxidative stress response in Caenorhabditis elegans model," *Nutrients*, vol. 11, no. 2, p. 232, 2019.

[47] E. Pawlowska, J. Szczepanska, A. Koskela, K. Kaarniranta, and J. Blasiak, "Dietary polyphenols in age-related macular degeneration: protection against oxidative stress and beyond," *Oxidative Medicine and Cellular Longevity*, vol. 2019, Article ID 9682318, 13 pages, 2019.

[48] R. Bejarano-Escobar, M. Blasco, G. Martín-Partido, and J. Francisco-Morcillo, "Light-induced degeneration and microglial response in the retina of an epibenthonic pigmented teleost: age-dependent photoreceptor susceptibility to cell death," *Journal of Experimental Biology*, vol. 215, no. 21, pp. 3799–3812, 2012.

[49] Z. Erisgin, M. A. Ozer, M. Tosun, S. Ozen, and S. Takir, "The effects of intravitreal H2S application on apoptosis in the retina and cornea in experimental glaucoma model," *International Journal of Experimental Pathology*, vol. 100, no. 5–6, pp. 330–336, 2020.

[50] D. Cervia, E. Catalani, and G. Casini, "Neuroprotective peptides in retinal disease," *Journal of Clinical Medicine*, vol. 8, no. 8, p. 1146, 2019.

[51] C. N. Thomas, M. Berry, A. Logan, R. J. Blanch, and Z. Ahmed, "Caspases in retinal ganglion cell death and axon regeneration," *Cell Death Discovery*, vol. 3, no. 1, pp. 1–13, 2017.

[52] Y. Zhang, C.-H. Cho, L.-o. Atchaneeyasakul, T. McFarland, B. Appukuttan, and J. Timothy Stout, "Activation of the mitochondrial apoptotic pathway in a rat model of central retinal artery occlusion," *Investigative Ophthalmology & Visual Science*, vol. 46, no. 6, pp. 2133–2139, 2005.

[53] R. A. Kowluru, P. Koppolu, S. Chakrabarti, and S. Chen, "Diabetes-induced activation of nuclear transcriptional factor in the retina, and its inhibition by antioxidants," *Free Radical Research*, vol. 37, no. 11, pp. 1169–1180, 2009.

[54] S. Raadde, P. J. Szczesny, K. Munz, and C. E. Remé, "Light damage in the rat retina: glial fibrillary acidic protein accumulates in Müller cells in correlation with photoreceptor damage," *Ophthalmic Research*, vol. 28, no. 2, pp. 99–107, 1996.

[55] C. L. Gupta, T. C. Nag, K. A. Jha et al., "Changes in the inner retinal cells after intense and constant light exposure in Sprague-Dawley rats," *Photochemistry and Photobiology*, vol. 96, no. 5, pp. 1061–1073, 2020.

[56] I. Iandiev, A. Wurm, M. Hollborn et al., "Müller cell response to blue light injury of the rat retina," *Investigative Ophthalmology & Visual Science*, vol. 49, no. 8, pp. 3559–3567, 2008.

[57] E. Jung and J. Kim, "Aloin inhibits Müller cells swelling in a rat model of thioacetamide-induced hepatic retinopathy," *Molecules (Basel, Switzerland)*, vol. 23, no. 11, article 2806, 2018.

[58] S. Hachana, M. Pouliot, R. Couture, and E. Vaucher, "Diabetes-induced inflammation and vascular alterations in the Goto-Kakizaki rat retina," *Current Eye Research*, vol. 45, no. 8, pp. 965–974, 2020.

[59] M. He, L. Pan, L. Guo, M. Zhang, S. Wang, and H. He, "Fushiming capsule attenuates diabetic rat retina damage via antioxidation and anti-inflammation," *Evidence-based Complementary and Alternative Medicine: Ecam*, vol. 2019, article 5376439, 13 pages, 2019.

[60] Y.-M. Shang, G.-S. Wang, D. H. Sliney, C.-H. Yang, and L.-L. Lee, "Light-emitting-diode induced retinal damage and its wavelength dependency in vivo," *International Journal of Ophthalmology*, vol. 10, no. 2, pp. 191–202, 2017.

[61] T. Okamoto, H. Kawashima, H. Osada et al., "Dietary spirulina supplementation protects visual function from photostress by suppressing retinal neurodegeneration in mice," *Translational Vision Science & Technology*, vol. 8, no. 6, p. 20, 2019.

[62] K. Ameri and A. L. Harris, "Activating transcription factor 4," *The International Journal of Biochemistry & Cell Biology*, vol. 40, no. 1, pp. 14–21, 2008.

[63] S. E. Kobylewski, K. A. Henderson, K. E. Yamada, and C. D. Eckhert, "Activation of the EIF2α/ATF4 and ATF6 pathways in DU-145 cells by boric acid at the concentration reported in men at the US mean boron intake," *Biological Trace Element Research*, vol. 176, no. 2, pp. 278–293, 2017.

[64] M. Carrara, F. Prischi, and M. Ali, "UPR signal activation by luminal sensor domains," *International Journal of Molecular Sciences*, vol. 14, no. 3, pp. 6454–6466, 2013.

[65] D. R. Hyduke, S. A. Amundson, and A. J. Fornace, "Chapter 257 - complexity of stress signaling," in *Handbook of Cell Signaling (Second Edition)*, R. A. Bradshaw and E. A. Dennis, Eds., pp. 2107–2125, Academic Press, San Diego, 2010.

[66] B. M. Gardner, D. Pincus, K. Gotthardt, C. M. Gallagher, and P. Walter, "Endoplasmic reticulum stress sensing in the unfolded protein response," *Cold Spring Harbor Perspectives in Biology*, vol. 5, no. 3, p. a013169, 2013.

[67] M. E. Fusakio, J. A. Willy, Y. Wang et al., "Transcription factor ATF4 directs basal and stress-induced gene expression in the unfolded protein response and cholesterol metabolism in the liver," *Molecular Biology of the Cell*, vol. 27, no. 9, pp. 1536–1551, 2016.

[68] R. F. Hillary and U. FitzGerald, "A lifetime of stress: ATF6 in development and homeostasis," *Journal of Biomedical Science*, vol. 25, no. 1, p. 48, 2018.

[69] S. X. Zhang, E. Sanders, S. J. Fliesler, and J. J. Wang, "Endoplasmic reticulum stress and the unfolded protein responses in retinal degeneration," *Experimental Eye Research*, vol. 125, no. 8, pp. 30–40, 2014.

[70] B. Luo, B. S. Lam, S. H. Lee et al., "The endoplasmic reticulum chaperone protein GRP94 is required for maintaining hematopoietic stem cell interactions with the adult bone marrow niche," *PLoS One*, vol. 6, no. 5, article e20364, 2011.

[71] NRC (US), *Nutrient Requirements of Laboratory Animals: Fourth Revised Edition, 1995*, National Academies Press (US), Washington (DC), 1995, https://www.ncbi.nlm.nih.gov/books/NBK231927/.

Hindawi
Oxidative Medicine and Cellular Longevity
Volume 2021, Article ID 6614028, 20 pages
https://doi.org/10.1155/2021/6614028

Research Article

Mechanism of Intestinal Flora and Proteomics on Regulating Immune Function of *Durio zibethinus* Rind Polysaccharide

Huimin Jiang,[1] **Jinmei Wang**,[1,2] **Qiongxin Liang**,[1] **Shengjun Jiang**,[1] **Changyang Ma**,[1,3] **Yan Zhang**,[4] **and Wenyi Kang**[1,2,3]

[1]*National R&D Center for Edible Fungus Processing Technology, Henan University, Kaifeng, 475004 Henan Province, China*
[2]*Joint International Research Laboratory of Food & Medicine Resource Function, Henan University, Kaifeng, 475004 Henan Province, China*
[3]*Functional Food Engineering Technology Research Center, Henan University, Kaifeng, 475004 Henan Province, China*
[4]*College of Forensic Medicine, Hebei Medical University, Shijiazhuang 050017, China*

Correspondence should be addressed to Changyang Ma; macaya1024@sina.com, Yan Zhang; snowwinglv@126.com, and Wenyi Kang; kangweny@hotmail.com

Received 17 November 2020; Revised 20 December 2020; Accepted 22 January 2021; Published 2 February 2021

Academic Editor: Daoud Ali

In this study, cyclophosphamide was injected intraperitoneally to establish an immunosuppressive mouse model to study the immune regulating effects of *Durio zibethinus* Murr rind polysaccharide (DZMP) through proteomics and intestinal flora. The results showed that the thymus and spleen indexes of the high-dose DZMP (200 mg/kg) group were significantly increased, and the tissue structure of the spleen was improved compared with the model group ($P < 0.01$). The contents of IL-2, IL-4, IL-6, and TNF-α in the high-dose group of DZMP were significantly increased ($P < 0.001$). Activities of acid phosphatase (ACP), lactate dehydrogenase (LDH), superoxide dismutase (SOD), and total antioxidant capacity (T-AOC) were increased in serum ($P < 0.01$). In the liver, catalase (CAT) activity was increased ($P < 0.001$) while the malondialdehyde (MDA) content was decreased and immune activity was increased ($P < 0.001$). Proteomics studies showed that the drug group could significantly increase the low-affinity immunoglobulin gamma Fc receptor III (FcγRIII) protein and protein kinase C-α (PKC-α) compared with the model group ($P < 0.001$). In addition, the result showed that those proteins were likely involved in the regulation of the metabolic pathways of autoimmune thyroid disease, *Staphylococcus aureus* infection, and NF-κB signaling pathway. Intestinal microbial studies showed that short-chain fatty acid (SCFA) content was increased as well as the relative abundance of beneficial bacteria *Akkermansia*, *Bacteroides*, and *Paraprevotella*, while the relative abundance of *Ruminococcus* and *Oscillospira* was decreased compared with the model group ($P < 0.001$). The results showed that DZMP might play a beneficial role in immune regulation by improving intestinal flora.

1. Introduction

The immune system consists of immune organs, immune cells, and immune molecules [1]. The immune system's stress response to external stimuli is considered as one of the important defense strategies for the human body to prevent and fight against foreign infections, inflammation, and cancer [2, 3]. Studies have shown that the main immunomodulatory mechanism of polysaccharides is to help the host form a strong immune response by activating the host's immune response [4, 5]. Previous studies showed that polysaccharide from *Ganoderma atrum* could significantly improve the immune organ index [6], *Epimedium brevicornu* Maxim polysaccharides could play an important role as immune adjuvant [7], and *Malus halliana* Koehne flower polysaccharide can regulate the content of cytokines and enhance the immune function of immunosuppressed mice [8].

Intestinal flora belongs to a complex microecosystem, which involves microbial interaction, nutrient metabolism, immune function, and diseases [9, 10]. The metabolism of the intestinal microbial community is closely related to the health of the host, among which beneficial bacteria can

regulate the absorption and utilization of nutrients in the intestinal tract [11, 12]. In some disease areas, such as cancer, colitis, and obesity, the adjuvant therapy of beneficial bacteria plays a good regulatory role [13]. Besides, existing studies showed that *Fructus morji* pectin polysaccharide and its metabolites have beneficial effects on health by regulating the growth of intestinal beneficial bacteria *Bacteroides taiotaomicron* [14]. Short-chain fatty acids (SCFAs) are key factors to regulate the intestinal flora [15]. Studies showed that SCFAs had important biological functions, including maintaining energy; adjusting colon and intracellular pH; and regulating cell ion transport, proliferation, and gene expression differentiation [16]. The concentration of SCFAs in the cecum and colonic cavity can be significantly changed by high-dose administration of *Pleurotus eryngii* polysaccharide, and the gastrointestinal function can be regulated [17].

In these studies, many omics techniques such as proteome, genome, and transcriptome have been used to study the action mechanism of some natural products on diseases. Proteomics technology focuses on the differences in the expression level, quantity, and modification status of proteomics among different experimental groups to identify the specific proteins, which are related to disease diagnosis and protein targets of drug therapy [18–21]. Wang et al. performed 2D-DIGE gel electrophoresis analysis on the liver proteins of mice from the normal group and the experimental group administrated with the *Dendrobium huoshanense* polysaccharide, and identified 18 differentially expressed proteins involved in glucose metabolism, amino acid metabolism, and other metabolic pathways [22]. Chao et al. compared the protein expression profiles related to the proliferation of mouse spleen monocytes before and after the effect of total polysaccharide from *Ganoderma* spore, and found out the target proteins with the functions of cell survival and proliferation, cell activation and migration, and cytoskeleton structure [23]. Wei et al. studied the *Hedysarum polybotrys* polysaccharide on the immune function of mice at the level of proteomics, and found out its significant improvement effect on the protein expression profile of thymus cells and the relationship of protein synthesis initiation factor 4, carbolic anhydrase, reductase 6, and proteasome with the thymus immune regulation in mice [24].

Cyclophosphamide (CTX), one immunosuppressive agent in the clinic, is usually taken as a common chemotherapy drug to decrease spleen index, lymphocyte proliferation, and phagocytic cell activity [25]. At the same time, polysaccharides are commonly used to improve the side effects caused by this chemotherapy drug. For example, in the treatment of intestinal tumor mice, carboxymethyl polysaccharide can alleviate the adverse effects of chemotherapy drugs and enhance the immunity of mice [26]. In addition, *Astragalus* polysaccharide, *Panax ginseng* polysaccharide, *Lentinula edodes* polysaccharide, and *Ganoderma lucidum* polysaccharide have been widely used as adjuvant drugs in cancer treatment.

The *D. zibethinus* rind is the husk of durian in Bombacaceae, and current researches mainly focus on its surface chemistry and adsorption function [27, 28]. Pharmacological studies show that durian skin extract has cough-relieving, bowel laxative, analgesic, antioxidant, and antibacterial activities [29–31]. Studies on the chemistry of DZMP mainly focus on flavonoids. The results of our preexperiment found that DZMP had an immunomodulatory effect.

Thus, in this paper, proteomics and intestinal flora were used to investigate the immune effect of DZMP on an immunosuppressed mouse model *in vivo*.

2. Materials and Methods

2.1. Materials and Chemicals. CTX (batch number: 19012825) was purchased from Jiangsu Hengrui Pharmaceutical Co., Ltd. *Lentinula edodes* polysaccharide tablets (batch number: 1903010) was from Hubei Guangren Pharmaceutical Co., Ltd. *D. zibethinus* rind was collected from supermarkets in Kaifeng City, Henan Province, and identified by Professor Changqin Li of The National Center for Edible Fungus Processing Technology, Henan University. Then, the *D. zibethinus* rind was chopped, dried, and used to extract the DZMP following the procedure from a previous research [30].

2.2. Animal Experimental Design. A total of 60 SPF Kunming mice (male, 20~22 g) were purchased from Henan Provincial Laboratory Animal Center with the following license number: SCXK (Yu) 2017-0004. Before the experiment, these mice were allowed to acclimate for 1 week (temperature: 25°C ± 2°C, lighting: 12 h light/12 h dark, and humidity: 40%~45%) before the experiment.

These mice were randomly divided into 6 groups: the blank group (BC), the model group (MC), the positive control group (PC), the DZMP high-dose group (HD), the DZMP medium-dose group (MD), and the DZMP low-dose group (LD) (with 10 mice in each group).

The BC and MC groups were given normal saline at 0.1 mL/10 g BW every day. In the PC group, *Lentinula* polysaccharide tablet, one common immunosuppression modulator in the clinic, was administered at 3 mg/kg BW by oral gavage. The HD, MD, and LD groups were given DZMP orally at 200, 100, and 50 mg/kg BW, respectively, once a day. All groups were treated for 21 days as described above. On the 18th, 19th, 20th, and 21st days, the BC group was intraperitoneally injected with normal saline, while the other groups were modeled by intraperitoneally injecting with CTX at 70 mg/kg BW.

2.3. Sample Collection. After treatments, the rats were weighed and fasted overnight (12–14 h). Blood was taken from the eyeball, placed for 30 min, centrifuged at 3500 g for 10 min, and then the serum was collected from the supernatant and stored at -20°C until analyzed. The spleen and thymus were taken and weighed for the organ index. Partial spleens of mice were cut and rinsed with PBS for the antioxidant capacity of this organ. The livers of each mouse were cut and stored at -80°C for later use in proteomics research. The cecum of each mouse was removed, 0.3 g of cecal contents were placed in a 4 mL centrifuge tube, and then the samples were stored at -40°C for SCFA determination. To determine the bacterial flora, the cecal contents of 3 mice in each cage were collected randomly and a total of 18 samples

Table 1: Chromatographic elution conditions.

Time/min	0-5	5-45	45-50	50-52	52-54	54-60
Mobile phase A (2% acetonitrile, 0.1% formic acid)	95%	75%	65%	20%	20%	95%
Mobile phase B (98% acetonitrile, 0.1% formic acid)	5%	25%	35%	80%	80%	5%

were stored at -80°C until (0.2 g/sample) taken for DNA extraction.

2.4. Thymus Index and Spleen Index. The spleen and thymus were taken, cleaned, and weighed. Spleen and thymus indexes were calculated according to the following formulas:

$$\text{Thymus index} = \frac{\text{thymus weight (mg)}}{\text{body weight (10 g)}},$$
$$\text{Spleen index} = \frac{\text{spleen weight (mg)}}{\text{body weight (10 g)}}. \quad (1)$$

2.5. Determination of Cytokine Content. The contents of IL-2, IL-4, IL-6, and TNF-α were determined by ELISA kits.

2.6. Determination of Antioxidant Stress Ability. About 50 mg of spleen was taken for tissue homogenization, and MDA content and CAT activity were, respectively, detected according to the kit instructions. The activities of SOD and T-AOC were examined according to the instructions of the kit. The activity values of lactate dehydrogenase (LDH) and acid phosphatase (ACP) were determined by microenzyme labeling and microplate method according to the instructions of the corresponding kits, respectively.

2.7. Histological Evaluation. The thymus and spleen parts of mice were rinsed and placed in 4% paraformaldehyde solution for 24 h. After that, they were dehydrated, embedded in conventional paraffin, and sliced. Hematoxylin-eosin staining was performed to the tissue slice for 5 min, and then dehydration was conducted. The slices were sealed with neutral gum.

2.8. Proteomics Research. From the BC, MC, and HD groups, 9 mice were randomly selected from each group for their livers. The liver tissues of every 3 mice were combined together as one sample, and a total of 9 samples were obtained for proteomics research.

2.8.1. Protein Extraction. The protein extraction procedure is as follows: take 300-500 mg of the liver tissue, add two steel balls and lysate, place it on ice for 5 min, and add dithiothreitol (DTT). Then, break and crack the tissue using a grinding apparatus (power: 60 Hz, time: 2 min). After that, centrifuge it at 25000 g and 4°C for 15 min, and take the supernatant. Keep on adding DTT, iodoacetamide, cold acetone, and sodium dodecyl sulfate L3 (SDSL3) in turn to extract the protein and repeat the centrifugation. The protein solution would then be obtained from the supernatant. Take 30 μg protein solution from each sample to determine the protein concentration by the SDS-PAGE method.

Table 2: Effects of DZMP on immune organs in mice ($n = 10$).

Groups	Thymus index (mg/10 g)	Spleen index (mg/10 g)
BC	24.72 ± 4.47	20.89 ± 4.36
MC	$6.40 \pm 0.98^{***}$	$8.87 \pm 1.33^{***}$
PC	$9.74 \pm 2.05^{\#\#}$	$11.87 \pm 1.88^{\#\#}$
HD	$9.07 \pm 2.07^{\#}$	$12.55 \pm 1.97^{\#\#}$
MD	6.59 ± 0.91	10.87 ± 1.94
LD	6.57 ± 1.32	10.06 ± 0.83

Compared with the BC group: $^{***}P < 0.001$, $^{**}P < 0.01$, and $^{*}P < 0.05$. Compared with the MC group: $^{\#\#\#}P < 0.001$, $^{\#\#}P < 0.01$, and $^{\#}P < 0.05$.

2.8.2. Proteolysis. 100 μg protein solution was added into a 1.5 mL centrifuge tube. Dilute it with 0.5 M triethyl ammonium bicarbonate (TEAB) until the final sodium dodecyl sulfate (SDS) concentration in the protein solution was lower than 0.1%. Add this into the solution of trypsin enzyme with a 1 : 20 proportion of enzyme (μg) and substrate protein (μg). After vortex oscillation, centrifuge it at low speed for 1 min and incubate it at 37°C for 2 h. After desalting the digested peptide and freeze-drying it, the target peptides would be obtained.

2.8.3. Peptide Labeling and Separation. Each tube with 2 mg isobaric tag (IBT) reagent was dissolved with 80 μL isopropanol and shaken for more than 1 min to fully dissolve. After enzymatic digestion and desalination, the peptide was dissolved in 0.2 M TEAB solution at a concentration of 4 μg/μL and shaken for more than 1 min to dissolve the peptide adequately. 100 μg of peptide and 80 μL of IBT reagent were rapidly mixed and centrifuged, and the pH value should be between 7.0 and 8.0. The peptide labeling operation was repeated for each channel of IBT reagent, and each of them was marked. Then, they were placed at room temperature for 2 h to let the peptide label sufficiently. The Shimadzu LC-20AB liquid phase system was used to separate peptides of the samples through a Gemini C18 column (5 μm, 4.6 × 250 mm).

2.8.4. LC Analysis. The extracted peptide samples were redissolved in mobile phase A (2% acetonitrile, 0.1% formic acid), centrifuged at 20,000 g for 10 min, and the supernatant was taken for sample injection. Separation was performed using the Thermo UltiMate 3000 UHPLC. The samples were first enriched and desalted in a trap column, followed by a series separation with a self-loaded C18 column (75 μm inner diameter, >3 μm particle diameter, and 25 μm column length) in a series with an effective gradient elution procedure at a flow rate of 300 nL/min (Table 1). One mass spectrometer was located at the end of the nanoliquid phase separation process.

Table 3: Effects of DZMP on the content of cytokines ($n = 10$).

Groups	IL-2 (ng/mL)	IL-4 (pg/mL)	IL-6 (pg/mL)	TNF-α (pg/mL)
BC	2.67 ± 0.77	420.23 ± 51.51	78.93 ± 7.75	73.12 ± 11.18
MC	1.78 ± 0.08***	341.23 ± 17.90***	69.19 ± 3.82**	36.44 ± 9.06***
PC	2.66 ± 0.06$^{\#\#\#}$	412.05 ± 47.39$^{\#\#}$	79.48 ± 6.56$^{\#\#}$	86.40 ± 2.39$^{\#\#\#}$
HD	2.63 ± 0.14$^{\#\#\#}$	392.63 ± 49.26$^{\#}$	79.49 ± 6.48$^{\#\#}$	99.83 ± 13.05$^{\#\#\#}$
MD	2.51 ± 0.12$^{\#\#\#}$	270.50 ± 35.41$^{\#\#}$	81.70 ± 6.92$^{\#\#\#}$	55.31 ± 8.90$^{\#\#\#}$
LD	2.42 ± 0.07$^{\#\#\#}$	274.37 ± 52.58$^{\#\#}$	73.51 ± 7.96	51.08 ± 5.25$^{\#\#}$

Compared with the BC group: $^{***}P < 0.001$, $^{**}P < 0.01$, and $^{*}P < 0.05$. Compared with the MC group: $^{\#\#\#}P < 0.001$, $^{\#\#}P < 0.01$, and $^{\#}P < 0.05$.

Table 4: Effect of DZMP on serum ACP and LDH activities ($n = 10$).

Groups	ACP (unit/100 mL)	LDH (U/L)
BC	8.89 ± 0.95	1580.44 ± 72.08
MC	4.01 ± 0.69***	1468.21 ± 42.44**
PC	6.75 ± 0.82$^{\#\#\#}$	1451.51 ± 79.53
HD	6.95 ± 1.20$^{\#\#\#}$	1560.86 ± 73.42$^{\#}$
MD	5.35 ± 1.09$^{\#\#}$	1541.97 ± 69.12$^{\#}$
LD	5.61 ± 1.01$^{\#\#}$	1448.96 ± 113.31

Compared with the normal group: $^{***}P < 0.001$, $^{**}P < 0.01$, and $^{*}P < 0.05$. Compared with the model group: $^{\#\#\#}P < 0.001$, $^{\#\#}P < 0.01$, and $^{\#}P < 0.05$.

Table 5: Effect of DZMP on the activities of SOD and T-AOC in serum ($n = 10$).

Groups	SOD (U/mL)	T-AOC (mg/mL)
BC	156.25 ± 3.98	0.51 ± 0.04
MC	79.34 ± 12.16***	0.32 ± 0.03***
PC	150.90 ± 10.85$^{\#\#\#}$	0.48 ± 0.06$^{\#\#\#}$
HD	132.81 ± 3.36$^{\#\#\#}$	0.41 ± 0.06$^{\#\#\#}$
MD	119.05 ± 4.28$^{\#\#\#}$	0.37 ± 0.08$^{\#}$
LD	112.04 ± 5.52$^{\#\#\#}$	0.33 ± 0.03

Compared with the normal group: $^{***}P < 0.001$, $^{**}P < 0.01$, and $^{*}P < 0.05$. Compared with the model group: $^{\#\#\#}P < 0.001$, $^{\#\#}P < 0.01$, and $^{\#}P < 0.05$.

Table 6: Effects of DZMP on CAT and MDA activities in the liver tissues ($n = 10$).

Groups	CAT (U/mgprot)	MDA (nmoL/mgprot)
BC	18.50 ± 0.74	0.95 ± 0.08
MC	12.01 ± 0.90***	1.35 ± 0.09***
PC	29.73 ± 0.79$^{\#\#\#}$	1.00 ± 0.05$^{\#\#\#}$
HD	22.81 ± 1.00$^{\#\#\#}$	0.99 ± 0.05$^{\#\#\#}$
MD	20.95 ± 1.12$^{\#\#\#}$	1.04 ± 0.06$^{\#\#\#}$
LD	19.00 ± 0.96$^{\#\#\#}$	1.21 ± 0.09$^{\#\#\#}$

Compared with the normal group: $^{***}P < 0.001$, $^{**}P < 0.01$, and $^{*}P < 0.05$. Compared with the model group: $^{\#\#\#}P < 0.001$, $^{\#\#}P < 0.01$, and $^{\#}P < 0.05$.

2.8.5. MS Analysis. After the liquid phase separation, the peptides were ionized by a nanoESI ion source and then transferred to Q Exactive HF-X (Thermo Fisher Scientific, San Jose, CA) in tandem mass spectrometry for detection in a data-dependent acquisition (DDA) mode. The main parameter was set as follows: the ion source voltage was set to 1.9 kV, the scanning range of primary mass spectrometry was 350~1500 m/z with a resolution of 60,000, and the initial m/z of the secondary mass spectrometry was 100 m/z with a resolution of 30,000. Under the condition of charge from 2^+ to 6^+, the first 20 parent ions with the highest ion peak, the strength of which were over 20,000, were classified as the parent ions of the secondary fragmentation. Ion fragmentation mode was set in HCD, and fragment ions were detected in Orbitrap. In addition, the dynamic exclusion time was set to 30 s and the automatic gain control targets (AGCs) of primary mass spectrometry and secondary mass spectrometry were to 3E6 and 1E5, respectively.

The work from extraction to analysis was done by the BGI Group in Shenzhen.

2.9. Western Blotting. About 30 mg of mouse liver was taken, fully ground in RIPA lysate, and centrifuged at 4°C and 12000 rpm/min for 10 min. The supernatant was taken and the protein concentration was determined by BCA protein quantitative assay kit (Solarbio). Both FcγRIII protein and PKC-α were analyzed by this method.

2.10. SCFAs Were Determined by HPLC. The amount of 0.3 g of the contents of cecum was dissolved into 1 mL deionized water, 5 mL ether was added, and the aqueous phase at the lower layer was discarded for extraction. The solution was reextracted with 500 L, 1 M NaOH, followed by filtration through a 0.22 m filter after adding 100 L HCl. The concentration of SCFAs in cecal contents including acetic acid, propionic acid, and butyric acid was analyzed by a Shimazu LC-20A HPLC with a C18 column according to previous research [30].

2.11. 16S rRNA Sequencing. The combined cecal content (200 mg) was evaluated by Qubit® dsDNA BR Assay Kit for DNA extraction. 30 ng of qualified genomic DNA samples were amplified in V3-V4 regions, and HiSeq platform was selected for sequencing. The DNA extraction and sequencing were carried out by the BGI Group in Shenzhen.

2.12. Bioinformatics and Statistical Analysis. The protein IBT was quantified, and the identified protein and peptide segments were obtained by 1% false discovery rate (FDR) filtration (PSM level:FDR ≤ 0.01). Euclidean distance and a hierarchical cluster method were used to cluster the differential proteins. The obtained differential proteins were

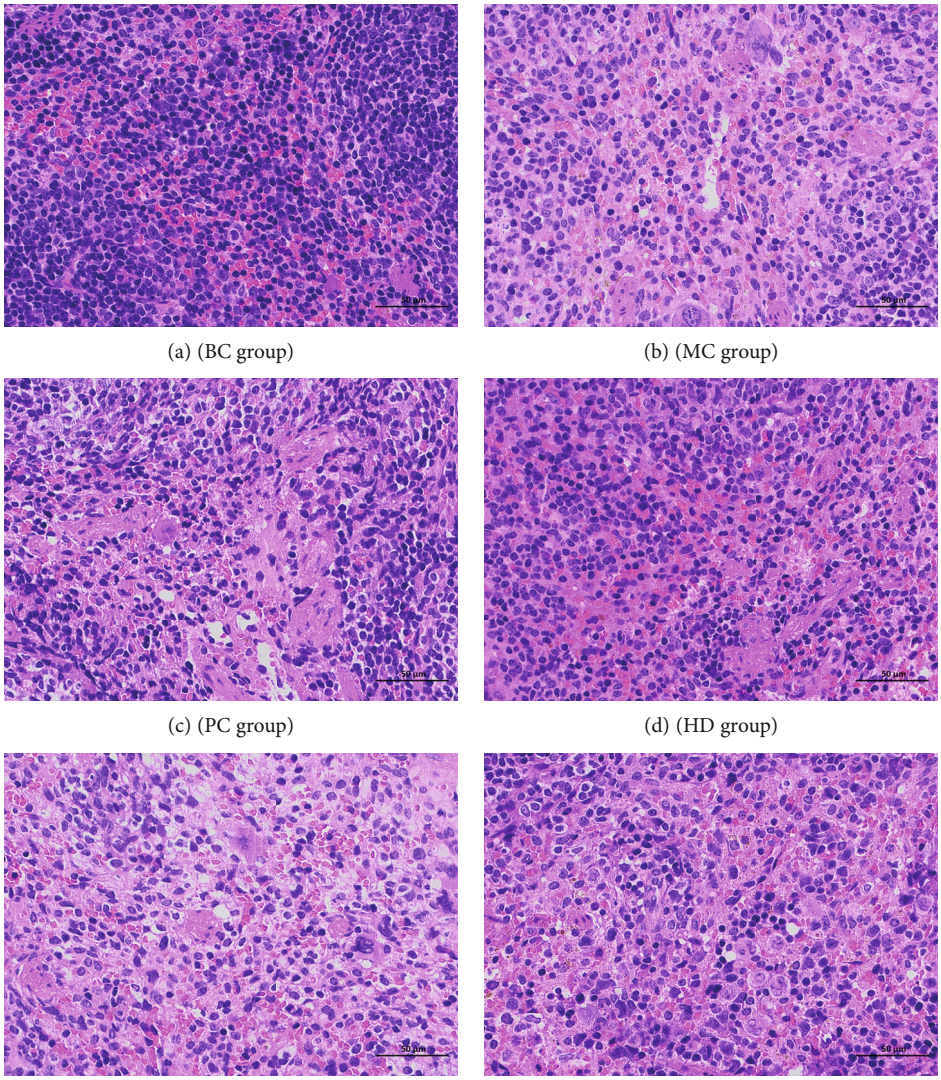

(a) (BC group) (b) (MC group)

(c) (PC group) (d) (HD group)

(e) (MD group) (f) (LD group)

Figure 1: Histopathological section of the spleen (400x).

compared with the NR database, and GO functional annotations were obtained. Besides, the KEGG Pathway Database was used to analyze metabolic abnormalities.

Reads obtained from sequencing cecal contents were spliced in pairs by FLASH software to get tags. After quality screening, OTU clustering was conducted with 97% similarity, and reference database Greengene was used for comparison. The data was analyzed taxonomically by the Ribosomal Database Program (RDP) classifier. Principal component analysis (PCA) was also carried out on the basis of a similarity coefficient matrix, and beta diversity comparison was performed by QIIME (V1.80).

All results were presented as the means ± standard error. Statistical significance was performed by SPSS 19.0 software with a single-factor analysis of variance (one-way ANOVA).

3. Results

3.1. Effects of DZMP on Thymus Index and Spleen Index. In Table 2, the spleen index and thymus index in the MC group were significantly lower than those in the BC group ($P < 0.001$) indicating that the model was successful. Compared with the MC group, the thymus and spleen indexes in the HD group were significantly increased ($P < 0.01$). The thymus index of the MD group and the LD group was higher than that of the MC group, despite at a nonsignificant level.

3.2. Effect of DZMP on Cytokine Content in Mice. In Table 3, the levels of IL-2, IL-4, IL-6, and TNF-α in the MC group were significantly lower than those in the BC group ($P < 0.01$), indicating that CTX could inhibit immune activity. The decreased levels of IL-2, IL-4, IL-6, and TNF-α in mice induced by CTX were improved after the gavage of different doses of DZMP; the HD group especially had the best effect, which was similar to that of the PC group. The results showed that DZMP could improve immunity from the CTX-induced immunosuppressive situation by regulating the level of cytokines.

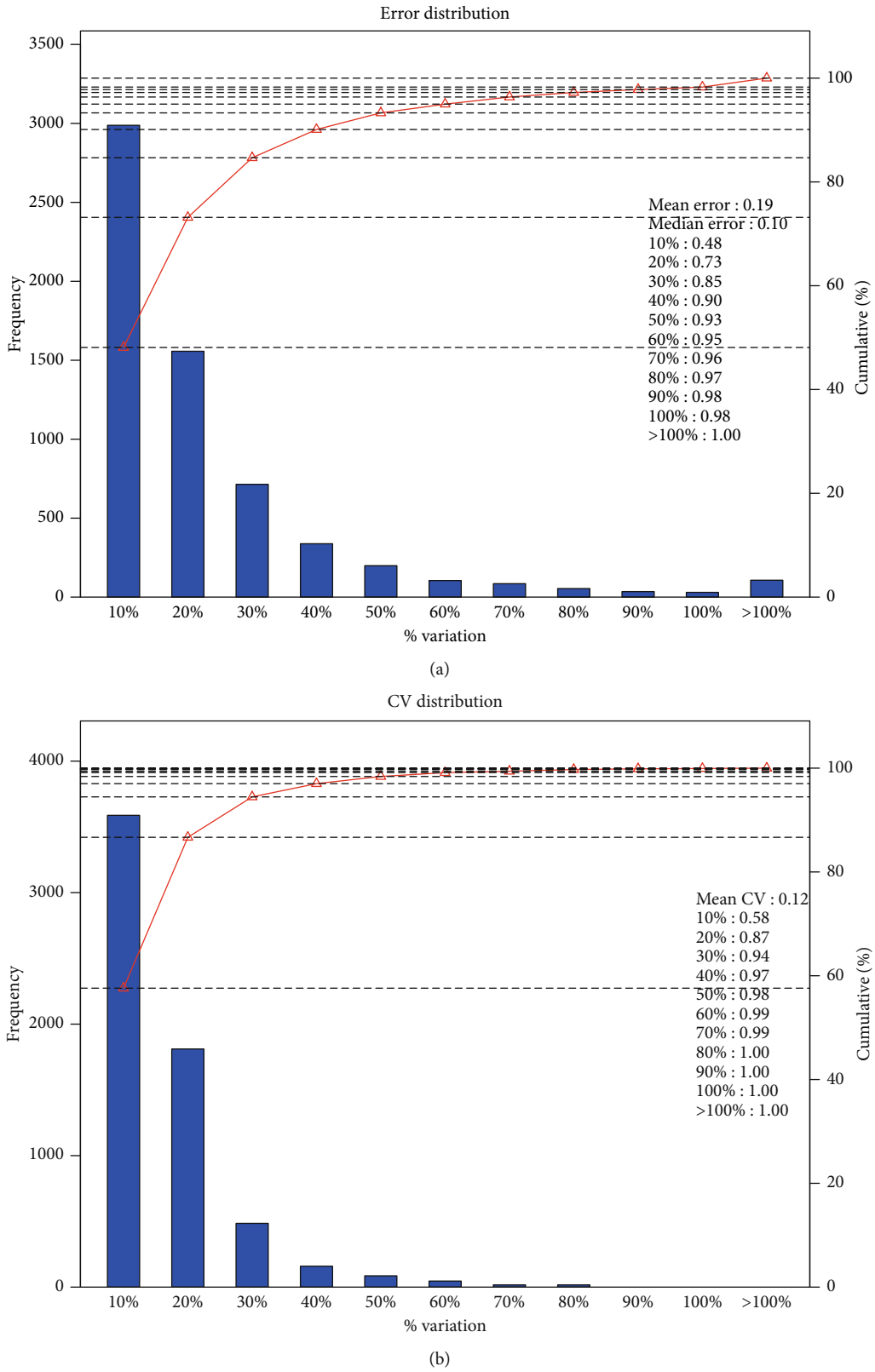

Figure 2: Intragroup and intergroup repeat experiment distribution.

3.3. Effect of DZMP on the Activity of ACP and LDH in Mice. In Table 4, the serum activities of ACP and LDH in the MC group were lower than those in the BC group. After corresponding treatments in the other groups, the activities of ACP in all the other 4 groups were significantly increased ($P < 0.01$) while LDH activities only in the HD and MD

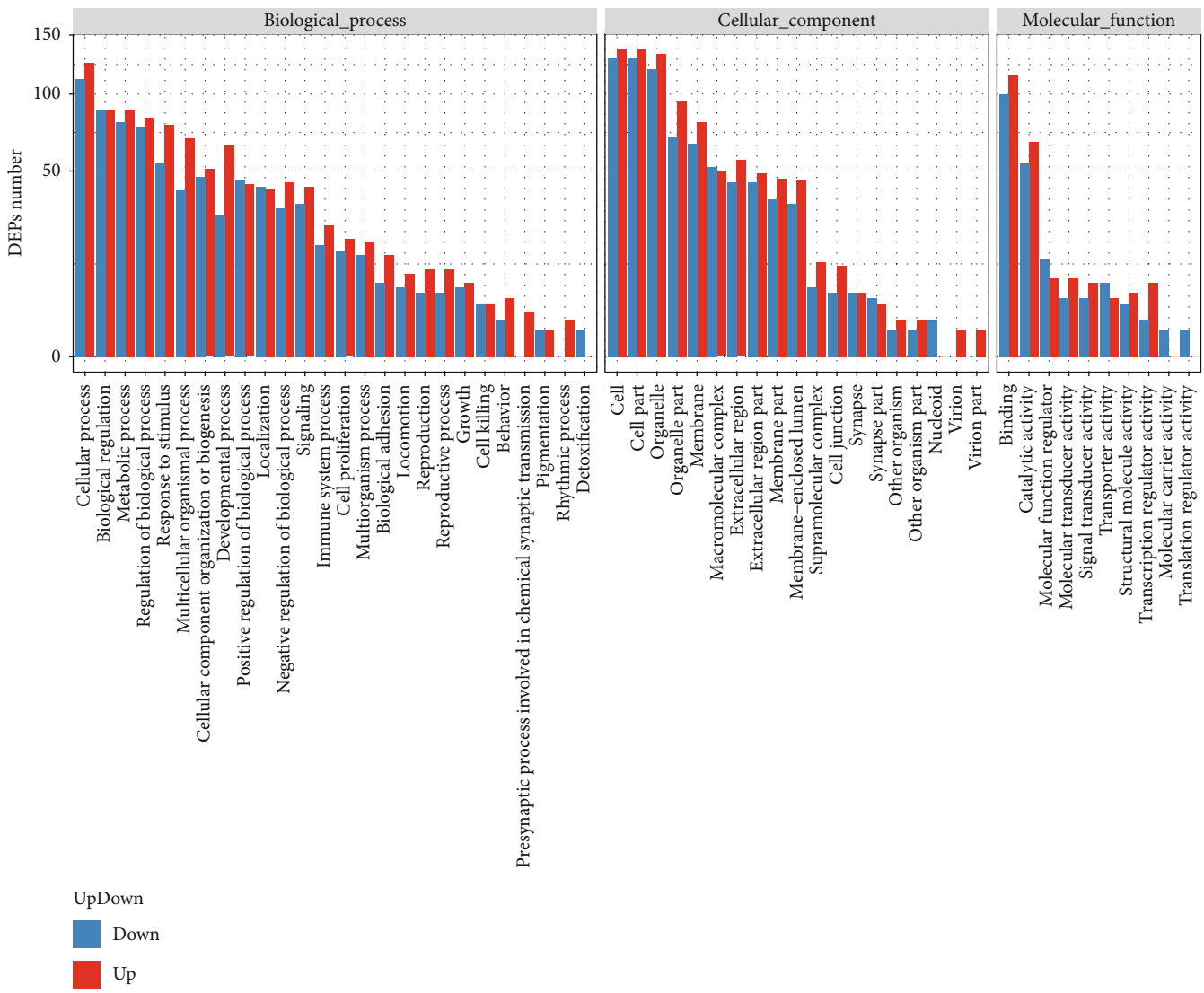

Figure 3: Statistical diagram of downregulated GO functional classification of differential proteins in the MC group and the HD group.

groups were significantly increased ($P < 0.05$). Among them, the activities of LDH in the HD and MD groups as well as ACP in the HD group were higher than that in the PC group. The results indicated that DZMP could significantly enhance the activity of ACP and LDH in mice.

3.4. Effect of DZMP on Antioxidant Capacity of Mice. In Table 5, SOD and T-AOC in the MC group were significantly lower than those in the BC group ($P < 0.001$), indicating that the antioxidant capacity was successfully inhibited by CTX. Both SOD and T-AOC activities showed a close level among the PC, HD, and BC groups. Therefore, compared with the MC group, administration with high-dose DZMP could almost recover the activities of SOD and T-AOC ($P < 0.001$). In addition, SOD activity in the MD and LD groups was also increased significantly ($P < 0.001$).

In Table 6, compared with the BC group, CAT activity in the MC group was significantly decreased ($P < 0.001$) and MDA activity was significantly increased ($P < 0.001$), indicating that the model was established. Compared with the MC group, the CAT activity of the PC group fed with *Lentinula edodes* polysaccharide tablets was the highest, followed by the HD, MD, and LD groups, which were all significantly higher than that of the MC group ($P < 0.001$). Meanwhile, the MDA activities of these groups were significantly lower than that of the MC group ($P < 0.001$) and the MDA content of the HD group was as low as the PC group. Thus, DZMP has antioxidant ability.

3.5. Effect of DZMP on Pathological Changes of Immune Organs in Mice. In Figure 1, spleen tissues of mice in the BC group were in normal shape, with no abnormal cell arrangement, while there had been disordered cell arrangement and a reduced number in the MC group. Compared with the MC group, administration of DZMP in the HD, MD, and LD groups increased the cell density and the cells were closely and orderly arranged. This result indicated that the DZMP could alleviate the injury of immune organs caused by CTX.

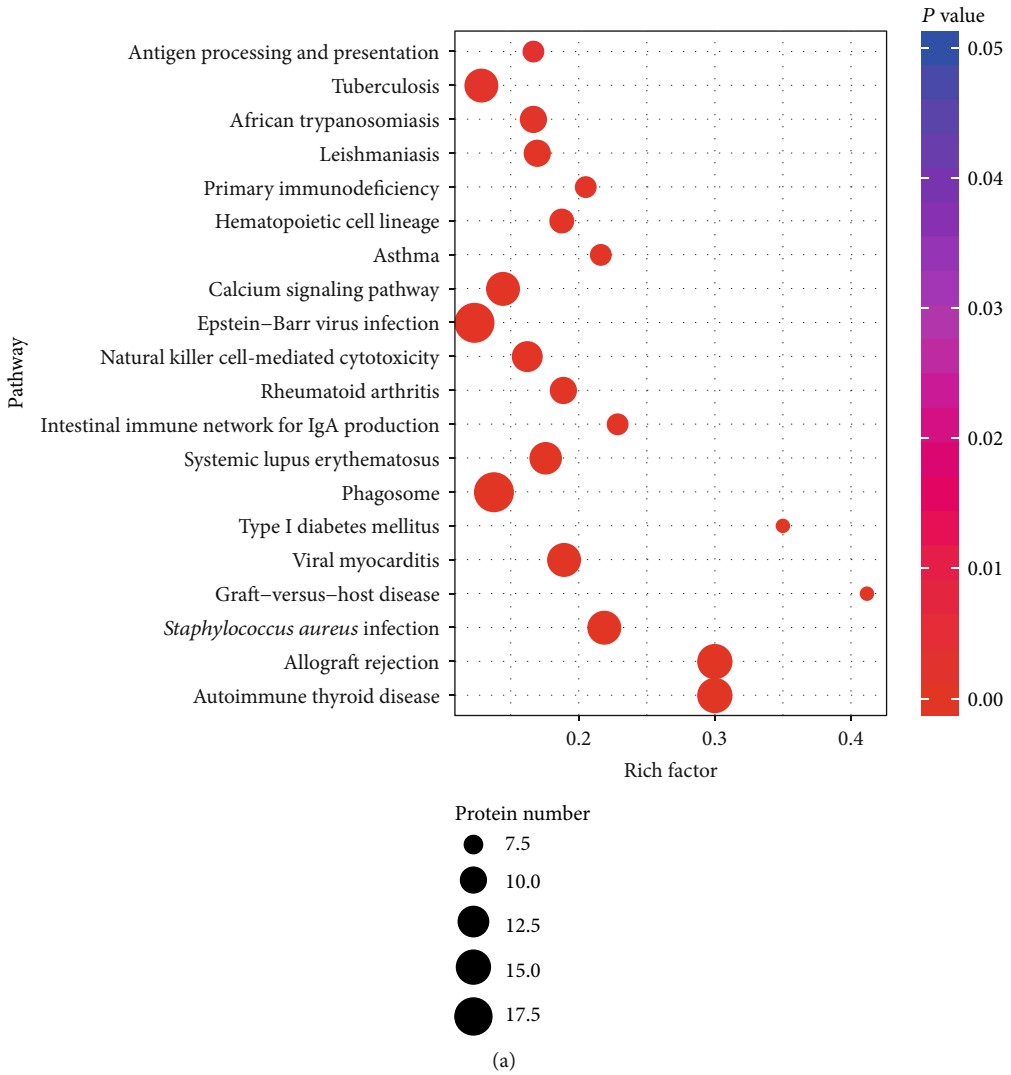

(a)

Figure 4: Continued.

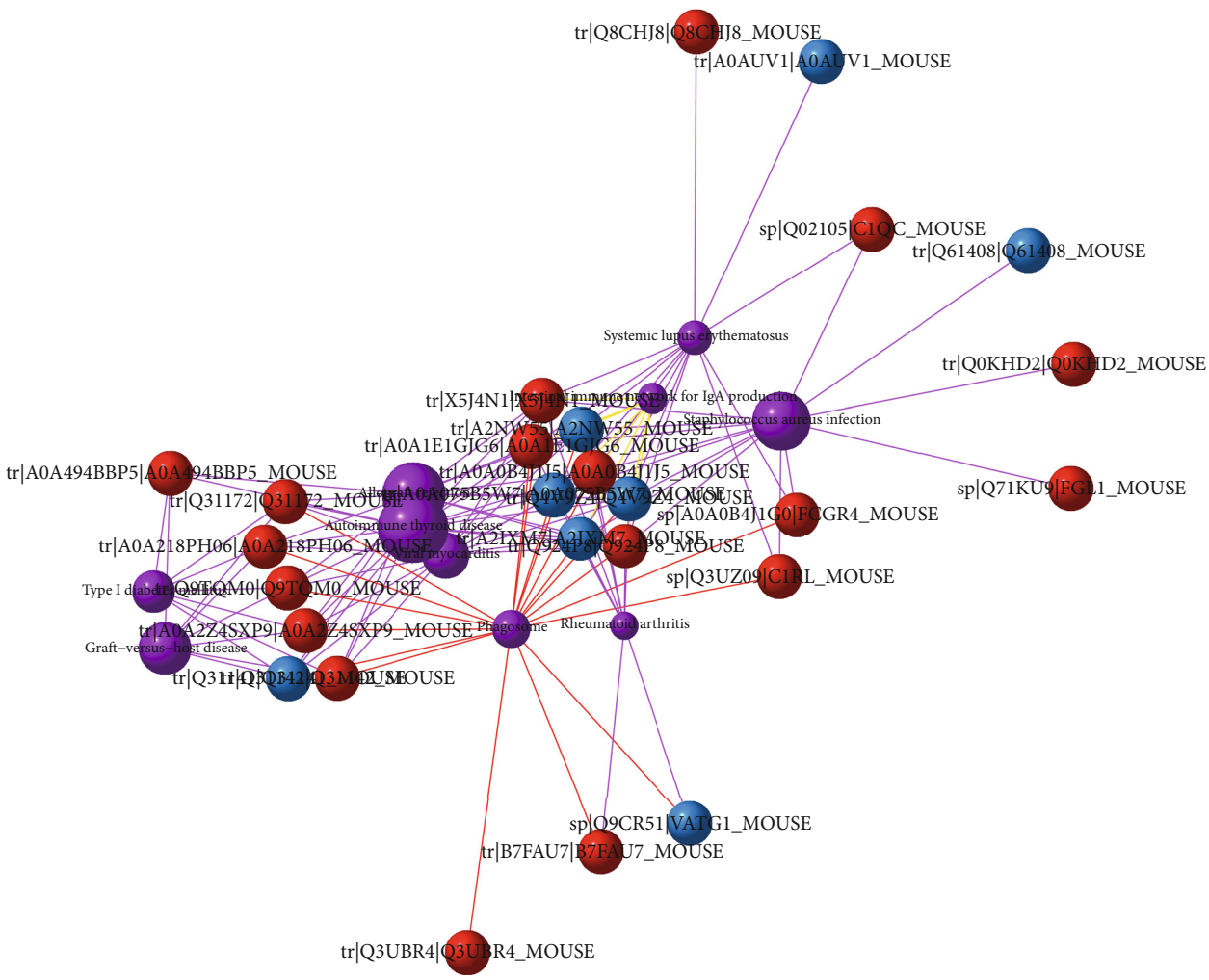

(b)

Figure 4: Pathways of significant enrichment (a) and the relationship network diagram (b) of the HD and MC groups. The purple balls are the top 10 enriched pathways, and the relative area of each ball is the richness of the corresponding pathway. The red balls and blue balls are the upregulation and downregulation differential proteins, respectively.

3.6. Enrichment Analysis of Differential Protein Function. There were a total of 9 samples with functional enrichment of differential proteins, which symbiotically formed 718,399 secondary spectrograms. A total of 36,679 peptides and 6229 proteins were identified under the "1% FDR" filtration standard. In Figure 2, the mean error value in the group was 0.19 and the mean CV value between the groups was 0.12. Moreover, the protein with a CV value less than 20% accounted for 87%, indicating that the biological repeatability between the sample groups was good. The differential proteins among different groups were screened by differential multiples and significance. Based on the functional enrichment analysis results of differential protein, it could indicate that FcγRIII and PKC-α mediate the effect among multiples.

Cluster analysis was carried out for GO entries with significant enrichment. In Figure 3, most of the differentially expressed proteins in the MC group and the HD group were in the biological process, cell component, and molecular function, and the most significant differences were cellular process, cell component, and binding, respectively.

The differentially expressed proteins in the HD and MC groups were mainly involved in 20 KEGG pathways, and about 10-45 differentially expressed proteins were involved in each pathway (Figure 4(a)). Figure 4(b) shows that protein upregulation was the majority in the top 10 enriched pathways. RichFactor is a parameter calculated by dividing the number of annotated differentially expressed proteins into all proteins identified in this pathway, and the higher the RichFactor is, the greater the proportion of differential proteins in the pathway is. In Figure 4, the four pathways, graft versus host disease, type I diabetes mellitus, allograft rejection, and autoimmune thyroid disease, owned the highest differential protein proportion, while Epstein-Barr virus infection, phagosome, and tuberculosis were the pathways with the highest number of different proteins. To analyze the interaction among differential proteins, they were imported into STRING, a protein interaction database, and

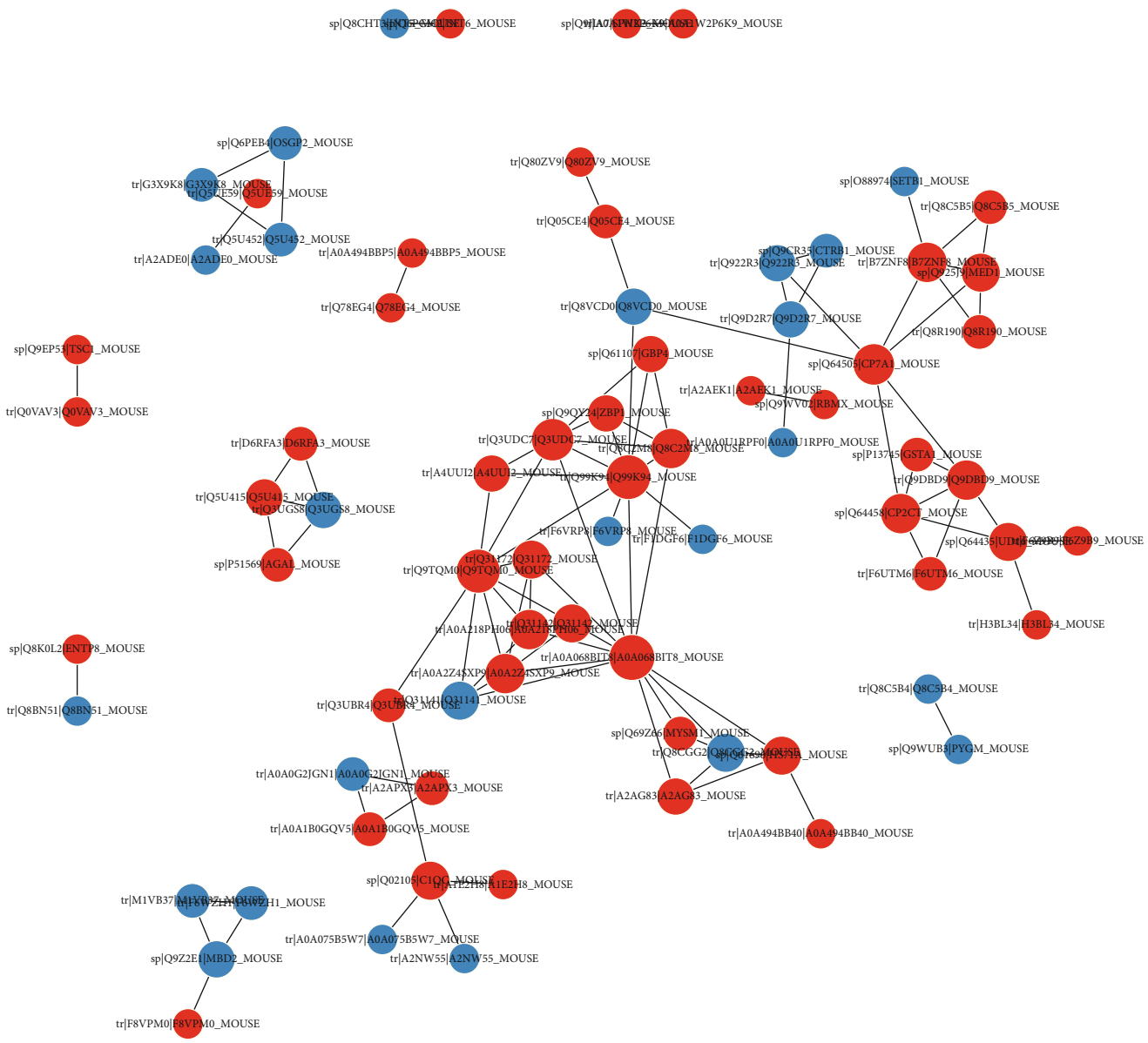

Figure 5: Network diagram of the differential protein interaction between the HD and MC groups.

compared. The protein interactions ranking at the top 100 in trustworthiness were plotted in Figure 5.

The proteins could participate in the various life activities of the cell only when they are transported to the right places after they are synthesized in the ribosome. WoLF PSORT and PSORTb were used to predict the subcellular location of proteins for eukaryotes and prokaryotes, respectively. In Figure 6, the subcellular localization results of HD and MC differential proteins reveal that the differential proteins were more widely distributed in the nucleus (nucl), cell fluid (cyto), extracellular fluid (extr), mitochondria (mito), and plasma membrane (plas).

3.7. Protein Validation. The results of FcγRIII and PKC-α protein in Figure 7 show that the protein expression in the MC group was significantly lower than that in the BC group. Compared with the MC group, the HD group significantly increased protein expression and it was consistent with the results of proteomics.

3.8. Evaluation of Microbial 16S rRNA Gene Sequencing. After gene sequencing and data quality filtering, a total of 2,301,428 high-quality readings were obtained, and about 1143,329 tags were spliced together. These tags were clustered into OTUs with 97% similarity, and a total of 756 OTUs were obtained. In Figure 8(a), the transverse bend line was wider, and the line eventually tends to be flat, indicating that the species composition in the tested samples was abundant and uniform. In Figure 8(b), the rising trend at the top of the OTU accumulation curve was gradually stable, indicating that the amount of sampling was sufficient to represent the community structure of the sample community in this experiment, and following data analysis was feasible.

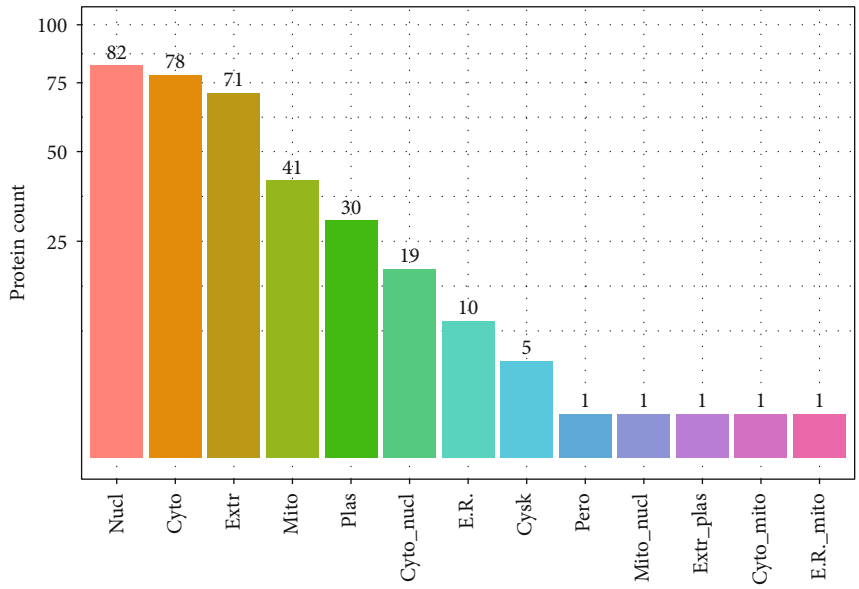

Figure 6: Histogram of subcellular localization of HD and MC differential proteins. nucl: nucleus; cyto: cytosol; extr: extracellular; mito: mitochondria; plas: plasma membrane; E.R.: endoplasmic reticulum; cysk: cytoskeleton; pero: peroxisome.

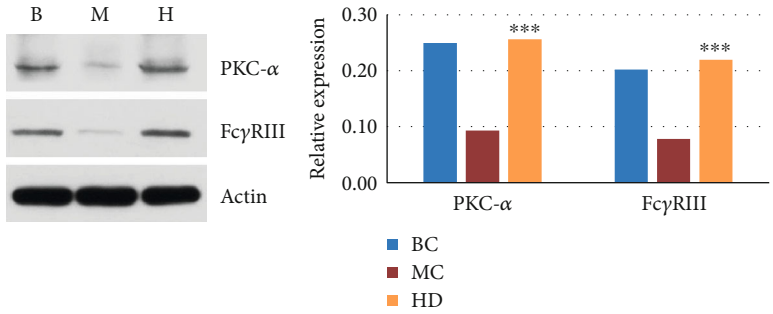

Figure 7: FcγRIII protein and PKC-α are expressed in different groups of the liver.

The microbial communities in different environments have certain similarity and specificity in species distribution. According to the OTU abundance information, Venn diagram analysis was performed to compare the commonness or uniqueness of OTUs between different groups. In Figure 9, each group had its special community representation. Among them, the BC group and the HD group had more specific OTUs than that of the MC group.

The analysis results of alpha diversity and beta diversity are shown in Figures 10 and 11, respectively. In Figure 10, the observed species index, Chao1 index, ACE index, and Shannon's index of the BC, LD, and MD groups were all higher than that of the HD, MC, and PC groups. It indicated that species richness was lower in the HD, MC, and PC groups. Good's coverage value of each group was higher than 99%, indicating that the sample library had a high coverage rate and the sequencing results were reliable and feasible. The similarity or difference of the composition of the sample flora is presented by principal component analysis in Figure 11(a). The results showed that the first principal component accounting for 47.35% was contributed mainly by the HD group. The results of hierarchical clustering (Figure 11(b)) showed that the microbial communities of each treatment group were close to each other on the whole, while the MC group was far away from the HD group.

In order to better identify the community composition of each sample, the taxonomic analysis of the microflora information was carried out. In Figure 12, *Firmicutes* and *Bacteroidetes* were the two dominant bacteria groups in the samples, accounting for about 85%~95% of all bacteria, followed by *Proteobacteria*. Observation showed that the relative abundance of *Firmicutes* and *Bacteroidetes* in the BC group (72.09%, 20.77%) was close to that of the corresponding bacteria species in the MC group (74.36%, 20.71%), indicating that the intra-abdominal injection of CTX had little impact on the two dominant bacteria groups. In the HD group, the relative abundance of *Firmicutes* decreased obviously (50.78%), while that of *Bacteroidetes* and *Proteobacteria* increased relatively (35.17%, 6.86%), compared with the BC group.

The species information of all samples detected at the genus level is plotted as a cluster heat map. In Figure 13,

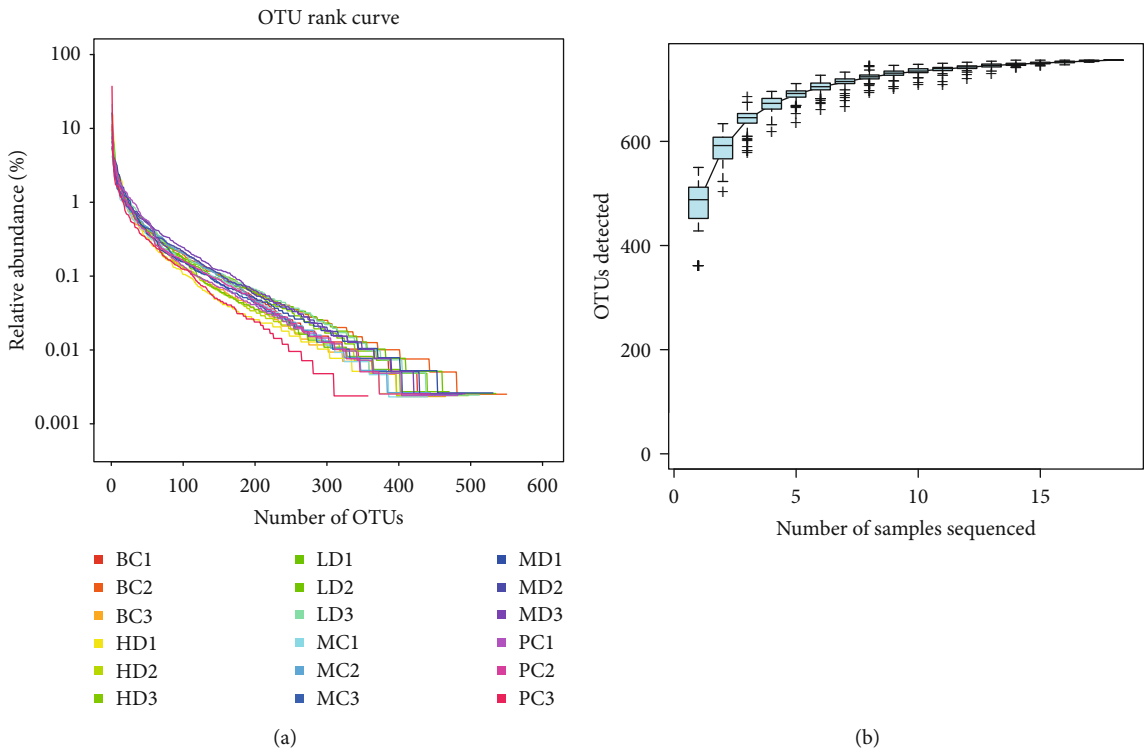

Figure 8: OTU rank curve (a) and OTU cumulative curve (b).

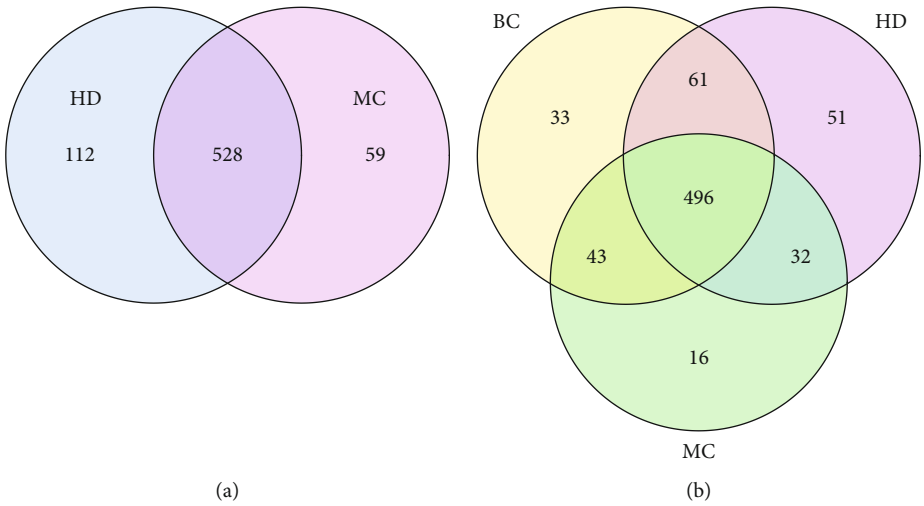

Figure 9: OTU Venn figure: comparison of the species similarity or specificity between groups.

the two genera with the highest relative abundance were *Oscillospira* and *Prevotella*, followed by *Ruminococcus* and *Bacteroidetes*. The relative abundance of *Proteobacteria* in the HD group was higher than that in BC group. At the same time, the relative abundance of *Bacteroides*, *Paraprevotella*, *Akkermansia*, *Roseburia*, *CF231*, *Helicobacter*, *Sutterella*, and *Coprobacillus* in the HD group were much higher than that in the MC group, while that of *Ruminococcus* and *Oscillospira* in the HD group were lower.

3.9. Effect of DZMP on SCFA Content. In Figure 14, compared with the BC group, the contents of acetic acid, propionic acid, and butyric acid in MC were significantly reduced, while the contents in the HD and PC groups were close to that in the BC group and significantly higher than that in the MC group. The results indicated that DZMP and *Lentinula* polysaccharide had a strong influence on the SCFA contents.

4. Discussion

Immune response is a series of immune reactions of the immune active cells in the immune system, including recognition of external stimuli as well as its activation,

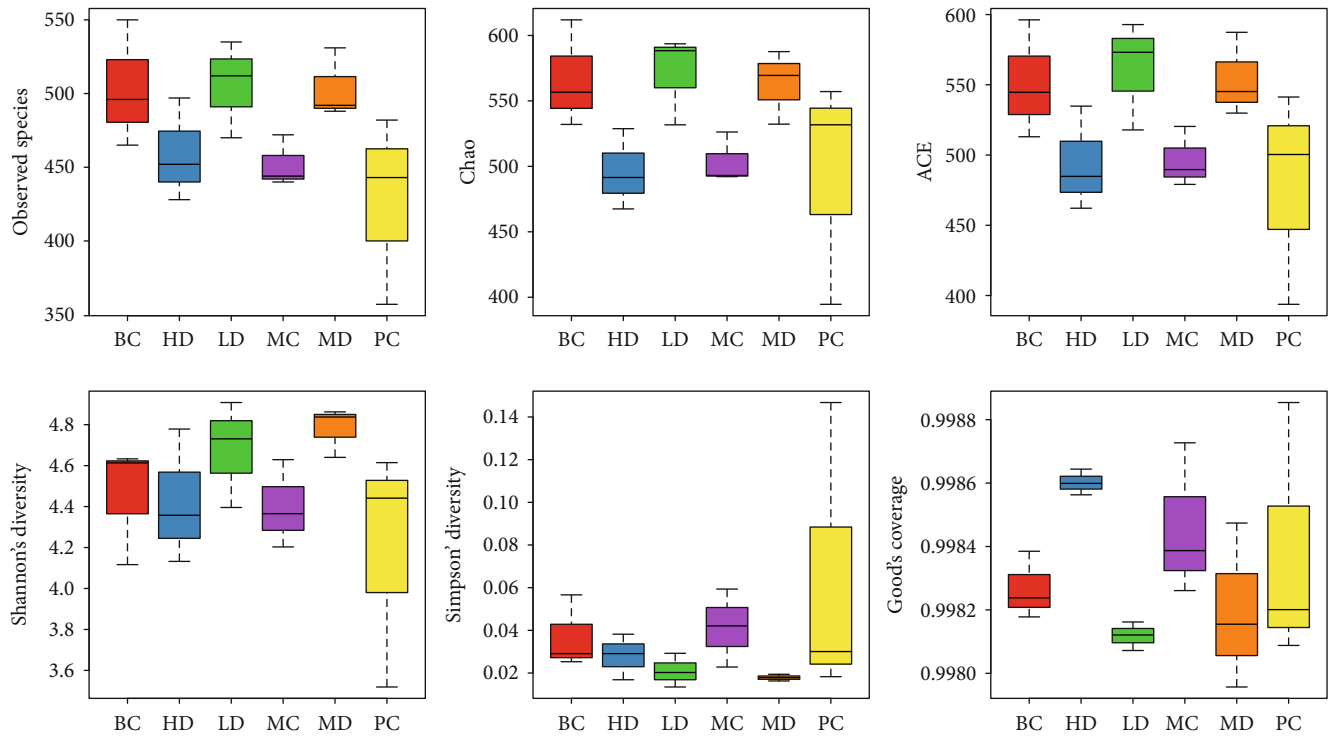

Figure 10: Alpha diversity box.

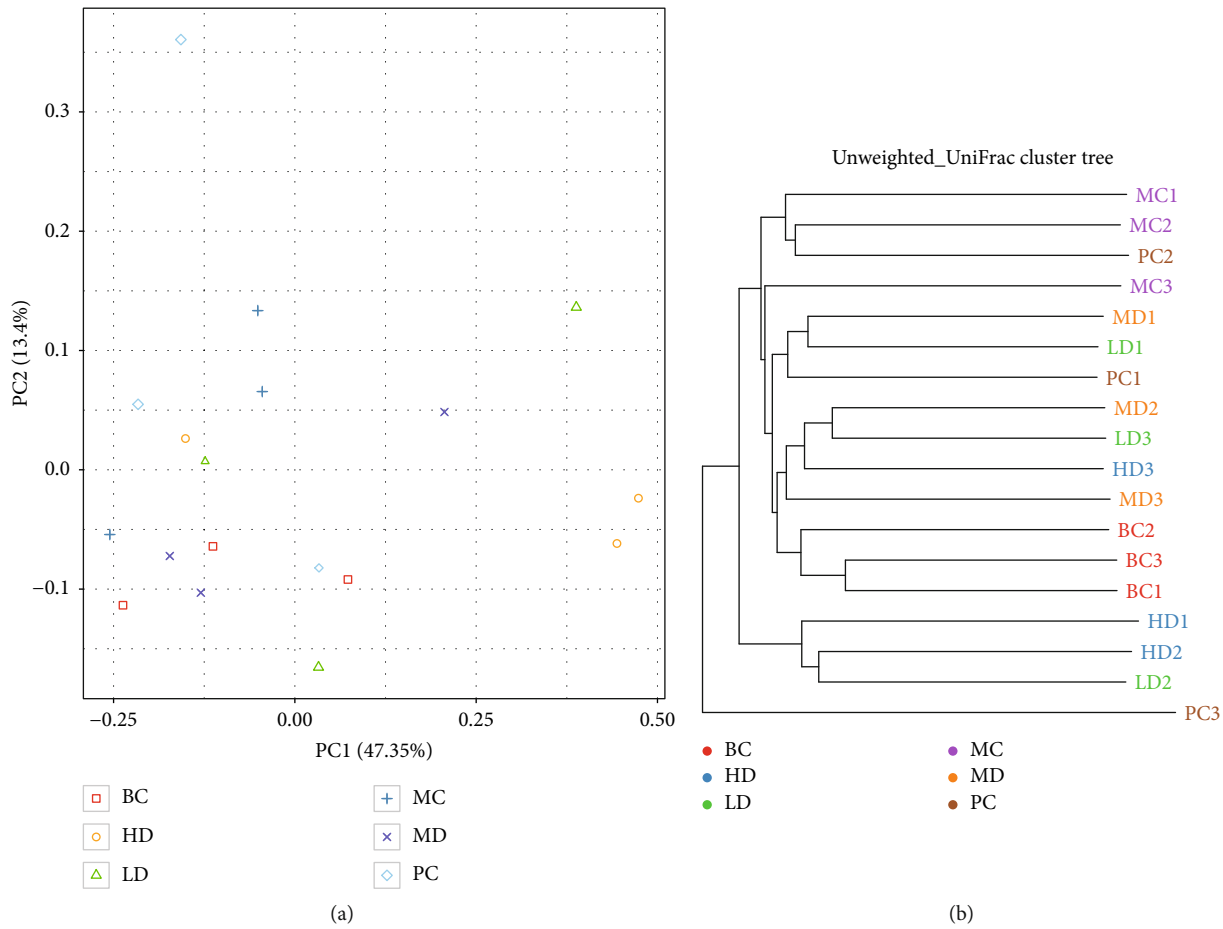

Figure 11: Beta diversity analysis. (a) Principal component analysis diagram. (b) Sample clustering tree (unweighted).

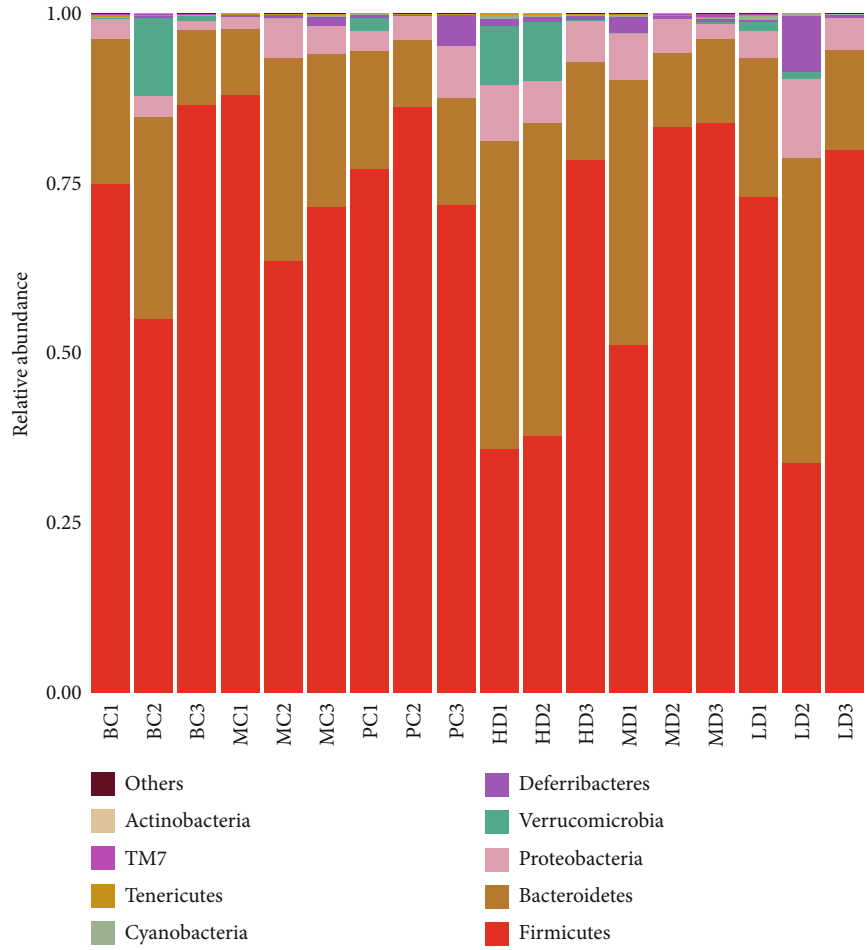

Figure 12: Relative abundance of major bacteria at phylum level.

proliferation, and differentiation [32–34]. Immune organs, including the thymus, spleen, and bone marrow, are important for the proliferation and growth of human immune cells. The changes of the thymus and spleen indexes can reflect intuitively the immune function of the body, and the decline of immune function usually accompanies with the shrinkage of immune organs [35]. Previous studies have shown that *Citrus pericarp* and *Litchi pulp* polysaccharides could significantly improve the thymus and spleen indexes in mice [36, 37]. In this experiment, the thymus and spleen indexes of mice were significantly decreased in the MC group, while they were significantly raised after the treatment of DZMP in the HD group, indicating that DZMP can alleviate CTX damage to the thymus and spleen and enhance the immune ability of the body.

Macrophages, an important type of immune cell, can participate in the immune response and protect the normal operation of the body by identifying antigens, killing/engulfing foreign pathogens, releasing cytokines, or secreting cytotoxic molecules after being activated [38]. The activity of ACP and LDH can directly reflect the activation of macrophages [39, 40]. In this study, ACP and LDH activities were significantly enhanced in the HD and MD groups compared with the MC groups. The results showed that DZMP could regulate the activities of LDH and ACP in mice and activate macrophages to participate in immune response. Previous studies have shown that cytokines have multiple immune functions [41]. In this experiment, IL-2, IL-4, IL-6, and TNF-α in the MC group were significantly decreased, indicating that CTX had an immunosuppressive effect, which was consistent with the results of Tang et al. [42]. The Th1 and Th2 subgroups of mice can secrete IL-2 and IL-4, respectively, and both IL-2 and IL-4 can promote the proliferation of T cells [43, 44]. In addition, IL-4 can also promote the expression of B cells, enhance the antigen presentation ability of B cells, increase IgG1 and IgE levels, and make the responses of immune system to antigen stimulation [45, 46]. Gong et al. found that *Bletilla baicalensis* polysaccharides could significantly enhance the levels of IL-2 and IL-4 in immunosuppressed mice [47] which is similar with the effect of DZMP in this paper. TNF-α and IL-6 are the major cytokines in macrophages. TNF-α, as a proinflammatory cytokine, can directly kill tumor cells [48], while IL-6 can promote the proliferation and differentiation of lymphocytes [49], and both of them play important roles in a variety of immune responses. The results of this experiment showed that DZMP could significantly increase the levels of IL-2, IL-4, IL-6, and TNF-α in serum of mice, thus playing an immunomodulation role.

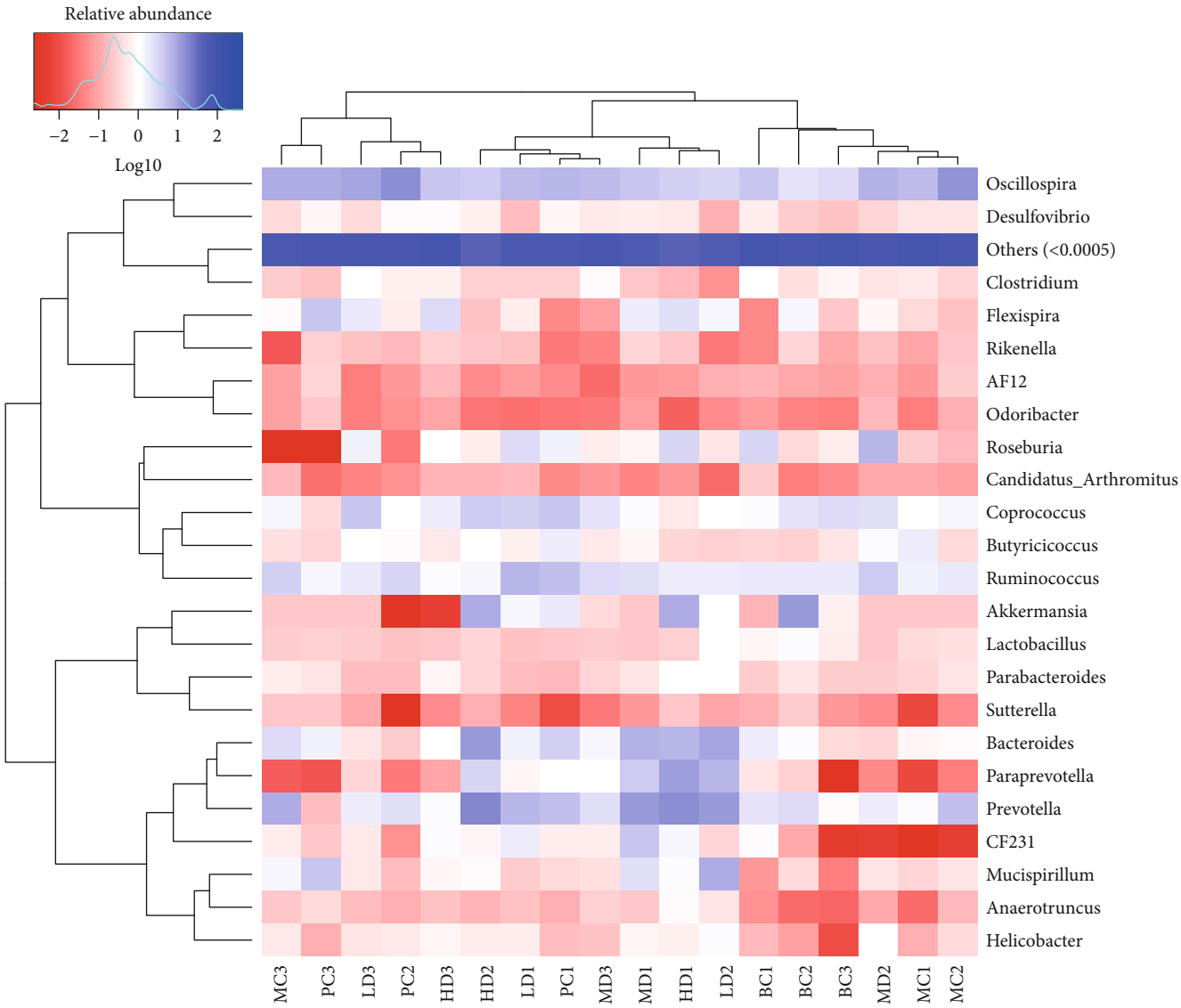

Figure 13: Relative abundance heat map of flora at genus level.

The liver is an important metabolic organ with a strong function of biotransformation [50]. The cytotoxicity of many chemotherapeutic drugs in the metabolic process of the body can easily cause organic damage to the liver as well as the activities of metabolic enzymes [51–53]. CTX is mainly converted into 4-hydroxycyclophosphamide and aldehyde phosphamide by CYP450 enzymes in the liver, and then distributed throughout the body. After that, CTX can enter target cells and alkylate DNA, generating strong cytotoxicity [50, 54]. Clinically, polysaccharides are often used as adjuvant drugs together with chemotherapy drugs to reduce their toxicity, improve the body's immunity, and strengthen the recovery [55–57]. Polysaccharides usually have many pharmacological activities, like multitargets and wide effects [22, 58]. For this reason, proteomics technology was used for the expression of proteins at the whole gene level, and IBT quantitative analysis for the key differential proteins, so as to provide analytical basis for studying specific drug action protein targets and their interactions. In this study, the differential proteins of untreated, immunosuppressed, and DZMP-treated mice were compared to find the protein targets.

The results showed that FcγRIII and PKC-α exerted regulatory effects on multiple pathways. FcγRIII consists of CD16a and CD16b, expressed by FcγR NK cells, and some other immune cells [59]. Both CD16a and CD16b can bind to IgG, a monomer on target cells, which plays an important role in the clearance of immune complexes and the function of NK cells, respectively [60, 61]. Both of the subtypes can rapidly undergo proteolysis when neutrophils and NK cells are subjected to various stimuli, and fall off from the surface of human white blood cells [62, 63]. Studies have shown that CTX can enhance the phagocytic activity of macrophages to treat tumors by upregulation of FcγRIII [64]. In this study, compared with the MC group, the expression of the FcγRIII receptor in the treatment group was significantly upregulated, providing a theoretical basis for the function of DZMP in the treatment of cancer. Protein kinase C (PKC) is a type of multifunctional enzyme involved in the regulation of

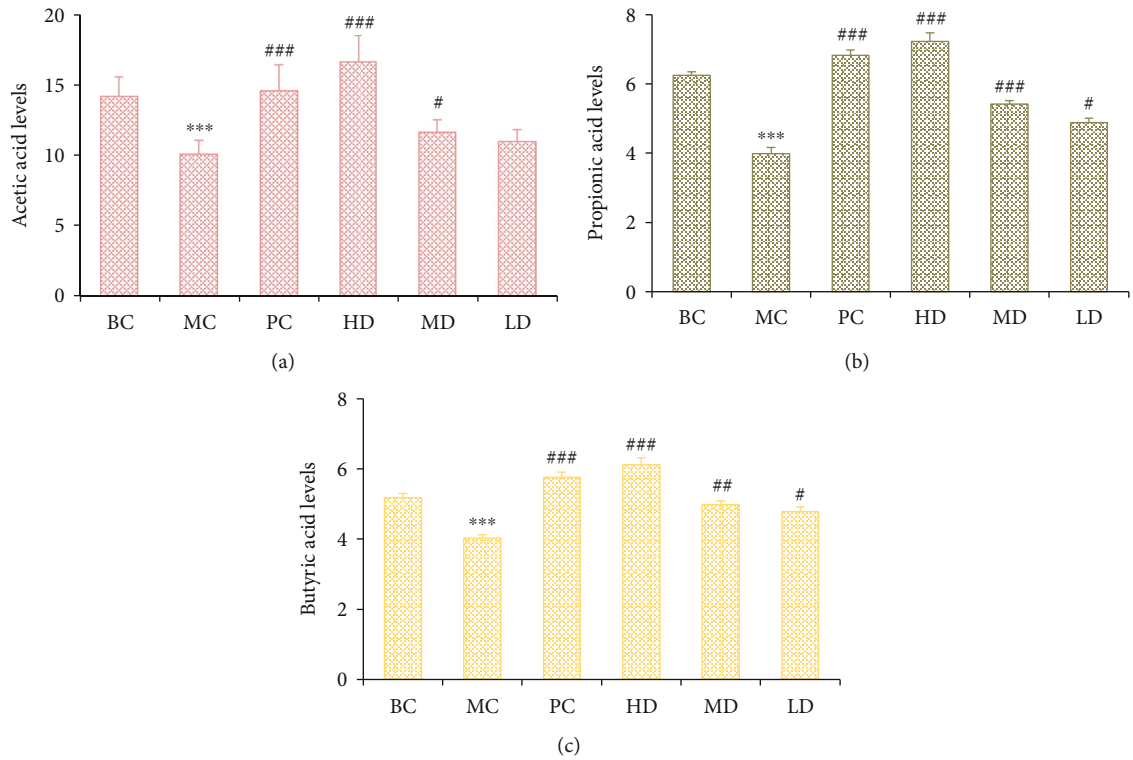

Figure 14: Acetic acid content in samples from each group (a), propionic acid content in each group (b), and butyric acid content in each group (c).

biochemical reactions by activating some enzymes in the cytoplasm. Meanwhile, it also acts on transcription factors in the nucleus and participates in the regulation of gene expression. Das et al. evidenced that PKC participated in the host protective immune response through the TLR2/PKC signal crosshair by the pretreatment of a TLR2 agonist, an Arabinosylated lipoarabinomannan (Ara-LAM), which could significantly increase the expression of conventional PKC in infected macrophages [65]. Mohammd et al. have shown that the extract of PKC has a probiotic and immunomodulatory effect on rats and enhances the antioxidant capacity of the rats' liver [66]. There are three isoforms, PKC-α, PKC-β, and PKC-θ, contributing to the nature of lymphocyte-specific effector responses *in vivo* [67]. Take PKC-α for example, acid phosphatase can activate its immune-stimulating activity by phosphorylating it [68]. In this study, the expression of PKC-α was increased in the HD group of DZMP. The above results indicated that DZMP might play a role in the immune regulation by upregulating the expression of FcγRIII and PKC-α to regulate the drug metabolism-related pathways such as autoimmune disease, *Staphylococcus aureus* infection, and the NF-κB signaling pathway.

The coexisting flora of the human gastrointestinal tract constitutes a relatively stable microecosystem. Rehman et al. proposed that the change of intestinal flora species number was related to the abnormal immune function [69]. Many previous studies also showed that probiotics combined with drugs could better treat gastritis, inflammatory bowel disease, allergic asthma, and other diseases in children, and enhance the immune function of the body [70]. Natural plant polysaccharides are one type of probiotics, which has been proven to regulate the physiological and immune functions of the body as well as improve the structure and composition of flora, and maintain the balance of intestinal microorganisms [14, 67–74]. The results of this study showed that the number of specific OTUs in the HD group was significantly higher than that in the MC group and its alpha diversity index is lower than that of the BC group, which revealed the regulation effect of DZMP on the dominant bacteria in the HD group.

In order to more accurately determine the changes in the composition of the intestinal microflora, the related assessments were carried out at different taxonomic levels. The research results show that *Firmicutes* and *Bacteroidetes* are two dominant bacteria, which promote polysaccharide metabolism through carbohydrate enzymes and enable the host to absorb and store energy [75, 76]. Turnbaugh et al. showed that the relative abundance of *Firmicutes* to *Bacteroidetes* in the intestinal flora of obese mice increased while that of *Bacteroidetes* decreased [77]. In our study, a high dose of DZMP can significantly reduce the relative abundance of *Firmicutes* and increase the relative abundance of *Bacteroidetes*, playing a beneficial regulatory role in the intestinal flora.

Plant polysaccharides also have beneficial effects on microbial fermentation of carbohydrates, such as short-chain fatty acids (SCFAs), which regulate body health [78, 79]. During the digestion of plant fibers, a particular genus of bacteria (*Roseburia*) in the gut can produce butyrate, which has been proven to be the main source of metabolic

energy of large intestine cells, helping to maintain normal metabolism of large intestine cells, control intestinal inflammation, and support genomic stability [80, 81]. Propionate, mainly produced by *Bacteroides*, a symbiotic bacterium in the human intestinal tract, can reduce the degradation of fat, the level of serum cholesterol, and the carcinogenic effect of other tissues [81, 82]. *Prevotella* and *Coprococcus* can degrade carbohydrates and polysaccharides to protect intestinal health [83–85]. *Prevotella* is also involved in the synthesis of multivitamins [86]. *Akkermansia* is a beneficial bacterium, which can reduce the risk of obesity, diabetes, inflammation, and other diseases, and maintain intestinal health [87–89]. In this paper, compared with the MC group, the relative abundance of *Bacteroides*, *Prevotella*, *Coprococcus*, and *Akkermansia* as well as the content of SCFAs in the HD group were significantly increased, which were consistent with the results of these mentioned study. Besides, *Ruminococcus* which was known to produce the acetic acid and formic acid and upregulate the barrier function of host intestinal epithelial cells was downregulated after the treatment of DZMP in this paper [90, 91]. Similarly, the relative abundance of *Oscillospira*, which was directly proportional to health [92, 93], increased in the MC group (consistent with the study of Tang et al. [42]) and decreased after the treatment of DZMP in the HD group (slightly higher than that in the BC group). All these above results showed the balance effect of DZMP on these intestinal florae in mouse intestinal tract.

5. Conclusion

DZMP can protect the immune organs of immunosuppressive mice, improve the content of mice immune factors, enhance the antioxidant capacity, change the content of SCFAs, upregulate FcγRIII and PKC-α protein expression, promote energy metabolism, balance the flora composition, maintain intestinal health, and play a role of immune regulation. Based on the results of this study, we will further explore the targeting role of the polysaccharides in immune-related metabolic pathways, and the regulation mechanism of probiotic *Akkermansia* on immunity.

Data Availability

The data used to support the findings of this study are included within the article.

Conflicts of Interest

All the authors declare that there is no conflict of interests regarding the publication of this paper.

Authors' Contributions

Huimin Jiang and Jinmei Wang contributed equally to this work.

Acknowledgments

We would like to thank all participants in the study. This work is supported by the Research Unit of Digestive Tract Microecosystem Pharmacology and Toxicology, Chinese Academy of Medical Sciences and the CAMS Innovation Fund for Medical Sciences (2019-I2M-5-055).

References

[1] D. Blau, "Contributions to the psychobiology of aging," *Psychosomatic Medicine*, vol. 29, no. 2, pp. 194-195, 1967.

[2] R. J. Vagnozzi, M. Maillet, M. A. Sargent et al., "An acute immune response underlies the benefit of cardiac stem cell therapy," *Nature*, vol. 577, no. 7790, pp. 405–409, 2020.

[3] A. T. Springer, "Adhesion receptors of the immune system," *Nature*, vol. 346, no. 6283, pp. 425–434, 1990.

[4] J. P. Bourgault, K. R. Trabbic, M. Shi, and P. R. Andreana, "Synthesis of the tumor associative α-aminooxy disaccharide of the TF antigen and its conjugation to a polysaccharide immune stimulant," *Organic & Biomolecular Chemistry*, vol. 12, no. 11, pp. 1699–1702, 2014.

[5] T. Ohta, K. Kusano, A. Ido, C. Miura, and T. Miura, "Silkrose:: a novel acidic polysaccharide from the silkmoth that can stimulate the innate immune response," *Carbohydrate Polymers*, vol. 136, pp. 995–1001, 2016.

[6] S. Zhang, S. Nie, D. Huang, J. Huang, Y. Feng, and M. Xie, "A polysaccharide from *Ganoderma atrum* inhibits tumor growth by induction of apoptosis and activation of immune response in CT26-bearing mice," *Journal of Agricultural and Food Chemistry*, vol. 62, no. 38, pp. 9296–9304, 2014.

[7] Y. Wu, Y. Y. Li, C. Liu et al., "Structural characterization of an acidic Epimedium polysaccharide and its immune-enhancement activity," *Carbohydrate Polymers*, vol. 138, pp. 134–142, 2016.

[8] Y. Y. Niu, J. Dong, H. M. Jiang et al., "Effects of polysaccharide from *Malus halliana* Koehne flowers in cyclophosphamide-induced immunosuppression and oxidative stress on mice," *Oxidative medicine and, cellular longevity*, vol. 2020, pp. 1–10, 2020.

[9] P. R. Desai, H. Tegtmeyer, G. F. Springer, S. Metcalfe, and R. J. Svvennsen, "Intestinal flora, carcinomata and erythrocytes evoke anti-Tn antibodies," *Naturwissenschaften*, vol. 74, no. 5, pp. 247-248, 1987.

[10] L. Wen, R. E. Ley, P. Y. Volchkov et al., "Innate immunity and intestinal microbiota in the development of type 1 diabetes," *Nature*, vol. 455, no. 7216, pp. 1109–1113, 2008.

[11] K. Honda and K. Takeda, "Regulatory mechanisms of immune responses to intestinal bacteria," *Mucosal Immunology*, vol. 2, no. 3, pp. 187–196, 2009.

[12] K. C. Mountzouris, "Nutritional strategies targeting the beneficial modulation of the intestinal microflora with relevance to food safety: the role of probiotics and prebiotics," *Food Safety*, vol. 1, pp. 133–152, 2007.

[13] B. S. Bhardwaj, "Gut flora and its modification as a therapy," *Reviews in Medical Microbiology*, vol. 24, no. 3, pp. 52–54, 2013.

[14] S. Li, M. Li, H. Yue et al., "Structural elucidation of a pectic polysaccharide from Fructus mori and its bioactivity on intestinal bacteria strains," *Carbohydrate Polymers*, vol. 186, pp. 168–175, 2018.

[15] S. Sivaprakasam, P. D. Prasad, and N. Singh, "Benefits of short-chain fatty acids and their receptors in inflammation and carcinogenesis," *Pharmacology & Therapeutics*, vol. 8, pp. 144–151, 2016.

[16] I. Kaji, T. Iwanaga, M. Watanabe et al., "SCFA transport in rat duodenum," *American Journal of Physiology-Gastrointestinal and Liver Physiolog*, vol. 308, no. 3, pp. G188–G197, 2015.

[17] G. Ma, B. M. Kimatu, L. Zhao, W. Yang, F. Pei, and Q. Hu, "In vivo fermentation of a Pleurotus eryngii polysaccharide and its effects on fecal microbiota composition and immune response," *Food & Function*, vol. 8, no. 5, pp. 1810–1821, 2017.

[18] A. Pandey, "Proteomics to study genes and genomes," *Nature*, vol. 405, no. 6788, pp. 837–846, 2000.

[19] B. M. Gadella, "Sperm surface proteomics," *Immune Infertility*, W. Krause and R. Naz, Eds., pp. 33–48, Springer, Berlin, Heidelberg, 2017.

[20] J. Wang, D. Mauvoisin, E. Martin et al., "Nuclear proteomics uncovers diurnal regulatory landscapes in mouse liver," *Cell Metabolism*, vol. 25, no. 1, pp. 102–117, 2017.

[21] L. M. Li, S. Q. Yan, B. C. Lin, Q. Shi, and Y. Lu, "Single-cell proteomics for cancer immunotherapy," *Advances in Cancer Research*, vol. 139, pp. 185–207, 2018.

[22] X. Y. Wang, *Proteomic and Metabolomic Studies of Dendrobium Huoshan Polysaccharide in the Intervention of Subacute Alcoholic Liver Injury in Mice*, Hefei University of Technology, 2014.

[23] C. Ma, S.-H. Guan, M. Yang, X. Liu, and D.-A. Guo, "Differential protein expression in mouse splenic mononuclear cells treated with polysaccharides from spores of _Ganoderma lucidum_," *Phytomedicine*, vol. 15, no. 4, pp. 268–276, 2008.

[24] D. F. Wei, *Proteomic Studies on the Immune Regulation and Anti-Tumor Effects of Astragalus Polysaccharide*, Lanzhou University, 2012.

[25] Q. Yu, S. P. Nie, J. Q. Wang et al., "Chemoprotective effects of _Ganoderma atrum_ polysaccharide in cyclophosphamide-induced mice," *International Journal of Biological Macromolecules*, vol. 64, pp. 395–401, 2014.

[26] X. J. Wei, T. J. Hu, J. R. Chen, and Y. Y. Wei, "Inhibitory effect of carboxymethylpachymaran on cyclophosphamide-induced oxidative stress in mice," *International Journal of Biological Macromolecules*, vol. 49, no. 4, pp. 801–805, 2011.

[27] M. F. Mokhtar, E. H. A. Latib, S. Sufian, and K. Z. Ku Shaari, "Preparation of activated carbon from *Durian* shell and seed," *Advanced Materials Research*, vol. 626, pp. 887–891, 2012.

[28] K. Y. Foo and B. H. Hameed, "Textural porosity, surface chemistry and adsorptive properties of durian shell derived activated carbon prepared by microwave assisted NaOH activation," *Chemical Engineering Journal*, vol. 187, pp. 53–62, 2012.

[29] S. Pongsamart and V. Lipipun, "Antimicrobial preparations using polysaccharide gel from durian fruit-rind," 2009, Patents, US20090149418.

[30] H. M. Jiang, J. Dong, S. Jiang et al., "Effect of _Durio zibethinus_ rind polysaccharide on functional constipation and intestinal microbiota in rats," *Food Research International*, vol. 136, p. 109316, 2020.

[31] M. Z. Wu, G. Xie, Y. X. Li et al., "Cough-relieving, analgesic and antibiotic effects of durian shell extracts: a study in mice," *Journal of Southern Medical University*, vol. 30, no. 4, pp. 793–797, 2010.

[32] Q. Guo, "Advances of immune checkpoint inhibitors in tumor immunotherapy," *IOP Conference Series: Materials Science and Engineering*, vol. 301, p. 012020, 2018.

[33] M. Ruslan, "Recognition of microorganisms and activation of the immune response," *Nature*, vol. 449, no. 7164, pp. 819–826, 2007.

[34] M. E. Selsted and A. J. Ouellette, "Mammalian defensins in the antimicrobial immune response," *Nature Immunology*, vol. 6, no. 6, pp. 551–557, 2005.

[35] Y. Wang, Q. Qi, A. Li et al., "Immuno-enhancement effects of Yifei Tongluo Granules on cyclophosphamide- induced immunosuppression in Balb/c mice," *Journal of Ethnopharmacology*, vol. 194, pp. 72–82, 2016.

[36] H. J. Suh, H. S. Yang, K. S. Ra et al., "Peyer's patch-mediated intestinal immune system modulating activity of pectic-type polysaccharide from peel of *Citrus unshiu*," *Food Chemistry*, vol. 138, no. 2-3, pp. 1079–1086, 2013.

[37] F. Huang, R. F. Zhang, Y. J. Liu et al., "Dietary *litchi* pulp polysaccharides could enhance immunomodulatory and antioxidant effects in mice," *International Journal of Biological Macromolecules*, vol. 92, pp. 1067–1073, 2016.

[38] N. V. Belska, A. M. Guriev, M. G. Danilets et al., "Water-soluble polysaccharide obtained from _Acorus calamus_ L. classically activates macrophages and stimulates Th1 response," *International Immunopharmacology*, vol. 10, no. 8, pp. 933–942, 2010.

[39] J. du, H. Zhu, P. Liu et al., "Immune responses and gene expression in hepatopancreas from _Macrobrachium rosenbergii_ challenged by a novel pathogen spiroplasma MR-1008," *Fish & Shellfish Immunology*, vol. 34, no. 1, pp. 315–323, 2013.

[40] X. Chen, J. Lu, Y. Zhang et al., "Studies of macrophage immuno-modulating activity of polysaccharides isolated from *Paecilomyces tenuipes*," *International Journal of Biological Macromolecules*, vol. 43, no. 3, pp. 252–256, 2008.

[41] J. J. Burns, L. Zhao, E. W. Taylor, and K. Spelman, "The influence of traditional herbal formulas on cytokine activity," *Toxicology*, vol. 278, no. 1, pp. 140–159, 2010.

[42] C. Tang, J. Sun, B. Zhou et al., "Effects of polysaccharides from purple sweet potatoes on immune response and gut microbiota composition in normal and cyclophosphamide treated mice," *Food & Function*, vol. 9, no. 2, pp. 937–950, 2018.

[43] W. Liao, J. X. Lin, and W. J. Leonard, "IL-2 family cytokines: new insights into the complex roles of IL-2 as a broad regulator of T helper cell differentiation," *Current Opinion in Immunology*, vol. 23, no. 5, pp. 598–604, 2011.

[44] T. Hu, Q. Huang, K. Wong, and H. Yang, "Structure, molecular conformation, and immunomodulatory activity of four polysaccharide fractions from *Lignosus rhinocerotis* sclerotia," *International Journal of Biological Macromolecules*, vol. 94, no. Part A, pp. 423–430, 2017.

[45] A. Kumar, L. Rani, S. T. Mhaske et al., "IL-3 receptor expression on activated human Th cells is regulated by IL-4, and IL-3 synergizes with IL-4 to enhance Th2 cell differentiation," *The Journal of Immunology*, vol. 204, no. 4, pp. 819–831, 2020.

[46] A. E. Zanno, M. A. Romer, L. Fox et al., "Reducing Th2 inflammation through neutralizing IL-4 antibody rescues myelination in IUGR rat brain," *Journal of Neurodevelopmental Disorders*, vol. 11, no. 1, p. 34, 2019.

[47] Z. H. Gong, J. R. Hu, Y. Q. Duan et al., "Effects of *Bletilla baicalensis* polysaccharide on serum IL-2R, IL-4 and caspase-8 expression in stomach tissue of model rats with gastric ulcer," *Journal of Traditional Chinese Medicine*, vol. 26, pp. 35–39, 2019.

[48] U. Gupta, S. K. Hira, R. Singh, A. Paladhi, P. Srivastava, and P. Pratim Manna, "Essential role of TNF-α in gamma c cytokine aided crosstalk between dendritic cells and natural killer

cells in experimental murine lymphoma," *International Immunopharmacology*, vol. 78, p. 106031, 2020.

[49] A.-C. Voirin, N. Perek, and F. Roche, "Inflammatory stress induced by a combination of cytokines (IL-6, IL-17, TNF-α) leads to a loss of integrity on bEnd.3 endothelial cells _in vitro_ BBB model," *Brain Research*, vol. 1730, p. 146647, 2020.

[50] R. P. da Silva, I. Nissim, M. E. Brosnan, and J. T. Brosnan, "Creatine synthesis: hepatic metabolism of guanidinoacetate and creatine in the rat in vitro and in vivo," *American Journal of Physiology-Endocrinology and Metabolism*, vol. 296, p. E256, 2009.

[51] R. Bahirwani and K. Reddy, "Drug-induced liver injury due to cancer chemotherapeutic agents," *Seminars in Liver Disease*, vol. 34, no. 2, pp. 162–171, 2014.

[52] X. J. Li, B. Li, and Y. Jia, "The hepatoprotective effect of Haoqin Qingdan decoction against liver injury induced by a chemotherapeutic drug cyclophosphamide," *Evidence-Based Complementary and Alternative Medicine*, vol. 2015, Article ID 978219, 8 pages, 2015.

[53] B. A. Baldo and N. H. Pham, "Adverse reactions to targeted and non-targeted chemotherapeutic drugs with emphasis on hypersensitivity responses and the invasive metastatic switch,," *Cancer and Metastasis Reviews*, vol. 32, no. 3-4, pp. 723–761, 2013.

[54] X. F. Xu and X. Zhang, "Effects of cyclophosphamide on immune system and gut microbiota in mice," *Microbiological Research*, vol. 171, pp. 97–106, 2015.

[55] D. M. Yang, J. Q. Zhang, and Y. F. Fei, "*Lycium* barbarumpolysaccharide attenuates chemotherapy-induced ovarian injury by reducing oxidative stress," *Journal of Obstetrics and Gynaecology Research*, vol. 43, no. 10, pp. 1621–1628, 2017.

[56] P. Luo, H. Z. Liu, X. Y. Le, H. Du, and X. H. Kang, "Squid ink polysaccharide prevents chemotherapy induced injury in the testes of reproducing mice," *Pakistan journal of pharmaceutical ences*, vol. 31, pp. 25–29, 2018.

[57] X. l. Meng, L. Xue, Z. W. Zhang et al., "Effect of *Portulaca oleracea* polysaccharide on immunological function in mice with cyclophosphamide-induced immunosuppression," *Chinese Journal of New Drugs*, vol. 26, pp. 1296–1300, 2017.

[58] C. Ma, S.-H. Guan, M. Yang, X. Liu, and D.-A. Guo, "Differential protein expression in mouse splenic mononuclear cells treated with polysaccharides from spores of Ganoderma lucidum," *Phytomedicine*, vol. 15, pp. 268–276, 2008.

[59] J. V. Ravetch and B. Perussia, "Alternative membrane forms of Fc gamma RIII(CD16) on human natural killer cells and neutrophils. Cell type-specific expression of two genes that differ in single nucleotide substitutions," *Journal of Experimental Medicine*, vol. 170, no. 2, pp. 481–497, 1989.

[60] A. Coxon, X. Cullere, S. Knight et al., "FcγRIII mediates neutrophil recruitment to immune Complexes," *Immunity*, vol. 14, no. 6, pp. 693–704, 2001.

[61] F. Nimmerjahn and J. V. Ravetch, "Fcγ receptors as regulators of immune responses," *Nature Reviews Immunology*, vol. 8, no. 1, pp. 34–47, 2008.

[62] Y. Wang, J. Wu, R. Newton, N. S. Bahaie, C. Long, and B. Walcheck, "ADAM17 cleaves CD16b (FcγRIIIb) in human neutrophils," *Biochimica et Biophysica Acta*, vol. 1833, no. 3, pp. 680–685, 2013.

[63] R. Romee, B. Foley, T. Lenvik et al., "NK cell CD16 surface expression and function is regulated by a disintegrin and metalloprotease-17 (ADAM17)," *Blood*, vol. 121, no. 18, pp. 3599–3608, 2013.

[64] A. Roghanian, G. Hu, C. Fraser et al., "Cyclophosphamide enhances cancer antibody immunotherapy in the resistant bone marrow niche by modulating macrophage FcγR expression," *Cancer Immunology Research*, vol. 7, no. 11, pp. 1876–1890, 2019.

[65] S. Das, O. Bhattacharjee, and A. Goswami, "Arabinosylated lipoarabinomannan (Ara-LAM) mediated intracellular mechanisms against tuberculosis infection: involvement of protein kinase C (PKC) mediated signaling," *Tuberculosis*, vol. 95, no. 2, pp. 208–216, 2015.

[66] M. Faseleh Jahromi, P. Shokryazdan, Z. Idrus, R. Ebrahimi, F. Bashokouh, and J. B. Liang, "Modulation of immune function in rats using oligosaccharides extracted from palm kernel cake," *BioMed Research International*, vol. 2017, Article ID 2576921, 10 pages, 2017.

[67] G. Baier and J. Wagner, "PKC inhibitors: potential in T cell-dependent immune diseases," *Current Opinion in Cell Biology*, vol. 21, no. 2, pp. 262–267, 2009.

[68] N. Perera, F.-L. Yang, Y.-T. Lu, L.-H. Li, K.-F. Hua, and S.-H. Wu, "Antrodia cinnamomeaGalactomannan elicits immuno-stimulatory activity through toll-like receptor 4," *International journal of biological sciences*, vol. 14, no. 10, pp. 1378–1388, 2018.

[69] A. Rehman, P. Lepage, A. Nolte, S. Hellmig, S. Schreiber, and S. J. Ott, "Transcriptional activity of the dominant gut mucosal microbiota in chronic inflammatory bowel disease patients," *Journal of Medical Microbiology*, vol. 59, no. 9, pp. 1114–1122, 2010.

[70] C. G. Zhang, W. J. Gong, Z. H. Li, D. W. Gao, and Y. Gao, "Research progress of gut flora in improving human wellness," *Food Science and Human Wellness*, vol. 8, no. 2, pp. 102–105, 2019.

[71] W. Xia, L. Z. Ke, L. Li, G. Wei, and F. Xu, "Clinical efficacy of probiotics for recurrent respiratory tract infections of children and its influence on immune function: a systematic review," *Drug evaluation study*, vol. 43, pp. 140–146, 2020.

[72] G. Q. Wang, H. Y. Tang, Y. Zhang, X. Xiao, and Y. J. Xia, "The intervention effects of _Lactobacillus casei_ LC2W on _Escherichia coli_ O157:H7 -induced mouse colitis," *Food Science and Human Wellness*, vol. 9, no. 3, pp. 289–294, 2020.

[73] S. Li, M. Li, H. Yue et al., "Structural elucidation of a pectic polysaccharide from _Fructus Mori_ and its bioactivity on intestinal bacteria strains," *Carbohydrate Polymers*, vol. 186, pp. 168–175, 2018.

[74] X. Wu, L. Zhou, X. Luo, X. L. Deng, R. Y. Wen, and J. W. Wu, "Effect of polysaccharide of Sijunzi decoction on gut flora and immune function in spleen-deficiency mice," *Pharmacology and Clinics of Chinese Materia Medica*, vol. 2, pp. 12–14, 2014.

[75] D. W. Cockburn and N. M. Koropatkin, "Polysaccharide degradation by the intestinal microbiota and its influence on human health and disease," *Journal of Molecular Biology*, vol. 428, no. 16, pp. 3230–3252, 2016.

[76] H. J. Flint, K. P. Scott, P. Louis, and S. H. Duncan, "The role of the gut microbiota in nutrition and health," *Nature Reviews Gastroenterology & Hepatology*, vol. 9, no. 10, pp. 577–589, 2012.

[77] P. J. Turnbaugh, R. E. Ley, M. A. Mahowald, V. Magrini, E. R. Mardis, and J. I. Gordon, "An obesity-associated gut

microbiome with increased capacity for energy harvest," *Nature*, vol. 444, no. 7122, pp. 1027–1031, 2006.

[78] M. G. Gareau, P. M. Sherman, and W. A. Walker, "Probiotics and the gut microbiota in intestinal health and disease," *Nature Reviews Gastroenterology & Hepatology*, vol. 7, no. 9, pp. 503–514, 2010.

[79] M. Delzenne, A. M. Neyrinck, F. Bäckhed, and P. D. Cani, "Targeting gut microbiota in obesity: effects of prebiotics and probiotics," *Nature Reviews Endocrinology*, vol. 7, no. 11, pp. 639–646, 2011.

[80] B. Seo, K. Jeon, S. Moon et al., "_Roseburia_ spp. Abundance Associates with Alcohol Consumption in Humans and Its Administration Ameliorates Alcoholic Fatty Liver in Mice," *Cell Host & Microbe*, vol. 27, no. 1, pp. 25–40.e6, 2020.

[81] Y. L. Feng, J. Zhu, and R. Sensenstein, "Development of a headspace solid-phase microextraction method combined with gas chromatography mass spectrometry for the determination of phthalate esters in cow milk," *Analytica Chimica Acta*, vol. 538, no. 1-2, pp. 41–48, 2005.

[82] D. Rachel, "Regulatory T cells: a helping hand from *Bacteroides fragilis*," *Nature Reviews Immunology*, vol. 10, p. 539, 2010.

[83] E. Hosseini, C. Grootaert, W. Verstraete, and T. van de Wiele, "Propionate as a health-promoting microbial metabolite in the human gut," *Nutrition Reviews*, vol. 69, no. 5, pp. 245–258, 2011.

[84] H. Ursula, "Microbiome: pro-inflammatory *Prevotella*?," *Nature Reviews Microbiology*, vol. 12, p. 5, 2014.

[85] D. A. Relman, "How to build healthy growth-promoting gut communities," *Nature Reviews Gastroenterology & Hepatology*, vol. 13, no. 7, pp. 379-380, 2016.

[86] M. Sakamoto, M. Umeda, I. Ishikawa, and Y. Benno, "*Prevotella multisaccharivorax* sp. nov., isolated from human subgingival plaque," *International Journal of Systematic and Evolutionary Microbiology*, vol. 55, no. 5, pp. 1839–1843, 2005.

[87] M. Derrien, "Akkermansia muciniphila gen. nov. sp. nov. a human intestinal mucin-degrading bacterium," *International Journal of Systematic & Evolutionary Microbiology*, vol. 54, no. 5, pp. 1469–1476, 2004.

[88] A. Everard, C. Belzer, L. Geurts et al., "Cross-talk between *Akkermansia muciniphila* and intestinal epithelium controls diet-induced obesity," *Proceedings of the National Academy of Sciences*, vol. 110, no. 22, pp. 9066–9071, 2013.

[89] M. C. Dao, A. Everard, J. Aron-Wisnewsky et al., "*Akkermansia muciniphila* and improved metabolic health during a dietary intervention in obesity: relationship with gut microbiome richness and ecology," *Gut*, vol. 65, no. 3, pp. 426–436, 2016.

[90] C. D. Owen, L. E. Tailford, S. Monaco et al., "Unravelling the specificity and mechanism of sialic acid recognition by the gut symbiont _Ruminococcus gnavus_," *Nature Communications*, vol. 8, no. 1, p. 2196, 2017.

[91] S. Fukuda, H. Toh, K. Hase et al., "*Bifidobacteria* can protect from enteropathogenic infection through production of acetate," *Nature*, vol. 469, no. 7331, pp. 543–547, 2011.

[92] T. Konikoff and U. Gophna, "_Oscillospira_ : a Central, Enigmatic Component of the Human Gut Microbiota," *Trends in Microbiology*, vol. 24, no. 7, pp. 523-524, 2016.

[93] U. Gophna, T. Konikoff, and H. B. Nielsen, "*Oscillospira* and related bacteria—from metagenomic species to metabolic features," *Environmental Microbiology*, vol. 19, no. 3, pp. 835–841, 2017.

Hindawi
Oxidative Medicine and Cellular Longevity
Volume 2021, Article ID 6695634, 11 pages
https://doi.org/10.1155/2021/6695634

Research Article

Oxidative Stress Mediated Cytotoxicity, Cell Cycle Arrest, and Apoptosis Induced by *Rosa damascena* in Human Cervical Cancer HeLa Cells

Mai M. Al-Oqail,[1] Nida N. Farshori,[1] Ebtesam S. Al-Sheddi,[1] Shaza M. Al-Massarani,[1] Quaiser Saquib,[2,3] Maqsood A. Siddiqui,[2,3] and Abdulaziz A. Al-Khedhairy[3]

[1]*Department of Pharmacognosy, College of Pharmacy, King Saud University, Riyadh 11495, Saudi Arabia*
[2]*DNA Research Chair, Zoology Department, College of Science, King Saud University, P.O. Box 2455, Riyadh 11451, Saudi Arabia*
[3]*Zoology Department, College of Science, King Saud University, P.O. Box 2455, Riyadh 11451, Saudi Arabia*

Correspondence should be addressed to Nida N. Farshori; nidachem@gmail.com
and Maqsood A. Siddiqui; maqsoodahmads@gmail.com

Received 5 November 2020; Revised 5 January 2021; Accepted 11 January 2021; Published 28 January 2021

Academic Editor: Hui-Min David Wang

Rosa damascena Mill (Damask rose), belonging to the Rosaceae family, is known for medicinal purposes in traditional medicine system. However, its anticancer activity has not been studied yet in detail. Herein, we aimed to investigate the cytotoxic effects of *R. damascena* hexane (RA-HE) and methanolic (RA-ME) extracts against human breast (MCF-7), lung epithelial (A-549), and cervical (HeLa) cancer cells. The RA-HE and RA-ME showed more potent cytotoxic effects against HeLa cells with an IC_{50} of 819.6 and 198.4 μg/ml, respectively. Further, cytotoxic concentrations of most effective extract (RA-ME) were used to evaluate the mechanism of cytotoxicity involved in HeLa cells. A concentration-dependent induction of lipid peroxidation (LPO) and reduction of glutathione (GSH) in HeLa cells treated with 250-1000 μg/ml of RA-ME confirms the association of oxidative stress. We also detected a noteworthy increase in reactive oxygen species (ROS) production and a decline in mitochondrial membrane potential (MMP) level in RA-ME-exposed HeLa cells. Flow cytometric data showed a strong dose-response relationship in cell cycle analysis between subG1 phase in HeLa cells and RA-ME treatment. Similarly, a concentration-dependent increase was recorded with Annexin V assay in HeLa cells going to late apoptosis. In conclusion, our findings suggest that RA-ME-induced cytotoxicity and apoptosis in HeLa cells are mediated by oxidative stress.

1. Introduction

Cancer is the second leading cause of the mortality worldwide and is main health problem globally because of the uncontrolled cell growth [1]. Cancer elaborates uncontrolled growth of normal cells triggered by genetic changes and variabilities, subsequent in the production of malignant cells, and initial of development of secondary malignant growths [2]. These genetic changes could be due to the exposure of pesticides, smoking, absorption of carcinogenic chemicals, or alterations in the immune system and hormonal balance [3]. As cancer is typically detected at an advanced stage, the diagnosis is poor and treatment is mainly unsuccessful [4]. The deficiency in early detection and lack of effective therapeutic agents are the foremost causes of poor cancer control and diagnosis [5]. The treatment of cancer includes chemotherapy, surgery, and/or radiation. Various chemotherapeutic agents often used have been found to be less effective and are associated with severe side effects such as damage to normal cells [6]. Hence, the search for alternative therapeutic effective agent with less side effects is needed. Globally, after breast and colon cancer, cervical cancer is the third leading malignancy among women [7]. Cervical cancer is one of the most common cancers in female living in middle- and low-income countries [8]. Although incidence and death rates have been declined in past decades, but due to the

population aging, the number of new cases and mortality has increased by 0.5%/year [9]. Because of population and aging, estimated number of new cases is expected to increase by 2025, if incidents remain the same at 2002 [10]. Further, in order to broadly report this serious health problem, initial recognition and medicine with clinical efficacy are to be required. The field of natural product research has become one of the most interesting subjects in the advancement of novel therapeutic agents [11]. Plants have played a leading role in the old system of remedy with particularly elongated history in the treatment of cancer diseases [12]. A number of plant extracts such as *cotinus coggygria* [13], *Aristolochia ringens* [14], *Tabernaemontana divaricate* [15], and *Artemisia annua* [16] have been reported to possess cytotoxic effects against HeLa cells. The earlier studies have demonstrated that the cytotoxic phytochemicals are capable to induce apoptosis/necrosis by obstructing different signaling pathways, which leads to cell cycle arrest and cell death [17]. Cancer cells have several molecular mechanisms to improve and suppress apoptosis that plays key role in cancer development [18]. Therefore, induction in apoptosis/-necrosis by cytotoxic agents can be a fundamental beneficial method towards cancer chemotherapy [19]. *Rosa damascena* Mill L (Damask rose), known as Gole Mohammadi, is one of the most important species of Rosaceae family. *R. damascena*, an ornamental plant, is primarily cultivated for the use in food industries and perfumes [20]. Apart from these, this plant is also being used for medicinal purposes in traditional medicine system [21]. A number of products and isolated constituents from seeds, flowers, and petals of *R. damascena* have been studied in different *in vivo* and *in vitro* model systems [22]. The beneficial effects of *R. damascena* extracts have been established for the management of menstrual bleeding and digestive problem [23], cough [24], gentle laxative [25], analgesic [26], brain function [27], and cardiovascular function [28]. The antioxidant [29], antimicrobial [30], anti-HIV [31], antidiabetic [32], antiageing [33], and anti-inflammatory [34] activities of *R. damascena* have also been well-documented. There are few reports that reveal that *R. damascena* extracts and oils induced cytotoxic effects against various cancer cell lines [35–38]. In another study, the cytotoxic potential of the leaf bud and flower extracts of *Crataegus microphylla* plant of Rosaceae family against HeLa cells have also been reported [39]. But there has been only limited investigation on the cytotoxic effects of *R. damascena*; however, detailed mechanistic studies have not been conducted yet. Therefore, this study was conducted to investigate the mechanism(s) of cytotoxicity induced by *R. damascena* against three different carcinoma cell lines, i.e., human breast (MCF-7), human lung epithelial (A-549), and human cervical (HeLa). In this study, firstly, we screened the cytotoxicity of hexane (RA-HE) and methanolic (RA-ME) extracts of *R. damascena* using MTT assay, neutral red uptake assay, and morphological changes. Secondly, the cytotoxic concentrations of most effective extract were used to evaluate the mechanism involved in the cytotoxicity against sensitive cancer cells, HeLa.

2. Material and Methods

2.1. Chemicals and Culture Medium. Cell culture medium (DMEM) with high glucose, sodium bicarbonate, MTT, neutral red, Rhodamine (Rh123), and $2',7'$-dichlorofluorescin (DCF-DA) dye was procured from Sigma Aldrich, USA. Fetal bovine serum (FBS), antibiotic-antimycotic (100x solution) (Cat. No. 15240-062, Gibco), and trypsin were procured from Gibco, Life Technologies, USA. Flow cytometric kits were purchased from Backman Coulter, USA. All other specified chemicals and reagents were obtained from Sigma Aldrich, USA, unless indicated otherwise.

2.2. Cell Culture. Human breast adenocarcinoma (MCF-7), human lung epithelial (A-549), and human cervical carcinoma (HeLa) cell lines were obtained from American Type Culture Collection (ATCC), USA. The cell lines were grown in DMEM with 10% FBS and 1% antibiotic solution. All cell lines were maintained in 25 cm^2 flasks at 37°C in a humidified atmosphere containing 5% CO_2.

2.3. Plant Collection and Extractions. The fresh *R. damascena* flowers were collected from a rose farm, Taif, Saudi Arabia. The roses were cut into small pieces, air-dried under shade at 25°C, and converted into a course powder. The extraction was done by maceration. Briefly, 10 g of powdered *R. damascena* was extracted with hexane and methanol, respectively. Then, the filtrate was collected in a beaker by filtration and dried at 40°C in a rotary evaporator. The extracts were separately obtained, and the dried hexane extract was named as RA-HE and methanolic extract as RA-ME. Both the extracts were stored at 4°C until further use. The extracts were diluted in dimethyl sulfoxide (DMSO) for bioassays. The final concentration of DMSO used in the assays was 0.02%.

2.4. Cytotoxicity Experiments. The *in vitro* cytotoxicity of RA-HE and RA-ME against MCF-7, A-549, and HeLa cells was determined by MTT, neutral red uptake, and cell morphology assays [40].

2.5. MTT Assay. Briefly, cells were seeded into a 96-well culture plate at 1×10^4 cells in each well. Cells were then exposed to varying concentrations (0-1000 μg/ml) of RA-HE and RA-ME. The plates were placed in a humidified 5% CO_2 incubator for 24 h. Then, MTT solution (10 μl of 5 mg/ml MTT stock) was added to each well and incubated for 4 h. The colored formazan crystal formed was dissolved in dimethyl sulfoxide. Finally, absorbance was measured at 550 nm using microplate reader [40].

2.6. NRU Assay. Following the protocol [40], the NRU assay was performed. In brief, all the cells were plated in a 96-well plate at a density of 10,000 cells/well. Then, cells were exposed to varying concentrations (0-1000 μg/ml) of RA-HE and RA-ME for 24 h. The cells were then incubated for 3 h in a medium supplemented with 50 μg/ml of NR dye. After incubation, the plates were washed and dye was extracted in ethanol: acetic acid: water (50 : 1 : 49). Finally, absorbance was measured at 550 nm using microplate reader. All the assays were performed in replicates for each RA-HE

and RA-ME concentrations. Three replicates were examined in each experiment. The percent cell viability was calculated as follows:

$$\%\text{survival} = \text{mean experimental absorbance}/\text{mean control absorbance} \times 100. \quad (1)$$

2.7. Morphology Assay. To analyze the cell morphology induced by RA-HE and RA-ME in MCF-7, A-549, and HeLa cells, 1×10^4 cells were seeded into a 96-well culture plate. After 24 h of exposure, alterations in the cellular morphology were observed at 20x magnification using a light microscope (Olympus, CKX41, Japan).

2.8. Oxidative Stress Measurements by LPO and GSH. To measure the LPO and GSH content, HeLa cells were plated in 6-well plates at 1×10^5 cells in every well. The cells were then exposed to 250, 500, and 1000 μg/ml of RA-ME for 24 h. After treatment, control and treated cells were harvested and sonicated and total protein was measured by Lowry et al. [41]. The LPO content in HeLa cells was measured by TBARS (thiobarbituric acid-reactive substance) method [42], and GSH content was measured according to the method of Chandra et al. [43].

2.9. Reactive Oxygen Species (ROS) Measurements. The intracellular ROS level in HeLa cells was determined by DCF-DA fluorescence dye following the method described earlier [44]. Briefly, HeLa cells were seeded into 24-well plates with a density of 2×10^4 cells/well in complete medium. Then, cells were exposed to 250-1000 μg/ml of RA-ME for 24 h. After that, cells were rinsed with PBS and then incubated with 20 μM of DCF-DA dye in dark for 1 h. The qualitative ROS level was examined under the microscope, and qualitative fluorescence of cells was measured by fluorescent reader at 485/530 nm excitation/emission (Fluoroskan Ascent, Thermo-Scientific, Finland).

2.10. Mitochondrial Membrane Potential (MMP) Analysis. Rhodamine 123-based fluorescence measurement was used to analyze the alterations of MMP in HeLa cells after the exposure of RA-ME using the method [44]. Briefly, HeLa cells were plated in 24-well plates with a density of 2×10^4 cells in each well. Then, cells were treated with 250-1000 μg/ml of RA-ME for 24 h. After that, cells were incubated with 10 μg/ml of Rh123 dye for 60 min in the dark and fluorescence of MMP was analyzed under fluorescence microscope. The quantitative measurements of MMP in HeLa cells were done by measuring the plate at 485/530 nm excitation/emission.

2.11. Cell Cycle Analysis. To analyze the cell cycle arrest induced by RA-ME, HeLa cells (5×10^4 cells/well) were seeded in 24-well culture. Cells were then exposed to 250-1000 μg/ml of RA-ME for 24 h. After treatment, cells were rinsed with PBS and fixed in 70% cold ethanol for 1 h. Further, cells were rinsed and dispersed in a staining solution containing 50 μg/ml propidium iodide (PI) and 50 μg/ml RNase A. After incubating at room temperature for 1 h, distribution of cells in each phase of cell arrest was examined by PI staining using Beckman Coulter Epics XL-MCL flow cytometer.

2.12. Apoptosis Assay. Apoptosis analysis in HeLa after the exposure of RA-ME was performed using commercially available Annexin V-PI apoptosis kit (Beckman Coulter, USA). Briefly, HeLa cells were plated in culture plate and treated with 0, 250, 500, and 1000 μg/ml of RA-ME for 24 h. After treatment, cells were collected and washed with chilled PBS. After centrifugation, the cell pellet of control and exposed cells was resuspended in 1× binding buffer containing 10 μl of each Annexin V and PI for 20 min in the dark. The distribution of apoptosis/necrosis cells was recorded by using flow cytometer (Beckman Coulter Epics XL-MCL).

2.13. Statistical Analysis. The data analysis was done by one-way analysis of variance (ANOVA) using Dunnett's test. The level of statistical analysis selected was $p < 0.05$ unless indicated otherwise. Results were expressed as mean ± SD obtained from three independent experiments.

3. Results and Discussion

3.1. Cytotoxicity. The cell viability of three carcinoma cell lines, MCF-7, A-549, and HeLa, was assessed by MTT and NRU assays after the exposure of RA-HE and RA-ME at 0-1000 μg/ml for 24 h. The results showed that all the cell lines responded to cytotoxic effects of RA-ME in a concentration dependent manner (Figure 1). However, RA-HE has not shown cytotoxic effects on MCF-7 and A-549 cells and less cytotoxic effects on HeLa cells in contrast to RA-ME. RA-ME at 500 and 1000 μg/ml significantly decreased the viability of MCF-7 and A-549 cells. The cell viability was recorded as 81% and 70% in MCF-7 and 72% and 48% in A-549 cells, respectively, at 500 and 1000 μg/ml of RA-ME. However, a significant reduction in the viability of HeLa cells was recorded even at 100 μg/ml and above concentrations. The cell viability was recorded as 71%, 37%, 25%, and 13% at 100, 250, 500, and 1000 μg/ml of RA-ME, respectively. The RA-HE was also found to reduce the cell viability of HeLa cells up to 75% and 39% at 500 and 1000 μg/ml, respectively. NRU assays also revealed similar kind of cytotoxic response of RA-HE and RA-ME against MCF-7, A-459, and HeLa cells. The results showed that RA-ME reduced the viability of all three cells in a concentration-dependent manner (Figure 2). The viability of cells was found to be 83% and 72% in MCF-7, 70% and 45% in A-549, and 27% and 15%, respectively, at 500 and 1000 μg/ml of RA-ME. However, RA-HE was found to be noncytotoxic to MCF-7 and A-549 cells, but the viability was reduced to 73% and 42% in HeLa cells at 500 and 1000 μg/ml. In contrast, RA-HE and RA-ME were found to induce cytotoxicity only in HeLa cell line, but RA-HE showed slightly less cytotoxic effects to HeLa cells even at higher concentrations compared to RA-ME. Therefore, RA-ME was chosen for further analysis in HeLa cells. The half maximal inhibitory concentration (IC_{50}) values of RA-HE and RA-ME obtained on MCF-7, A-549, and HeLa

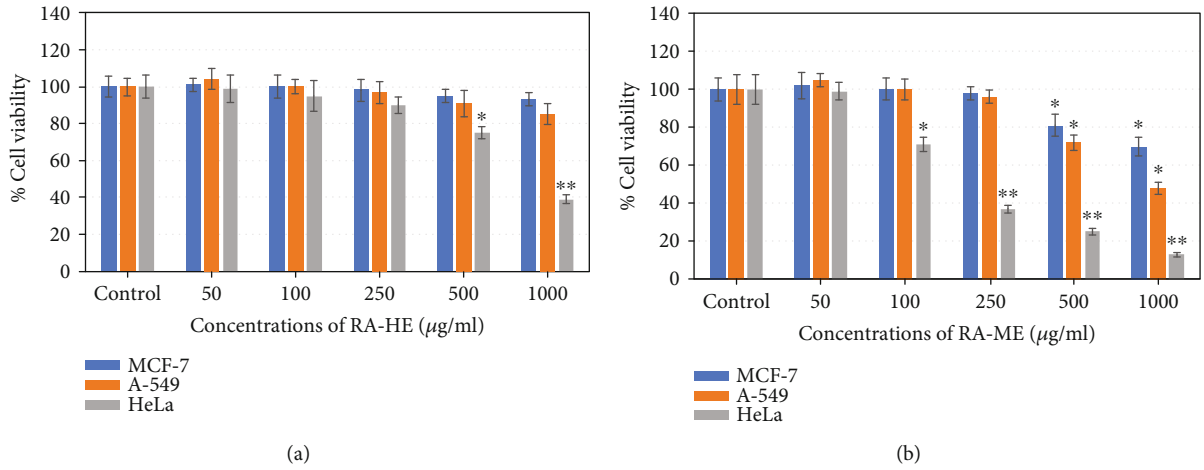

Figure 1: Cytotoxic potential of (a) RA-HE and (b) RA-ME against human breast (MCF-7), human lung (A-549), and human cervical (HeLa) carcinoma cell lines. MCF-7, HeLa, and A-549 cells were treated with increasing concentrations (0-1000 μg/ml) of RA-HE and RA-ME for 24 h. Cell viability was determined by MTT assay. Each diagram represents as mean ± SD of three experiments. Significant difference $^{*}p < 0.5$ and $^{**}p < 0.01$ from the control.

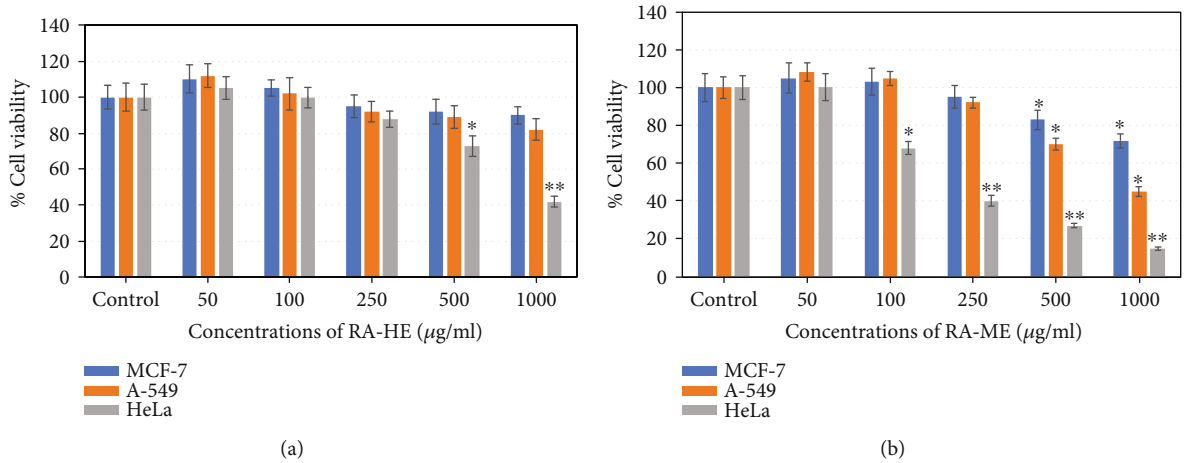

Figure 2: Cytotoxic potential of (a) RA-HE and (b) RA-ME against human breast (MCF-7), human lung (A-549), and human cervical (HeLa) carcinoma cell lines. MCF-7, HeLa, and A-549 cells were treated with increasing concentrations (0-1000 μg/ml) of RA-HE and RA-ME for 24 h. Cell viability was determined by neutral red uptake (NRU) assay. Each diagram represents as mean ± SD of three experiments. Significant difference $^{*}p < 0.5$ and $^{**}p < 0.01$ from the control.

cells are presented in Table 1. These findings were also substantiated by morphological observations. As shown in Figure 3, RA-ME decreased the maximum density of HeLa cells compared to MCF-7 and A-549 cells. In this study, we used MTT and NRU assays to assess the cytotoxic potential of RA-HE and RA-ME in MCF-7, A-549, and HeLa cells. These assays are routinely being used to screen the cytotoxic potential of plant extract against cancer cell lines [45]. The live cells reduced yellow MTT to purple formazan crystal by mitochondrial dehydrogenase enzyme [46]. Neutral red is a weak cationic weak dye which accumulates in lysosome of living cells but not in dead cells by nonionic passive diffusion [47]. The amount of dye taken up by cells is assumed to be relative to the total number of live cells present. Our results showed that MTT and NRU assays revealed a concentration-dependent cytotoxicity of RA-HE and RA-ME against cancer cell lines. The results showed that RA-ME at 100 μg/ml and above concentrations inhibits the cell viability of HeLa cells. Our results are consistent with previous reports showing that alcoholic extracts of *Rosa damascena* induced cytotoxic effects against HeLa cell line in the range of 100-1000 μg/ml concentrations [36]. In our study,

Table 1: Inhibitory concentration (IC_{50}) of the RA-HE and RA-ME on MCF-7, A-549, and HeLa cell lines.

Cell lines	IC_{50} (μg/ml)	
	RA-HE	RA-ME
MCF-7	>1000	>1000
A-549	>1000	961.5
HeLa	819.6	198.4

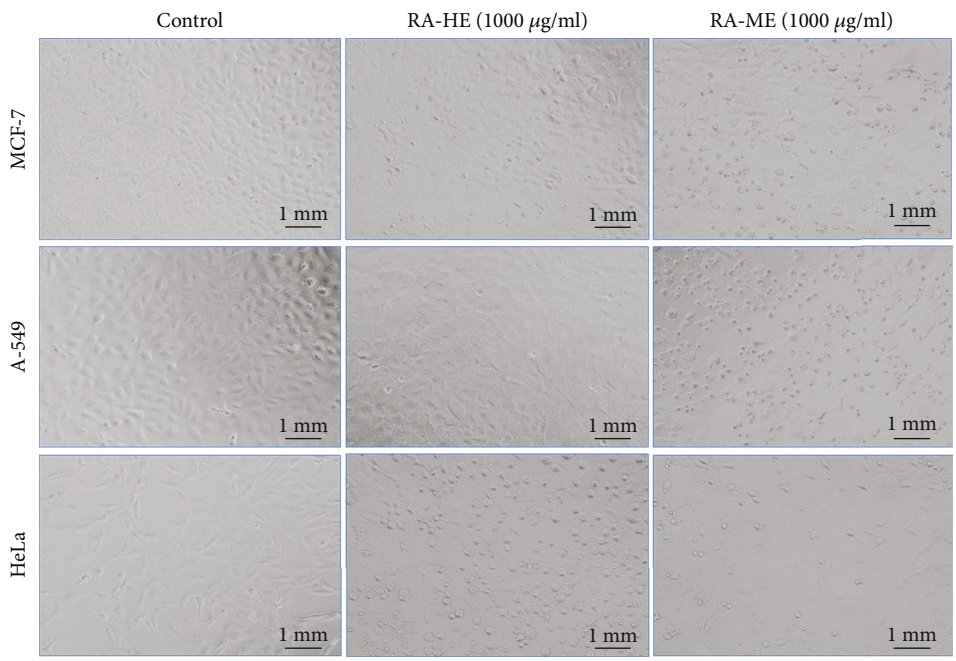

Figure 3: Representative light microscopy images of MCF-7, A-549 cells, and HeLa treated with their higher concentration, i.e., 1000 μg/ml for 24 h. The images were taken with magnification of 20x.

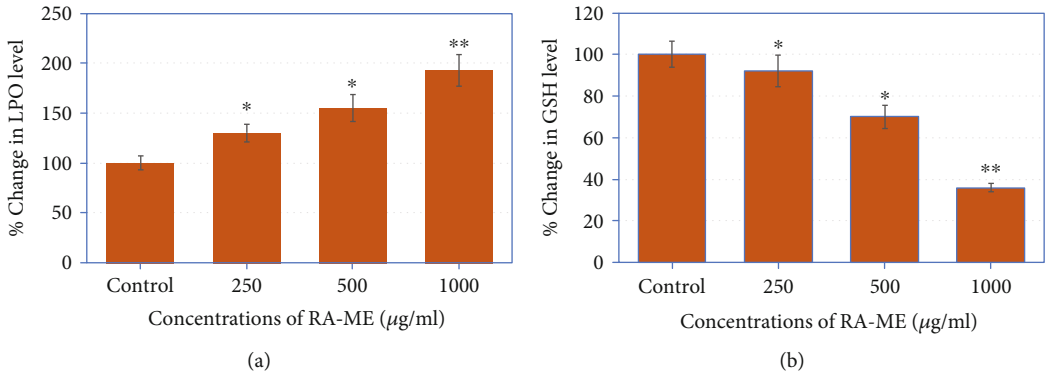

Figure 4: RA-ME-induced oxidative stress in human cervical carcinoma (HeLa) cells. The cells were treated with increasing concentrations (0-1000 μg/ml) of RA-ME for 24 h. (a) Percent increase in lipid peroxidation (LPO) level and (b) depletion in glutathione (GSH) level. Significant difference $^{*}p < 0.5$ and $^{**}p < 0.01$ from the control.

methanolic extract of R. *damascena* (RA-ME) showed highest cytotoxic response in HeLa cell line with IC_{50} ~200 μg/ml, which is consistent with Artun et al. [13], who have shown that methanolic extract of *R. damascena* exhibited cytotoxicity effects on HeLa cells with IC_{50} of 265 μg/ml. Other reports have also showed cytotoxic activities of *Rosa damascena* and its ingredients against human prostate, lung, and breast cancer cell lines [35]. Hagag et al. [48] have also shown that *Rosa damascena* exhibited anticancer potential against MCF-7 and HepG2 cells.

3.2. Oxidative Stress Measurements by LPO and GSH. Oxidative stress is well-known to be associated with the molecular mechanism of bioactive constitutes induced apoptosis and cytotoxicity [49]. To study the role of oxidative stress in RA-ME-induced HeLa cell death, we have performed the LPO and GSH assays (Figure 4). Our results obtained from LPO assay exhibited a significant dose-dependent increase in the LPO in RA-ME-exposed HeLa cells. A 35%, 55%, and 93% enhancement in LPO in HeLa cells was recorded at 250, 500, and 1000 μg/ml of RA-ME, respectively (Figure 4(a)). Our results clearly showed that RA-ME significantly induced the LPO level in HeLa cells. Many studies have also shown that plant extracts exhibited oxidative stress-mediated cancer cell death by increasing the LPO and decreasing the GSH activities [50, 51]. GSH plays a significant part in the defense of cells on oxidative stress [52]. It has also been documented that cellular GSH level is an important component for the activity of anticancer agents [53]. In this study, we found that GSH level was significantly reduced in RA-ME-treated HeLa cells. A maximum reduction of 64% was observed at 1000 μg/ml of RA-ME followed

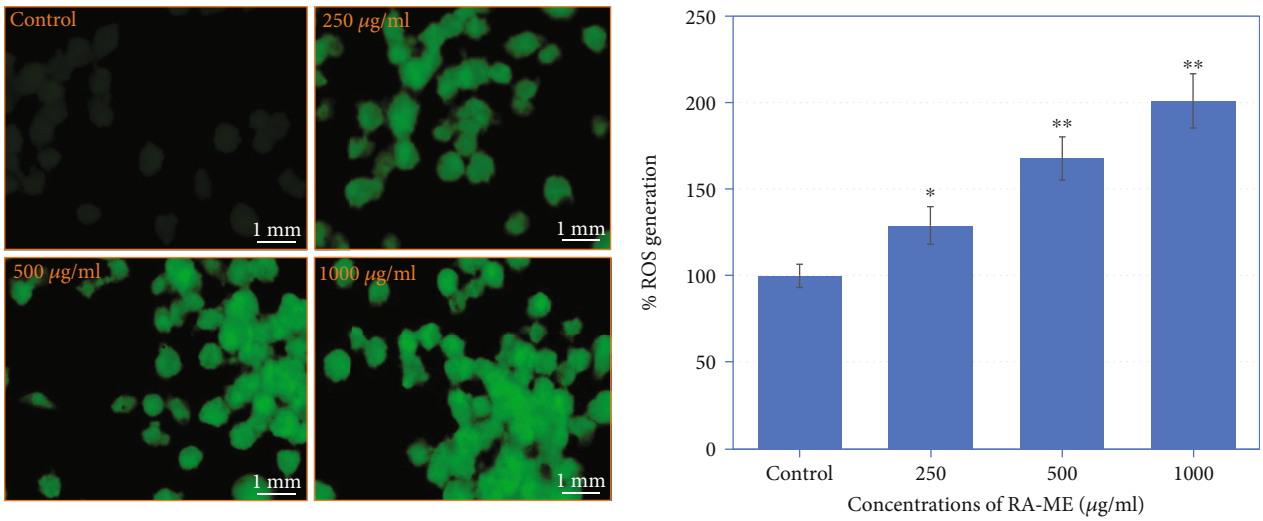

Figure 5: (a) Green fluorescence staining using DCF-DA dye showing ROS generation in HeLa cells. Cells were treated with 250-1000 μg/ml of RA-ME for 24 h. (b) Bar diagram showing percent induction in ROS generation. Significant difference $^{*}p < 0.5$ and $^{**}p < 0.01$ from the control.

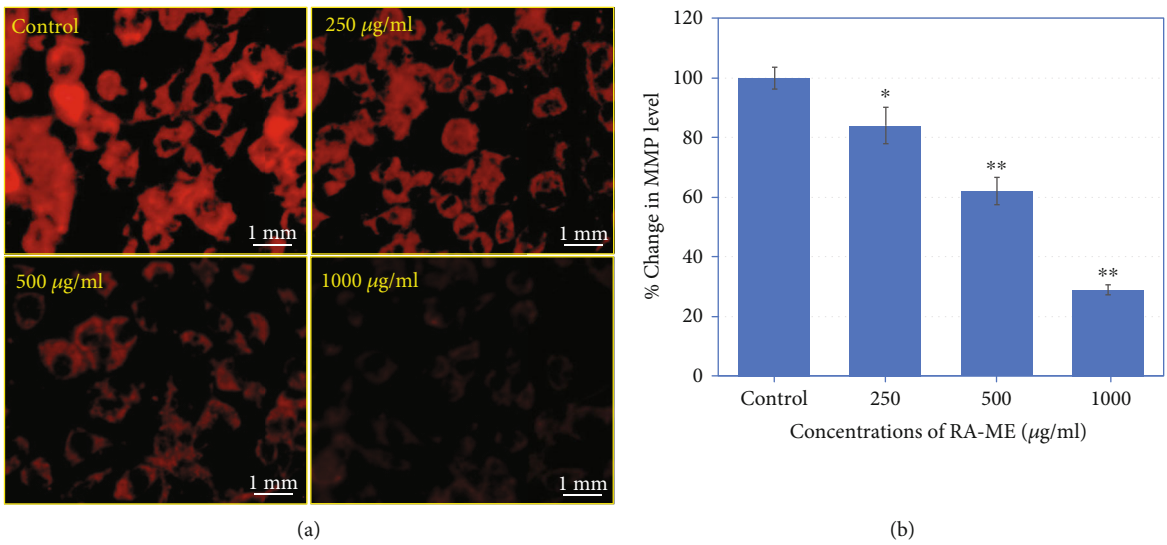

Figure 6: (a) Mitochondrial membrane potential (MMP) staining using Rhodamine 123 in control and treated HeLa cells with RA-ME. Cells were exposed to 250, 500, and 1000 μg/ml of RA-ME for 24 h. (b) Bar diagram showing percent change in decreased mitochondrial membrane potential. Significant difference $^{*}p < 0.5$ and $^{**}p < 0.01$ from the control.

by 30% and 8% at 500 and 250 μg/ml of RA-ME as compared to untreated control (Figure 4(b)). The depletion in GSH content in HeLa cells could be resulted due to the increased intercellular oxidation of GSH or inhibition of GSH synthesis by the plant extract. These findings suggest that reduction in GSH level by RA-ME may contribute to increase of ROS generation in the cells producing redox imbalance which leads to oxidation of biomolecules causing cell death. Similarly, Wageesha et al. [54] reported that treatment of HeLa cells with "Le Pana Guniya" (LPG), a well-known anticancer herbal medicine, caused depletion in GSH level.

3.3. ROS Measurement. The increase ROS production has been reported as one of the major causes of apoptosis in cancer cells and has been recognized into a promising therapeutic approach for the cancer treatments [55]. Herein, we have measured the quantitative and qualitative ROS production in HeLa cells exposed to cytotoxic concentrations of RA-ME. As shown in Figure 5(a), RA-ME significantly induced ROS generation in HeLa cells as examined by fluorescence microscope. An increase of 29%, 68%, and 101% in ROS generation was observed at 250, 500, and 1000 μg/ml, respectively, in HeLa cells exposed to RA-ME for 24 h as measured by using fluorescence spectrophotometer (Figure 5(b)).

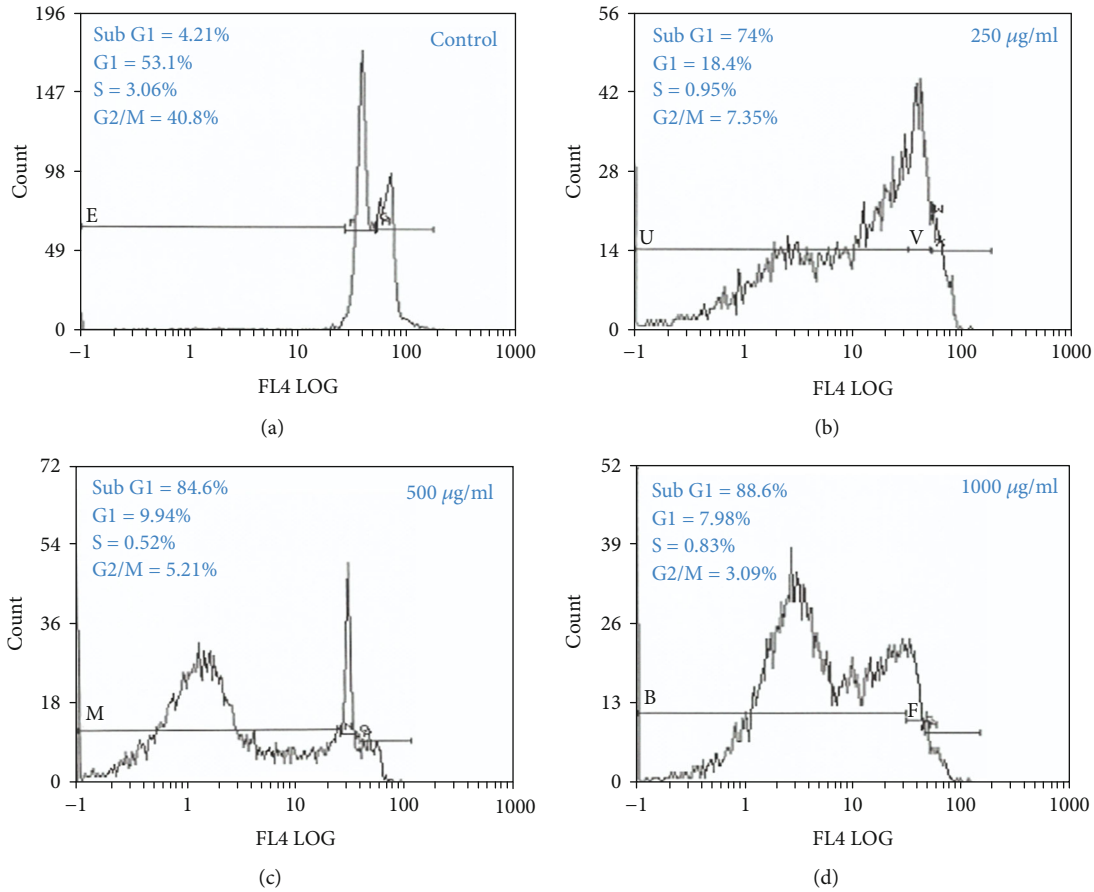

Figure 7: Flow cytometric images presenting cell cycle arrest in HeLa cells treated with RA-ME at 250, 500, and 1000 μg/ml for 24 h. The images showing an increase in subG1 peak with the increasing doses of RA-ME.

Based on obtained data showing an increase in ROS generation indicated that RA-ME-induced cytotoxicity and apoptosis in HeLa cells are mediated through ROS generation. The increase level of ROS production has also been reported to be involved in the process of anticancer mechanism of potential anticancer drugs [56] and plant extract-induced apoptosis in human prostate (CA-2B), human breast (MCF-7), and human lung (PC-9) cancer cells [57].

3.4. MMP Analysis. Depolarization in MMP is known as one of the properties of apoptosis progression in cells [58]. To confirm this process, we measured the mitochondrial membrane potential in HeLa cells. The cells were exposed to RA-ME at 250-1000 μg/ml for 24 h. As given in Figure 6, the florescence images revealed a concentration-dependent decrease in MMP (Figure 6(a)). The quantitative data also exhibited that RA-ME decreased the MMP by 16%, 38%, and 71% at 250, 500, and 1000 μg/ml, respectively (Figure 6(b)). As observed here, a decrease in the intensity of dye which indicated a disruption of MMP suggests that the HeLa cell death induced by RA-ME is mitochondrial dependent. The cytotoxicity and apoptosis responses through disruption of MMP in other cancer cells have also been investigated [59]. Numerous studies also revealed the apoptotic possessions of Rosa species, such *Rosa canina* extract in human colon cancer [60] and human lung and prostate cancer cells [61] through depolarization in mitochondrial membrane potential.

3.5. Cell Cycle Analysis. The cell cycle arrest in HeLa cells treated with *R. damascena* extract (RA-ME) was analyzed by flow cytometer. As shown in Figure 7, there was a strong dose-response relationship between subG1 phase in HeLa cells and RA-ME treatment. All the concentrations of RA-ME used significantly increased the cell numbers in subG1 phase (apoptosis cells). After 24 h of treatment, percentages of cells in subG1 phase were 4.21%, 74%, 84.6%, and 88.6% in control in 250, 500, and 1000 μg/ml of RA-ME, respectively (Figures 7(a)–7(d)). Our results showed that RA-ME induced a dose-dependent accumulation of cells in G1 phase. Consistent with our results, Kilinc et al. [61] in *Rosa canina* extract arrested cell cycle of human lung and human prostate cancer cells in subG1/G0 phase. Similarly, one of the main components of Rose, Geraniol-treated pancreatic cancer cells, has also exhibited dose-dependent increases in the percentage of cells in subG1/G0 phase of cell cycle and decreases the cells present in G2/M phases [62].

3.6. Apoptosis Assay. To investigate the apoptotic effects of *R. damascena* extract (RA-ME) on HeLa cells, the flow cytometric analysis was performed. Apoptosis analysis was done using Annexin V-PI apoptosis assay. As shown in

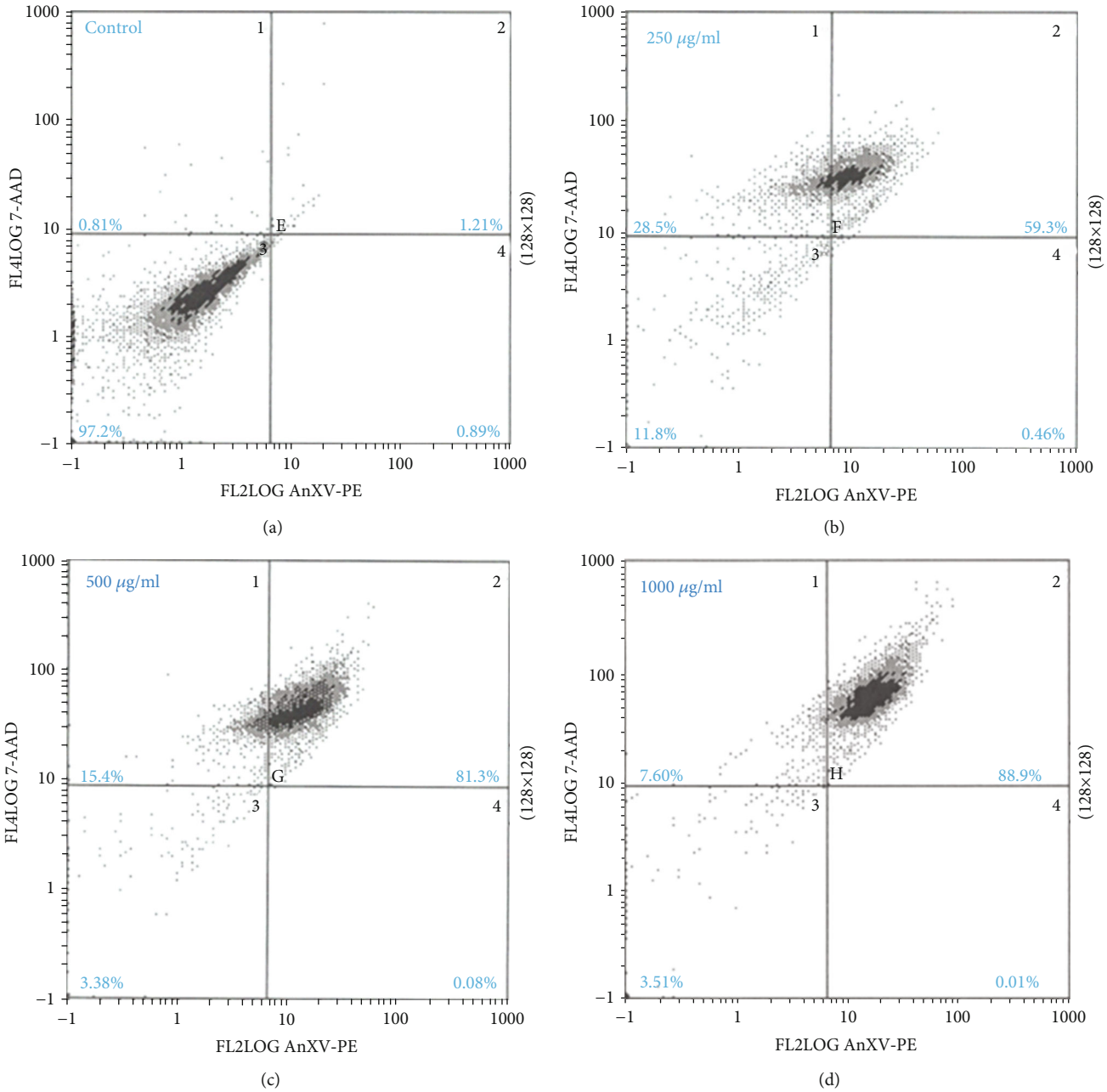

Figure 8: Representative flow cytometry analysis results obtained from Annexin V-FITC/PI assay. The HeLa cells were exposed to RA-ME at 250, 500, and 1000 μg/ml for 24 h. Percentage of early apoptotic, late apoptotic, and necrotic cells are shown by the scatter plots.

Figures 8(a)–8(d), a dose-dependent increase in the percentage of late apoptosis (quadrant 2) cells was found in HeLa cells. The percentages of apoptosis cells in untreated control and RA-ME-treated cells (quadrant 2) were 1.21%, 59.3%, 81.3%, and 88.9% in 0, 250, 500, and 1000 μg/ml, respectively (Figures 8(a)–8(d)). Our results showed that RA-ME induces cellular apoptosis in human cervical cancer (HeLa) cells with the increasing concentrations. These apoptosis cells show an increase expression of Annexin V positive cells in RA-ME-exposed HeLa cells compared to control. The maximum apoptosis cells were found at 1000 μg/ml of RA-ME. Our results are also supported by Khatib et al. [63], who have shown that *R. damascena* oil induced cytotoxicity in gastric cancer cell line (MKN45) through apoptosis mechanism. Turan et al. [60] have also demonstrated that *Rosa canina* extract exhibits concentration-dependent cytotoxic effects against human colon cancer cells by inducing apoptosis. Induction in cancer cell apoptosis has been extensively studied, making it an important indicator for the development of anticancer agents [55]. Earlier reports have also demonstrated that cytotoxic phytochemicals either induced apoptosis or block the signaling pathways, thus leading to cell cycle arrest or cell death [64]. Cancer cells are known to possess molecular mechanism that alleviates apoptosis which plays an important role

in the progression of cancer [19]. Therefore, induction in apoptosis induced by cytotoxic agents can be an essential therapeutic method in the direction of cancer chemotherapy.

4. Conclusions

In conclusion, the present study demonstrated the mechanism of *R. damascena* against cancer cells *in vitro*. Our findings revealed that RA-ME-induced apoptosis and cytotoxicity in HeLa cells are associated with oxidative stress formation, ROS production, mitochondrial depolarization, and cell cycle arrest. Based on results obtained in the present investigation, we can assume that the cell death induced by RA-ME in HeLa cells is due to the oxidative stress. The cytotoxic effects of *R. damascena* observed in this study provide a detail insight knowledge on it. However, further studies are required to understand specific mechanism(s) involved in *R. damascena*-induced cancer cell death.

Data Availability

The data used to support the findings of this study are included within the article.

Conflicts of Interest

The authors declare that they have no conflicts of interest.

Acknowledgments

The authors are grateful to the Deanship of Scientific Research, King Saud University for funding through Vice Deanship of Scientific Research Chairs.

References

[1] H. Nagai and Y. H. Kim, "Cancer prevention from the perspective of global cancer burden patterns," *Journal of Thoracic Disease*, vol. 9, no. 3, pp. 448–451, 2017.

[2] K. Mazumder, B. Biswas, I. M. Raja, and K. Fukase, "A review of cytotoxic plants of the Indian subcontinent and a broad-spectrum analysis of their bioactive compounds," *Molecules*, vol. 25, no. 8, p. 1904, 2020.

[3] K. Kaur and R. Kaur, "Occupational pesticide exposure, impaired DNA repair, and diseases," *Indian Journal of Occupational and Environmental Medicine*, vol. 22, no. 2, pp. 74–81, 2018.

[4] L. Caplan, "Delay in breast cancer: implications for stage at diagnosis and survival," *Frontiers in Public Health*, vol. 2, p. 87, 2014.

[5] S. Bratulic, F. Gatto, and J. Nielsen, "The Translational Status of Cancer Liquid Biopsies," *Regenerative Engineering and Translational Medicine*, 2019.

[6] R. W. Johnstone, A. A. Ruefli, and S. W. Lowe, "Apoptosis: a link between cancer genetics and chemotherapy," *Cell*, vol. 108, no. 2, pp. 153–164, 2002.

[7] J. Ferlay, I. Soerjomataram, M. Ervik et al., *GLOBOCAN 2012 v1.0, Cancer Incidence and Mortality Worldwide: IARC CancerBase No. 11. International Agency for Research on Cancer*, Lyon, France, 2013.

[8] M. Arbyn, X. Castellsagué, S. de Sanjosé et al., "Worldwide burden of cervical cancer in 2008," *Annals of Oncology*, vol. 22, no. 12, pp. 2675–2686, 2011.

[9] L. Denny, R. Herrero, C. Levin, and J. J. Kim, "Cervical cancer," in *Disease control priorities*, H. Gelband, P. Jha, R. Sankaranarayanan, and S. Horton, Eds., pp. 69–84, World Bank Group, 2015.

[10] D. M. Parkin, M. Almonte, L. Bruni, G. Clifford, M. P. Curado, and M. Pineros, "Burden and trends of type-specific human papillomavirus infections and related diseases in the Latin America and Caribbean region," *Vaccine*, vol. 26, pp. L1–L15, 2008.

[11] H. I. Ciftci, M. Can, D. E. Ellakwa et al., "Anticancer activity of Turkish marine extracts: a purple sponge extract induces apoptosis with multitarget kinase inhibition activity," *Investigational New Drugs*, vol. 38, no. 5, pp. 1326–1333, 2020.

[12] A. I. Kuruppu, P. Paranagama, and C. Goonasekara, "Medicinal plants commonly used against cancer in traditional medicine formulae in Sri Lanka," *Saudi Pharmaceutical Journal*, vol. 27, no. 4, pp. 565–573, 2019.

[13] F. T. Artun, A. Karagoz, G. Ozcan et al., "In vitro anticancer and cytotoxic activities of some plant extracts on HeLa and Vero cell lines," *Journal of BUON*, vol. 21, pp. 720–725, 2016.

[14] A. J. Akindele, Z. Wani, G. Mahajan et al., "Anticancer activity of *Aristolochia ringens* Vahl. (Aristolochiaceae)," *Journal of Traditional and Complementary Medicine*, vol. 5, pp. 35–41, 2014.

[15] A. S. Dantu, P. Shankarguru, D. D. Ramya, and H. B. Vedha, "Evaluation of in vitro anticancer activity of hydroalcoholic extract of *Tabernaemontana divaricate*," *Asian Journal of Pharmaceutical and Clinical Research*, vol. 5, pp. 59–61, 2012.

[16] T. Efferth, F. Herrmann, A. Tahrani, and M. Wink, "Cytotoxic activity of secondary metabolites derived from Artemisia annua L. towards cancer cells in comparison to its designated active constituent artemisinin," *Phytomedicine*, vol. 18, article 959969, 2011.

[17] V. A. Silva, A. L. Alves, M. N. Rosa et al., "Hexane partition from Annona crassiflora Mart. promotes cytotoxity and apoptosis on human cervical cancer cell lines," *Investigational New Drugs*, vol. 37, no. 4, pp. 602–615, 2019.

[18] M. Hassan, H. Watari, A. AbuAlmaaty, Y. Ohba, and N. Sakuragi, "Apoptosis and molecular targeting therapy in cancer," *BioMed Research International*, vol. 2014, Article ID 150845, 23 pages, 2014.

[19] R. Kim, M. Emi, and K. Tanabe, "The role of apoptosis in cancer cell survival and therapeutic outcome," *Cancer Biology and Therapy*, vol. 5, pp. 1429–1442, 2014.

[20] Z. Jabbarzadeh and M. Khosh-Khui, "Factors affecting tissue culture of Damask rose (Rosa damascena Mill.)," *Scientia Horticulturae*, vol. 105, no. 4, pp. 475–482, 2005.

[21] T. Hongratanaworakit, "Relaxing effect of rose oil on humans," *Natural Product Communications*, vol. 4, no. 2, pp. 291–296, 2009.

[22] M. H. Boskabady, M. N. Shafei, Z. Saberi, and S. Amini, "Pharmacological effects of Rosa damascena," *Iranian Journal of Basic Medical Sciences*, vol. 14, no. 4, pp. 295–307, 2011.

[23] A. Sharafkhandy, *Ave-Sina. Law in Medicine. Interpreter, Teheran*, Ministry of Guidance Publication, 1990.

[24] M. N. Shafei, H. Rakhshandah, and M. H. Boskabady, "Antitussive effect of Rosa damascena in guinea pigs," *Iranian Journal of Pharmaceutical Research*, vol. 2, pp. 231–234, 2003.

[25] R. Arezoomandan, H. R. Kazerani, and M. Behnam-Rasooli, "The laxative and prokinetic effects of Rosa damascena Mill in rats," *Iranian Journal of Basic Medical Sciences*, vol. 14, pp. 9–16, 2011.

[26] H. Rakhshandah, K. Dolati, and M. Hosseini, "Antinoceptive effect of Rosa damascena in mice," *Journal of Biological Sciences*, vol. 8, pp. 176–180, 2008.

[27] S. Awale, C. Tohda, Y. Tezuka, M. Miyazaki, and S. Kadota, "Protective Effects of Rosa damascena and Its Active Constituent on Aβ(25–35)-Induced Neuritic Atrophy," *Evidence Based Complementary and Alternative Medicin*, vol. 2011, article 131042, 8 pages, 2011.

[28] M. H. Boskabady, A. Vatanprast, H. Parsee, and M. Ghasemzadeh, "Effect of aqueous-ethanolic extract from Rosa damascena on guinea pig isolated heart," *Iranian Journal of Basic Medical Sciences*, vol. 14, pp. 116–121, 2011.

[29] N. Kumar, P. Bhandari, B. Singh, and S. S. Bari, "Antioxidant activity and ultra-performance LC-electrospray ionization-quadrupole time-of-flight mass spectrometry for phenolics-based fingerprinting of Rose species: Rosa damascena, Rosa bourboniana and Rosa brunonii," *Food and Chemical Toxicology*, vol. 47, no. 2, pp. 361–367, 2009.

[30] S. Ulusoy, G. Boşgelmez-Tınaz, and H. Seçilmiş-Canbay, "Tocopherol, carotene, phenolic contents and antibacterial properties of rose essential oil, hydrosol and absolute," *Current Microbiology*, vol. 59, no. 5, pp. 554–558, 2009.

[31] N. Mahmood, S. Piacente, C. Pizza, A. Burke, A. I. Khan, and A. J. Hay, "The anti-HIV activity and mechanisms of action of pure compounds isolated from *Rosa damascene*," *Biochemical and Biophysical Research Communications*, vol. 229, no. 1, pp. 73–79, 1996.

[32] A. Gholamhoseinian and H. Fallah, "Inhibitory effect of methanol extract of *Rosa damascena* Mill. flowers on α-glucosidase activity and postprandial hyperglycemia in normal and diabetic rats," *Phytomedicine*, vol. 16, no. 10, pp. 935–941, 2009.

[33] M. Jafari, A. Zarban, S. Pham, and T. Wang, "R*osa damascena* decreased mortality in adult Drosophila," *Journal of Medicinal Food*, vol. 11, no. 1, pp. 9–13, 2008.

[34] G. Latifi, A. Ghannadi, and M. Minaiyan, "Anti-inflammatory effect of volatile oil and hydroalcoholic extract of Rosa damascena Mill. on acetic acid-induced colitis in rats," *Research in Pharmaceutical Sciences*, vol. 10, no. 6, pp. 514–522, 2015.

[35] Y. Zu, H. Yu, and L. Liang, "Activities of ten essential oils towards *Propionibacterium acnes* and PC-3, A-549 and MCF-7 cancer cells," *Molecules*, vol. 15, no. 5, pp. 3200–3210, 2010.

[36] A. Zamiri-Akhlaghi, H. Rakhshandeh, Z. Tayarani-Najaran, and S. H. Mousavi, "Study of cytotoxic properties of *Rosa damascena*extract in human cervix carcinoma cell line," *Avicenna Journal of Phytomedicine*, vol. 1, pp. 74–77, 2011.

[37] B. Venkatesan, V. Subramanian, A. Tumala, and E. Vellaichamy, "Rapid synthesis of biocompatible silver nanoparticles using aqueous extract of *Rosa damascena* petals and evaluation of their anticancer activity," *Asian Pacific Journal of Tropical Medicine*, vol. 7, pp. S294–S300, 2014.

[38] E. S. Abdel-Hameed, S. A. Bazaid, and H. A. Hagag, "Chemical characterization of Rosa damascena Miller var. trigintipetala Dieck essential oil and its in vitro genotoxic and cytotoxic properties," *Journal of Essential Oil Research*, vol. 28, pp. 121–129, 2015.

[39] F. T. Bura, R. A. Firuzja, and F. Nemati, "Cytotoxic effect of the flower and leaf bud extract of Crataegus microphylla C. Koch on HeLa cell line," *IIOAB Journal*, vol. 7, pp. 214–218, 2016.

[40] M. M. Al-Oqail, E. S. Al-Sheddi, N. N. Farshori et al., "Corn silk (Zea mays L.) induced apoptosis in human breast cancer (MCF-7) cells via the ROS-mediated mitochondrial pathway," *Oxidative Medicine and Cellular Longevity*, vol. 2019, Article ID 9789241, 9 pages, 2019.

[41] O. H. Lowry, N. J. Rosebrough, A. L. Farr, and R. J. Randall, "Protein measurement with the Folin phenol reagent," *Journal of Biological Chemistry*, vol. 193, no. 1, pp. 265–275, 1951.

[42] J. A. Buege and S. D. Aust, "Microsomal lipid peroxidation," *Methods in Enzymology*, vol. 52, pp. 302–310, 1978.

[43] D. Chandra, K. V. Ramana, L. Wang, B. N. Christensen, A. Bhatnagar, and S. K. Srivastava, "Inhibition of fiber cell globulization and hyperglycemia-induced lens opacification by aminopeptidase inhibitor bestatin," *Investigative Ophthalmology and Visual Science*, vol. 43, no. 7, pp. 2285–2292, 2002.

[44] M. A. Siddiqui, M. P. Kashyap, V. Kumar, A. A. Al-Khedhairy, J. Musarrat, and A. B. Pant, "Protective potential of trans-resveratrol against 4-hydroxynonenal induced damage in PC12 cells," *Toxicology In Vitro*, vol. 24, no. 6, pp. 1592–1598, 2010.

[45] E. Studzińska-Sroka, H. Piotrowska, M. Kucińska, M. Murias, and W. Bylka, "Cytotoxic activity of physodic acid and acetone extract from Hypogymnia physodes against breast cancer cell lines," *Pharmaceutical Biology*, vol. 54, no. 11, pp. 2480–2485, 2016.

[46] T. Mosmann, "Rapid colorimetric assay for cellular growth and survival: application to proliferation and cytotoxicity assays," *Journal of Immunological Methods*, vol. 65, no. 1-2, pp. 55–63, 1983.

[47] G. Cudazzo, D. J. Smart, D. McHugh, and P. Vanscheeuwijck, "Lysosomotropic-related limitations of the BALB/c 3T3 cell-based neutral red uptake assay and an alternative testing approach for assessing e-liquid cytotoxicity," *Toxicology In Vitro*, vol. 61, article 104647, 2019.

[48] H. A. Hagag, S. A. Bazaid, E. S. Abdel-Hameed, and M. Salman, "Cytogenetic, cytotoxic and GC–MS studies on concrete and absolute oils from Taif rose, Saudi Arabia," *Cytotechnology*, vol. 66, no. 6, pp. 913–923, 2014.

[49] C. G. Yedjou and P. B. Tchounwou, "In vitro assessment of oxidative stress and apoptotic mechanisms of garlic extract in the treatment of acute promyelocytic leukemia," *Journal of Cancer Science and Therapy*, vol. 2012, Supplement 3, p. 6, 2012.

[50] A. S. Abdullah, A. S. Mohammed, A. Rasedee, and M. E. Mirghani, "Oxidative stress-mediated apoptosis induced by ethanolic mango seed extract in cultured estrogen receptor positive breast cancer MCF-7 cells," *International Journal of Molecular Sciences*, vol. 16, no. 2, pp. 3528–3536, 2015.

[51] M. M. Al-Oqail, M. A. Siddiqui, E. S. Al-Sheddi et al., "V*erbesina encelioides*: cytotoxicity, cell cycle arrest, and oxidative DNA damage in human liver cancer (HepG2) cell line," *BMC Complementary and Alternative Medicine*, vol. 16, no. 1, p. 126, 2016.

[52] D. H. Kwon, H. J. Cha, H. Lee et al., "Protective effect of glutathione against oxidative stress-induced cytotoxicity in RAW 264.7 macrophages through activating the nuclear factor erythroid 2-related factor-2/heme oxygenase-1 pathway," *Antioxidants*, vol. 8, p. 82, 2019.

[53] N. Traverso, R. Ricciarelli, M. Nitti et al., "Role of glutathione in cancer progression and chemoresistance," *Oxidative Medicine and Cellular Longevity*, vol. 2013, Article ID 972913, 10 pages, 2013.

[54] N. D. Wageesha, P. Soysa, K. Atthanayake, M. I. Choudhary, and M. Ekanayake, "A traditional poly herbal medicine "Le Pana Guliya" induces apoptosis in HepG 2 and HeLa cells but not in CC1 cells: an in vitro assessment," *Chemistry Central Journal*, vol. 11, pp. 1-2, 2017.

[55] J. Pi, H. Cai, H. Jin et al., "Qualitative and quantitative analysis of ROS-mediated oridonin-induced oesophageal cancer KYSE-150 cell apoptosis by atomic force microscopy," *PLoS One*, vol. 10, no. 10, article e0140935, 2015.

[56] W. P. Tsang, S. P. Chau, S. K. Kong, K. P. Fung, and T. T. Kwok, "Reactive oxygen species mediate doxorubicin induced p53-independent apoptosis," *Life Sciences*, vol. 73, no. 16, pp. 2047–2058, 2003.

[57] I. González-Chavarría, F. Duprat, F. J. Roa et al., "Maytenus disticha extract and an isolated β-dihydroagarofuran induce mitochondrial depolarization and apoptosis in human cancer cells by increasing mitochondrial reactive oxygen species," *Biomolecules*, vol. 10, no. 3, p. 377, 2020.

[58] J. Jakubowicz-Gil, E. Langner, D. Bądziul, I. Wertel, and W. Rzeski, "Apoptosis induction in human glioblastoma multiforme T98G cells upon temozolomide and quercetin treatment," *Tumor Biology*, vol. 34, no. 4, pp. 2367–2378, 2013.

[59] V. Kuete, A. R. Donfack, A. T. Mbaveng, M. Zeino, P. Tane, and T. Efferth, "Cytotoxicity of anthraquinones from the roots of Pentas schimperi towards multi-factorial drug-resistant cancer cells," *Investigational New Drugs*, vol. 33, no. 4, pp. 861–869, 2015.

[60] I. Turan, S. Demir, K. Kilinc et al., "Cytotoxic effect of Rosa canina extract on human colon cancer cells through repression of telomerase expression," *Journal of Pharmaceutical Analysis*, vol. 8, no. 6, pp. 394–399, 2018.

[61] K. Kilinc, S. Demir, I. Turan et al., "Rosa canina extract has antiproliferative and proapoptotic effects on human lung and prostate cancer cells," *Nutrition and Cancer*, vol. 72, no. 2, pp. 273–282, 2020.

[62] D. A. Wiseman, S. R. Werner, and P. L. Crowell, "Cell cycle arrest by the isoprenoids perillyl alcohol, geraniol, and farnesol is mediated by p21Cip1 and p27Kip1 in human pancreatic adenocarcinoma cells," *Journal of Pharmacology and Experimental Therapeutics*, vol. 320, no. 3, pp. 1163–1170, 2007.

[63] H. Khatib, M. Rezaei-Tavirani, S. H. Keshel et al., "Flow cytometry analysis of Rosa Damascena effects on gastric cancer cell line (MKN45)," *Iranian Journal of Cancer Prevention*, vol. 6, pp. 30–36, 2013.

[64] T. Sa and T. Das, "Anti cancer effects of curcumin: cycle of life and death," *Cell Division*, vol. 3, no. 1, p. 14, 2008.